

5-24-2019

An Experimental Study on the Impacts of Using Multiple PDC Cutters on Rock Cutting Process

Kian Sheikhezai

Follow this and additional works at: https://digitalcommons.lsu.edu/gradschool_dissertations



Part of the [Other Engineering Commons](#)

Recommended Citation

Sheikhezai, Kian, "An Experimental Study on the Impacts of Using Multiple PDC Cutters on Rock Cutting Process" (2019). *LSU Doctoral Dissertations*. 4937.

https://digitalcommons.lsu.edu/gradschool_dissertations/4937

This Dissertation is brought to you for free and open access by the Graduate School at LSU Digital Commons. It has been accepted for inclusion in LSU Doctoral Dissertations by an authorized graduate school editor of LSU Digital Commons. For more information, please contact gradetd@lsu.edu.

AN EXPERIMENTAL STUDY ON THE IMPACTS OF USING MULTIPLE PDC CUTTERS ON ROCK CUTTING PROCESS

A Dissertation

Submitted to the Graduate Faculty of the
Louisiana State University and
Agricultural and Mechanical College
in partial fulfillment of the
requirements for the degree of
Doctor of Philosophy

in

The Department of Petroleum Engineering

by

Kian Sheikherezaei

B.S., Amirkabir University of Technology, 2008

MBA, Payam Noor University of Tehran, 2011

August 2019

©Copyright 2019
Kian Sheikhrzaei
All rights reserved

To my beloved wife, Marmar

& my dear parents

for their endless love and support...

ACKNOWLEDGEMENTS

Above all, I am grateful to the almighty Allah, for blessing me this far. Then, I would like to express my sincere appreciation, primarily, to my major advisor, Dr. Babak Akbari. Undoubtedly, this dissertation would not have been possible without his great support, understanding and encouragement. I would also like to appreciate my co-advisor, Dr. Arash Dahi Taleghani, for providing me with insights toward my academic work. I want to express my gratitude to my committee members, Dr. Andrew Wojtanowicz, Dr. Michael M. Khonsari, Dr. Patricia Persaud and Dr. Jianhua Chen for their valuable advice throughout this work.

I gratefully acknowledge financial support from Dr. Karsten Thompson and the Craft & Hawkins Department of Petroleum Engineering at LSU and Dr. Marc Bird in Baker Hughes. I would like to thank companies and individuals who contributed to this research. BHGE and NOV for providing the rock samples. Mr. Roy Ledgerwood and, Dr. Reza Rahmani, for their technical comments and insights. Dr. Michelle Osborn, Dr. Kip Matthews, Dr. Juan Lorenzo, Mr. Nic Dinecola (ME shop), and LTRC (concrete lab) all at LSU for their helpful collaboration in different parts of this work.

I appreciate all my friends in the departments of petroleum, mechanical, civil and electrical engineering for their kind assist in conducting this experimental study. I would like to write with tribute in memory of Dr. Denis Klimenko, a great friend in our research group.

Finally, I thank my wife, Marmar, my parents, my parents' in-law, my sister, Mahdieh, my brother, Kaveh and all my family for their ongoing support and unconditional kindness throughout the PhD career and my entire life.

TABLE OF CONTENTS

ACKNOWLEDGEMENTS	iv
ABSTRACT.....	vii
CHAPTER	
1 BACKGROUND	1
1.1 Introduction	1
1.2 Problem Statement	4
2 CURRENT STATE OF KNOWLEDGE.....	7
2.1 PDC Cutter	7
2.2 Rock Cutting Experiments by PDC Cutters in Literature	9
2.3 Rock Cutting Force Modelling.....	13
2.4 Cutters Arrangements on Bit.....	18
3 ROCK CHARACTERIZATION	25
3.1 Introduction	25
3.2 Compressive Strength Test	27
3.3 Scratch Test.....	34
3.4 Sonic Test.....	36
3.5 Rock Cutting Simulation via Finite Element Method.....	39
4 EXPERIMENTAL SETUP.....	47
4.1 Multi-Point Cutter Facility (MPC).....	47
4.2 Rock Preparation	52
4.3 Arranging the Cutters on the Designed Bit	53
4.4 Force Components on Bit Profile.....	54
4.5 Method of Experiments.....	55
4.6 Engagement Area	58
4.7 Equivalent Cut Thickness (ECT)	64
4.8 Electrical and Mechanical Power, Torque & MSE	66
5 EXPERIMENTAL RESULTS.....	69
5.1 Results for Single Cutter Tests.....	69
5.2 Results for Double Cutter Tests	76
5.3 Results for Triple Cutter Tests	77
5.4 Conclusion on Triple Cutter Results	86
5.5 Grooves and Cuttings Remain on Bit and Rock Sample	87
6 RESULT ANALYSIS.....	94
6.1 Single Cutter Force Model	94
6.2 Impact of Triple Cutters on Force Model.....	97
6.3 Proposed Model to Experiments	104
6.4 Impact of Cutters Arrangements on Bit Performance	112
6.5 Bit Design.....	119

7	APPLICATIONS	128
7.1	Different Cutters Arrangements on a Bit	128
7.2	Simulation of Cutting Process via FEM.....	134
7.3	Applied Forces Model to Cutters on Various Bits	137
7.4	Summary	144
8	CONCLUSIONS AND FUTURE WORK RECOMMENDATIONS	146
	REFERENCES	151
	APPENDIX A: μ – CT SCANNING OF A SAMPLE AFTER CUT	158
	APPENDIX B: SAMPLE PREPARATION.....	170
	APPENDIX C: COMPARING RESULTS: EXPERIMENTS & MODEL.....	174
	APPENDIX D: SHALE SPECIFICATIONS (<i>X-RAY & XRF</i>)	176
	APPENDIX E: GROOVES AND CUTTING REMAIN AFTER CUT.....	179
	APPENDIX F: EMPRICAL RELATIONS TO OBTAIN UCS	183
	APPENDIX G: SENSOR PROTECTIVE BOX.....	184
	VITA.....	185

ABSTRACT

The ultimate goal in drilling in oil and gas applications is to improve the rate of penetration (ROP) and one important factor that affects the ROP enhancement is Drill Bit. Today, PDC bit plays a significant role in drilling all types of formations. Besides the material development, bit design or a way of cutters arrangements on a bit is a regular challenge for bit designers to improve the bit performance. This concept has been experimentally studied in this work.

Different sets of cutters arrangements containing three 13 – *mm* PDC cutters on a flat bit profile have been used to conduct a variety of experiments under atmospheric pressure on different rock samples including shale, sandstone and limestone. Different cutters arrangements including spiral and reverse spiral sets, and different spacing between the cutters are selected to investigate these bit design parameters. The measured forces for those two specific sets (spiral and reverse spiral) show the equal normal force but different forces on the bit plane. It is found that radial force on a cutter besides the cutter engagement area is also affected by changes in the cutting shape, or cutting area. The efficiency of one specific cutters layout can be recognized by MSE and lateral force, as a tool to indicate stability. A force model is proposed to predict the acting forces on one PDC cutter and then, to integrate it into a full PDC bit. The model can be used as a reliable tool to study the rock-cutter interactions during the cutting process to avoid cyclic loading and damage to the cutters and to enhance the bit life. The experimental results show that cutters arrangements on bit strongly affect the bit performance. In the scope of this work, lower MSE can be obtained by a reverse spiral set of cutters arrangement but regards to the lateral force and stability, arranging the cutters spirally can provide better results.

1 BACKGROUND

1.1 Introduction

For drilling engineers, fundamental understanding of the mechanics of rock cutting in downhole conditions is crucial to overcome the challenges of drilling for deep hydrocarbon resources, such as low rates of penetration and bit balling. Understanding the rock behavior while it is being cut by a drilling bit is beneficial to increase the drilling efficiency and decrease costs. The strength and stress-strain behavior of rocks under confining stresses are also important to understand the cutting process, rock failure and behavior of bits on different types of rocks and formations and to develop techniques for improving Rate of Penetration (ROP). The characterization and modeling of mechanical behavior of the rocks are necessary for the stability analysis of structures.

Drill (or drilling) bit is responsible for shearing or crushing rock as it drills into the subsurface. They are critical components in entire drilling process; and therefore they have a significant impact over the entire project economics. This is an important role that must be evaluated through elements and parameters involved in bit rock interactions. In rotary drilling that relies on continuous circular motion of bit to break the rock at the bottom of the hole, most bits in use today can be broadly classified as either roller cone or fixed cutter bits. Since the introduction of PDC bits -which fail the rock in shear-, they have come to dominate market share over roller cones. In 2015, more than 90% of worldwide footage drilled in oil and gas applications were done by PDC bits [1]. A regular challenge for bit designers has continuously shifted between materials development and advancing bit design to expand the materials capabilities [2]. In addition, the arrangements and different layouts of the PDC cutters on bits play an important role in bit drilling efficiency and bit stability [3].



Figure 1-1: rotary drilling bits (www.slb.com)

Knowledge of PDC cutter and rock-cutter interaction is a necessity to improve drilling performance to increase ROP and reduce time and cost. To reach this goal, many researchers have studied effects of different parameters such as geometry, process, and field conditions on PDC cutters performance [4-6]. Obviously, any factor that imposes delay in drilling process should be investigated and then mitigated. For example, bit balling is one of the drilling operational issues that can cause several problems such as reduction in rate of penetration and surface torque and raising cutter temperature that might shorten bit life [6, 7]. It occurs when the drilled rock or cuttings accumulate and attach to the bit during the drilling process [8]. Some formations such as claystone and shale are prone to be balled up even in oil base mud (OBM) or inhibitive water base mud (WBM). Swollen clays can become plastic and stick to the cutters and the body of the drill bit. PDC bits, due to their shear cutting action and the mechanism of chip generation, are especially susceptible to bit balling [9]. Bit wear and failure due to the erosion by fluid or cutting abrasive formations is another factor to be considered. It is strongly desired to have a bit with longer life to save time, cost, and to increase the drilling efficiency. This objective is usually pursued by optimizing geometrical design of cutters placement.

Designing an optimized PDC bit, with higher efficiency and stability, is always a main objective for the development engineers. A full PDC bit consists of many cutters spatially arranged and brazed on body of the bit. In fact, with the help of the same PDC cutters, many different types of drill bits are designed to drill into various formations. Technically, optimization of bit design refers to better efficiency and life duration of the bits for the given formation properties. Drilling efficiency is evaluated by Mechanical Specific Energy (MSE) and the bit life refers to the duration that drilling can continue without the need to pull the bit out, due to reasons *e.g.* wear and erosion.

Two sets of variables are usually being considered by bit designers, local and global variables. The former include cutter size, rake angles, chamfer size, *etc.* and, the latter encompass number of cutters, blades and way of distributing the cutters on a bit, *etc.* In single cutter models, only the local variables can be inputted. The bit-rock interactions model integrates single cutter models and incorporated the global variables [10]. It can be concluded from studying the design variables that the cutters layout on a PDC bit plays a significant role in optimizing the bit performance. Although, many researchers have worked on the PDC single cutter process, lack of insight on impact of multiple cutters on rock cutting process is strongly felt [6, 7, 11]. Therefore, providing accurate laboratory experiments with multiple cutters can provide valuable results assisting bit design.

Numerical modeling can be used to better understanding on the cutting process. It often yields reliable results for a given set of conditions, and sometimes offers effective visualization of breakage processes, although it includes some important simplifications. Finite element methods (FEM) is found to be a reliable method for simulating the rock cutting process, due to its flexibility in handling material heterogeneity, nonlinearity and boundary conditions [12, 13]. Rock cutting process is a challenging problem from the modelling point of view, due to complexity of the

physics from cutter rock interaction to the fracture process and propagation. Thus, development of numerical tools (FEA) benefitting from analytical methods for more accurate analysis accompanied with experimental laboratory scales (single or triple cutter tests) could improve the understanding of major issues in subsurface drilling.

Last, to propose an accurate model, it is essential to obtain the parameters of the rock through proper experiments including unconfined compression test. In this study, rock strength is obtained based on the experimental results of UCS test and measuring travel time through the rock samples. The obtained parameters based on the current samples are then used in rock cutting simulation and in force model development.

1.2 Problem Statement

The dream of the drillers all around the world is to drill as quickly as possible *i.e.* from casing shoe to the next casing point without compromising borehole quality and rig safety. The drill bit (which is also called *bit* or *drilling bit*) is central to achieving this goal because it must withstand variations in lithology, formation compressive strength and many other factors.

Drilling efficiency as a measure to evaluate the drilling process plays a key role to determine the viability of potential hydrocarbon plays. It is highly dependent on the drilling tool performance owing to the fact that drill bits are responsible for shearing or crushing the rocks and drilling into the subsurface. They are critical components in the whole drilling process and have a paramount impact over the entire project economics.

Therefore, the bit design becomes a substantial part of drilling process, which could be developed by accurate laboratory experiments of rock cutting process. Drilling into a formation requires rotation of a bit coupled with axial force applied to the cutting face of the bit. The rotation

causes torque on bit (TOB) which is responsible for shearing (dragging) job. The axial force is called weight on bit (WOB) and is distributed over the cutters on bit. As a bit rotates and penetrates into the formation, each PDC cutter involves with the formation exerts forces on the bit, which can be estimated from the kinematic laboratory models for that specific drilling condition and formation. If the forces acting on a bit become zero or minimum, it may avoid excessive vibrations, damaging the cutters, shortening the bit life, and reducing the drilling efficiency. It can be investigated through summations of linear and moment force vectors which highly depend on the cutting structure [14].

Bit imbalance forces are generally generated by the bit geometry and/or the formation anisotropy that impose non-symmetric moment and forces to the cutters. Potential sources of out-of-balanced forces caused by bit geometry can be named as giving rise to the radial components at the cutters for non-flat bits, non-zero sum of circumferential cutting forces on the cutters, side rake angle of the cutters, and uneven mass distribution of the cutters density on a bit [15]. From another side, the main reason may cause the bit instability can be created through the transitional drilling *i.e.* drilling through the boundary of two formations. Simply, the forces on bit, make it oriented, push one side of the bit against the wellbore and create the frictional forces. Then, the torque on the bit may couple with the friction and pull the bit off the rotational geometric center toward the wellbore. This phenomenon would accelerate the wear, mitigate the penetrating rate, enlarge the borehole, and deviate the well [15]. Therefore, force-balancing techniques are valuable to reduce any downhole vibrations and deviation caused by the bit's cutting action.

Considering the importance of cutters layout and reliable force model, this study aims to provide a better knowledge of bit design to enhance drilling efficiency. The current work is built to investigate the cutting process by applying triple PDC cutters on different blades on a flat bit.

This method of experiment has been scarcely studied by scholars. We focus to investigate the impact of using multiple cutters on different aspects for the process including force equilibrium on bit plane, optimum cutters arrangement on a bit, reducing the possible vibrations on bit. A novel model is proposed to predict the forces acting on PDC cutters on a bit. The model is verified by conducting series of experiments on cutting the rock samples using tripe PDC cutter. Then, based on the suggested model, a desired application of arranging cutters on a ring of bit is implemented. The model can be assumed as the conditions of transitional drilling where the depth of cut is constantly changing due to changes in drilling formation from hard to soft or vice versa. Besides, the results of conducting several cutting tests on various rock samples provide a good measure on efficient cutters arrangement on different formations.

Hence, the current work investigates the effect of applying different cutters arrangements on different sets (including spiral and reverse spiral sets of cutters) on the rock cutting process. The spacing between the cutters on some rock samples is another factor that is studied experimentally. A force model is proposed to predict the acting forces on the PDC cutters on a bit plane, which can be integrated into a full PDC bit. The proposed model develops a reliable and efficient method to study the rock-cutter interactions on a bit. It can significantly enhance the durability of the PDC cutters and consequently, increase the bit life.

In chapter 1, the introduction and the problem is stated. In chapter 2, the current state of knowledge on modeling and experiments by PDC cutters and PDC bits is presented. In chapter 3, rock characterization is reported based on the tests and finite element method. In chapter 4, the experimental setup and methodology are described. Next chapter is the report of the experimental results. In chapter 6, the analysis of the results is presented in depth. Chapter 7 provides an

application of the model on PDC bit design. In chapter 8, the conclusion and summary are stated. Last, appendices and references are presented.

2 CURRENT STATE OF KNOWLEDGE

2.1 PDC Cutter

One of the most significant impacts on the overall cost of drilling wells is the slow penetration rate problem. Many empirical, analytical and numerical models have been proposed to estimate ROP in subsurface drilling [6, 16, 17]. To develop those models, it is highly desired to consider the interactions between cutters on a bit and confining stress, frictional forces, pore fluid and porous nature of rock. Understanding the major factors affect the penetration rate is an essential step to provide a robust model to study the issues mitigate the rate of drilling and to detect its solutions. Two major types of these factors are described; formation factors such as changes in pressure, temperature, permeability, and rock strength; and dysfunction phenomena *e.g.* bit, cutter or bottom-hole balling, and bit dullness.

As The predominant method for researchers to study the influential factors in rock cutting process is applying Polycrystalline Diamond Compact (PDC) cutters. PDC cutters were first introduced with the concept of cutting rock by shearing action by General Electric in 1973. A specific commercial product for application in oil filed bits was introduced in 1976. With advantages of higher rates of penetration (ROP) and longer life, PDC bits have gained prominent use for drilling different formations [9]. The thin layer of synthetic diamond compact on the leading face of the cutter is called Polycrystalline Diamond Compact (PDC), which is inserted on tungsten carbide stud. The main duty of PDC cutter is to fail the rock.



Figure 2-1: Polycrystalline Diamond Compact (PDC) Cutter (13 mm dia.)

At the cutting face, the interface force can be resolved in three directions: normal or axial force, side or radial force toward the center, and cutting or tangential force, which acts tangent to the groove path (Figure 2-2). In this study, we will use the same nomenclature as described.

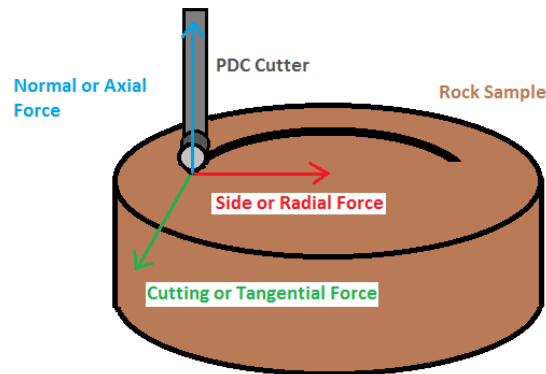


Figure 2-2: Forces on sharp single cutter cutting the rock sample

2.1.1 Mechanical Specific Energy (MSE)

Mechanical specific energy (MSE) is an important measurement to evaluate the drilling performance by quantifying a complex process of rock cutting. For the first time, this concept was introduced by Teale in 1965 as the amount of mechanical energy required to remove a unit volume of rock (Equation 2-1) [18]. He formulated this concept in rotary drilling based on the work done

by weight on bit (axial force) and torque on bit (rotational force) to drill a volume of rock. The general definition for mechanical specific energy is seen as Equation 2-2.

$$MSE = WOB/A_b + 120.\pi.RPM.T/(A_b * ROP) \quad (2-1)$$

where WOB is weight on bit, A_b is bit area, RPM is revolution per minute, T is torque on bit, and ROP is rate of penetration.

$$MSE = \left(\frac{Total\ Energy\ Input}{Removed\ Volume} \right) = \left(\frac{Vertical\ Energy\ Input}{Removed\ Volume} \right) + \left(\frac{Rotational\ Energy\ Input}{Removed\ Volume} \right) \quad (2-2)$$

2.2 Rock Cutting Experiments by PDC Cutters in Literature

2.2.1 Single PDC Cutter Tests

The purpose of single cutter experiments is to study different aspects of rock cutting process in laboratory scale for better insights into drill bit design in field scale drilling. Fundamental understanding of the mechanics of rock cutting in downhole conditions is crucial to overcome the challenges of drilling for deep hydrocarbon resources, such as low rates of penetration. Many scholars have studied experimentally various aspects of using single cutter in cutting process. One of the first important investigations on PDC cutters under atmospheric pressure was conducted by Glowka [7]. He found a relation between the cutting forces and depth of cut, regardless of cutter geometry. Zijsling in 1987 studied the effect of temperature on cutters and reported the advantages of using a thin diamond layer on them. It can improve heat conduction and reduce the maximal cutting-edge temperature. Zijsling proposed a method for a single cutter tester to study the cutting process with PDC cutters under simulated borehole conditions in shales drilling. He discussed the drilling characteristics of PDC bits in shales and bit/cutter design aspects in order to improve the bit performance by facilitating the bit cleaning [19]. Smith presented both laboratory and field data to illustrate the benefits of applying a mirror polished surface to the face

of PDC cutters in drilling stressed formations [6]. In 1998, Sinor *et al.* evaluated the effect of cutter density, back rake angle, size, and speed on the steady state wear rate and performance of PDC cutters[5]. The effects on the friction coefficient between the rock and the PDC cutter caused by the back rake angle was another interesting topic for researchers. Kuru and Wojtanowicz (1995) indicated that in comparison to the back rake angle, parameters such as normal force or the rock type would not be able to change the friction coefficient remarkably [20]. Richard (1999) explained that changing the back rake angle would alter the flow regime ahead of the cutter which leads to vary the friction angle [11]. The author studied and verified his claim later in 2010 in other work [21]. He studied the influence of cutting geometry on the cutting force acting on a sharp cutter tracing a groove on the surface of a rock sample and showed that the geometry of the groove being traced could strongly affect the intrinsic specific energy. Rafatian *et al.* (2010), conducted a series of experiments in atmospheric and pressurized conditions on single cutter to propose a theory to explain unexpected behavior that even at low pressures, significant increase in MSE was observed compared to atmospheric tests [22]. Rajabov *et al.* (2012) presented the results of 150 tests that showed the effect of both rake angles on MSE of PDC cutters [23]. In 2013, Akbari *et al.* experimentally investigated on effect of rock pore pressure on MSE. The corresponding author later in 2014, systematically tested the impacts of rake angles, cutter size, and cutter chamfer size on the MSE. The abovementioned studies and some others [24, 25] were all focused on the force models by single cutter.

2.2.2 Double or Triple PDC Cutter Tests

An important investigation on PDC cutting with multiple PDC cutters was done by Glowka [7]. He conducted various laboratory tests in atmospheric pressure with single PDC cutters and provided some relations between the forces on the cutters and rock type, cut depth, and cutter-wear

state. He identified two distinct modes of wear. He studied the effects of interaction among closely spaced cutters and then developed a model to account the impacts on the adjacent cutters. The effect of water jet assistance was also considered in his work. Glowka reported that in atmospheric pressure, interaction could be important if the cutters cut the grooves closely enough to have interconnection. Then, the cross-sectional area of rock removed by each cutter, therefore, would be the parameter that characterized cutter interaction and that controlled cutter forces. He found that in shallow depth of cut, PDC cutters did not cause much rock breakage outside the projected area of the cutter profile. He ran some linear parallel cuts at top surface of the rock sample to study the effects of interacting cuts. Cuts made with PDC cutters were assisted by the high-pressure water jets. Cutter wear-flats were measured. Two types of cut were used: interacting and non-interacting. Figure 2-3 demonstrates the cut track whether has the interconnection with adjacent cutters or not.

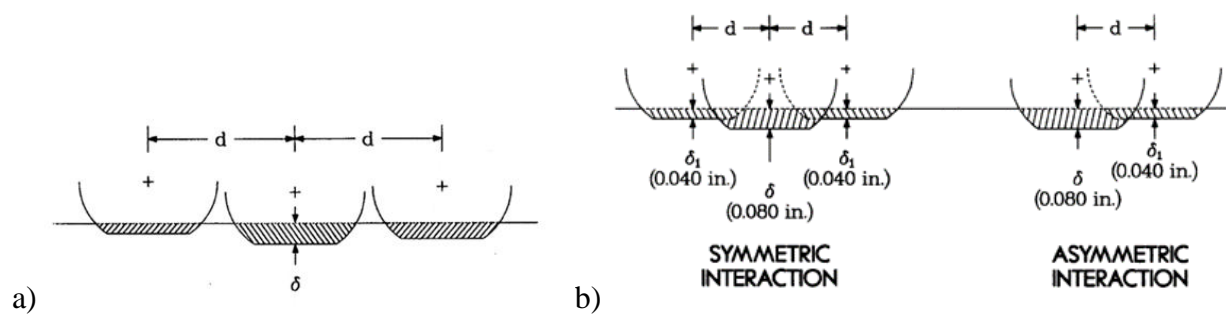


Figure 2-3: interacting and non-interacting cutting the rock sample after [7]

By comparing the cuts, he concluded that the ratio of horizontal force to vertical force in a given rock is not heavily dependent on degree of interacting or depth of cut. Furthermore, he implied that larger cutters are more effective than small ones from MSE perspective. By conducting series of experiments on PDC cutters, he reported that similar to the sharp cutters where the vertical force is proportional to the cutter's engaging area, the penetrating or vertical force

imposed on a worn PDC cutter at a given cut depth is nearly proportional to the wear-flat area in contact with the rock. Based on the results of the interacting tests, he then suggested a method to achieve a uniform state of the wear on the cutters. He recommended radially shifting the cutters and providing large number of the cutters in regions of excessive wear and low number of the cutters in regions of low wear.

2.2.3 Full PDC Bits Experiments

In 1988, Kerr [26] reviewed the development of PDC bits from their introduction in 1973 in different aspects such as body material, cutter density, etc. and their effect on the bit performance. Feenstra [27] in the same year studied the characteristics, development, and outlook for PDC bits and treated applications of PDC bits, including suitable locations, types of hole, and uses. Knowlton and Kester [28] worked on enhanced thermal stability and a radius of curvature on the diamond table of PDC cutters on bits. Knowlton in 1990 developed a new concept in bit technology with applying larger diameter of cutters, curved cutters and placing critical spacing between the cutters [29]. Warren and Armagost [8] analyzed laboratory drilling performance and reported that at equal weight on bit, as cutter density of a PDC bit or the back rake angle of the cutters increased, ROP and the depth of cut decreased. Proper bit selection will highly affect the cleaning, ROP and durability.

Appl and Wilson [30] in 1993 presented a series of cutting experiments to better understand the effects of cutter temperatures and forces on PDC bit life. Andersen and Azar conducted laboratory tests at borehole conditions, investigating the effects of differential pressure on Polycrystalline Diamond Compact (PDC) drill bit performance; observing that differential pressure reduced PDC bit performance due to rock strengthening, chip hold down, and bit balling. Chip hold-down occurs when the pressure holds the cuttings down in a path of cut by the bit [31].

Zijsling and Illerhaus (1993) proposed a new concept in PDC bits to comprise a hydraulic layout that would optimize bit cleaning and cuttings removal in soft and sticky formations [32]. Bit whirl occurs when the center of rotation moves about the bit face as the bit rotates. This phenomenon would break the cutters and accelerate wear for PDC bit. Weaver and Clayton in 1993, developed new whirl resistant PDC bits that in laboratory experiments showed validation with field results obtained from PDC bit performances in six different fields with variety of formation types [33]. They stated that positioning the PDC cutters in concentric rings with little or no overlap between cutters produced a bottom-hole profile with deep grooves. Those grooves acted as guide tracks for the PDC cutters and provided a restoring force to resist off-center rotation. Ersoy in 2003 evaluated the optimum performance of PDC based on maximum feed rate at minimum specific energy. Similarities between the rock strength and drilling specific energy were reported to provide a relationship between specific energy, drilling rate and the mechanical rock properties [34]. Hareland *et al.* (2009) introduced the specific volume factor to evaluate the cutting efficiency of PDC bits. This showed that the cutting efficiency was a function of the back rake angle, the depth of cut and the rock properties [35].

2.3 Rock Cutting Force Modelling

2.3.1 Single Cutter Force Models

The first analytical model to describe the cutting process was developed by Merchant in 1945 [36] by considering the metal cutting. In next decades, many scholars have developed the models for rock cutting process, [7, 37-39]. One of the best method to study the influential factors is applying Polycrystalline Diamond Compact (PDC) cutters in the investigations. With advantages of higher rates of penetration (ROP) and longer life, PDC bits have gained prominent use for drilling different formations during last decades [9]. In 1979, Cheatham and Daniels [40]

may be the first researchers who performed a series of shale cutting tests using a set consisting of different shapes of PDC cutters, concluded that the cutting force was proportional to the cutting area and had no dependence on the shape of cutting area [40]. Following these pioneers in using PDC cutters, Zijsling and Glowka in two different works but both in 1987 also developed the force models for circular PDC cutters [7, 19]. [7] reported that ratio of horizontal force to vertical force (μ) is independent from whether the grooves are interconnected or not. Besides, regardless of the size or shape of the wear flat or diameter of the cutters, the relationship between the forces and depth of cut are followed as equations below.

$$F = C\delta^n \quad (2-3)$$

$$F/A_w = C\delta^n \quad (2-4)$$

where F is normal force, A_w is worn area, and C & n are rock-dependent constants and δ is depth of cut. The relation between the cutting force and depth of cut (DOC) have been considered by many authors; while some propose a linear relation between these parameters [40-42], some have obtained a power law variation of the cutting force with DOC [41, 43]. It should be noted that the linear relation has mostly been seen for shallow depth of cut while by increasing DOC, a power law relation is observed.

Fairhurst and Lacabanne (1957) [44] suggested two processes to characterize the rock cutter interaction. Based on their hypothesis, Detournay and Defourny in 1992 [39], developed a model (DD model) for both sharp and blunt cutters by dividing the rock cutter interaction for a single circular PDC cutter into pure cutting process and frictional contact [39, 44]. The cutting force is proportional to the cut area and the acting force on wear flat is independent of cut depth. They introduced some parameters such as intrinsic specific energy ϵ , the ratio of vertical to

horizontal forces acting on the cutting face ζ , and friction coefficient on the wear flat rock interface, μ . By combining the two processes, a model called E-S was presented which shows the relation between specific energy (E) and drilling strength (S). Later, the DD model was developed to rectangular cutters and to triangular cutters [21, 45]. They considered a cutter tracing a groove of constant cross sectional area on a horizontal rock surface via constant horizontal velocity and zero vertical velocity, therefore depth of cut is constant.

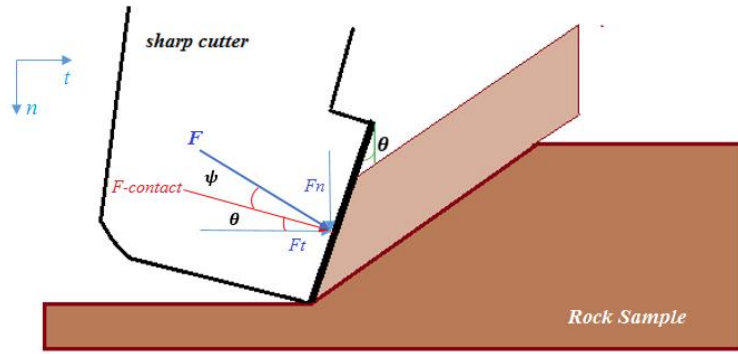


Figure 2-4: Cutting configuration for sharp cutter

Assuming a sharp cutter cutting a slab, the only acting force on the rock can be decomposed into two components of vertical and horizontal which are proportional to the cross sectional area. For a blunt cutter, the frictional forces should be considered based on a friction coefficient.

$$F_t = \varepsilon A \quad (2-6)$$

$$F_n = \zeta \varepsilon A \quad (2-7)$$

where $\zeta = \tan \alpha$ characterizes the inclination $\alpha = \psi + \theta$ of the cutting force on the cutting face with respect to the direction of the cutter motion. It should be noted θ is the back rake angle of the cutter and ψ is the interfacial angle between the failed rock and the cutting face. In their model,

they did not define a relationship for the radial force when the side rake angle is zero. In this work to predict the forces on a cutter, the same definition to the abovementioned model is used for the normal force and the tangential force. To obtain the radial force a new relation will be developed.

In 1999, Richard [11] by studied the depth of cut and the cutting forces and proposed two relations proportional to the cut area based on the failure mode (ductile and brittle). The experiments were conducted under atmospheric pressure, using a rectangular cutter to scratch or scoop the rock by constant linear speed. He concluded that in the ductile mode and lower depth of cut, the rock fails ahead of cutter by shearing and crushing at the tip and cutting forces are proportional to cut area. In the brittle mode or larger depth of cut, propagation of cracks at the tip or chipping is the reason of rock failure and cutting forces are related to material toughness due to fracture propagation.

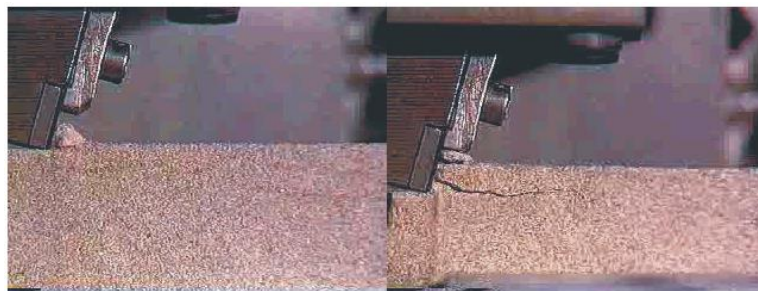


Figure 2-5: : Two failure mechanism, ductile (left) and brittle (right) mode (after [11])

In 2006, Gerbaud *et al.* [46] presented a new cutter rock interaction model including several improvements based on the presence of a build-up edge of crushed materials on the cutting face [46]. Three years later, Hareland *et al.*, [35] analyzed the cutting efficiency based on a force model for a single PDC cutter and reported that the efficiency directly related to the internal angle of friction of the rock being cut. Effect of confining pressure on rock cutting by using a single PDC cutter was studied based on the Smith' experiments on shale cutting and an analytical force model

was described by Rahmani *et al.* [47]. They published a model built upon the metal cutting basics, assuming ductile failure for impermeable rocks such as shale under confining pressure by accounting the effects of the confined shear strength of the rock. It simply assumes for a sharp cutter, the failure in front of cutter face similar to deformation of stacks of card which sets constraint for different angles *e.g.* back rake (θ), internal friction (ψ) and shear angle (α) (equation 2-5). The model matches the experimental results after [6], including bit balling phenomena.

$$2\alpha + \theta + \psi = \pi/2 \quad (2-5)$$

2.3.2 Full PDC Bits Force Model

The models presented so far are based on the prediction of the forces on a single cutter. Transition from single to full PDC bit in which tens of single cutters are arranged on the bit profile and engaged with a formation, requires more accurate integrated modeling in full scale. In 1985, Ziája by conducting a series of single cutter tests and analyzing the results of forces along with cross section area of cut, proposed a model for PDC bit by simply treating all cutters as equal in cutting action and defining mean area and mean radius for them [48]. Later, in 1999 he developed an advanced model by considering the complexity of cutters pattern into a geometry of a given PDC bit design as well as the imbalance force resulting from non-symmetric distribution of drilling forces [15]. Warren and Sinor [49] presented their PDC bit model by taking precisely the geometry profile into account. They assumed the forces remain constant during drilling which decreases the accuracy of the loads and ROPs. Then, they developed their model based on the laboratory tests for evaluating the mechanical design of a particular bit.

[39] modeled the drilling action of a PDC bit based on their single cutter model which they characterized interactions into cutting and frictional contacts [39]. To consider the influence of bit design, they defined parameters such as bit constant (γ) and density factor which relate to bit

profile and cutters quantity on the bit, respectively. In 2008, Detournay *et al.* [50] developed that model into a more complete model for drag bits by further investigations on previous version. They considered three phases for the response of ROP to WOB with constant RPM based on the depth of cut. In the first phase, the frictional force is dominant, then the depth of cut increases and the contact stress reaches a maximum limit and, in the final phase, at high depth of cut, due to cutting accumulation and increasing the contact forces, the efficiency drops. Behavior in latter phase can be followed by two paths. Path A shows a kinematic controlled DOC (which is not seen realistically in the fields) and path B shows a typical response to increasing WOB that is generally controlled in field applications.

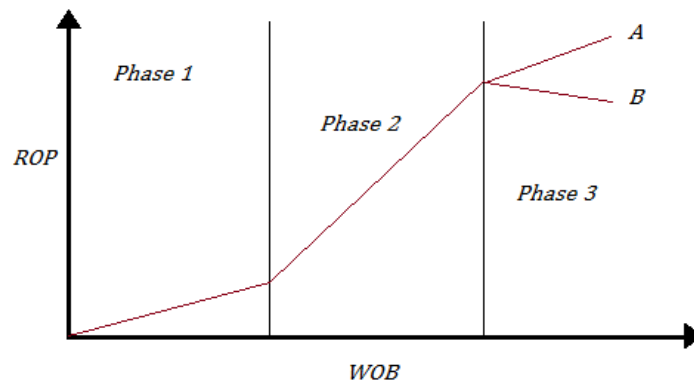


Figure 2-6: Conceptual response of ROP to WOB (after [50])

2.4 Cutters Arrangements on Bit

A full PDC bit consists of tens of cutters spatially arranged and brazed on body of the bit. The cutters are expected to engage the formation to shear the rock with a continuous scraping motion. For efficient drilling, the cutters are also required to maintain their geometrical properties; *i.e.* their shapes. Dull (wear) and broken cutters reduce the efficiency. The bit body is designed to hold the cutters in place and to convey mechanical and hydraulic power to cut the rock [2]. PDC bits are manufactured from steel or tungsten carbide powder infiltrated with a binder alloy (matrix).

The cutters are brazed on steel bulges called blades. Total axial or normal force on a bit is called weight on bit (WOB). Similarly, total torque on bit (TOB) is the torque applied in the direction of bit axis.

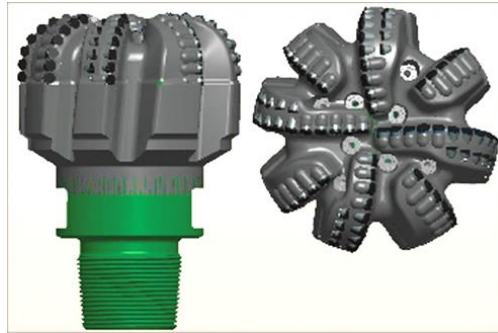


Figure 2-7: PDC drill bits with 8 blades. (drillingcontractor.com)

The PDC cutters are laid out on the bit face starting from the bit center toward the bit gauge, following a spiral direction either clockwise or counter-clockwise. Cutters may have different distances from the bit center. They could have relative exposure or different heights, which indicates how far the cutter face extends from the blade surface. If cutters are rotationally projected into a 2D plane passing through the bit axis, then, the impact of the adjacent cutters on the cutting geometry of the neighboring cutters are better illustrated. It is seen that heeding a cutter individually without the adjacent cutters does not provide a reliable understanding. In Figure 2-8 different zones are presented. PDC cutters on a drill bit can be considered in different zones based on their locations. Generally, the first section is called cone zone where a few PDC cutters are dispersed and they are less involved with dragging action. In a regular 8 ½" drill bit, the cone zone can be recognized from the bit center to ~2" distance. The second zone, called nose zone, receives the most attention from the bit designers. Due to the fact that plenty of cutters engaging with the formation are compacted in this zone. It can start from ~2" to ~5" in that regular bit. The cutters in the shoulder zone are less engaged with the formation and slightly less compacted than the nose

cutters. The last area on the bit is called the gauge zone where the cutters are mostly involved with the wellbore.

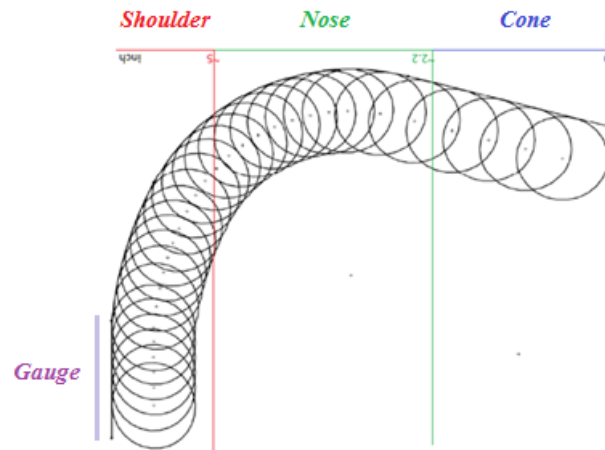


Figure 2-8: 2D overlay of a PCD-cutter layout on bit profile. (modified after [51])

Bit interaction with the formation affects the bit stability. Stability is defined based on the ability of the bit to resist the drilling vibrations. These vibrations negatively impact the PDC cutters and, thereby reduce the bit life by causing failure and damage to cutters and wearing the bit that ultimately reduces the drilling efficiency [14]. The vibrations encompass three types of axial, torsional and lateral movements (Figure 2-9). Axial vibration that is also called bit bounce, which occurs when the string moves up and down. Torsional vibration known as stick-slip or non-uniform bit rotation that takes place when the bit periodically stops rotating. Lateral vibration is bit whirl or eccentric rotation of the bit to high speed [14]. PDC bits can generate higher vibrations by larger cutter size, lower number of cutters or blades, or lower back rake angle. Changes in drilling conditions including number of revolution per minute or weight on bit can increase or decrease the torsional or lateral vibrations. It is found in field that ratio of RPM to WOB is a good criterion to control and treat the vibrations [52].

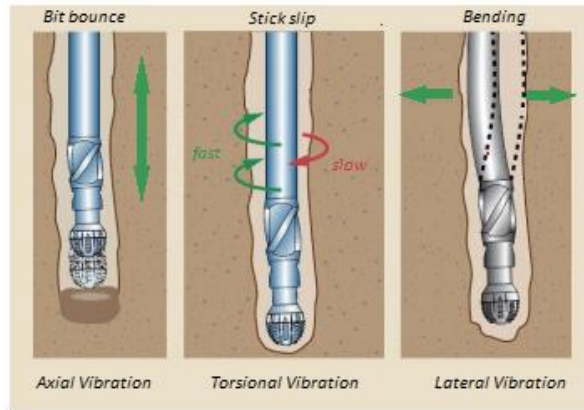


Figure 2-9: different types of vibrations that cause instability (modified after slb.com)

A ring of cutters on the bit profile can be assumed if those cutters are involved in removing a ring of rock. They could have the same relative exposure or height and engage with the formation at the same time. These cutters can be considered to study the force groups on them. In other words, instead of heeding a cutter individually, a ring of cutters as described is considered. If the total force on the plane on this ring of cutters is tended to zero or minimized, then the forces are in balanced or equilibrium. Forming the forces in a balanced state on a bit would be enhanced by laying out the cutters to minimize the lateral force. Therefore, it can be concluded that the cutters layout on a bit plays a major role in reducing the lateral force, which can be interpreted as the bit stability. Generally, in today's PDC bits, two general principals are followed to lay out the cutters; single set and track set. If at least two cutters are placed at the same radial and axial positions on a bit but just on different blades, it is called track set. While having no cutter at the same axial and radial position after projecting them into a radial plane is called single set [53].

Figure 2-10 (a) depicts 9 PDC cutters with various distances to the center brazed on 4 blades. If they are projected into a 2D plane passing the bit axis, it is shown how the adjacent cutters in a plane but on different blades can affect each other. A drill bit always rotates to the right. If the cutters (starting from bit center toward the bit gauge) traverse a spiral direction, similar

to the bit rotation, then it would be called spiral set of cutters (10-c). If they traverse spirally but in opposite direction of the bit rotation, then it is called reverse spiral set of cutters. The spiral set of cutters arrangement is a traditional way of laying out the cutters on a bit profile that provides desired stability when all cutters are in engagement with a uniform formation [54].

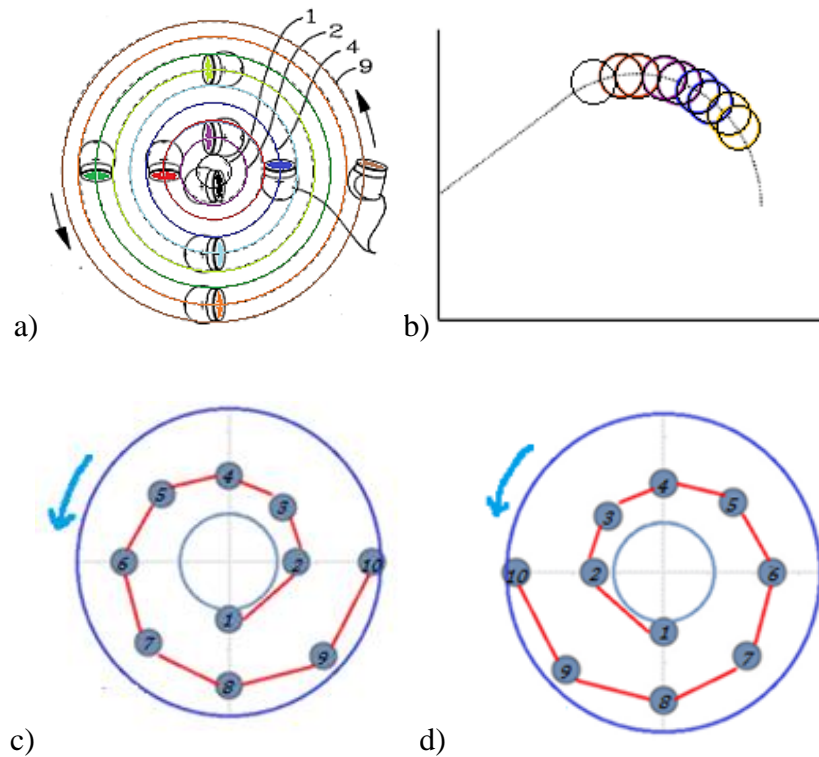


Figure 2-10: (a) cutters on bit profile (b) cutters on 2D layout (c) spiral set (d) reverse spiral set

Chen *et al.* [53] presented a new layout for PDC bit performance in transitional drilling where the formation lithology changes from soft to hard. For drilling into this type of formations, usually single set placement style of cutters causes misbalancing because the cutters around the nose may be subjected to more loading. Therefore, they developed a cutters arrangement to solve this issue. This style of cutters layout will be used in chapter 7 to compare the performance of the bits with different sets of cutters arrangements.

Chen and his colleagues in 2016 [55] proposed that the cutting forces are not only dependent on the cutting area but are also related to the shape of the cutting area, as well (Figure 2-11). These cutting shapes mainly depend on the cutters arrangements on the bit. They proposed a new cutter force model as a function of shape of cutting area with consideration of crack trajectory, which makes the rock chips. The impact of the shape of the cutting area

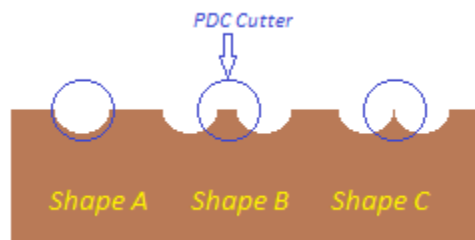


Figure 2-11: *different shapes of cutting area (modified after [55])*

A group of researchers [56] presented a study to correlate the laboratory results and field scale performance, which finally led to build and deploy a new laboratory machine to accelerate development of PDC cutter elements. In their work, they studied the cutter performance (WOB, TOB and MSE) on two types of bits. An important part of their job was designing a bit with 3 and 6 cutters on a flat cutting profile as shown in Figure 2-12. They proposed that for better understanding the performance of one type of cutter individually, a model of 3 cutters on a ring of bit would give the best measurements on different aspects of a cutter such as resistance to wear. Thus, following their suggestion, in this study, a ring of 3 cutters with different radiuses are considered in a ring of cutters with different arrangements.

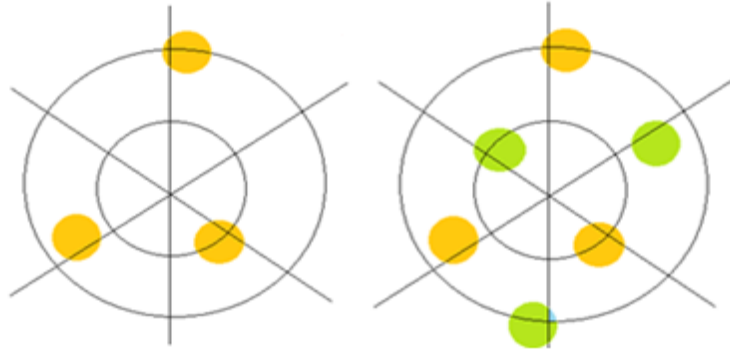


Figure 2-12: two cutter layouts (a) 3 cutters, type A. (b) 6 cutters (A & B). (modified after [56])

Apparently, most works have been dedicated to study the drilling bit behavior directly by running a bit in a field scale or indirectly by employing a single PDC cutter and integrating the model to a full PDC bit. The first one is desired but is not always available due to its cost and complexity and the second option may not cover all the essential parameters regarding a full bit. Due to difficult access to run a full PDC bit in a field scale to obtain comprehensive insight on cutter rock interactions compared to single cutter tests, another method is developed in this study. It is planned to investigate the rock cutting process by applying triple PDC cutters on different arrangements on a flat bit. This method has been scarcely studied by scholars; the work with the same concept was done by Glowka [7] who considered the effect of adjacent cutters and grooves. The main outcome of this way of cutters arrangement is to focus on the cutting area of every cutter and the effect of adjacent cutters on the cutting process.

3 ROCK CHARACTERIZATION

In this chapter, rock characterization is studied to obtain the rock properties before cutting the sample with using the PDC cutters. Some parameters such as rock strength and friction coefficient are needed to build a force model on a cutter on a bit and integrate it to a full PDC bit. Rock strength as a significant factor in characterization, can be investigated through different methods including sonic test or travel time. Rock cutting process based on the obtained parameters is simulated to study the validity of a hypothesis regards to the possible impacts of the cutters arrangements on the cutting performance. Due to some limitations, in measuring the rock strength of the rock samples, only the travel time measurement has been applied to all the samples. UCS test has been adopted on only shale sample. Therefore, a correlation between the sonic test results and UCS test on shale sample is provided. Then, the best empirical relations reported by [57] is used to measure the rock strength of the samples.

3.1 Introduction

Rock mechanical properties are essential for accurate geomechanical evaluations and drilling problems analysis including wellbore stability analysis, drill bit design, bit selection, pipe sticking, and other applications. In general, best relationship between physical properties and rock strength could be developed based on the calibration on rock cores from the field through the laboratory tests [57]. Despite that, due to lack of access to core samples, the other reliable method for rock characterization is to use the empirical strength equations based on the measureable physical properties such as P-wave velocity (or interval transit time), Young's modulus and Porosity. There are many empirical correlations in literature between these properties and UCS [57]. Rock mechanical properties which are typically required to build a geomechanical model, can be categorized into formation properties (*e.g.* compressive or tensile strength), elastic and

plastic properties. To study the rock properties, the behavior under different stress controlled tests is precisely investigated.

3.1.1 Definitions

Stress (σ) is defined as the internal force applied to a unit area of material, which could be either compressive, tensile, or shear stress. Strain (ε) is the deformation experienced by a material in response to an applied stress. Shear strength (S_u) shows the strength of the material resistance against the structural failure when occurs due to shear (equations 3-1 to 3-4). Elastic response is when the material returns to its original shape and size once the stress is removed; while in plasticity, if the applied stress exceeds the material's elastic limit, the material experiences permanent deformation. If rupture takes place before significant plastic deformation occurs, the material is described as brittle; and if the material ruptures only after experiencing significant plastic deformation, it is considered ductile. Based on this definition, sedimentary rocks usually exhibit brittle behavior under atmospheric pressure. Under high pressure conditions, the failure mechanism could transfer from brittle to ductile [58].

$$\varepsilon = \frac{\Delta L}{L_0} = \frac{\text{difference in length}}{\text{initial length}} \quad (3-1)$$

$$\sigma = \frac{F}{A} = \frac{\text{force}}{\text{area}} \quad (3-2)$$

$$UCS = \frac{P}{A} = \frac{(\text{failure load})}{(\text{area})} \quad (3-3)$$

$$S_u = \frac{1}{2} q_u (\text{or } \sigma_1) \quad (3-4)$$

Rock strength parameters are unconfined compressive strength (UCS), and internal friction angle (φ) or coefficient of internal friction ($\mu = \tan\varphi$). Elastic moduli including two most

common constants, Poisson's Ratio (ν) and Young's modulus (E). Poisson's ratio shows the phenomenon in which a material tends to expand in directions perpendicular to the direction of compression. Young's modulus is a mechanical property that demonstrates the stiffness of a solid material and measures the material's ability to withstand changes in length under tension or compression [59]. Rock elastic moduli can be derived from well logs *e.g.* sonic log and density log; some other rock strength properties such as UCS can be obtained through specific laboratory tests on core samples *e.g.* triaxial compression test, uniaxial compression test, sonic test, scratch test, *etc.*

3.2 Compressive Strength Test

Triaxial compressive tests are typically conducted on identical samples for a range of confining pressures to establish a relationship between the axial load at failure and the confining pressure. By measuring axial and radial stresses and strains, the static Young's modulus and Poisson's ratio are obtained. In this test, stress is applied to a sample based on some prescribed conditions while stress along one axis is different from the stresses in perpendicular directions.

Due to cost and time constraints, triaxial test cannot be available for all cases required in analysis. Therefore, the uniaxial or unconfined compressive strength test is commonly used to acquire the rock strength. In this test, zero confining pressure is applied to the rock sample. Then, the axial stress at failure is a direct measure of UCS. To present a constitutive model for the description of elastoplastic behavior of rocks, a simple method that could be accessible in most fields is presented. This method is based on the uniaxial compression test that is a well-known standard test for rocks. It is applied to some rock samples in this study. For some other rocks that have not been tested through UCS test, another reliable method is used to measure the travel time of a rock sample to obtain the rock strength.

3.2.1 Mohr-Coulomb Failure Criterion

The Mohr–Coulomb (MC) failure criterion is a set of linear equations in principal stress space describing the conditions for which an isotropic material fails by neglecting effect of intermediate principal stress, σ_2 . It can be written as a function of either major or minor principal stresses, (σ_1 or σ_3), or normal stress σ and shear stress τ on the failure plane [59].

$$\tau = \pm (C + \sigma_n \tan \varphi) \quad (3-5)$$

where τ shear stress at failure, C cohesive resistance, σ_n normal stress at failure, φ angle of internal friction. The angle of internal friction is a measure of dependency of rock strength on confining pressure such that a higher value of φ indicates a higher sensitivity of strength to confining pressure [57]. This equation in rock cutting process is based on the work of metal orthogonal cutting. It follows the assumptions of Mohr-Coulomb failure criteria on shear plane. In Mohr-Coulomb failure criterion, yielding or fracturing occurs when the shear stress exceeds the sum of the cohesive resistance of material and the frictional resistance of slip planes or fracture plane [60].

The Mohr-Coulomb failure model is based on plotting Mohr's circles for states of stress at failure in the plane of the maximum and minimum principal stresses. The failure envelope is the best straight line that tangents the cycles. Then, friction angle and cohesion values for Mohr-Coulomb (MC) failure envelope can be obtained by drawing a tangent line. The slope indicates the friction angle and the intercept presents the cohesion (Figure 3-1).

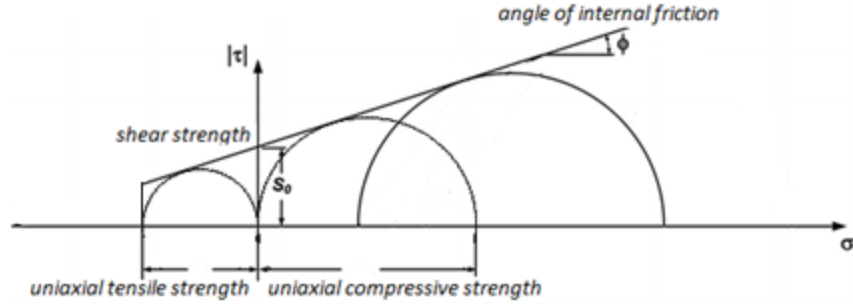


Figure 3-1: Mohr–Coulomb failure criterion, a linear envelope in the Mohr diagram

3.2.2 Drucker-Prager Criterion

Unlike metals, for soils and granular materials, a few yield criteria exist which are dependent on the hydrostatic stress component. Recognizing this, Drucker and Prager (1952) [61] extended the well-known von Mises yield condition to include the hydrostatic component of the stress tensor.

The Drucker-Prager plasticity model is an isotropic elasto-plastic model that has been used in many studies in the literature to represent the behavior of granular materials such as soils and rocks. Three stress invariants are used in this model to provide a possibly noncircular yield surface in the deviatoric plane to match different yield values. The Drucker Prager yield criteria can be used to study the plastic behavior of a rock that the compressive yield strength is greater than tensile strength and exhibits pressure dependent yield. It means that the rock gets stronger as the pressure increases [62].

The linear Drucker-Prager model given as follows:

$$F = q - p \times \tan\beta - d = 0 \quad (3-6)$$

$$q = \sigma_0 - \sigma_3 \quad (3-7)$$

$$p = (2\sigma_3 + \sigma_0)/3 \quad (3-8)$$

where p is mean effective stress, q is the Mises equivalent stress, β is the slope of the linear yield surface in the p - q stress plane and is commonly referred to the friction angle of the material, d is the cohesion of the material, and σ_0 is yield stress at different confining pressures. For the linear Drucker-Prager (DP) model, the general finite element package requires the yield surface to be defined as the line plotted in Figure 3-2. The yield line of Drucker-Prager can be obtained from Mohr-Coulomb friction angle (φ) and cohesion C . From geometry, trigonometry and the relationships between p - q stresses and principal stresses the Mohr-Coulomb failure line is plotted in p - q space to represent a Drucker-Prager failure criterion. It is shown that the angle of the failure line in p - q stress space, β , and cohesion, d are determined from equations 3-9 to 3-11 [62].

$$\sigma_{0c} = d / (1 - \frac{1}{3} \tan \beta) \quad (3-9)$$

$$\tan \beta = \frac{6 \sin \varphi}{(2 - \sin \varphi)} \quad (3-10)$$

$$d = \frac{6C \sin \varphi}{(3 - \sin \varphi)} \quad (3-11)$$

where σ_{0c} is the yield stress and the confining stress is zero $\sigma_2 = \sigma_3 = 0$.

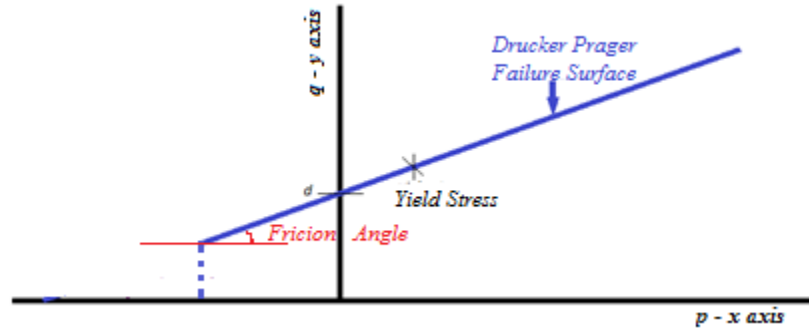


Figure 3-2: Drucker Prager yield condition in p-q stress space

3.2.3 Stress-Strain Profile

As The compression test provides stress-strain history of a rock. By plotting the experimental results, a typical stress-strain curve in rock deformation is built. [63] has described a

typical stress-strain curve for a rock into five main stages. It is interpreted as (1) initial nonlinear stress change associated with crack and pore dilation and closure, (2) elastic stage (linear or nonlinear), (3) nonlinear strain hardening associated with the onset of brittle micro-cracking and plasticity, (4) continued hardening characterized by progressive crack coalescence in a fracture process zone; and finally, (5) ultimate failure, strain softening, and macroscopic crack propagation (Figure 3-3). Shortly, one can divide the stages of deformation into (1) crack/pore closure, (2) linear elasticity, (3) strain hardening and micro-cracking, (4) crack coalescence and formation of a process zone, and (5) macroscopic propagation.

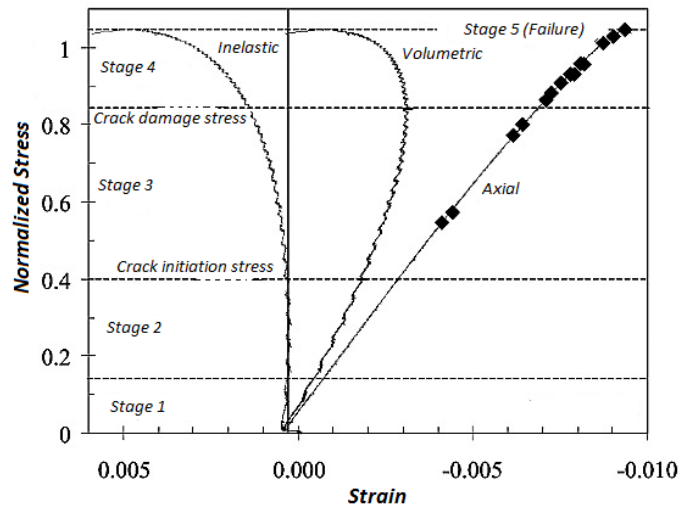


Figure 3-3: A typical stress strain curve (Modified after [63])

3.2.4 Results of UCS Test

UCS test is conducted on sample of Catoosa shale; it is cored at the surface in Eastern Oklahoma. Unconfined compression test are carried out on the sample. The height of the cylindrical sample is almost double its diameter. In this test, a core sample is subjected only to an axially controlled load and the load increases until the material fails. The load cell measures the

load on the rock sample until material failure. The rate is set as the smallest possible to be able to assume the process is done in a constant vertical strain rate.

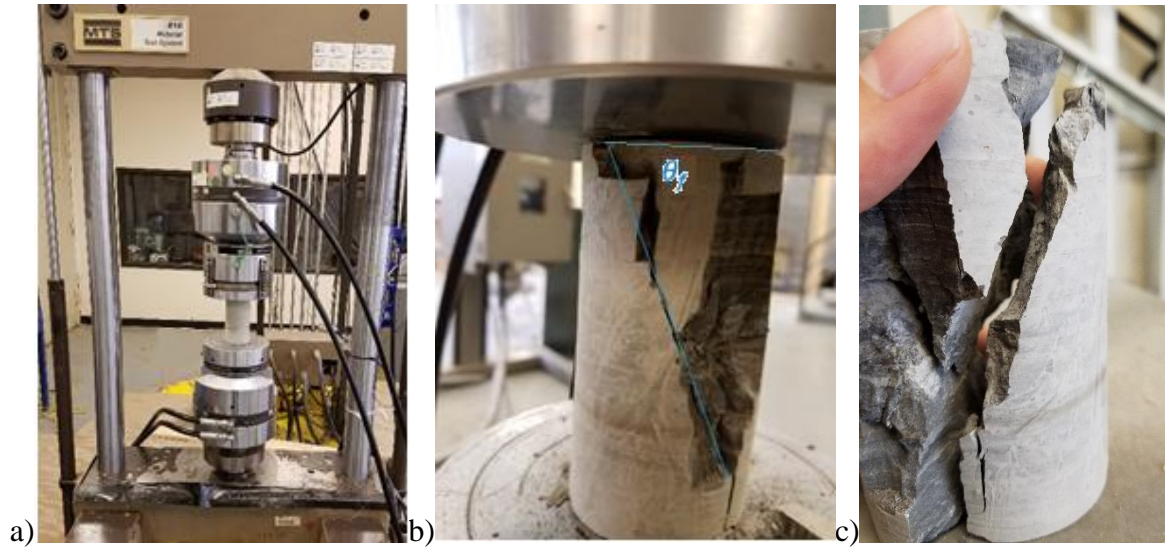


Figure 3-4: (a) test equipment (b & c) major crack on sample after the compression test

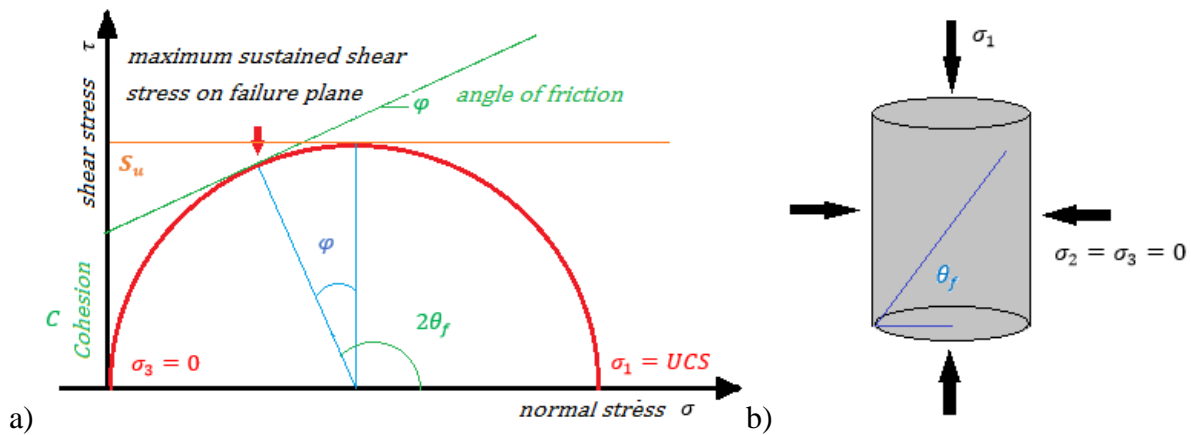


Figure 3-5: (a) Mohr-Coulomb failure envelope. (b) Schematic of loading on a sample

Figure 3-5 demonstrates the components of Mohr-Coulomb failure envelope. The relation between θ_f (the angle shows the inclination of the failure plane) follows equation 3-12. It should be noted that this angle is equal to the angle between the normal to the failure plane and principal

stress axis. [64] reported that if σ_t is tensile strength, then UCS and tensile strength can be expressed in terms of the cohesion and friction angle following below equations.

$$2\theta_f = \frac{\pi}{2} + \varphi \quad (3-12)$$

$$\sigma_c = \frac{2C \cos \varphi}{1 - \sin \varphi} \quad (3-13)$$

$$\sigma_t = \frac{C \cos \varphi}{2 - \sin \varphi} \quad (3-14)$$

$$\frac{\sigma_c}{\sigma_t} = \frac{2(2 - \sin \varphi)}{1 - \sin \varphi} \quad (3-15)$$

$$C = \frac{\sigma_c \sigma_t}{2 \sqrt{\sigma_t(\sigma_c - 3\sigma_t)}} \quad (3-16)$$

where C is the cohesion, σ_1 or σ_c is the uniaxial compressive strength, and φ is the friction angle. Based on the test observation (Figure 3-4), the angle between the failure plane and the minor stress, is 60° which makes the friction angle equals to 30° . As the sample failed at 11620 lb and surface area was 4.06 in^2 , then $\sigma_c = 2860 \text{ psi}$. Cohesion is $C = 825.6 \text{ psi}$ and shear strength or $S_u = 1430 \text{ psi}$. Therefore, the Mohr-Coulomb failure criteria can be written as:

$$\tau = \pm (\sigma_n \tan \varphi + c) = 0.5775 * \sigma_n + 825.6 \quad (3-17)$$

The stress-strain profile for the unconfined compressive test for Catoosa shale at constant rate of 0.02 in/min is illustrated in Figure 3-6.

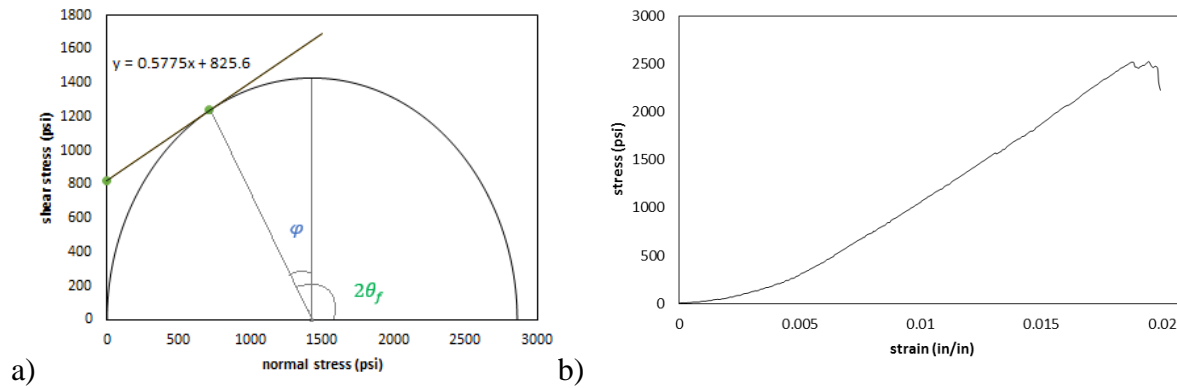


Figure 3-6: (a) Mohr-Coulomb failure envelope (b) stress-strain profile for UCS test for Catoosa shale

To convert parameters from Mohr-Coulomb criterion to Drucker-Prager criterion following equations are used to obtain the linear Drucker-Prager model. This model and the parameters are used in rock cutting simulation through finite element method in section 3-4. All units are in *psi*.

$$\tan\beta = \frac{6\sin\phi}{(2-\sin\phi)} = 2 \quad (3-18)$$

$$d = \frac{6c \sin\phi}{(3-\sin\phi)} = 990 \quad (3-19)$$

$$\sigma_{0c} = \frac{d}{1-\frac{1}{3}\tan\beta} = 2972 \quad (3-20)$$

$$p = \frac{2\sigma_3 + \sigma_0}{3} = 991 \quad (3-21)$$

$$q = \sigma_0 - \sigma_3 = 2972 \quad (3-22)$$

where p is the mean stress, q is the von Mises equivalent stress, β is friction angle which defines as slope of linear yield surface, d is material cohesion, and σ_{0c} is yield stress.

3.3 Scratch Test

A non-destructive strength test is called scratch test and developed in University of Minnesota in 1990's. A single sharp cutter is employed to scratch the rock sample and measure the forces in vertical and horizontal directions [65]. This technique also provides rock strength properties *e.g.* uniaxial compressive strength. The test is controlled as the cutter has a constant velocity and horizontally cuts the rock surface with a fixed depth of cut. Depending on the depth of cut, two failure modes are described. Ductile mode in shallower depth of cut and brittle regime in deeper cut [11]. The work for cutting a unit volume of rock represents the intrinsic specific energy (ε). The term *intrinsic* emphasizes the fact that this energy characterizes the pure cutting action [39].

$$\varepsilon = F_H x / w dx = F_H / w d = F_H / A \quad (3-23)$$

where ε is intrinsic specific energy (with unit of stress), d is depth of cut, w is width of rectangular cutter, A is area of cutter, and F_H is horizontal force.

3.3.1 Results of Scratch Test

A series of scratch test experiments is conducted on three rock samples (Carthage marble, Pierre shale and Berea sandstone) by using single PDC cutter with 13 mm diameter. The apparatus has two load cells and a linear actuator that provides horizontal linear momentum for the cutter to cruise at a constant velocity and depth of cut (DOC). The forces in horizontal and vertical directions are measured. The scratching process is done in shallow depth of cut range from 0.2 – 0.75 mm. By knowing the area of cut and cutting force in direction parallel to cut path, the scratch hardness or rock strength can be obtained. Figure 3-7a shows a sample of force measurement which is captured from a scratch test on a sample of Carthage Marble with a depth of cut equal to 0.42 mm. The results of several tests on Berea sandstone and Carthage marble is presented in Figure 3-7b. Following the equation 3-23, the slope of a best line fitted through different tests for a given rock gives the rock strength. Therefore, the strength for unsaturated rocks is 7250 psi for sample of Carthage marble, for shale sample is 3150 psi and 3800 psi for Berea sandstone.

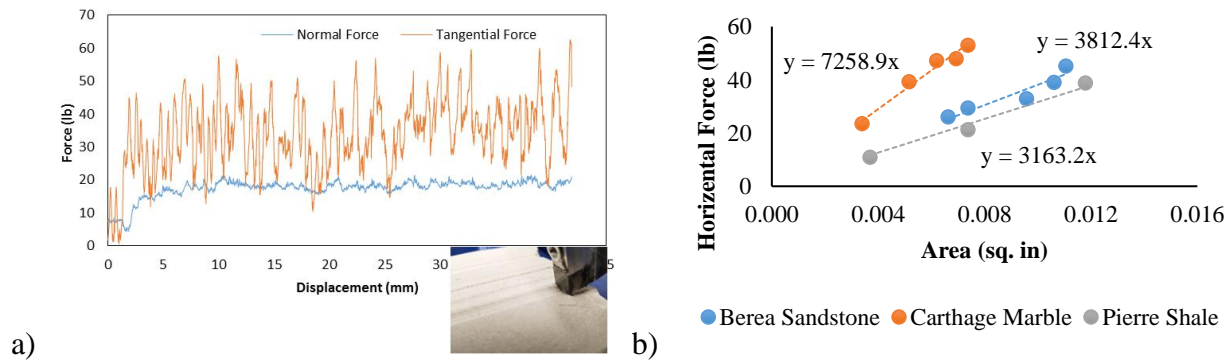


Figure 3-7: (a) force measurement and PDC cutter of the scratch test on Carthage (b) obtained rock strengths for three rock samples

3.4 Sonic Test

A common technique used mostly for reservoir evaluation and rock mechanical studies is sonic travel time test. This test reflects the effect of lithology, porosity and fluid content. There are many empirical relationships available in literature [57, 66, 67] between UCS and the physical properties including wave velocity or transit time, Young's modulus and porosity for various formations. In this method, the time duration lasts for signal to travel through the sample from one side to another side is measured. The travel time provides the wave velocity (v_p) and by knowing the density (ρ), Young modulus (E) can be obtained. [57, 68] proposed a comprehensive study on the empirical relations between unconfined compressive strength (UCS) and other physical properties in different sedimentary rocks. Based on the known properties of the rock sample, an empirical relationship is selected and UCS can be found. Only a few globally applicable relationship for different sedimentary rocks, are presented here and a list of relations is presented in Appendix F.

$$v_p = \sqrt{E/\rho} \quad (3-24)$$

$$UCS = 1200 * \exp(-0.036 * \Delta t) \quad (\text{for sandstones}) \quad (3-25)$$

$$UCS = 1.35 * (304.8/\Delta t)^{2.6} \quad (\text{for shales}) \quad (3-26)$$

$$E = 0.3752 * UCS + 4.428 \quad (\text{for carbonates}) \quad (3-27)$$

where v_p is in m/s , E is in MPa , ρ is in kg/m^3 , UCS is in MPa and Δt is in $\mu s/ft$.

3.4.1 Results of Sonic Test

A set of sonic test experiments is conducted to measure the transit time for a signal passing through a sample. For this purpose, a signal produced by a signal generator enters one side of rock and exits the other side. By using an oscilloscope to process the signal behavior (Figure 3-8) and measuring the rock thickness, P-wave velocity (v_p) is obtained. For instance, signal from

transmitter (yellow curve) enters the sample at point A (letters in red) and it takes $13.2\ \mu\text{s}$ to exit from the other side and enters the receiver at point B (blue curve). The measured time by this method should be calibrated. In fact, the transit time must be zero if the transmitter and receiver are contacted to each other with no material in between. Table 3-1 provides the rock strengths for various samples using the abovementioned method. By applying the empirical relations proposed in [57] for different formations based on the known rock properties on every sample, UCS for a given rock is estimated. It should be noted that travel time can be assumed from the beginning of first signal jump to beginning of second signal jump (this method is used in this study), or top (or middle) of first signal to top (or middle) of second one, respectively. Since, the available rock samples in this study are not perfect known, we name them based on the category they belong. However, just some of them are certainly known, for sake of simplicity, they are named by numbers.

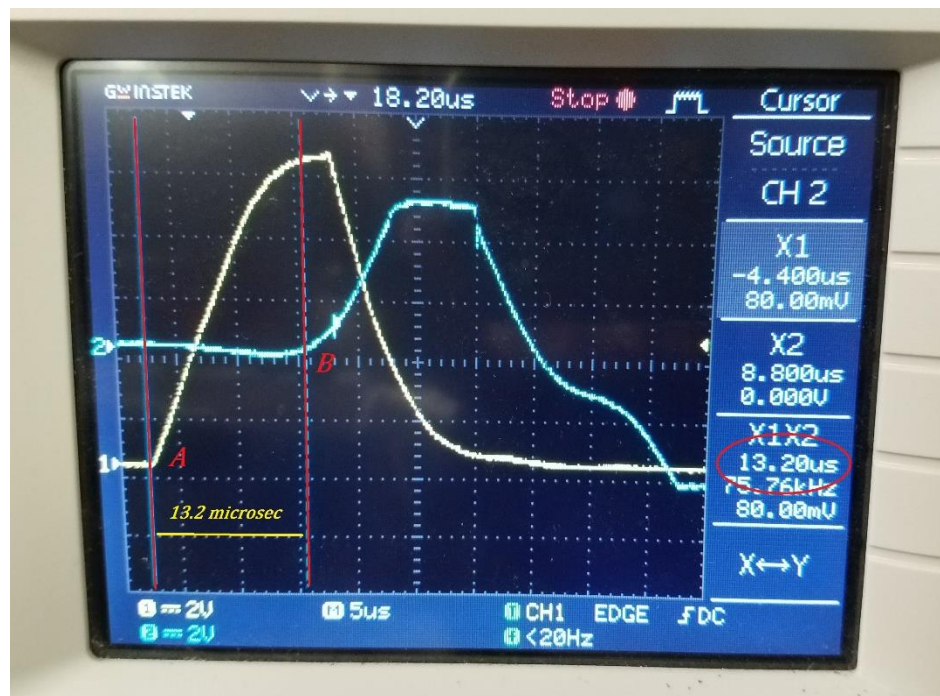


Figure 3-8: Screenshot of oscilloscope shows the travel time between A and B

Table 3-1: Results of sonic travel time tests on different samples

Rock Sample	Name	Travel Time ($\mu s/ft$)	UCS (psi)
Shale	<i>Catoosa</i>	112.32	264
Sandstone 1	<i>Torrey Buff</i>	92.73	618
Sandstone 2	<i>Crab Orchard</i>	94.81	573
Sandstone 3	<i>Unknown</i>	87.45	748
Sandstone 4	<i>Unknown</i>	99.77	481
Sandstone 5	<i>Berea</i>	96.72	535
Limestone 1	<i>Indiana</i>	101.26	535
Limestone 2	<i>Unknown</i>	103.81	419
Marble 1	<i>Unknown</i>	107.35	752
Marble 2	<i>Unknown</i>	89.47	108

The strength of the shale sample based on the UCS test is calculated as 2860 psi . It is used to find the best correlation between the sonic test results and UCS of the samples based on the empirical relations. The measured travel time provides the UCS of the shale sample equal to 2645 psi . The acceptable results verifies this method of travel time measurement and less than 10% error is considered to measure the UCS of all other samples. The rock strength for *marble 1* (most likely Carthage marble) based on the scratch test also gives a result (7258 psi from scratch test); however, this method was not available for all the samples. Hence, in our case it seems the rock properties obtained from sonic test and the proposed equations by [57] provide the UCS of the samples in a passable range. By knowing the rock strength, measuring the bulk density, obtaining the Young Modulus from stress-strain curve, Mohr-Coulomb and Drucker-Prager parameters (cohesive, and friction angle) the required inputs for simulating the cutting process is available.

3.5 Rock Cutting Simulation via Finite Element Method

Generally, scientists classified research methods in machining process modeling into three groups; analytical, experimental, mechanistic, and numerical. The latter one is simulation, where a problem is broken into a whole bunch of smaller problems to be solved by computers. Similarly, these methods are widely used in rock cutting processes. Due to limited applicability of analytical models in terms of the geometry and material properties, numerical modeling plays a significant role to obtain a better understanding of the mechanics of drilling. Many simulation studies on rock cutting process have been done by using finite element methods (FEM) [69-71] and using discrete element method (DEM) [24, 72, 73]. For instance, [71] have modeled the single cutter experiments through FEM to analyze the specific conditions in borehole drilling operation. In another study, [69] have developed a FEM within LS-DYNA to estimate the cutting forces on results of the scratch test in addition to capture essential characteristics of the process. As an example of a study by DEM, work of [58] can be mentioned where they used 2D DEM to model rock cutting dynamics by single cutter. The results demonstrated the significant relationship between rock failure modes and cuttings morphology (chip to ribbon). In the current study, a simple method is proposed based on a characterized rock that can form a modeling tool. It gives good insights to the role of cutting mechanics on bit's performance. The obtained failure model is introduced into a commercial FEA package, ABAQUS, through already available subroutines in it.

3.5.1 General Structure of FEM

Finite element methods (FEM) have two structures. The explicit FEM which is widely used in wave propagation, impact engineering, failure analysis, underwater simulations, etc. and the implicit FEM. The latter becomes expensive due to taking thousands of time steps in order to solve a dynamic problem. This occurs due to cost of inverting stiffness matrices to solve the large sets

of nonlinear equations. While in explicit, by setting short-time steps, there is no need of forming the global stiffness matrix. In fact, the solution is obtained on an element-by-element basis. It also provides easier way to implement and accurately treat to general nonlinearities [12]. To incorporate a robust modeling that can simulate the rock cutting process by PDC cutters, the properties of the model should be well calibrated to reproduce the experimental mechanical behavior of the rock. Afterwards, the model will be used to analyze the effect of using triple PDC cutter on drilling parameters such as MSE.

3.5.2 Simulation of Uniaxial Compression Test

First step is simulating the uniaxial compression tests and then, comparing to the experimental results to calibrate the parameters for modeling the rock. For this purpose, geometry of the sample is designed by scale of 1:1 to the real sample used in the test. Then, the sample is put between two rigid plates. The initial boundary conditions (BC) is applied as followed to the reference point of bottom surface of rock by giving zero degree of freedom to it. Then, in a compress step, all displacements and rotations are constraint whereas; there is only vertical displacement equal to 3 *mm* in 1 *sec*. In 3D mesh model, approximate global size of elements in sample surface is 1.5 *mm* which totally provide a fine mesh of rock sample with number of 67321 elements and the plates have 196 elements. Figure 3-9 illustrates the breakage of a sample under uniaxial loading. There are some steps to define the required parameters and build a model in ABAQUS to simulate the rock cutting process, which are explained below.

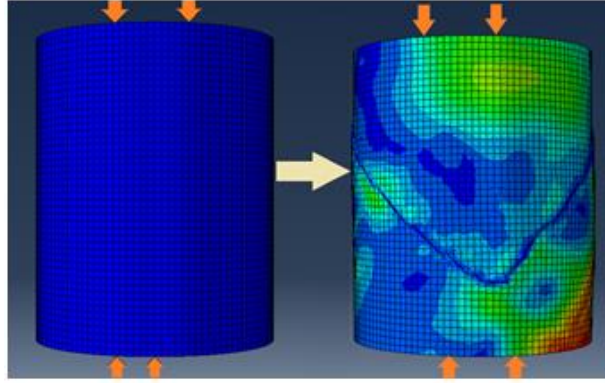


Figure 3-9: uniaxial loading on a sample until failure

Generally, in rock cutting simulation, the rock surface exposed after the cut depends only on the properties of the rock itself. Unlike the metal machining that, the cutting surface is known in advance. So, it is needed to adopt an erosion contact model to solve this issue. The erosion contact model removes the elements from the mesh once the material stiffness is fully degraded. Normally, an element calls it is failed when all section points on integration point lose the load carrying capacity [71]. In numerical simulations, an isotropic damage model which represents the degradation of mechanical properties *e.g.* stiffness and strength, is defined by a scalar variable such as D that has a range from zero (no damage) to one (fully damaged).

Theoretically, damage occurs when plastic deformation is present. Therefore, plastic strain values determine the beginning of the degradation and fully damaged state of rock properties. To get the plastic strain values, a criterion that is called ductility, is defined to predict the initiation of the damage. By applying this criterion, it is assumed that the plastic strain values at damage initiation are a function p/q in Drucker Prager, which is called stress triaxiality (η). In 1997 [74] recommended that a point on a stress strain curve which represented a significant change on the mechanical behavior of the rock (usually the peak strength or the yield stress (σ_0)) would be the plastic damage initiation (ε_0^{pl}). Therefore, by picking the maximum strain in stress-strain profile

of the compression test, the onset of damage is available (Figure 3-10). To complete the definition of the damage model parameters, it is only needed to consider plastic deformation as an indicator of damage initiation. It can be determined through calibrations as a critical plastic displacement. At critical plastic displacement, element detaches from the mesh and let the cutter progress.

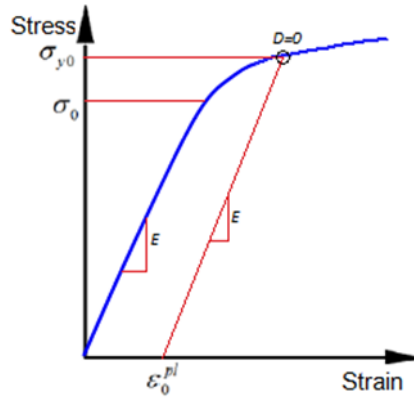


Figure 3-10: typical stress-strain behavior of brittle material and onset of damage

By obtaining all abovementioned inputs, (from the experiment, Drucker Prager model, and Damage model), the simulating of UCS test is implemented. In post-processing, the axial reaction force and the axial transition on the top surface are outputs to obtain the stress and the strain of the test. The importance of applying damage model is shown in stress-strain profile that compares the numerical and experimental results (Figure 3-11); where the numerical response follows the rock behavior only if damage model is applied.

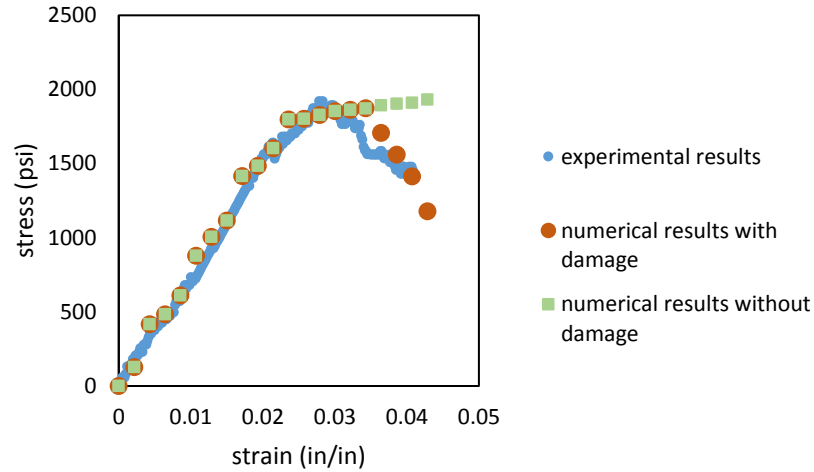


Figure 3-11: comparing the experimental and numerical results with and without applying damage

3.5.3 Simulation of Rock Cutting Process

By validating the input parameters in simulation of UCS test in previous part, a FEM model is proposed to model the rock behavior cutting by using three PDC cutters. To this purpose, a rock sample is designed with a square surface of 200 mm and 100 mm height. Height is divided into two partitions of 15 and 85. This division helps saving computational time of simulation to have a finer mesh only on top part of rock. A rigid round plate is assigned as a bit profile having three 13 mm round rigid shells in different locations presenting cutters. Cutters have 20° inclination to the plate (back rake angle); two of them are set in x axis, and one in y axis, all with different radiuses (in range of 60 to 71 mm distance from the center of plate). Four blades are designed on the plate, cross-shape and each contains one cutter (Figure 3-12). It is assumed that the cutters are perfectly sharp with no chamfer and zero side rake angle. The numerical mesh near the surface that experiences the cutting by the cutter should be tenth of total depth of cut to guarantee that no boundary will influence over the element stresses in the cut zone. Nevertheless, it will cause an inaccuracy if the size of elements is bigger than the size of actual particles. Therefore, a fine mesh

with average element size of 0.5 mm is formed on top of the sample, while a coarse mesh with average element size of 3.5 mm is distributed throughout the rest of the rock piece. It is desired for the fine mesh to have at least 10 elements on penetration. Element type C3D8R (an 8-node linear brick, reduced integration, hourglass control) is set to the elements in top partition of rock. Bit spins around z axis which passes through the center of the rock. To tune up and calibrate the required parameters, initially single cutter cutting is simulated to compare the numerical results with experiments. This model for single cutter cutting is similar to the triple cutter model but only one cutter is designed on a bit plane. To get the best results match to the experiments, dilation angle of the rock should be set to 5° and yield stress as 2900 psi . Table 3-2 shows the results for single PDC cutter cutting when depth of cut is 1 mm/rev , and rpm is 120. Drucker Prager failure criterion and hardening with ductile damage are used to compose the material constitutive model. For boundary conditions, the bottom surface of the rock is constrained with no displacement or rotation in any direction. The bit is moving toward the rock with speed of 2 mm/sec and rotational speed of 12.56 rad/sec , therefore, DOC be 1 mm/rev .

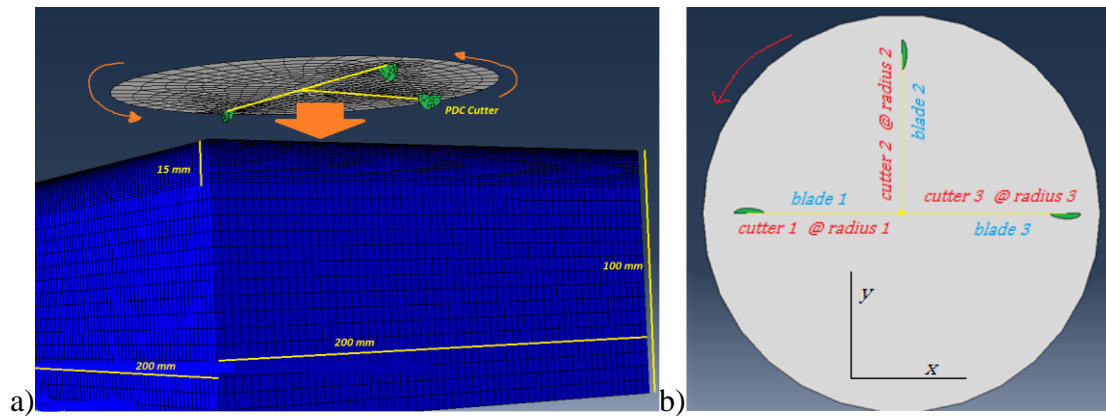


Figure 3-12: a) Assembly of rock model with a plate of cutters. b) Face of bit with cutters

All parameters required in rock cutting simulation are obtained from the simulation of UCS test and single cutter test. A set of simulations for different sets of cutters is conducted which

implies the rings of cutters on a bit. The cutters have different arrangements with various radiuses. The forces in three directions and the number of the removed elements are measured. Four sets of cutters arrangements are studied and the results show the best arrangements which have less MSE and more stability is *set 4* where the cutters are placed reverse spirally. MSE is calculated based on equation 3-29 and stability is recognized as zero or minimum lateral force.

$$MSE = [(F_z \times V_z + \tau \times \omega) / V_{cut}] \times time \quad (3-28)$$

where F_z is normal force, V_z is vertical displacement, τ is torque on bit, ω is rpm and V_{cut} is the volume of removed rock and τ is torque on bit plate around z -axis.

It should be noted that in Table 3-2, *Set 1* is spiral set of cutters and *Set 4* is reverse spiral set. The radiuses in the table are in millimeter.

Table 3-2: summary of the rock cutting simulation for different sets of triple cutters

SET	C1 mm	C2 mm	C3 mm	F _x lb	F _y lb	F _z lb	F _H lb	Vol (cu. in)	MSE psi
Set 1	60	65.5	71	-22	-6	152	24	0.611	4312
Set 2	71	60	65.5	-26	-54	243	60	0.641	4700
Set 3	65.5	71	60	-13	10	220	17	0.640	4636
Set 4	71	65.5	60	-5	6	145	8	0.605	4172

3.5.4 Conclusion on Simulation

The simulation process is beneficial to structure a hypothesis on the effect of cutters arrangement on drilling performance. Despite some thoughts that only consider the cutting area as an important factor on acting forces on every cutter on a bit, it seems that, the way of arranging cutters on a ring of bit would matter and affect the bit performance. The numerical results support this claim that although spirally and reverse spirally arranging the cutters on a bit (*Set 1* and *Set 4*) provide the same engagement area for each cutter, the forces on bit planes (F_x and F_y) for those sets are not equal. Therefore, it can be concluded that among those 4 different sets of cutters, first

of all the cutters layout affect the acting forces on the cutters, and it also shows even the bit performance varies for spiral and reverse spiral sets of cutters. The other outcome of the numerical calculation is to present the optimum set of cutters on a bit. It indicates, within the frame of this study, arranging the cutters in a reverse spiral set gives the best lowest MSE. The validity of the outcomes will be investigated in chapters 5 and 6.

4 EXPERIMENTAL SETUP

4.1 Multi-Point Cutter Facility (MPC)

Main goal of this research is to study the rock cutting process experimentally by using multiple PDC cutters. Various sets of cutter arrangements is designed to investigate the effect of different arrangements on a bit. For this purpose, Single Point Cutter (SPC) apparatus is selected for the tests. The equipment was donated to LSU by Baker Hughes, in 2005. This valuable property of the Craft and Hawkins Department of Petroleum Engineering at LSU is capable to simulate the subsurface drilling conditions under the elevated pressures and in presence of any drilling fluids.

The MPC facility has three main components composed of electrical panel, hydraulic panel, and mechanical parts that are shown in Figure 4-1. The electrical panel has two motors for providing and controlling the rotational motion and vertical displacement. It can provide the necessary power to spin the bit as fast as 1000 revolution per minute (*RPM*) and to penetrate into the rock sample (*ROP*) with velocities up to 15 *mm/sec* (177 *ft/hr*). The hydraulic panel is made of three different pumps and a set of pipes and hoses to carry the drilling mud into the system. It is capable of increasing the pressure (wellbore pressure) inside the vessel up to 10,000 *psi*. The mechanical panel is composed of three vessels, named as pressure, separation, and compensation vessels; to create the subsurface drilling conditions while rock-cutting process. The data acquisitions system rigorously collects data of the process. With the help of LabVIEW software, the raw data is recorded and processed into the host computer. The schematic of all components of the LSU MPC facility is presented in Figure 4-3.

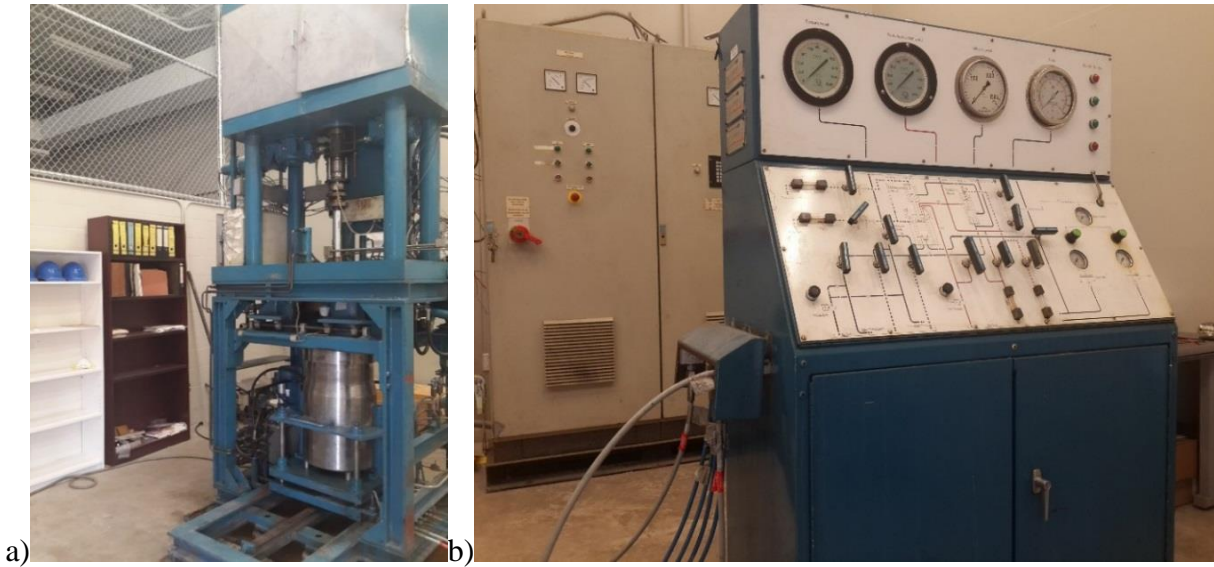


Figure 4-1: (a) MPC apparatus (b) Hydraulic and Electrical panels

The polished PDC cutters used in this study, have 13 *mm* diameter, and chamfer of 45° with 0.010" length. They are brazed into the stainless steel cutter holders with constant 20° back rake angle. PDC cutters and a cutter holder are shown in Figure 4-2.



Figure 4-2: PDC cutters and a cutter holder used in this study

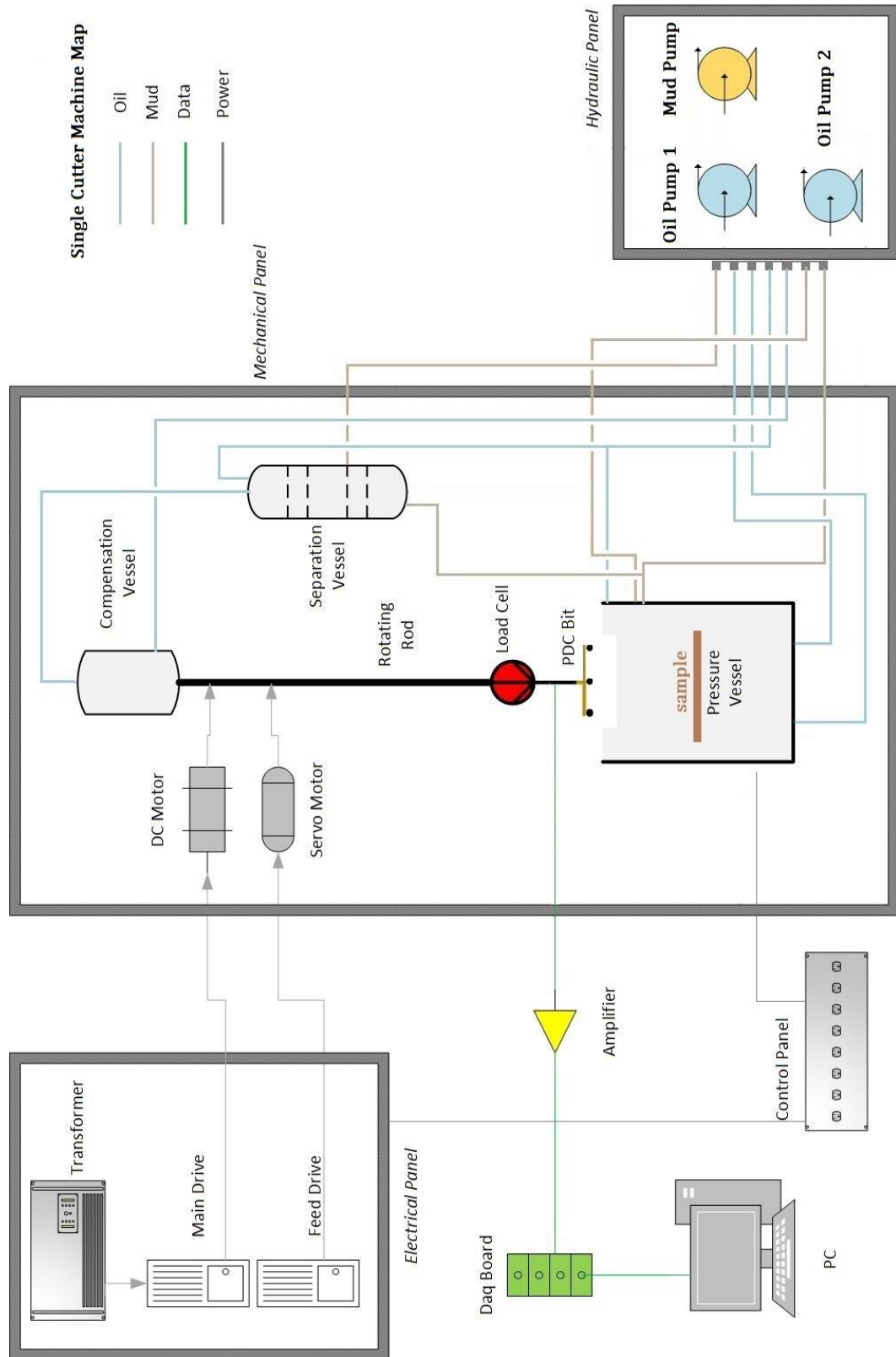


Figure 4-3: Schematic of all components in SPC lab

While cutters scratch and scoop the rock surface, forces in three directions are measured by a tri-axial load cell. The sensor has the capacity of 5000 *lb* in *z* axis and 2500 *lb* in both *x*, and *y* directions. An amplifier is designed next to the sensor to boost the signal and avoid missing data through the wiring. Although, the rock cutting tests are all run under atmospheric pressure, to protect the sensor in the harsh environment inside the vessel, a customized protective box is designed and built. The load cell is put into the box. Bottom flange of the box, plays the role of bit profile and cutters are attached to it. The top flange has two cylinders containing pistons to balance the pressure between inside and outside of the box, if the test is to be performed under elevated pressure. Load cell and relevant box are shown in Figure 4-4. The engineering design of the box can be found in Appendix G.



Figure 4-4: Tri-axial load cell and protective box

Before conducting the experiments, the facility had to be prepared to meet the project objectives. Besides fixing and repairing the apparatus, the capability of running the test with single cutter was enhanced to using up to four cutter on a flat bit. Therefore, the single cutter apparatus was upgraded to a multiple PDC cutter tester. A flat 7" diameter plate, made of stainless steel was designed with four perpendicular trails, imitating the blades on a bit. Based on that, up to four PDC

cutters with different radii (ranging from 25 mm to 80 mm distance from the bit center) could cut the rock, simultaneously. This would serve as a valuable tool to study the effect of adjacent cutters with interconnected grooves on rock cutting process. Figure 4-5 visualizes how the cutters are set on the bit profile.

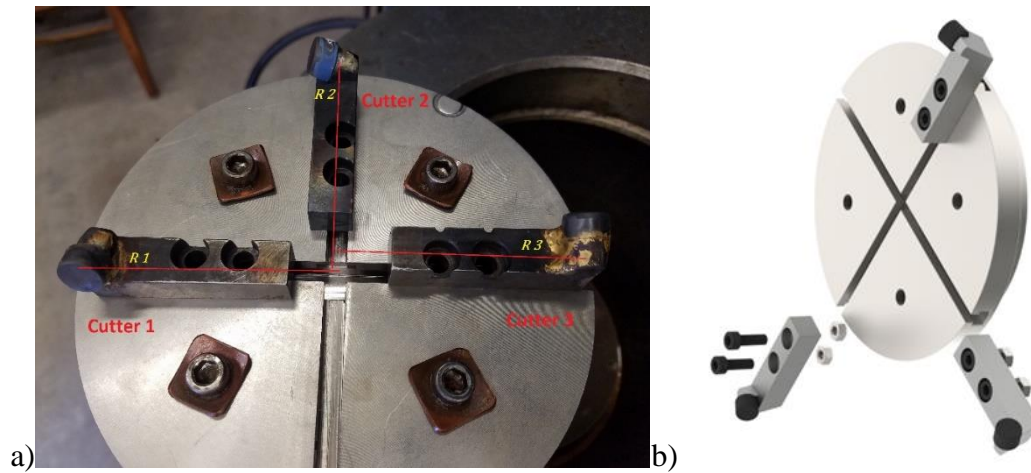


Figure 4-5: (a) bottom view of bit profile, (b) 3 cutters with various radiuses can sit on bit

In this project, the rotational speed (RPM) and the rate of penetration (ROP) are inputs and set by the operator. Forces in three directions and time intervals are measured and recorded via the sensor. Torque on bit is measured indirectly, and extracted from converting the electrical power to mechanical power, consumed by the main motor to rotate the shaft. Volume of the rock, which is removed by the cutters, can be measured after the test by the operator.

Rock sample must be fixed on its designed plate in the vessel. The plate is placed on top of a 11" piston. This piston divides the vessel into two sections that are totally sealed and separated from each other. The lower part is filled with hydraulic oil; and the top part where rock sample and PDC cutters are located, contains drilling fluid. In case of cutting tests under elevated pressures, the piston is pushed up by the high-pressure oil to compress the drilling fluid. This pressure can be assumed as wellbore pressure [6]. Furthermore, in this equipment due to its special

design, wellbore pressure can be considered as confining pressure, as well. Because the rock sample is exposed to the same fluid circumferentially and could freely expand laterally (Figure 4-6).



Figure 4-6: the rock sample is placed in the vessel

4.2 Rock Preparation

It is said that the cutters located in nose zone on a drill bit are significant in rock cutting. To assume the rock sample in our study is cutting by the nose cutters, the 8" diameter rock samples are needed. Thanks to our rock cores providers (*Baker Hughes and NOV*), different cores (as big as 64" *L* and 16" *Dia*) were provided. The entire process of preparation and sample cutting to the desired size was done at the MPC facility. First, rock sample was cored to 8" diameter by using core driller and then, by using a rock saw, it was sliced and cut into 1" thickness cores. Coring and cutting the Catoosa shale should be done by using hydraulic oil as the cutting fluid. In case of cutting limestone and sandstone, water can be used, as well.

The procedure of sample preparation is illustrated in details in Appendix B. X-Ray Fluorescence technique, which is a non-destructive analytical technology, was applied to

determine the chemistry and elemental composition of the Catoosa shale sample, as well. The XRF data for Catoosa shale can be found in Appendix D.

4.3 Arranging the Cutters on the Designed Bit

Although the flat bit can hold up to four PDC cutters, targeting to magnify out-of-balance forces, a set of three PDC cutters was selected to use to build different cutters arrangements. In fact, intentionally, non-symmetric arrangement was designed to investigate the effect of adjacent cutters and their impact on the acting forces on the bit. Accordingly, different sets of cutters arrangements were defined. Table 4-1 describes the radii of the cutters for the sets used in different parts of the study. The cutters are numbered same to Figure 4-5. It should be noted that *Set 1, 5, and 9* are spiral sets of cutters and *Set 4, 8, and 12* are reverse spiral sets. The cutters distances were ranged between 60 *mm* to 71 *mm*. Setting the cutters in this range ($\sim 2\frac{1}{2}$ *inch* distance from the bit center) may be typical to the radial location of cutter in the nose zone of certain bits. The maximum distance between the centers of cutters was 11 *mm*, and the minimum 5 *mm*, while the diameter of the PDC cutter was 13 *mm*. This range would allow the cutters to have interconnected grooves, which could show the effect of adjacent cutters in the cutting process. By arranging the cutters same to the table description, it is possible to study the effect of the cutters spacing on the rock cutting process. In first group, sets from 1 to 4, the spacing between the cutters is 5.5 *mm*, and then reduces to 4 *mm* and finally to 2.5 *mm* between the cutters radiuses. However, the arrangements of the cutters in all groups are the same.

Table 4-1: cutters distances from the bit center in different arrangements

SET	C1 mm	C2 mm	C3 mm
Set 1	60	65.5	71
Set 2	71	60	65.5
Set 3	65.5	71	60
Set 4	71	65.5	60
Set 5	60	64	68
Set 6	68	60	64
Set 7	64	68	60
Set 8	68	64	60
Set 9	60	62.5	65
Set 10	65	60	62.5
Set 11	62.5	65	60
Set 12	65	62.5	60

4.4 Force Components on Bit Profile

Generally, as mentioned in chapter 2, acting forces on a single PDC cutter can be resolved in three directions of normal force (F_n), tangential force (F_t), and radial force (F_r). Hence, the forces measured by the load cell, can be decomposed to the components as shown in Figure 4-7.

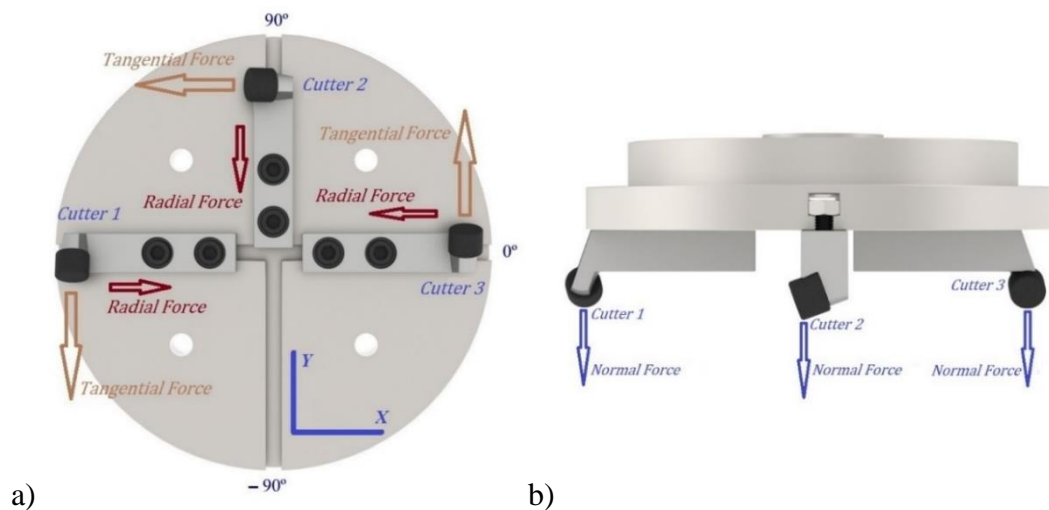


Figure 4-7: force components on the cutters on the bit

The forces on the bit can be calculated by the equations below (i is the cutter number).

$$F_x = \sum_{i=1}^{n=3} F_{x_i} = Fr_1 - Ft_2 - Fr_3 \quad (4-1)$$

$$F_y = \sum_{i=1}^{n=3} F_{y_i} = -Ft_1 - Fr_2 + Ft_3 \quad (4-2)$$

$$F_z = \sum_{i=1}^{n=3} F_{z_i} = Fn_1 + Fn_2 + Fn_3 \quad (4-3)$$

where F_x , F_y , and F_z are forces in three dimensions

To better analyze the effect of different arrangements, term of lateral force (F_H) is presented. The direction of this force on the bit plane can be computed as θ . The lateral force could serve as a good tool to compare the stability of different bits. It can be considered as the preferential force on the bit that intends to pull the bit laterally off the axis and causes the imbalance force on the bit. It can push one side of the bit against the wellbore and creates new frictional forces. If it couples with the torque on bit, then it moves the bit's instantaneous center of rotation off the bit axis and may cause a phenomenon called bit whirl, which reduces the bit life.

$$F_H = \sqrt{(F_x^2 + F_y^2)} \quad (4-4)$$

$$\theta = \arctan(F_y/F_x) \quad (4-5)$$

4.5 Method of Experiments

This section describes the method of rock cutting tests in this work. Once a rock sample with 8" diameter and about 1" thickness is prepared (cored and cut), it will be fixed inside the vessel on a metal disc plate with 6 clamps. The clamps are evenly distributed around the sample, to impose balanced lateral forces on sample and avoid stress concentration points. The cutters on the flat bit, all have the same height; in the drill bit jargon, it is said that the cutters have no relative exposure (tips of the cutters located in same horizontal plane); therefore, they all meet the flat rock

surface at the same time. For this assumption to be as close to reality as possible, the rock surface should be accurately cut to be completely level. In the case of samples with uneven rock surface, before running the test, a correction cutter with a long tip (to cover the range of cutters), is used to correct the surface. By rotating a few revolutions, it makes the surface totally leveled. Figure 4-8 shows the correction cutter with 40 mm edge and a sample corrected by this cutter.

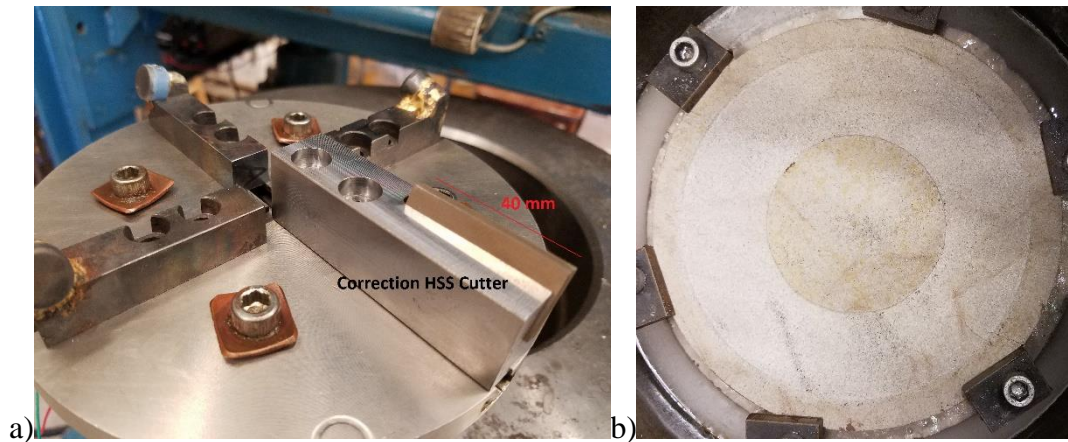


Figure 4-8: correction cutter used to level the surface

Once, the rock sample is placed and secured in its position, the drilling fluid is poured into the vessel to cover the sample. In this study, for most of the tests, water is used as the drilling fluid; while, for Catoosa shale tests, hydraulic oil is used as the drilling fluid.

As described before, the load cell is placed inside its protective box and the box is attached to the rotational shaft. Bit profile is the bottom plate of the protective box, and the cutters are arranged on the plate based on the test specification. Thus, the shaft, the sensor and the cutters spin as whole (rigid body assumed) at the same velocity that is set as the input (*RPM*). In this study, two rotary speeds are tested, namely 120, and 75*RPM*. The lowering velocity of the shaft when the cutter assembly starts engaging with the rock is another input for the test. This vertical

displacement is known as the rate of penetration and in this study, it is set to 1 mm/s or 1.25 mm/s .

Besides the acting forces on the bit, the electrical power used by motors to run the test, is measured as well. Voltage and current for both rotational and vertical motors are needed to get the relevant mechanical power. Data for the rotational motor can be used to estimate the torque on the bit, and the MSE is obtained using the data from both motors. The method of analyzing these results is explained at the end of this chapter.

Once the run is stopped and the sample is released, the trace of the cutters can be observed on the rock surface. The removed volume of the rock is now can be acquired by filling out the grooves by any powder and then weighing the amount of that powder. In this study, both flour and salt are used to double check the volume. Knowing the density, gives the powder volume. For instance, Figure 4-9 displays a sample after cut with triple cutter and the grooves filled by flour. Pictures of the grooves for different sets on various samples can be found in Appendix E. Cuttings remaining on the cutters after the test, may indicate the potential of the formation for sticking to the bit or bit balling (Figure 4-9). The picture of the cutters after the test are documented, as well in Appendix E.



Figure 4-9: (a) grooves created after cut (b) powder to fill them out (c) stuck cuttings on cutters

In this system, by every revolution when the cutters penetrate into the rock sample, the engagement area on a cutter increases due to its particular geometry. The maximum cutting area on a cutter never can be reached in this system. The process has to be stopped before reaching the steady state condition; and therefore the trend of the forces look like that of Figure 4-10. The forces increase and then start decreasing when the process is stopped and the bit is being pulled up (in the figure below, it stopped after ~3 seconds).

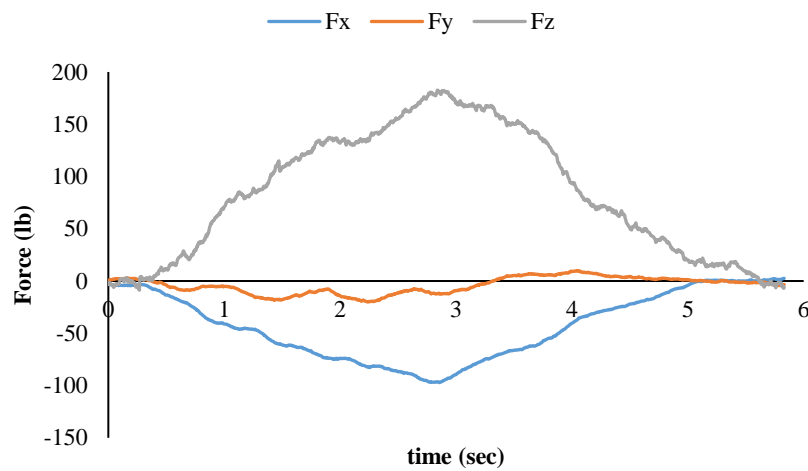


Figure 4-10: Force sampling for a reverse spiral set on a limestone sample

4.6 Engagement Area

The force models presented in literature for single cutter tests, demonstrate the importance of the cutting area of a PDC cutter. The cutting or engagement area of each cutter is defined as the [instantaneous] area where the cutter is engaged with the rock. The cutters are placed out on cross-shape trails where they make 90° . Once, a cutter rotates 90° , it arrives at a groove which is already cut by the front cutter, and it may have a different shape; which can change the engagement area of that cutter in new quarter of revolution. Aiming to study the potential effect of the cutting area,

a computer-aided design application is employed to measure the cutting area precisely for every cutter on every quarter of revolution.

The assumptions should be considered for measuring the engagement area are listed.

- The cutting area is constant in one quarter of revolution.
- Depth of cut is constant during one quarter of revolution.
- In every quarter of revolution, the cutter penetrates $\frac{1}{4}$ of DOC deeper. Therefore, the cutter goes $\frac{1}{4}$ DOC deeper than its trailing groove.
- Every cutter meets the groove of the front cutter, which may affect its engagement area.
- Every cutter has a 20° back rake angle. Projecting the cutter into a 2D vertical plane would convert the circle into an oval/ellipse. For instance, in this study, the whole area and the diameter is decreased by a factor of $\cos(20) = 0.94$, when projected onto a plane that is normal to the direction of cutter velocity (Figure 4-11).

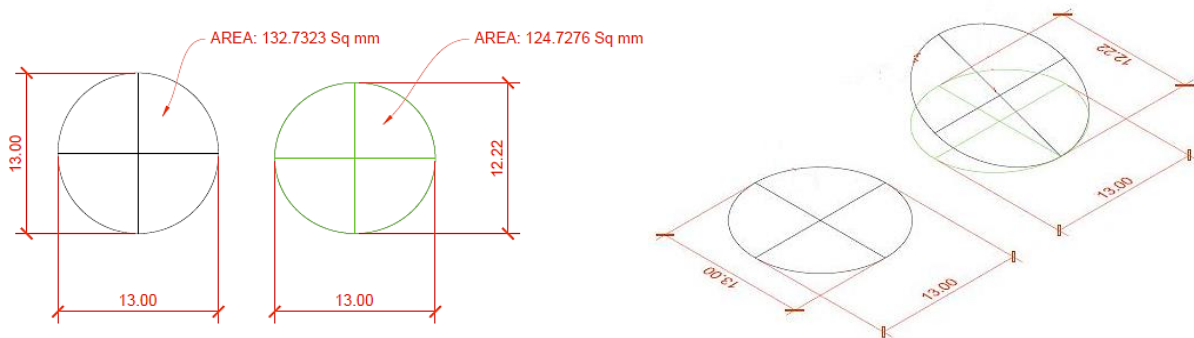


Figure 4-11: changes in shape by projecting the cutter into a vertical plane by 20° .

The series of figures below, present the schematic of the cutting area for all cutters in different quarters of one revolution. For better visualization, the 13 mm cutters are set with 4 mm distance from each other while the depth of cut is 1 mm/rev. In all figures, the purple and green

ellipses present the main cutter and the shape of the rock (which is already cut in previous revolution), respectively. The distance between the centers of these two ovals is equal to the depth of cut. The orange horizontal line represents the level of the formation. The solid white zone presents the cutting area that is engaged with the formation in that specific quarter of revolution. The light brown oval is the neighbor cutter. It leaves a groove after itself and may affect the amount of formation that the main cutter was supposed to cut.

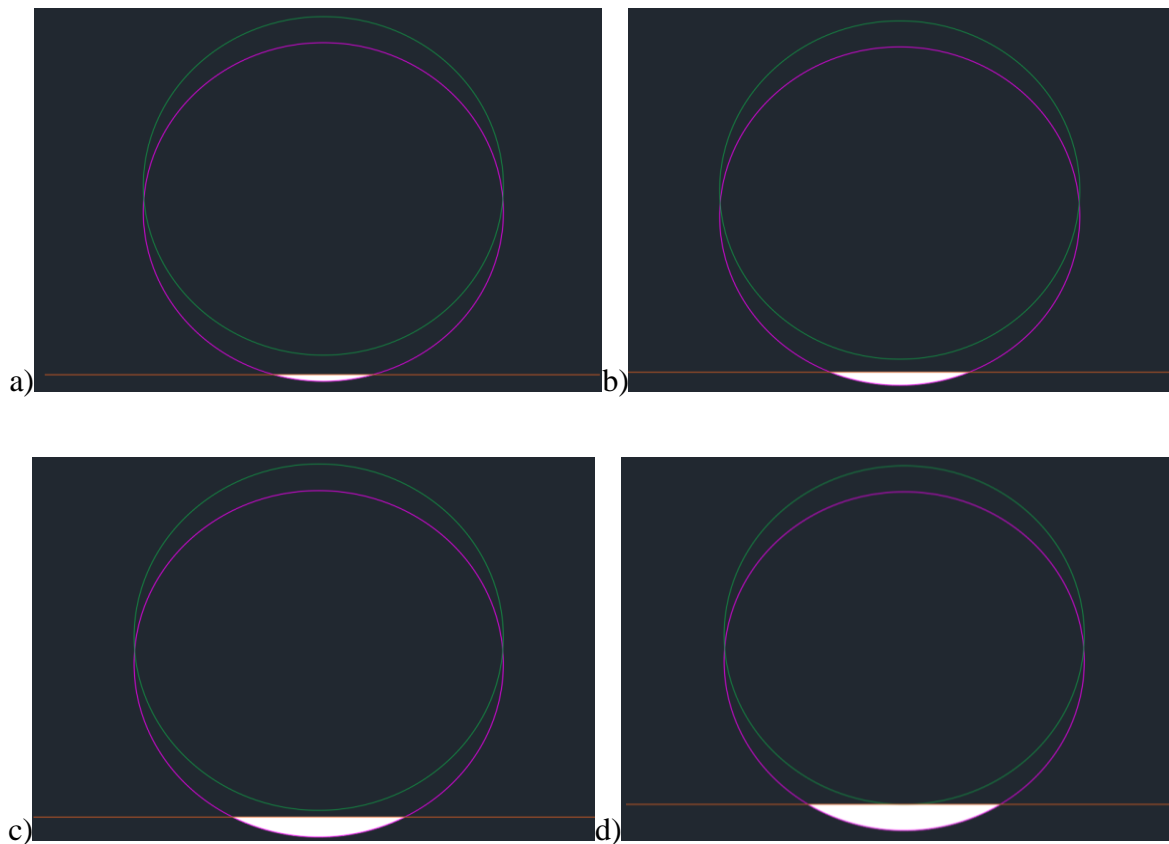


Figure 4-12: changes in cutting area for ONE cutter in 1st revolution (all 4 quarters). It still has not affected by the adjacent cutter.

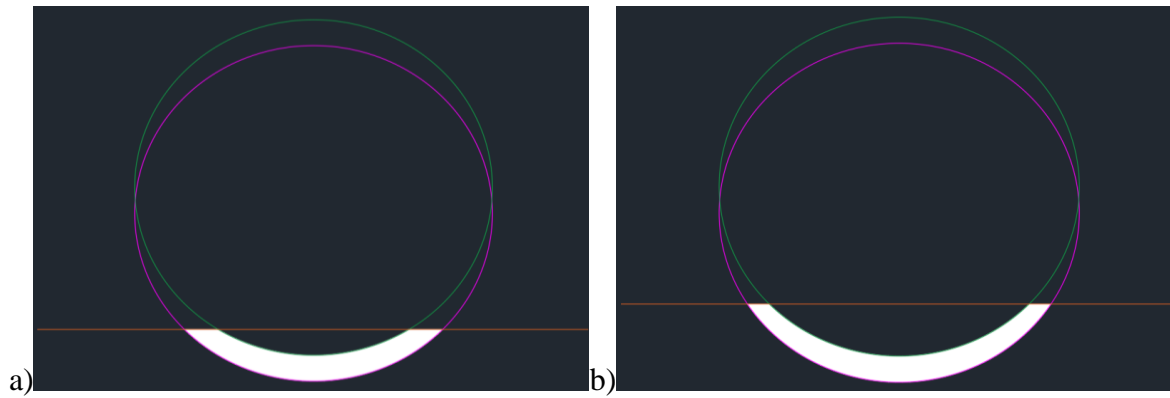


Figure 4-13: the same cutter at the end of its 2nd and 3rd revolution.

In the figures above, the white area shows the amount of formation that one cutter can see in different locations, before reaching the grooves of front cutter. It can be inferred to *cutter 1*, in its first 2 quarters, or to *cutter 2* and *cutter 3* in their first quarters. Figures below highlight the impact of the front cutter. For instance, Figure 4-14 depicts what happens to *cutter 1*, when it reaches the 3rd quarter and sees the groove already left by *cutter 3*.

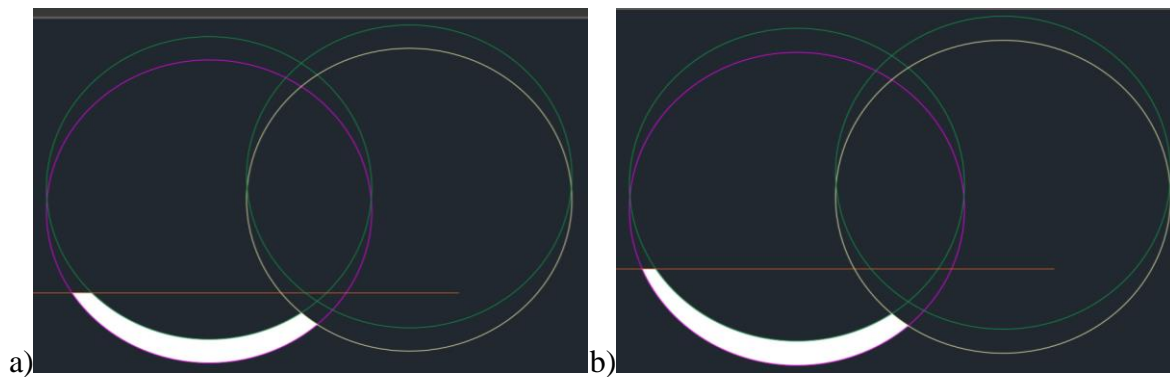


Figure 4-14: Effect of adjacent cutter. Cutter 1 arrives into 3rd quarter and sees groove of cutter 3
(a) after 2 revolutions (b) after 3 revolutions

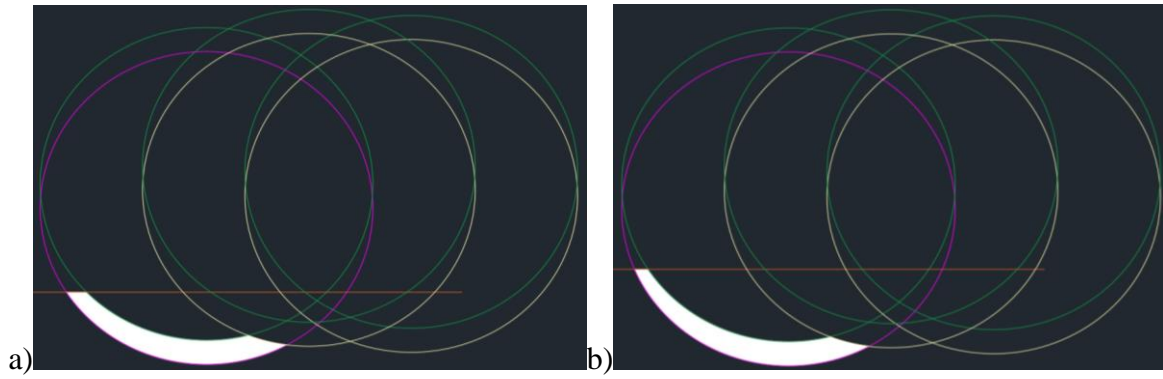


Figure 4-15: cutter 1 arrives to 4th quarter. It sees remained groove of both front cutters, revolution 2 & 3

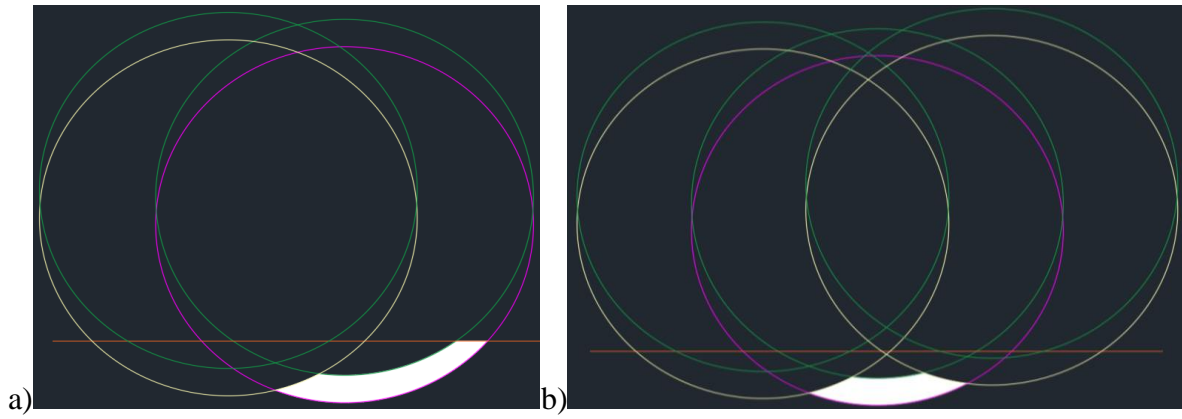


Figure 4-16: cutting area for cutter 2 in 2nd and 3rd quarter. (4th quarter would be as same as 3rd one)

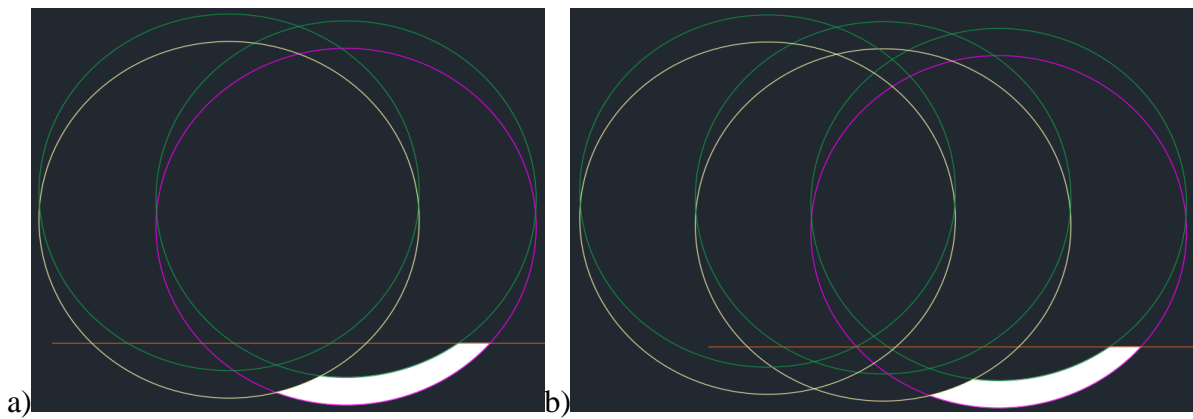


Figure 4-17: cutting area for cutter 3 in 2nd and 3rd quarters. (4th would be the same as 3rd one)

The cutting area for different cutters have been precisely measured from the beginning of the cutting process to the maximum area when the steady state condition initiates. The measurement shows that the area for either spiral or reverse spiral set of cutters is the same, if other parameters kept constant (DOC, RPM and ROP). For instance, the cutting area for *set 1* and *4* in Table 4-1 (spiral and reverse spiral arrangement) when depth of cut is 1 mm/s , $RPM = 75$, $ROP = 1\text{ mm/s}$ and presented in Figure 4-18. The distance of the cutters from the bit axis is $60, 65.5$, and 71 mm . The graph shows that most of the work of rock removing is done by *Cutter 1*, while *Cutter 2* has the least contribution in the rock removing process. In fact, either cutters arranged spirally or reverse spirally; the cutting area for every cutter is the same in both sets.

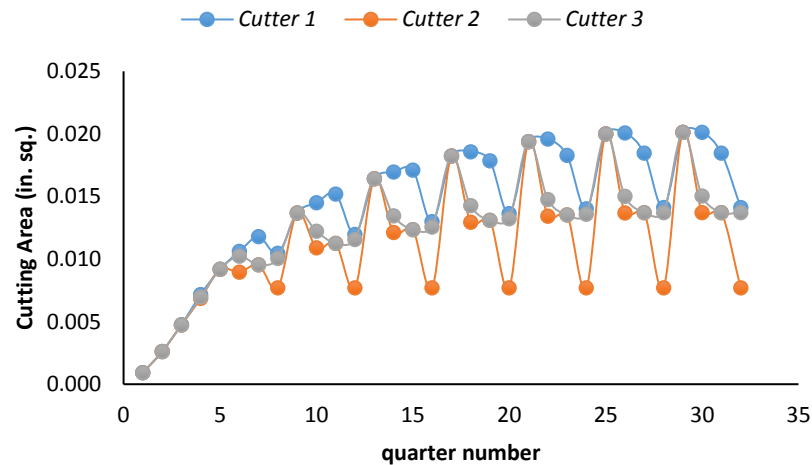


Figure 4-18: cutting area for both set 1 and 4 (triple cutter) is the same.

A comparison between cutting area for a single cutter and a triple set is presented in Figure 4-19 to better representing the impact of using multiple cutters a bit. The average cutting area of single cutter and triple cutter sets for every revolution is shown in the same figure, as well, in orange and purple squares, respectively. Yellow dots show the total area of a triple set in every quarter of revolution. Blue triangles depicts the area of a single cutter. It can be concluded a single

cutter can cut 34% to 43% of what a triple cutter set of cutters can, if three 13mm PDC cutters are placed as *Set 1* (or *Set 4*). It means that increasing the number of cutters does not increase the engagement area linearly.

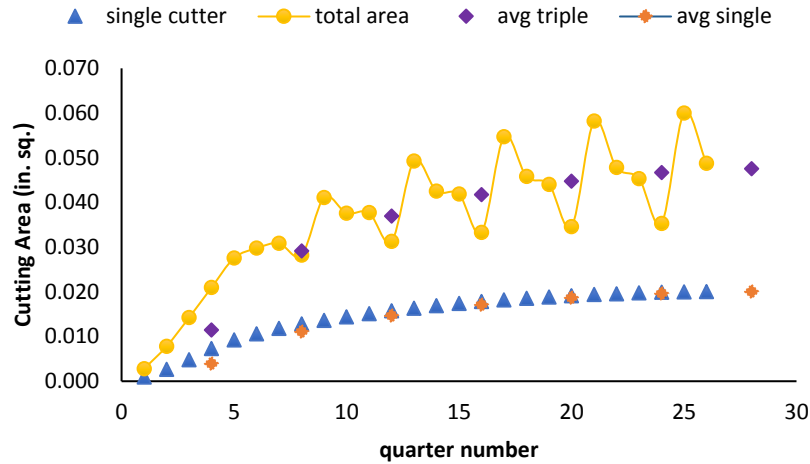


Figure 4-19: Comparing the cutting area between a single cutter and triple cutter set

4.7 Equivalent Cut Thickness (ECT)

As discussed, the steady state drilling condition cannot be reached due to particular system. The cutters are not allowed to cut the rock sample long enough to achieve the maximum engagement area of the cutter face. Hence, it can be said that in all tests conducted in this study, the process is stopped, before reaching the maximum area. In fact, although the cutter penetrates into the rock by fixed rate, it cannot be interpreted as the depth of cut, which is typically assumed in the field. Depth of cut and consequently, rate of penetration are the parameters that are used in steady state drilling, if the cutters fully engaged with the formation and stays constant beyond that.

Therefore, a parameter is defined to solve this issue. It is called “*Equivalent Cut Thickness*” (ECT), and is obtained by dividing total area of the cut at each quarter of revolution per total width

of the cut (equation 4-6). The unit of this parameter is mm/rev , same to depth of cut. It is introduced by [10] as the equivalent cutting height. Figure 4-20 illustrates how it obtains.

$$ECT = (total\ area)/(total\ width) \quad (4-6)$$

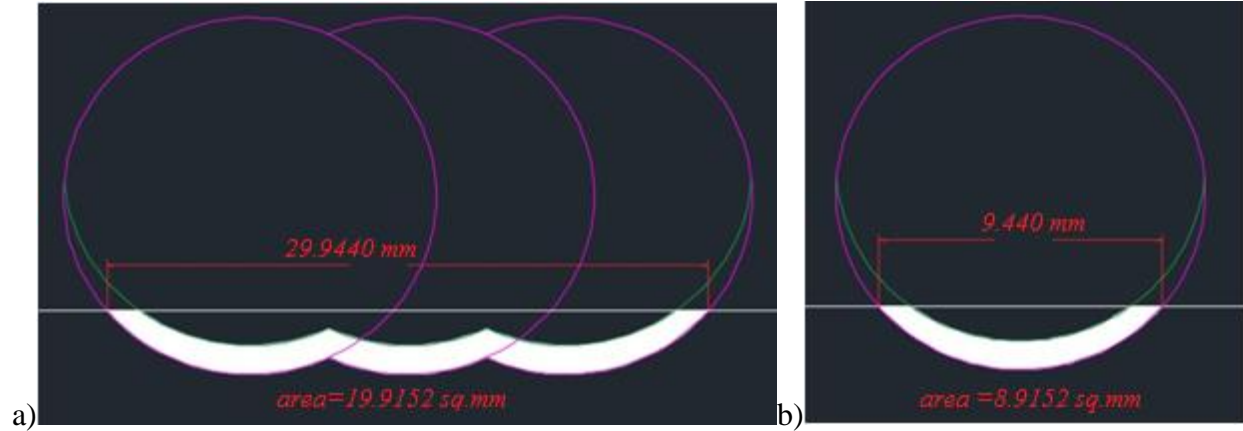


Figure 4-20: obtaining ECT by width and area of cut for (a) triple set (b) single cutter

The issue of unsteady state drilling condition may convey the transitional drilling concept where a drill bit travels from softer formation to harder formation. It happens due to heterogeneous formations; where formations are not homogenous and different anisotropic layers are drilled by the drill bit. At this situation, depth of cut is constantly changing, due to the various strengths of the formations. It can be doubled or halved quickly; therefore, the steady state condition is not dominant. The efficient bit design for transitional drilling is an interesting challenge that can be dominated to some extent, by the cutters arrangement on the bit [53]. Figure 4-21 compares the ECT for a single cutter and a triple cutter set after every revolution.

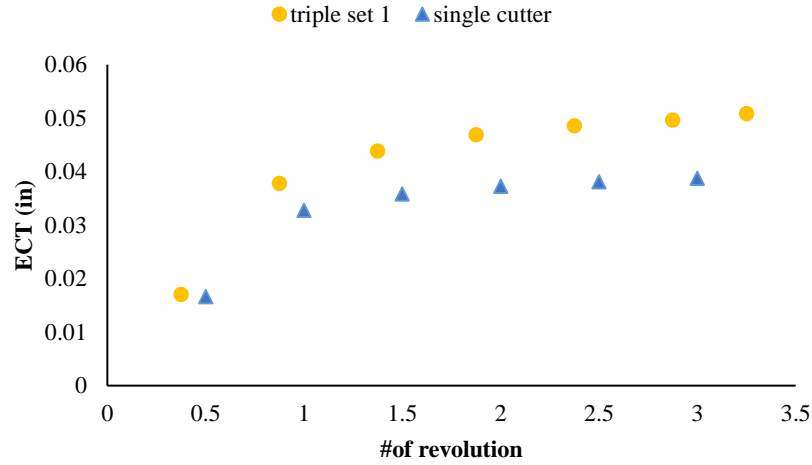


Figure 4-21: comparing the ECT between a single cutter and triple cutter set

4.8 Electrical and Mechanical Power, Torque & MSE

Due to the way the instrumentation is set up, torque for a bit with multiple cutter cannot be directly obtained from the sensor. To solve this problem, the electrical power generated to run the motors is considered to measure the torque and the required energy for cutting the rock. In drilling with fixed cutter bits, MSE is the summation of the works done by both rotational motor and vertical motor (below equations).

$$\text{Vertical work} = \text{total time} * (\text{force} * \text{travelled distance}/\text{time}) = t * (F * \frac{d}{t}) \quad (4-7)$$

$$\text{Rotational work} = \text{total time} * (\text{torque} * \text{angular velocity}) = t * (T * \omega) \quad (4-8)$$

$$\text{MSE} = \text{time} * ([F * d/t + T * \omega]/\text{removed volume}) \quad (4-9)$$

Mechanical power is typically defined as the work done divided by the time. In the current study, all the work is generated by two electrical motors. Under the assumption that the electrical power consumed is directly correlated with the real mechanical power performed (with a certain constant efficiency), measuring the electrical power gives the mechanical power. In other words, the electrical power can be converted to the mechanical power if the efficiency is known. The

efficiency here is the one due to loss of energy in conversion of electrical potential to mechanical work in the motors. The following equations clarify this relation. In this study, unit for mechanical power is horsepower (*HP*), and unit of electrical power is watt (or kilowatt (*Kw*)).

$$\text{Mechanical Power (HP)} = \text{Electrical Power (Kw)} * \text{efficiency} \quad (4-10)$$

$$\text{Electrical P. (Watt)} = \text{voltage (volt)} * \text{current(amp)} \quad (4-11)$$

$$1 \text{ HP} = 0.746 \text{ Kw} \quad (4-12)$$

$$\text{HP} = \text{Torque} * \text{RPM}/5252 \quad (4-13)$$

Therefore, to find the torque and consequently, obtain the MSE, the voltage and amperage consumed during each cutting test is measured for both motors. The energy conversion factor to convert electrical power to mechanical power is set to 0.90 and assumed constant for all the tests. This factor is obtained based on the single cutter tests; where, torque is measured directly from the cutting force and cutter distance to the bit center and can be measured indirectly from the work done by the rotating motor. The changes of amperage and voltage are recorded every 0.5 second. Then, they are plotted based on time. The area under the curve (by integration of $y = f(x)$) gives the electrical power with unit of watt. Equation (4-14), gives the torque from the area below the curve in unit of (*in – lb*). Equation (4-15) provides MSE in *psi* directly obtained from the area. Figure 4-22 shows the graph for the electrical power of a triple set on Carthage with *DOC* = 0.5 *mm/rev*.

$$\text{Torque (in – lb)} = \left[\frac{\text{total area}}{0.0118} * \frac{\text{efficiency}}{\text{RPM}} \right] * \frac{1}{\text{time}} \quad (4-14)$$

$$\text{MSE (psi)} = [\text{total area} * \text{efficiency} * 145] * \frac{1}{\text{removed volume}} \quad (4-15)$$

It is worth noting that in this method for calculating the torque, the electrical energy should be considered only from the rotational motor; while, for the MSE the summation of electrical power for both motors is required.

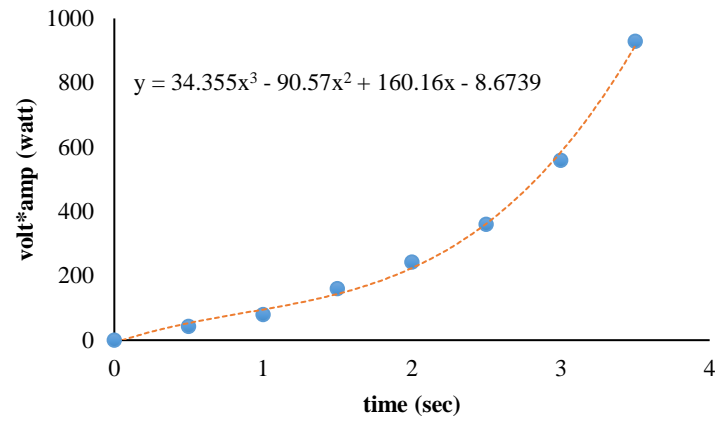


Figure 4-22: electrical power consumed to run a test is obtained from voltage and amperage

5 EXPERIMENTAL RESULTS

In the current chapter, results for various rock cutting experiments have been provided. This chapter partially includes single cutter tests and double cutter tests and mainly is composed of triple cutter test results.

5.1 Results for Single Cutter Tests

A reliable method to study the rock cutting process is applying single PDC cutter to rock cutting. This method has resulted many valuable applications, studied and analyzed in literature [7, 19, 39]. In this work, single cutter test is applied on various rock samples and in different conditions. All tests have been conducted under atmospheric pressure, and in presence of water or oil as the drilling fluid. A sharp single PDC cutter with 13 mm diameter and 20° back rake angle is used for this series of tests. Forces in 3 dimensions are measured by a tri-axial load cell, and, volume of removed rock is measured after each test. Because unique bit has been used in the entire project for single and multiple cutter tests, the cutting/engagement area for a single cutter is acknowledged via a computer design program, for every quarter of revolution. The width of the cut is also measured. The equivalent cut thickness (ECT) is then calculated for each quarter of revolution to represent the depth of cut. In single cutter tests, torque (*in – lb*) is obtained if the tangential force is multiplied by the cutter distance from the bit center, and, MSE (*psi*) is calculated by following the equation below.

$$MSE = time * ([F * d/t + T * \omega] / removed\ volume) \quad (5-1)$$

where, F is normal force (*lb*), d/t is feeding rate (*in/sec*), T is torque (*in – lb*), and ω is the angular velocity (*rev/sec*).

The forces on a single cutter are shown in Figure 5-1, where the normal force is in z -axis, and perpendicular to the 2D plane. The load cell starts to measure these forces when the cutter

touches the rock surface. The cutting process is finished when the feeding motor stops proceeding and starts to raise the cutter gradually off the rock. For instance, in Figure 5-2, the motor is stopped after 3.5 second.

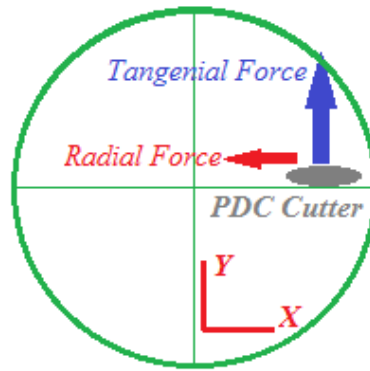


Figure 5-1: forces on a single cutter that rotates counter-clockwise to the viewer

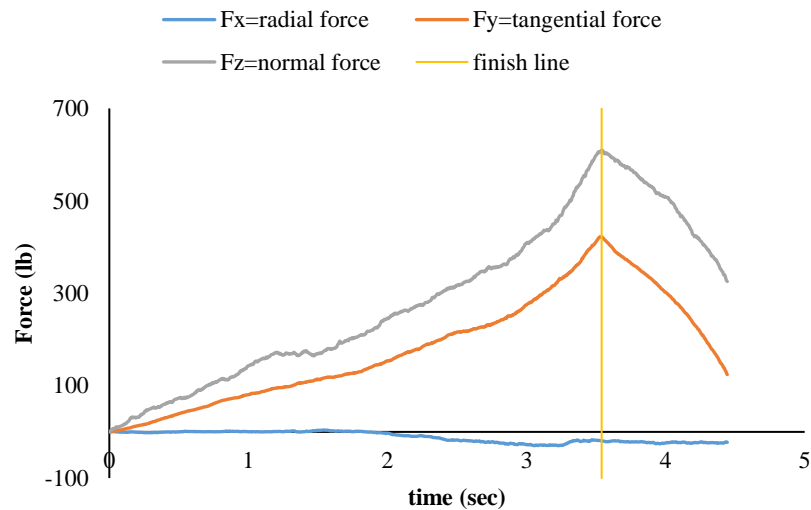


Figure 5-2: force sampling for single cutter cutting the marble

For 3 sets of input parameters, width of the cut, the engagement area and ECT are calculated and plotted in figures below. Because of some limitations on the feeding motor used in this work, the velocity of vertical displacement (ROP) cannot exceed 1.25 mm/sec. Therefore, to acquire different depth of cuts, both ROP and RPM have to be changed. This mechanical restriction

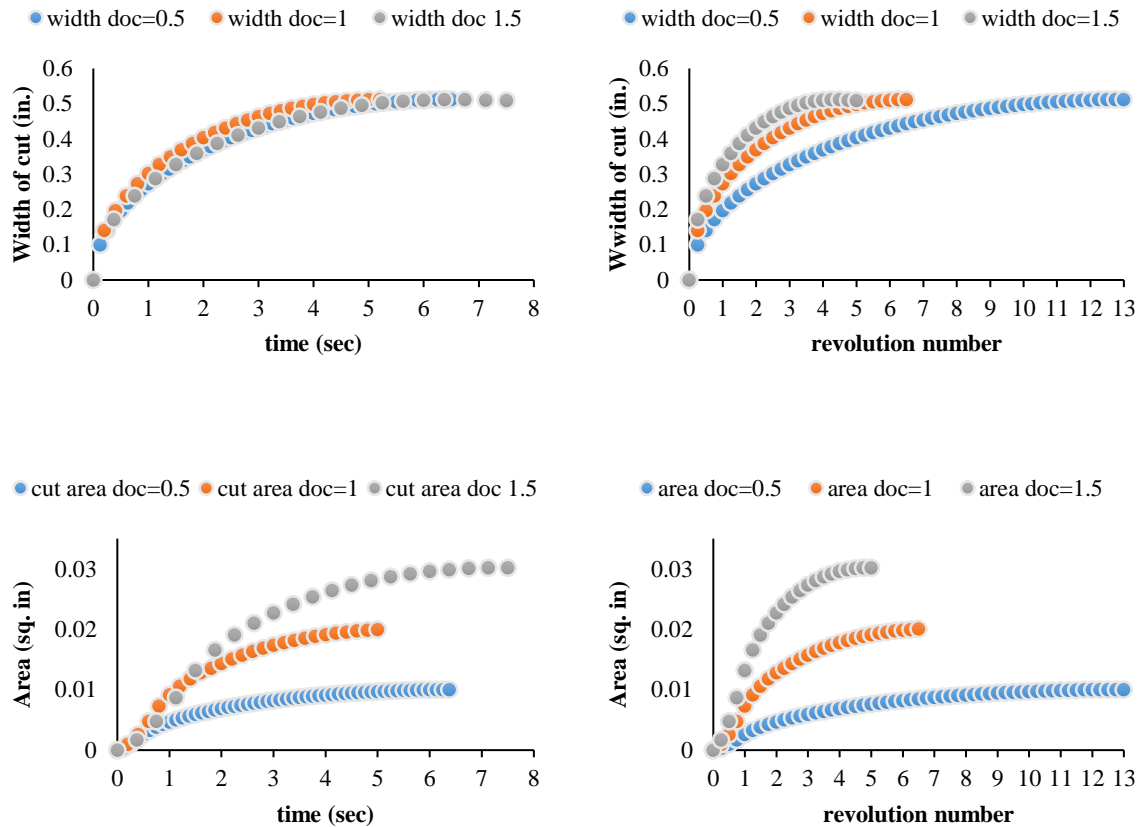
should be considered on analyzing the outputs of Figure 5-3. Depth of cut is obtained based on equation 5-2. Input parameters are seen in Table 5-1.

$$DOC = ROP/RPM \quad (5-2)$$

Table 5-1: categories of different input parameters for single cutter tests

Category	RPM	ROP (mm/s)	DOC (mm/rev)
1	120	1	0.5
2	75	1.25	1
3	40	1	1.5

The effect of depth of cut on width of cut, cutting area and equivalent cut area for different drilling categories for single cutter testing is presented in Figure 5-3, it is seen that higher depth of cut would need less number of revolutions to reach the steady state condition. Consequently, the width of cut and ECT remain constant at their maximum values.



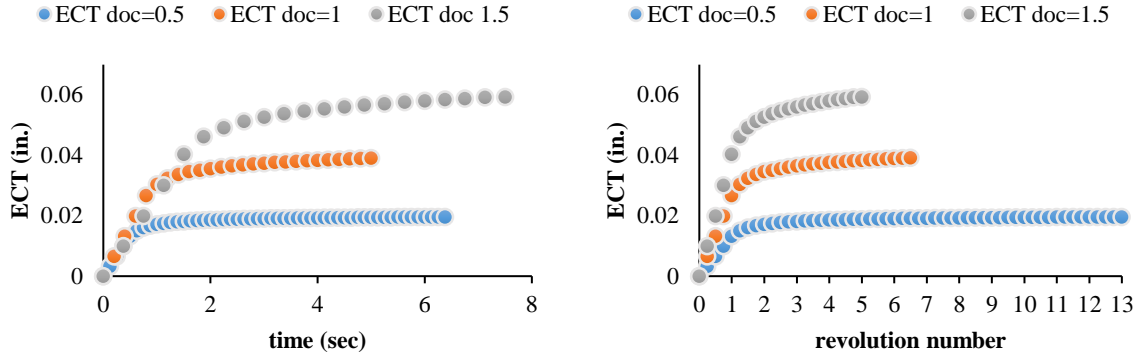


Figure 5-3: Width, Area and ECT for the single PDC cutter with different depth of cuts

The average results of conducting a series of experiments on several rock samples by applying a single PDC cutter is presented in Table 5-2.

Table 5-2: results for single cutter tests

Sample (Saturated Fluid)	DOC (mm)	Normal Force, F_N (lb)	Tangential Force, F_T (lb)	Radial Force, F_R (lb)	MSE (psi)
Sandstone 1 (oil)	0.5	133	113	-27	22400
Sandstone 1 (water)	0.5	150	84	-24	18200
Sandstone 1 (water)	1.0	120	94	3	16100
Sandstone 1 (water)	1.5	207	170	-41	13500
Shale (oil)	0.5	40	31	6	6700
Shale (oil)	1.0	63	39	-3	4200
Marble 1 (water)	0.5	283	90	7	43000
Marble 1 (water)	1.0	253	97	-1	39600
Marble 1 (water)	1.5	183	145	8	38200

5.1.1 MSE and DOC

It is shown in Table 5-2 that MSE tends to declines when depth of cut is increased. In shallower depth of cut (ductile mode), this phenomenon is usually seen owing to the fact that by increasing DOC, the equivalent cut thickness is increased and causes a major change in removed volume of rock and consequently, a drop in MSE. Using oil and water as drilling fluid for cutting

sandstone samples indicates that MSE is higher if the cutting process is done in presence of oil. This effect is also experienced in rock cutting by using multiple PDC cutter, which the details can be found at the end of this chapter. Figure 5-4 shows that for all rock samples MSE is decreased by increasing DOC.

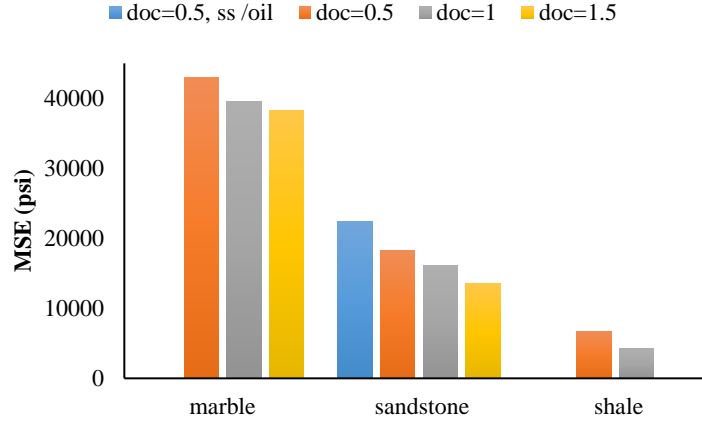


Figure 5-4: MSE and DOC for different rock samples

5.1.2 Cutting Force and DOC

Since the single cutter is fixed along the x -axis, the tangential force is F_Y and the radial force is equal to F_X that are measured by the load cell in our system (Figure 5-1). Combination of tangential force (F_t) and radial force (F_r) on the horizontal plane represents lateral force (F_H). The magnitude and direction of this force is calculated by using equations in section 4.4. As, the side rake angle for the single PDC cutter in this study is zero, the radial force is usually very small and negligible. Thus, it is reasonable to consider the lateral force almost equals to the tangential force in the single cutter tests. However, when more than one cutter is involved in the rock cutting process, these two forces are differentiated. Tangential force for various rock samples in single cutter tests is plotted in Figure 5-5.

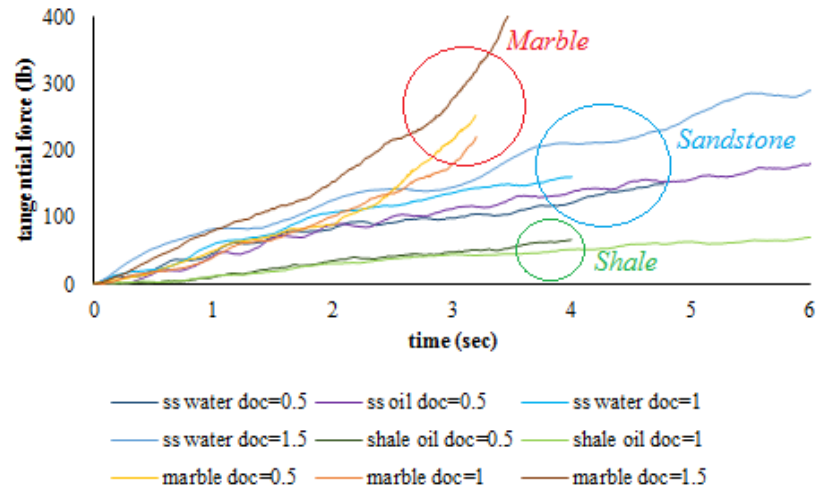


Figure 5-5: comparison of tangential forces for several samples and DOC's in single cutter tests

The effect of radial force on the lateral force in single cutter tests is very small. Meaning that the lateral force and the tangential force should have almost similar directions, perpendicular to the cutting face.

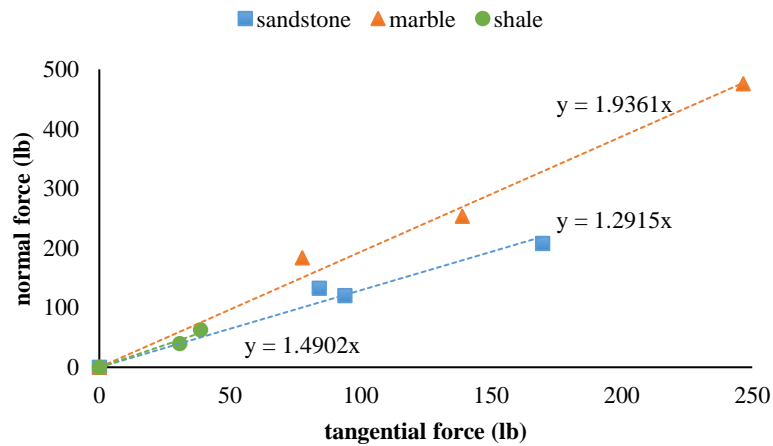


Figure 5-6: relation between the tangential force and normal force for three samples (DOC=0.5 mm/rev)

Another set of tests have been conducted by using a single cutter with 40 mm distance to the center of bit on different rock samples. In this set, nominal depth of cut is 1 mm/rev and RPM

is 75. The relation between the tangential forces and normal forces of the rocks based on the equivalent cut thickness is presented. The similar curvature of the graphs in Figure 5-7 represent that as the cutting area (or the equivalent cut thickness) is reaching its maximum value, the magnitude of the forces is rapidly increased. It can be seen that forces on the cutter in the first revolutions (or quarter of revolutions) are very low and when $\sim 1/3$ of the ECT is achieved, the forces on the cutters are raising quickly. It can also be concluded that in the transitional drilling where the depth of cut is constantly changing, even slightly change in ECT, can drastically affect the load on the cutters. Furthermore, sudden changes and impacts can imitate the bouncing on the cutters that accelerates the damage or breakage to the cutters.

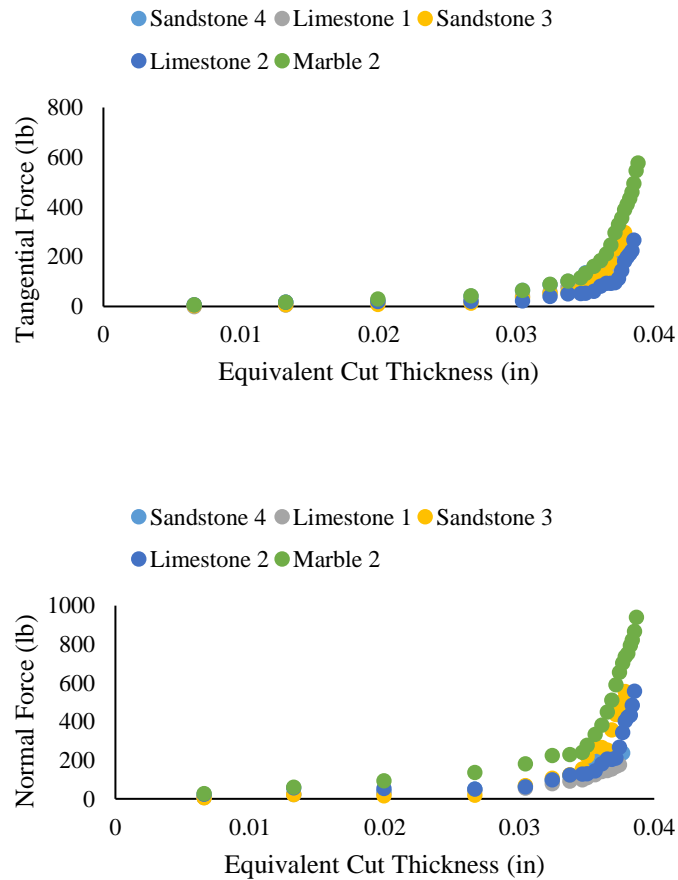


Figure 5-7: forces on the single cutter based on ECT for different rock samples

5.2 Results for Double Cutter Tests

A few tests were conducted by using two PDC cutters where they are placed symmetrically, in two blades on the x axis with 180° degrees angle between them. The distances from the bit center are 60 and 71 mm for *cutter 1* and *cutter 2*, respectively. By assuming the cutters meet the flat rock surface at the same time, the calculated engagement area shows the exact same area for each cutter on every quarter of revolution. The results for different tests can be found in Table 5-3. Figure 5-8 shows the arrangements of the cutters on a bit along with the acting forces.

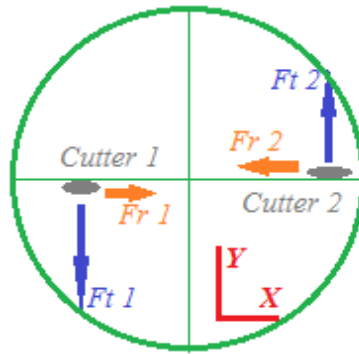


Figure 5-8: Double cutter arrangement on the bit that rotates counter-clockwise to the viewer

It might be expected to observe zero or very small forces on the bit plane where the forces may be cancelled each other out. Contrarily, the measured forces, specifically in x direction, show non-zero value for the radial force. The radial forces on the plane can effect on direction of lateral force (θ) that causes the inclination from 90° . This issue, having radial force when there are more than one cutter on plane and side rake angle is zero, will be studied in the next chapter.

Table 5-3: results of using two PDC cutters to cut the rock samples (DOC=1 mm/rev, RPM=75)

Sample (<i>all in water</i>)	F_X (lb)	F_Y (lb)	F_Z (lb)	F_H (lb)	θ°	Torque/V (psi)	MSE (psi)
Marble 1	-	26	418	27	-71	185	26000
Limestone 1	-	-	167	24	80	145	9300
Limestone 2	-	32	342	35	-66	309	23500

5.3 Results for Triple Cutter Tests

The main experimental part of this study is focused on the rock cutting using three PDC cutters in different arrangements on the bit. For this purpose, totally 12 different sets of arrangements have been defined in Table 4-1. On the other hand, 8 different rock samples including *sandstone*, *marble*, *limestone* and *shale* formations, are provided in this study to be drilled in presence of drilling fluid, and under atmospheric pressure. The results for different series of experiments are explained in the following sections. It should be noted that the duration of the cutting process might vary for every test in a range of 2 to 5 second; therefore, the tables presented in this chapter, are based on the total time of that particular test. In next chapter, to have a consistent analysis, an equal process duration for all tests will be considered to analyze. Figure 5-9 shows the arrangements of the cutters on a bit along with the acting forces.

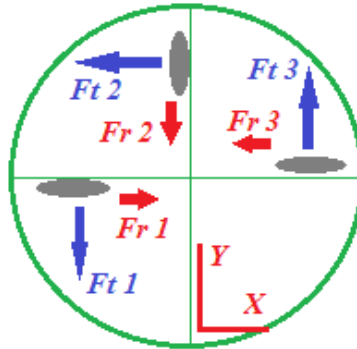


Figure 5-9: schematic of triple cutter arrangement on a bit that rotates counter-clockwise to the viewer

5.3.1 Triple Cutter Tests on Sandstone (*Torrey Buff*)

A set of rock samples in this work are called *sandstone 1*, most likely they are Torrey Buff sandstone. (Unfortunately, there is no certainty on the exact name of the samples, and only the formation type is clear to us). Totally, 9 sets (*out of 12*) of cutter arrangements are tested on this sample, in presence of the drilling fluid including air, water, or oil. Depth of cut is set to

0.5 mm/rev and RPM is 120. Torque is measured indirectly from the electrical energy consumption by the rotational motor. MSE is calculated based on the torque of the rotational motor (as described in previous chapter). Table 5-4 presents the results for different sets used to cut *sandstone 1*. (Torque and MSE are only measured when drilling fluid is liquid.) It is seen that different cutters arrangements causes various cutting results on a given rock sample. (The first column gives the distance between the radiuses).

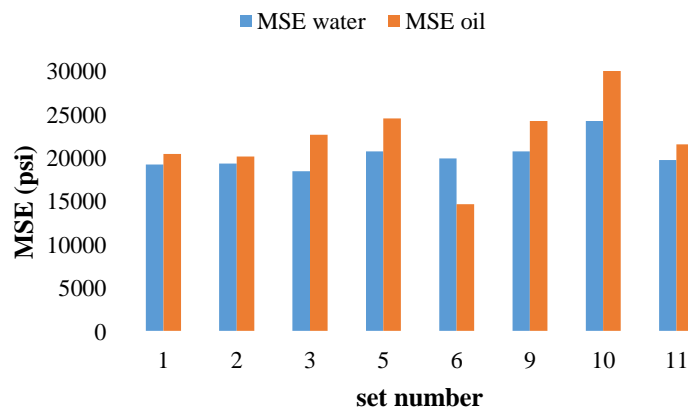
Table 5-4: Results of triple cutter cutting on Sandstone 1 (DOC=0.5 mm/rev, RPM=120)

Distance	SET	Drilling Fluid	F _H (lb)	θ°	F _N (lb)	Vol Rate (ml/sec)	Torque/V (psi)	MSE (psi)
d= 5.5 mm	1	water	36	23	89	2.57	408	19300
	1	oil	28	15	94	1.77	495	20500
	2	water	59	24	120	2.67	332	19500
	2	oil	47	21	95	2.14	424	20200
	3	water	58	-7	165	3.38	368	18500
	3	oil	76	-23	168	3.17	302	22700
d= 4 mm	5	water	20	60	89	3.00	263	20800
	5	oil	29	65	96	2.20	369	24600
	6	water	86	48	159	3.27	277	20000
	6	oil	65	44	116	3.11	241	14700
d= 2.5 mm	9	water	21	-73	93	2.50	259	20800
	9	oil	20	72	120	2.00	402	24300
	10	water	96	51	140	2.45	334	24400
	10	oil	110	51	141	1.88	383	30500
	11	water	65	4	148	3.14	214	19800
	11	oil	66	3	119	2.83	287	21600

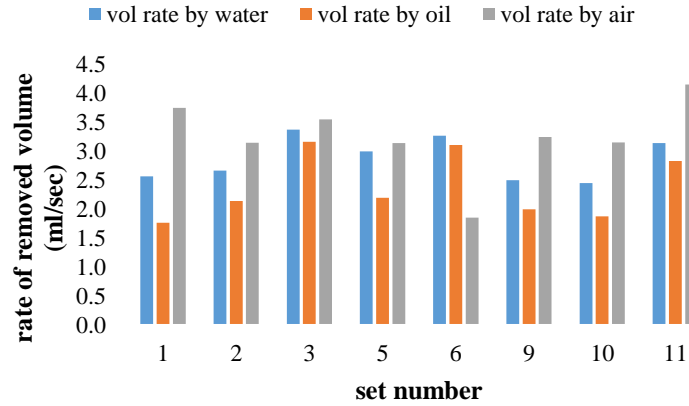
Generally, the results show that using water as the drilling fluid to cut this type of sandstone under atmospheric pressure is more efficient than oil, where the MSE is lower and the rate of removed volume of rock per unit of time is higher. The reason behind this issue is studied at the

end of this chapter in section 5-4. The bit performance in this set of tests can be studied based on different parameters such as MSE, lateral force, removed volume of rock per unit of time and torque per rock volume. For instance, analyzing the effect of cutters arrangements on the bit shows that the lowest MSE in an every group is obtained for the sets 1, 5, and 9; where, the cutters are distributed spirally on the bit. Lateral force on the bit (F_H), which may be considered as the bit stability and might indicate how much the bit plate is being pulled off the bit center. Volume rate shows the amount of rock which is removed in unit of time. Torque per volume represents the amount of torque is needed to remove a unit volume of rock and lower is preferred.

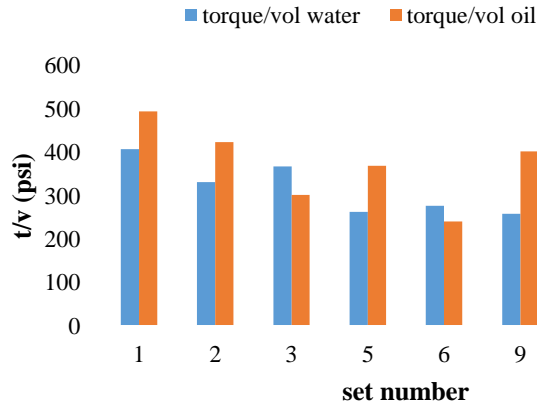
A few of the tests were repeated by only using the air (dry cutting). The rate of removed volume (the method is explained in section 4-5) increased by 15 % compared to water and 44 % comparing to the oil. Figure 5-10 compares the effect of different cutters arrangements on cutting *sandstone I* with using different drilling fluids when all other drilling parameters are set constant. It should be noted that distance between the cutters for sets 1 to 4 is 5.5 mm, for sets 5 to 8 is 4 mm, and for sets 9 to 12 is 2.5 mm. Therefore, analyzing on the graphs can be done based on the cutters spacing.



a)



b)



c)

Figure 5-10: the effect of different cutters arrangements on cutting sandstone 1 with using different drilling fluids

5.3.2 Triple Cutter Tests on Shale (*Catoosa shale*)

A set of experiments is conducted on Catoosa shale samples by using oil as the drilling fluid. All sets of arrangements, (described in Table 4-1), have been used in this part of study to compare the effect of different cutters distribution on the bit. The summary of the results is presented in Table 5-5. It should be reminded that the steady state condition is not reached during these tests, and the time duration of the cutting process varies. (The first column gives the distance between the radiuses).

Table 5-5: results for cutting the shale samples with oil (DOC=0.5 mm/rev, RPM=120)

Distance	SET	F_H (lb)	θ°	F_N (lb)	Vol Rate (ml/sec)	Torque/V (psi)	MSE (psi)
d= 5.5 mm	1	10.05	6	35	4.72	136	4300
	2	42.52	41	55	3.33	113	6400
	3	23.09	-5	71	2.8	208	6500
	4	33.3	41	60	5	95	3600
d= 4 mm	5	12.04	85	49	4	91	4600
	6	43.28	50	83	4	122	6100
	7	27.07	4	41	4.45	85	5900
	8	25.24	34	32	4	102	4400
d= 2.5 mm	9	6.32	72	41	4	51	3200
	10	50.99	48	58	3.76	107	6000
	11	21.02	-3	41	3.87	90	5100
	12	41.18	29	72	4.44	84	4700

It seems that generally in every group of cutter radiuses, the reverse spiral set of cutters arrangements gives the least MSE, although sets 9 and 10 responded differently. That would be most likely due to the experimental error. Considering the lateral force on the bit, it is seen that among all cutters sets, the spiral sets (sets 1, 5, and 9) generate less lateral forces, while sets 3, 7, and 11 generate the highest forces. Therefore, the spiral sets of cutters may present more stable bits for cutting this type of shale, although higher MSE is needed. The amount of removed rock per time for the reverse spiral set of cutters is more than other sets in a group.

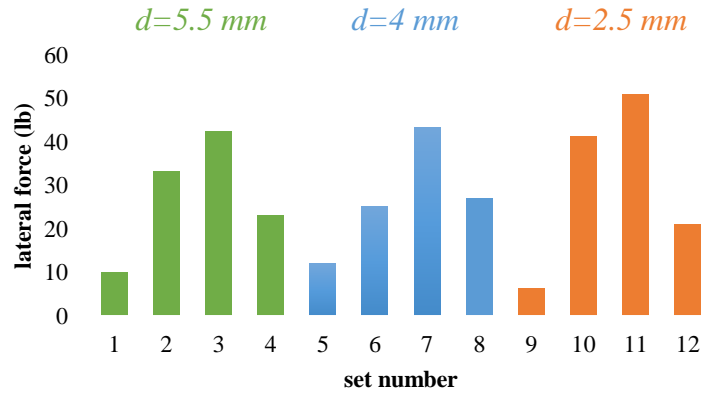


Figure 5-11: lateral forces on different sets for cutting the shale samples

5.3.3 Triple Cutter Tests on Marble (*Carthage Marble*)

Other series of tests are conducted on rock samples called *marble 1*, which possibly are Carthage marble. For this set, only spiral (*sp*) and reverse spiral (*rev sp*) sets of cutters are selected to focus on the effect of these two common ways of cutters arrangement on the bit and to find the optimum distance between the cutters. The details of results are presented in Table 5-6.

Table 5-6: Results for cutting the marble 1 samples with water (DOC=0.5 mm/rev, RPM=120)

Distance	SET	F_H (lb)	θ°	F_N (lb)	Vol Rate (ml/sec)	Torque/V (psi)	MSE (psi)
d= 5.5 mm	1	23.0	34	135	0.83	932	4110
	4	63.6	37	302	0.87	1071	4060
d= 4 mm	5	12.2	-55	342	1.58	835	4210
	8	77.9	-13	290	1.49	834	3940
d= 2.5 mm	9	21.4	79	313	1.60	778	3920
	12	100.6	6	248	1.41	716	3830

MSE for both sets of *sp* and *rev sp* in every group is almost the same, although yet the reverse spiral set consumes less energy to cut unit volume of rock. It is seen again that arranging the cutters spirally would generate less lateral force on a bit plane. Placing the cutters closer to the

adjacent cutters may increase the cutting performance on a hard rock such as Carthage marble. Based on the measured MSE better result is obtained, when cutters only have 2.5 *mm* distance from each other.

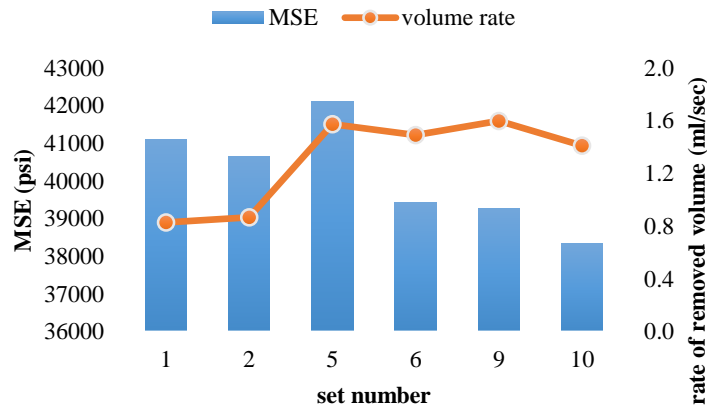


Figure 5-12: MSE and rate of removed rock volume for cutting the marble samples

5.3.4 Triple Cutter Tests on a Variety of Rock Samples ($DOC=1\text{ mm/rev}$)

Depth of cut for all conducted tests with triple PDC cutter so far, was 0.5 *mm/rev* and RPM was 120. Hence, it can be mentioned that the cutting process was partially done by the chamfer of the cutter. Cutting on chamfer is not an interest in this study. Therefore, to better analyze the effect of cutters arrangements, depth of cut is doubled. For the next series of experiments, using three PDC cutters, RPM is set to 75 and depth of cut is 1 *mm/rev*.

Various rock samples are used for this set of tests including 3 types of sandstone, 2 types of limestone, and 1 type of marble. The focus in this part is mainly on two sets of cutters arrangements; called spiral (*sp*) set and reverse spiral (*rev sp*) set. The distance between the cutters is set to 5.5 *mm*, therefore, only *set 1* and *set 4*, among all sets in Table 4-1 are tested. The same procedure as previous section is repeated. The forces in three directions are measured via the load cell, torque is obtained from the motor, and the removed rock volume by the cutters is measured

after the test by using the powder to fill out the grooves. The average of outputs for different rock samples are presented in Table 5-7.

Table 5-7: results for cutting various rock samples, (DOC=1 mm/rev, RPM=75)

Sample	SET	F_H (lb)	θ°	F_N (lb)	Vol Rate (ml/sec)	Torque/V (psi)	MSE (psi)
Limestone 1 (LS 1)	1 <i>Sp</i>	24.3	-9	140	3.40	354	13900
	4 <i>Rev Sp</i>	53.2	5	104	2.67	459	10800
Limestone 2 (LS 2)	1 <i>Sp</i>	21.0	3	151	2.11	537	16000
	4 <i>Rev Sp</i>	116.9	10	372	2.68	422	14700
Sandstone 2 (SS 2)	1 <i>Sp</i>	76.7	22	260	2.00	833	19700
	4 <i>Rev Sp</i>	51.5	18	170	1.92	715	16900
Sandstone 3 (SS 3)	1 <i>Sp</i>	53.2	12	349	1.17	1873	44300
	4 <i>Rev Sp</i>	47.5	-8	193	1.27	1393	32900
Sandstone 4 (SS 4)	1 <i>Sp</i>	27.5	33	138	2.44	535	18900
	4 <i>Rev Sp</i>	43.6	-9	121	1.82	695	15000
Marble 2	1 <i>Sp</i>	25.0	-2	204	1.43	1023	28200
	4 <i>Rev Sp</i>	57.9	-10	234	1.66	842	23200

It is found that MSE can be enhanced from 9 % to 22 % by arranging the cutters reverse spirally. The changes for the rate of removing rock volume is not consistent and seems depends on the rock strength; whereas, for softer formations (e.g. limestone 1, sandstone 4), the rate is higher for spiral sets and for harder formations (e.g. limestone 2, and marble 1), higher rate belongs to the reverse spiral sets. The apparent reason for experiencing lower MSE for reverse spiral sets is due to lower torque measured during the cutting for those sets. Torque on the bit plane is built based on the acting forces on the cutters, such as tangential and radial forces. It will be explained in section 6.2.2 that the direction of the radial forces for the reverse spiral sets of cutters is opposite to the spiral sets. These forces may be interfered as the centrifugal force or centripetal force that apparently affect the torque on bit and consequently the MSE.

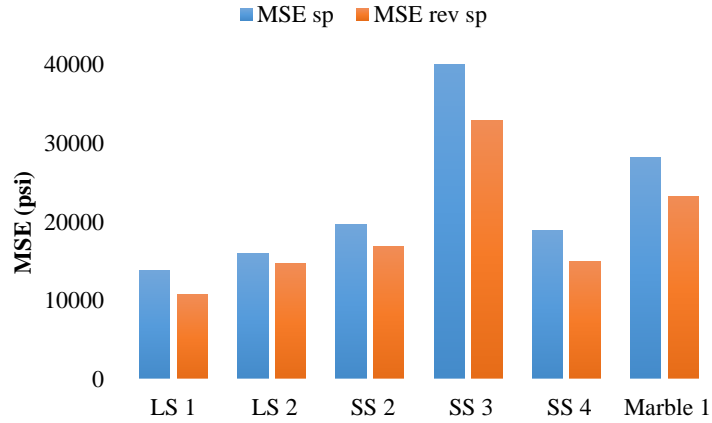
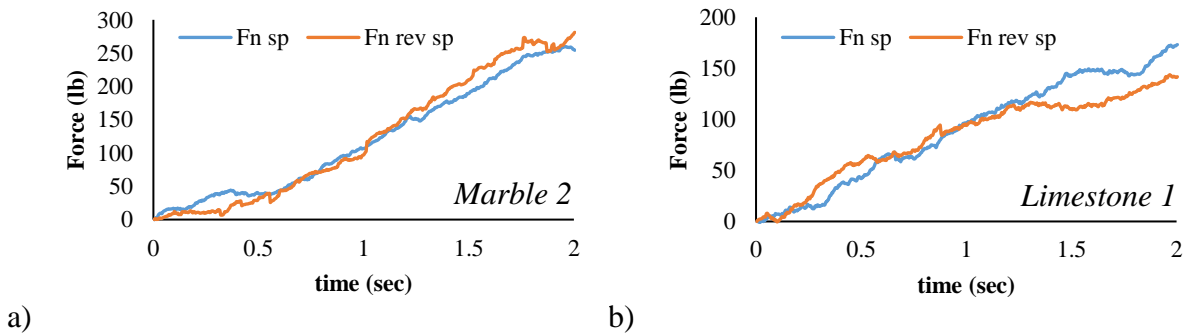


Figure 5-13: comparing the MSE for both sets of cutters arrangements

All drilling parameters are constant for all the tests presented in Table 5-7, only total time for the tests may vary between 3 sec to 4.5 sec. However, if the forces are plotted in the same time duration for every pair of test, then normal force for both sets (spiral and reverse spiral arrangement) becomes almost equal. It appears that normal force for the reverse spiral set on *marble 2* in his first $\frac{1}{4}$ of revolution slightly cut the sample and the entire assigned area was not engaged due to possibly uneven surface of the sample. Besides, lateral force is larger for the reverse spiral set than spiral set. Therefore, the measured force in *z-axis* shows a drop at the beginning. It can be concluded that although the cutting area on the cutters for both sets in the same amount of time (or number of revolutions) are equal, they generate different lateral forces on the bit plane.



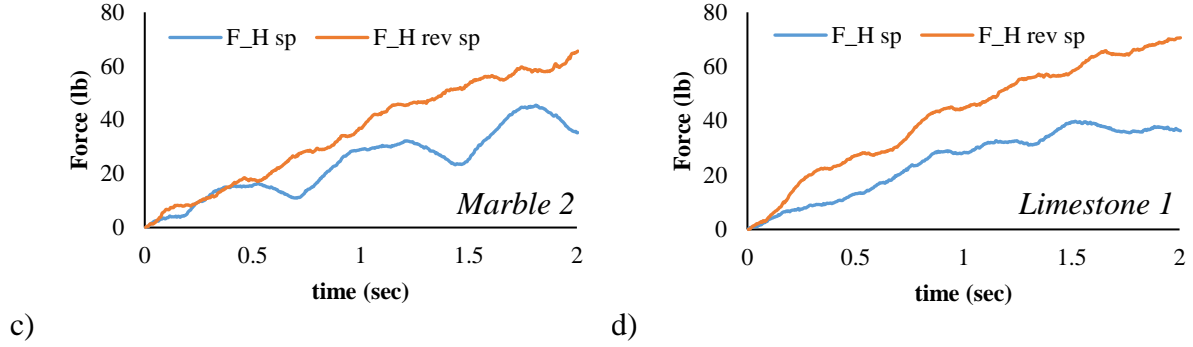


Figure 5-14: (a & b) normal force (c & d) lateral force for spiral and reverse spiral sets for two samples

The direction of lateral force (θ), shows that the reverse spiral set of cutters arrangement is more stable rather than the spiral set which fluctuates harder. θ is the angle between the lateral force and y-axis, in a range of $-\frac{\pi}{2}$ to $\frac{\pi}{2}$. The severe fluctuation of the lateral force on the bit plane might lead to bit instability or damage to the cutters, if it causes the bit to hit to the wellbore, periodically. In a reverse spiral set of triple cutters, the direction of lateral force shows smoother behavior, although this needs more study specially in steady state drilling.

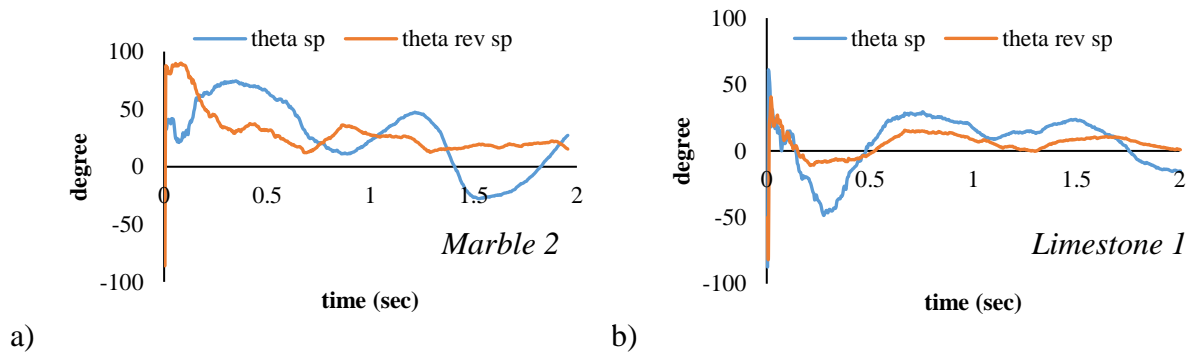


Figure 5-15: direction of lateral force (θ) on every moment of the cutting process

5.4 Conclusion on Triple Cutter Results

Various sets of triple cutters arrangements on a bit are used to cut several rock samples. Forces in three directions are measured via the load cell and torque is obtained through the

electrical power consumed to rotate the rotational rod. Mechanical specific energy (MSE), then, is calculated based on the removed rock volume, which is measured at the end of each test. The results are averaged from the beginning of the test ($t = 0$) to the last cutting point, when the rotation is stopped. Comparing the spiral set and reverse spiral set shows MSE is lower for reverse spirally arranging the cutters while the lower lateral force mostly is obtained for spiral sets. Here, is a conflict in purposes for bit design or bit selection, where the lower MSE is achievable but the lateral force increases. Although, the cutters arrangement in this study intentionally is not designed to be symmetric, generating higher forces on the bit plane in reverse spiral sets of cutters along with lower MSE is a significant outcome of the experiments that should be considered in bit design or bit selection.

5.5 Grooves and Cuttings Remain on Bit and Rock Sample

Grooves of the cutters remain after the cut can be assumed as the fingerprint of every set of cutters. They show the interconnection of the cutters and the relative involvement of the cutters in the cutting process. Figure 5-16 depicts some of the grooves on *sandstone 1*. The close up of the grooves shows that for instance, if *set 2* is used for cutters arrangement (c), the middle cutter has the lowest engagement but using *set 1*, most likely gives the equal share for all the cutters. However, the wettability of the rock samples should be considered, as well.

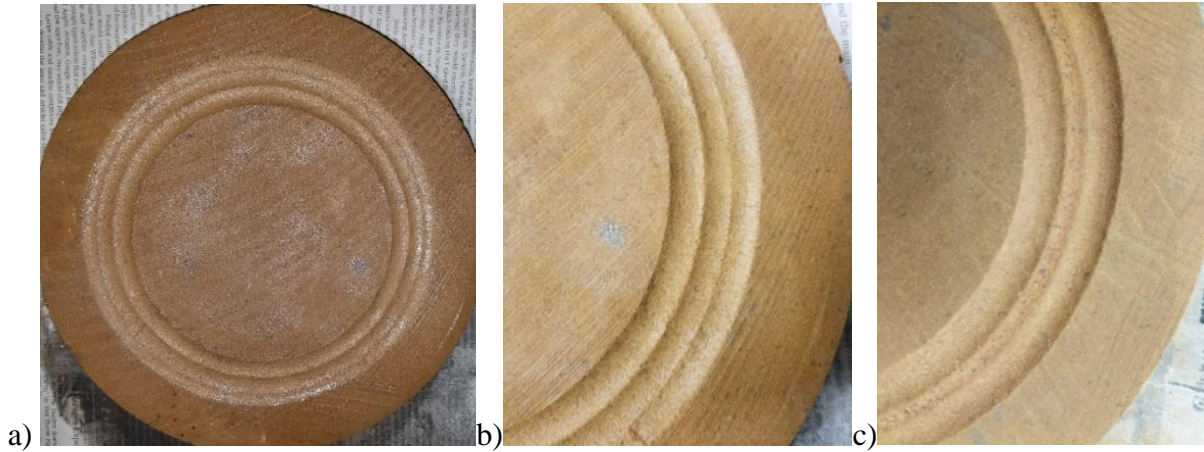
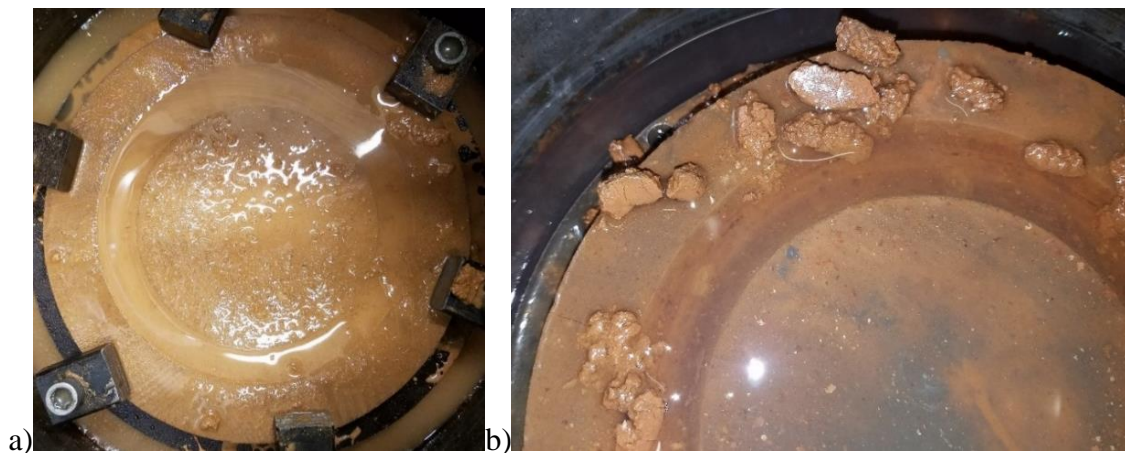


Figure 5-16: (a) full view of grooves remain on a 8" sample, (b) grooves for set 1, (c) grooves for set 2

After the cutting process is done, the remaining cuttings on the rock surface or on the cutter face can also be considered. The properties of the cuttings strongly depend on the drilling fluid and the wellbore pressure [6]. In the current work, the wellbore pressure is equal to the atmosphere pressure; hence, the difference in cuttings properties is mostly a result of the fluid type. For instance, Figure 5-17 shows that in the process of cutting *sandstone 1 (Torrey Buff)* by using two different fluids as the drilling fluid and the saturation fluid. If water is used, the cuttings spread over the rock sample like a fine mesh powder; while using oil to saturate the sample and the drilling fluid, causes the accumulation of the cuttings, and makes relatively large but very soft pieces.



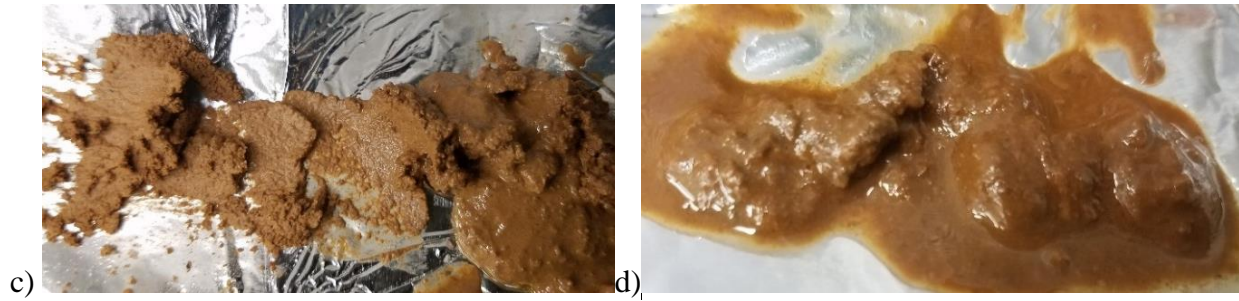


Figure 5-17: (a) a thick layer of powder-like cuttings on the sample after cutting water saturated sample, (b) large and soft mobilized particles after cutting oil saturated sample (c) collected cuttings of water saturated sample (d) collected remaining cuttings of oil cut

The reason behind the difference between the nature of the remaining cuttings after oil and water used and their impact on the cutting performance should be studied. As seen in Table 5-4, MSE for cutting *sandstone 1* is less for water than oil. It should be noted that all samples have been immersed in the drilling fluid in atmospheric pressure for at least two days prior to the test. In that way, it can be assumed they are partially saturated. It is well known that the strength of all types of rock is reduced by the fluid saturation [75-77]. For shale and quartz-sandstones even up to 50% UCS reduction has been reported due to full saturation with water [77]. The saturated status strongly affect the clay-rich sandstones rather than siliceous sandstones in strength reduction in compare to dry samples [76]. In general, the mineral composition plays a key role in controlling the sensitivity to water saturation. Tan and Wu have reported that fluid saturation on sandstones generally decrease the strength and Young's modulus and increase Poisson ratio. The degree of affection depend on the clay volume. It is said that the effect of oil saturation for all the above-mentioned parameters are less than water saturation. This phenomenon can be due to reduction in molecular cohesive strength (surface energy), chemical effect (cation exchange of water molecules) or developing capillary pressure (mostly for tight rocks such as shales) [75].

Despite, the reduction in the rock strength occurs due to the water or oil saturation, the effect of drilling fluid on the grains and fines distribution is important to study. After cutting the oil saturated sandstone sample, the larger particles appears to be accumulated and left on the rock surface. These large but soft particles might cause the misunderstanding on the cutting efficiency and efficient brittle failure. Since, usually cutting the larger cuttings only needs to fail the sand grain bonds in the shear plane of failure rather than overcoming the cohesive bonds between the individual fines of sandstone. Nevertheless, in fact, the rationale behind this phenomenon seen in the figures is owing to the fines mobilization of the grains. Mobilization of loosely bond fine particles is occurred considerably greater in the presence of oil than water. Because of the extra contribution from mineral particles associated with the oil deposit films on grain walls. The oil phase carries and redeposits the fines [78]. The amount of quartz in the sandstone plays a role in the mobilization. Torrey buff sandstone is composed of quartz (~50%), kaolin (*clay mineral*) (~16%), and dolomite (~24%). The mineral decomposition of Torrey buff sandstone supports the claim on higher strength reduction due to water and fines mobilization and redepositing due to oil saturation.

The cuttings adhering to the bit profile or on the cutters, is another factor that directly affects the cutting efficiency. Accumulation of formation in front of cutter or sticking to the cutter faces may cause a major drilling problem such as bit balling. This usually occurs when a formation containing water-sensitive clays (*e.g.* shales) is drilled. The cuttings absorb water from the drilling fluid, and stick to the bit or the cutters. Cuttings remain on the cutters due to cutting different samples are depicted in figures below. It is seen that the volume and the shape of sticking formation to the cutter face depend on the rock type, drilling fluid and saturation.

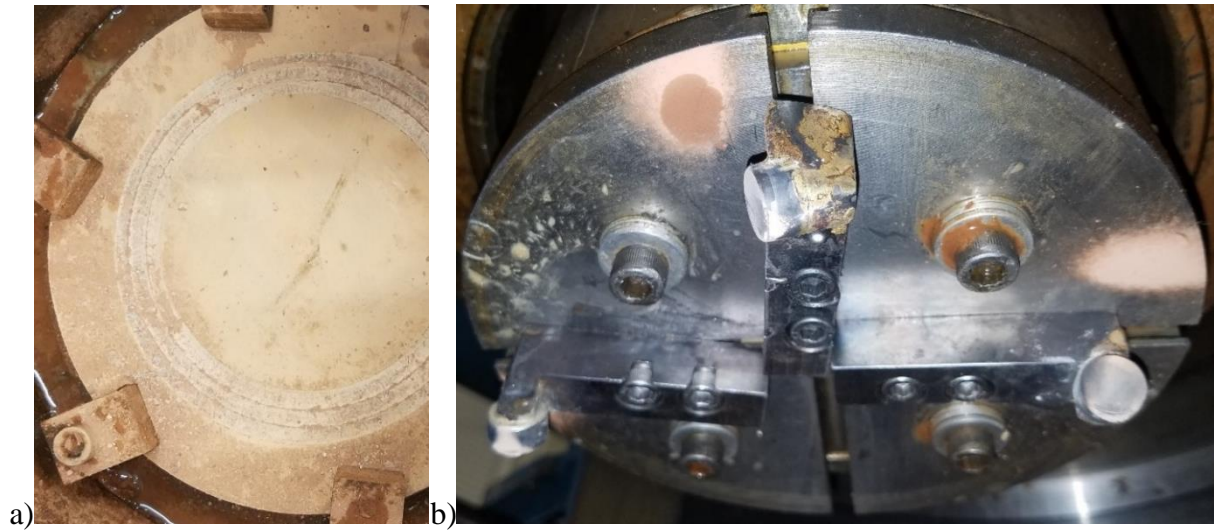


Figure 5-18: using air as drilling fluid for cutting dry and unsaturated sandstone

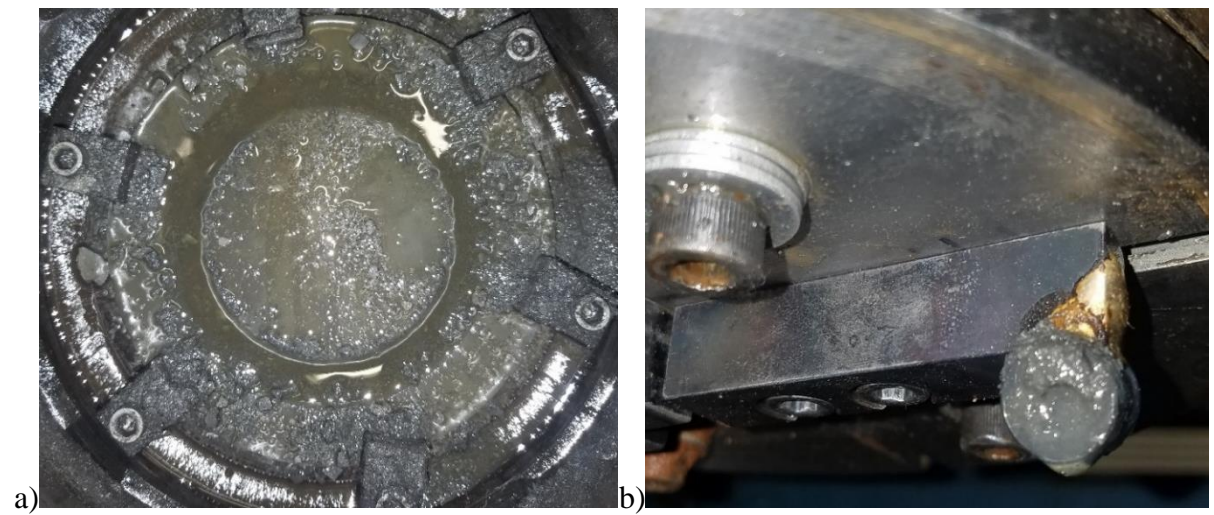


Figure 5-19: cutting the oil saturated shale sample and remained cuttings on the cutter

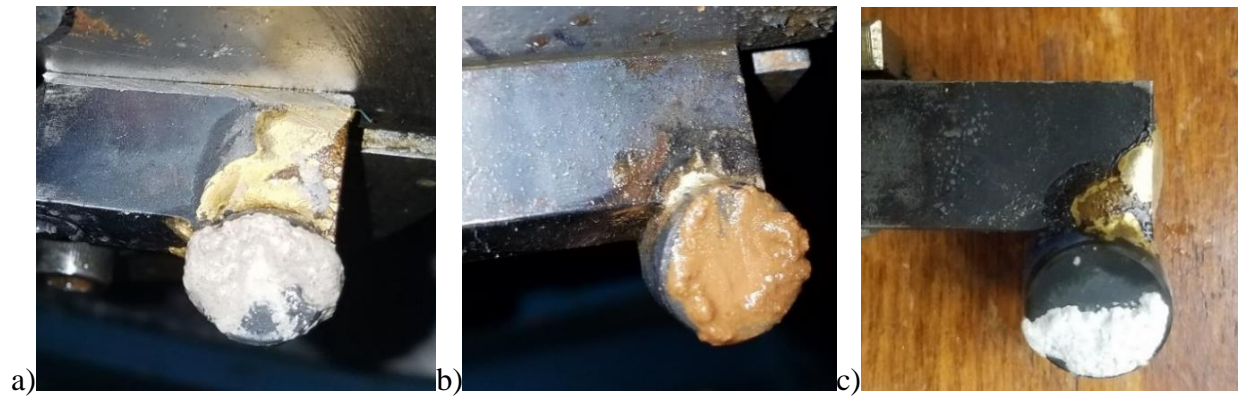


Figure 5-20: cutting the saturated samples (a) limestone / water (b) sandstone / oil (c) marble / water

It might be possible in some cases, to recognize the cutters arrangement by looking at the formation particles stick to the cutters. For instance, Figure 5-21 schematically shows the engagement area of the cutters in a spiral set and how the formation may engage with cutters. Figure 5-22 shows the cutter faces after a test with a spiral arrangement on the bit. The left side of *cutter 1* (a) is mostly covered by the muddy formation; *cutter 2* is fully covered due to accumulation of the cutting in the center of grooves (b). In fact, although the middle cutter has least engagement area, the cuttings are swept by the sided cutters and pushed inward, then, are collected by the middle cutter. The right side of *Cutter 3* (c) is covered with the sticking formation, as well. It appears that generally in Torrey buff samples, the cuttings made when oil is used are less prone to stick to the PDC cutter face.

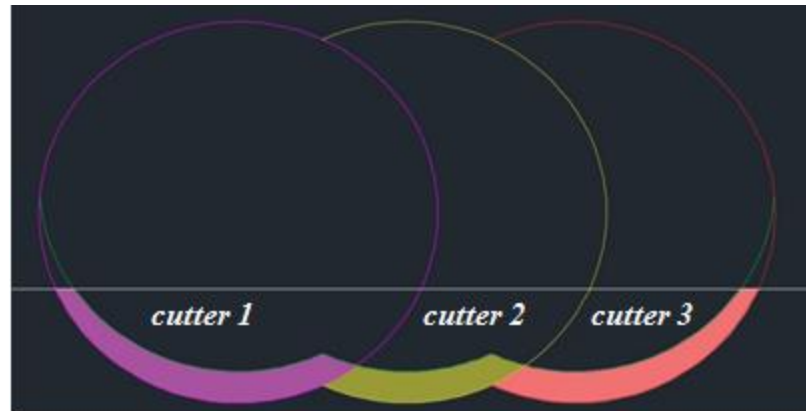


Figure 5-21: schematic of the engagement area for every cutter. The colorful zone shows the cutting area.



Figure 5-22: remaining cuttings on the cutters (a) cutter 1 (b) cutter 2 (c) cutter 3

6 RESULT ANALYSIS

In this chapter, a force model is developed based on the single cutter experiments. Then, the model is upgraded to match the triple cutter experiments, and last it is integrated to a full PDC bit. The effects of various cutters arrangements on different parameters have been studied as well. The experimental results have been employed to investigate on bit design affective parameters at the end of the current chapter.

6.1 Single Cutter Force Model

Single cutter experiments is a common method among the scholars to investigate on rock-cutter interactions. Forces on a sharp single PDC cutter in ductile regime (shallow depth of cut) are decomposed into normal (or axial) force (F_n), tangential (or cutting) force (F_t), and radial (or side) force (F_r) (Figure 6-1). Following the force model proposed by [39], normal force and tangential force on a single cutter can be obtained based on the engaged area of the cutter, rock strength and the ratio of normal to tangential force. . It is assumed that if the side rake angle of the cutter is zero, then, there is no side force on the cutter, perpendicular to cutting path. Generally, any force on the single cutter is a function of these parameters.

$$F = f(\varepsilon, \zeta, A, \mu, \beta, \alpha) \quad (6-1)$$

where ε is the intrinsic specific energy, A is the cutting area, μ is the friction between the rock and the cutter face, β is the back rake angle, and α is the side rake angle. The ratio of the normal force to tangential force is $\zeta = \tan(\psi + \theta)$ that characterizes the inclination of the cutting force on the cutting face with respect to the direction of the cutter motion. θ is the back rake angle of the cutter and ψ is the interfacial angle between the failed rock and the cutting face. The equations to predict the forces on the sharp single cutter are presented below.

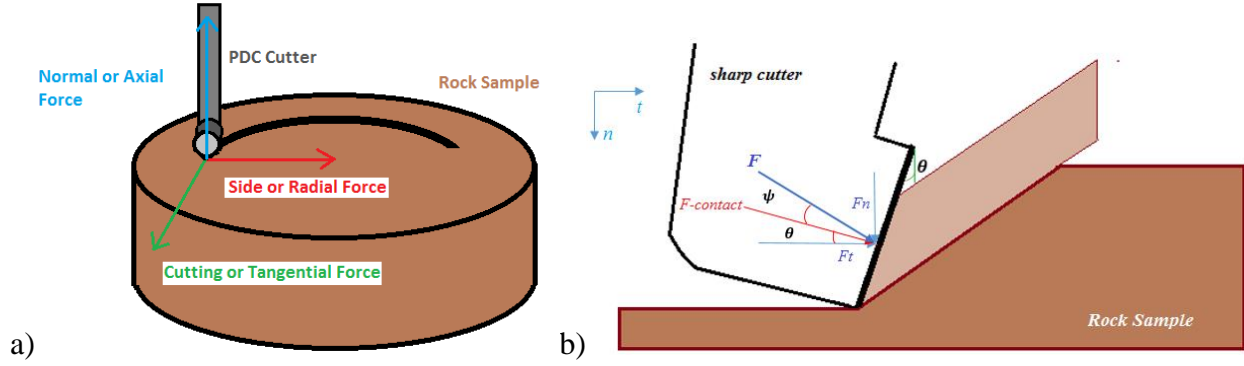


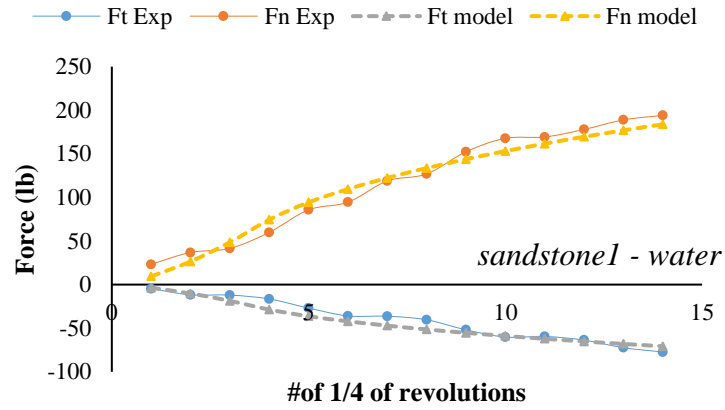
Figure 6-1: Forces on a single cutter

$$F_n = F * \sin(\theta + \psi) = \zeta \varepsilon A \quad (6-2)$$

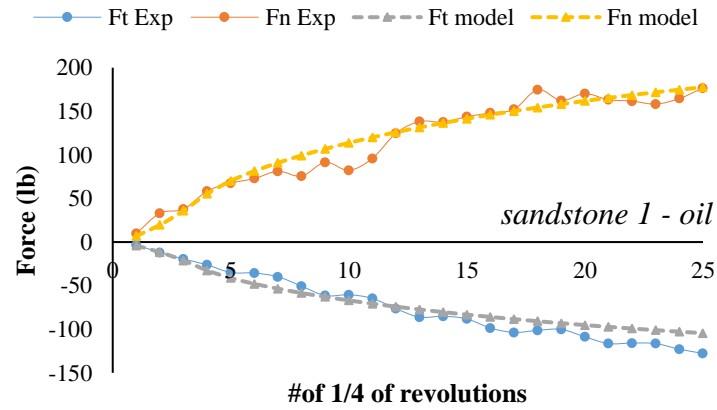
$$F_t = F * \cos(\theta + \psi) = \varepsilon A \quad (6-3)$$

$$\zeta = \tan(\theta + \psi) \quad (6-4)$$

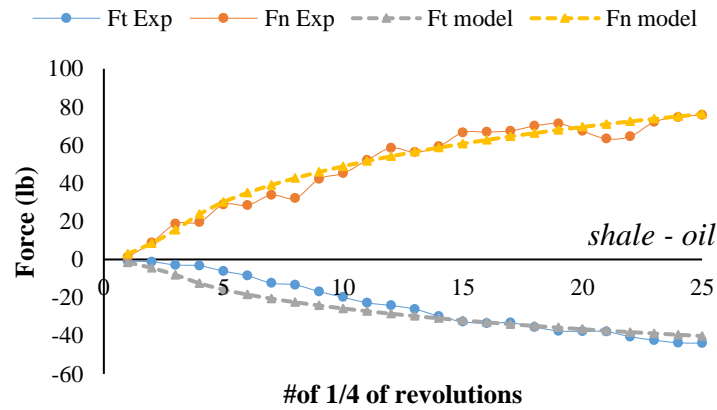
To predict the forces on the single cutter based on the proposed force model, the precise engagement area of the cutter at every moment of cutting is needed. By using CAD program, the cutting area for a single area is calculated (Figure 5-3). Again, it is assumed this area on a cutter is constant, at least at every quarter of revolution. Nine different experiments on various shale, sandstone and marble samples are selected to develop the force model for them and compare with the measured forces by the sensor. It is seen that there is a good agreement between the model and experimental results (Figure 6-2). Therefore, it seems that the validity of the model is verified at least for the single cutter tests.



a)



b)



c)

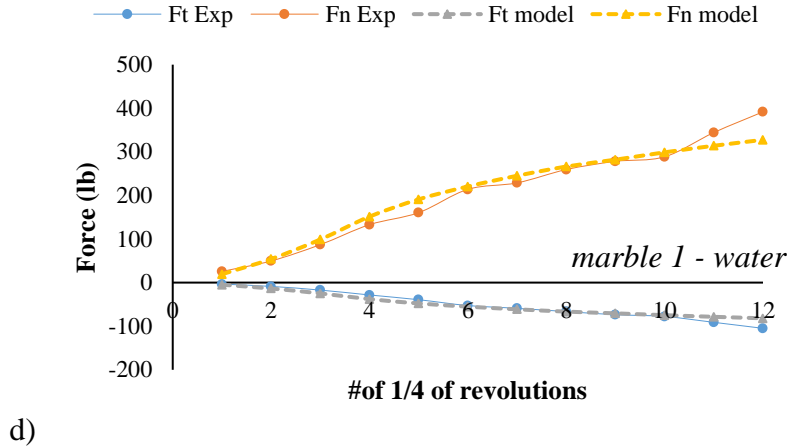


Figure 6-2: comparing single cutter experimental results with proposed model (RPM=120, DOC=0.5) (a) sandstone 1 with water (b) sandstone 1 with oil (c) shale with oil (d) marble 1 with water.

The rock strength and the ratio of the normal to tangential force for every rock is obtained on the force model to find the best fitted line with the experimental results. In this case, the rock strengths used in the model for triple cutters are ~25% less than the estimation from the sonic test.

Table 6-1: rock parameters obtained to model forces on all other samples

Sample	ϵ (psi)	ζ	Sample	ϵ (psi)	ζ
Sandstone 1	11000	2.6	Sandstone 3	10500	1.5
Marble 1	6000	3.5	Limestone 1	7200	1.2
Shale	4800	1.9	Limestone 2	5000	2.5
Marble 2	9000	2.2	Sandstone 4	9700	1.25

6.2 Impact of Triple Cutters on Force Model

It was discussed in previous chapter that the results of the triple cutter experiments shows the cutters arrangements affect the bit performance. It was explained that spiral and reverse spiral sets of cutters have the same cutting area but the measured forces in the same drilling condition, are different. Therefore, there should be another factor to explain the variety of the results when the above-mentioned parameters (ϵ , ζ , A , α) are the same for spiral and reverse spiral sets of cutters.

6.2.1 Radial Force

It is assumed that radial force depends on the side rake angle of the cutter and when that angle is zero, then, there should be no side force measured during a test. This assumption was verified in the single cutter experiments. However, as discussed in section 5-2, in double cutter tests, the forces measured in the bit plane shows a type of side force on the cutters should be considered. Comparing the results of using three PDC cutters for spiral and reverse spiral cutters arrangements highlights the existence of the radial force on the cutters with unknown direction.

The authors in [39] mention in their model that a ratio of ζ , implies the friction existence at the rock-cutter interface. However, since a symmetric cut has been assumed in their study on scratch test, no horizontal force orthogonal to the direction of the cut (*side or radial force*) is expected. This assumption cannot be hired in this study. The cutting area is constantly changing due to having multiple cutters in a ring of the bit and applying the vertical displacement (while in scratch test there is no vertical movement). Therefore, a horizontal force on the cutter face caused by the friction can be expected in frame of these experiments. This force can be assumed as the radial force on the cutting face. However, the friction coefficient on the cutting face could be smaller than the friction coefficient at the wear flat of the cutter, due to the different strengths of the materials and the level of stresses acting on them [42].

6.2.2 Center of Mass (CM) of PDC Cutters

Center of mass (CM) is a fictional parameter defined for a physical object. It considers the average location of the weight of an object. In fact, the motion of any object through space can be described in terms of translation of the CM. Center of mass and center of gravity are described at the same point if the gravitational field is uniform, which in this study is assumed to be. Based on

the definition, any object *e.g.* the PDC cutter in rock cutting process, can be represented by its center of mass/gravity; then, translation or rotation of CM represents the movement of the object.

Following the force models proposed by many scholars, the portion of the cutter face, which is engaged with the formation, is a significant factor to model the forces on a cutter. For a fixed depth of cut, the engagement area of a single cutter increases until it reaches the maximum value and beyond that point it remains constant (steady state). For a ring of cutters on a bit, the cutting area on every cutter is continually changing, because every cutter in every revolution may see different shape of grooves remained from the front cutter. The fluctuation in the cutting area could be seen for a few revolutions until the cutters reach their maximum area (if the formation is uniform). Otherwise, the depth of cut due to lithology and different layers of formations continuously oscillates, so does the cutting area. Accordingly, the changes in the cutting area causes the variation in the location of center of mass (CM) of the cutter. It can be thought that the formation ahead of the cutter pushes away the cutter face, perpendicular to the cutting path and causes the radial force on the cutter face. Therefore, the existence of the radial force depends on the changes in the location of CM. It is found that the direction of this radial force depends on the direction of this movement.

By employing a computer-aided design application, the location of CM at any moment for every cutter in a ring of cutters on a bit is obtained. The direction of CM movement for every cutter is used to specify the direction of the radial force on every cutter. Arranging the cutters spirally or reverse spirally would leverage the radial force toward different directions. Therefore, the radial force can be obtained through the equation below as long as changes in location of CM is occurred. Hence, the radial force is defined based on the following equations (please see Figure 6-1b).

$$F_{contact} = [F_n \sin(\theta) + F_t \cos(\theta)] \quad (6-5)$$

$$F_r = v_{CM} \cdot \mu \cdot F_{contact} = v_{CM} \cdot \mu \cdot [F_n \sin(\theta) + F_t \cos(\theta)] \quad (6-6)$$

$$v_{CM} = \{-1, 0, +1\}$$

where μ is friction coefficient, $F_{contact}$ is the force normal to the cutting face. v_{CM} only accepts 3 values $\{-1, 0, +1\}$. If the direction of movement of CM is toward the bit center $v_{CM} = -1$. If it is toward the bit shoulder, then $v_{CM} = +1$, and if there is no changes in the location of CM, then $v_{CM} = 0$. For instance, for the spiral set in Figure 6-3 v_{CM} is $+1, +1$, and -1 for *cutter 1*, *cutter 2*, and *cutter 3*, respectively. (The friction coefficient at the cutting face in this work obtained by calibrating and tuning up the parameters in the proposed force model.)

Radial force can be considered on the cutting face in both horizontal direction (x -axis) and vertical direction (y -axis) due to the feeding rate. Therefore, the changes in vertical direction of CM, also generates an upward force parallel to the cutting face, which should be added to the normal force of the cutter. Nevertheless, since this force is too small compared to the normal force, the vertical movement of CM of the cutter can be neglected and only the generated radial force in horizontal direction on the cutting face is considered.

Figure 6-3 schematically demonstrates the movement of CM and its direction at the end of every revolution (out of scale). After 7 revolutions, it reaches the steady state condition and stays constant. Radial force for any cutter on the bit follows the direction showed in Figure 6-4. The bit in this figure is rotating counter-clockwise on the plane.

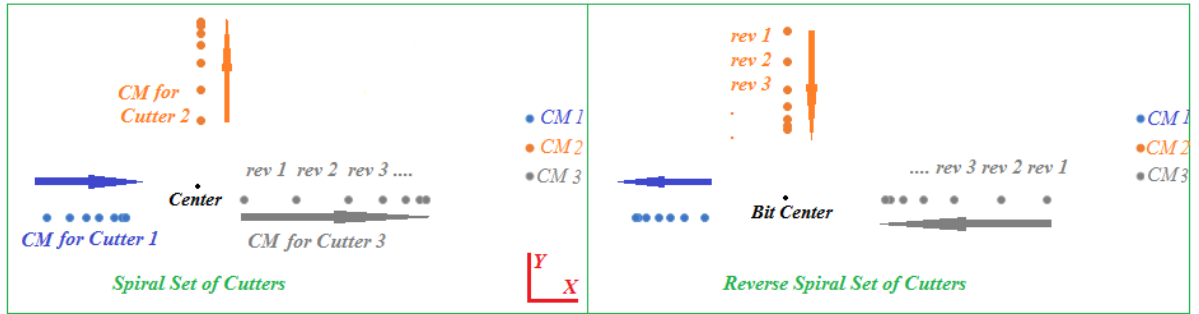


Figure 6-3: direction of CM movement for cutters in both sets

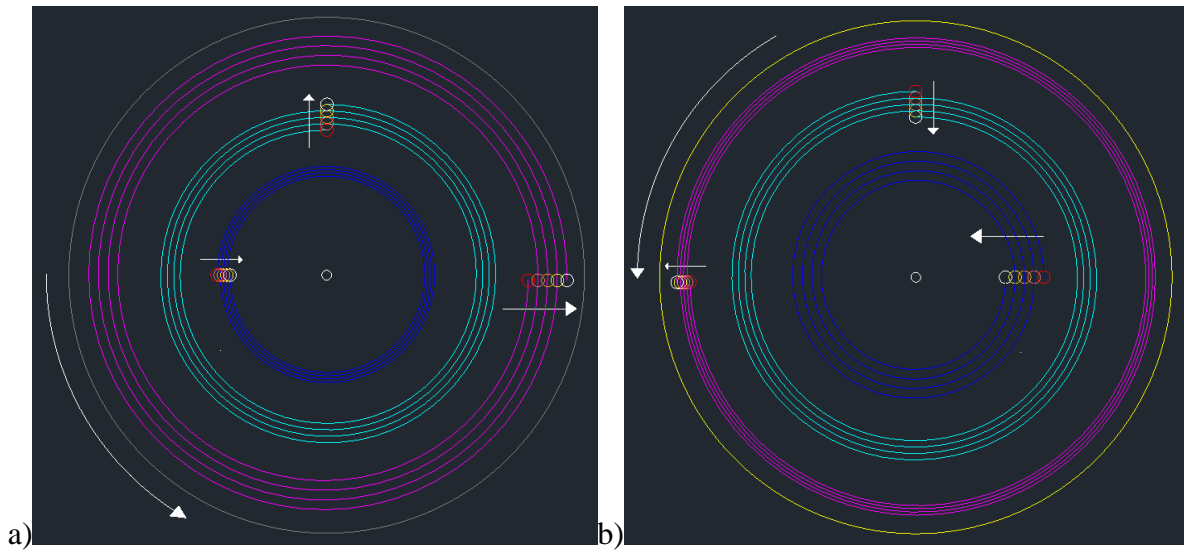


Figure 6-4: CM movement for (a) spiral set (b) reverse spiral set of cutters

6.2.3 Force Model on Full PDC Bit

A scaling approach for adapting a single cutter model to full-scale PDC bit can be modified based on the proposed force model to predict the forces in three directions on every single cutter on the bit. A rigorous model is presented solely based on the cutters arrangements and bit geometry, the cutting area of every cutter at any moment, the rock strength, the inclination of normal force to the cutting face, and the friction coefficient on the cutting face. The model is evaluated by the experimental results of using triple PDC cutters and with the numerical results of the proposed bit designs with five PDC cutters in Chapter 7.

To study the full bit response, first the cutters should be projected on a 2D plane layout. The adjacent cutters then should be divided into particular rings, where, every ring of cutters may cut a ring of rock. The full bit response is composed of the responses of every ring of cutters. The proposed force model is applied on every cutter (assumed sharp) in a ring to predict normal force, tangential force, and radial force of the PDC cutter. The impact of neighboring cutters have to be considered in calculating the engagement area and movement of center of mass (CM). The rock strength, friction coefficient and the inclination ratio (ζ) can be assigned properly based on the previous tests. The force equations are repeated below.

$$F_n = \zeta \varepsilon A \quad (6-2)$$

$$F_t = \varepsilon A \quad (6-3)$$

$$F_r = v_{CM} \cdot \mu \cdot [F_n \sin(\theta) + F_t \cos(\theta)] \quad , v_{CM} = \{-1, 0, +1\} \quad (6-6)$$

These equations provide the acting forces on every single cutter on the bit. To obtain the full response, the summation of the forces on a ring is needed with consideration of the force direction. To better presentation, it is assumed that 5 cutters are recognized on a ring on a flat bit. It is assumed that the cutters are arranged spirally; then, the direction of the radial force for every cutter is specified based on the movement of the CM and is shown in Figure 6-5. The normal force on every cutter is perpendicular to the plane (assumed flat bit). The, the tangential and radial forces on every cutter can be broken into x and y directions.

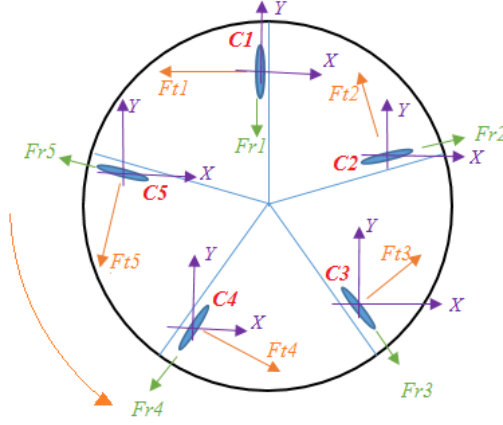


Figure 6-5: example of how the cutters are considered in the model.

Therefore, the cutters responses on a ring on the bit can be calculated as follows.

$$Fx = \sum_{i=1}^{n=5} Fx_i = Fx_1 + Fx_2 + Fx_3 + Fx_4 + Fx_5 \quad (6-7)$$

$$Fy = \sum_{i=1}^{n=5} Fy_i = Fy_1 + Fy_2 + Fy_3 + Fy_4 + Fy_5 \quad (6-8)$$

$$Fz = \sum_{i=1}^{n=5} Fz_i = Fz_1 + Fz_2 + Fz_3 + Fz_4 + Fz_5 \quad (6-9)$$

This example will be explained (as one the designed bits) in chapter 7, where the angular difference between all the blades is equal to 72° ; therefore, the forces along x -axis and y -axis can be decomposed as:

- $\bullet \quad \mathbf{Fx} = (-Ft_1) + (-Ft_2 \sin 18 + Fr_2 \cos 18) + (Ft_3 \cos 36 + Fr_3 \sin 36) +$
 $(Ft_4 \cos 36 - Fr_4 \sin 36) + (-Ft_5 \sin 18 - Fr_5 \cos 18)$
- $\bullet \quad \mathbf{Fy} = (-Fr_1) + (Ft_2 \cos 18 + Fr_2 \sin 18) + (Ft_3 \sin 36 + Fr_3 \cos 36) +$
 $(-Ft_4 \sin 36 - Fr_4 \cos 36) + (-Ft_5 \cos 18 + Fr_5 \sin 18)$
- $\bullet \quad \mathbf{Fz} = (Fn_1 + Fn_2 + Fn_3 + Fn_4 + Fn_5)$

Similar method can be used for any designed set of cutters arrangements on the bit. There is only needed to know the angular difference between the blades and possible side rake angle of the cutters. Then, the tangential and radial forces on any cutter can be predicted by applying the proposed model. The summation of horizontal forces is used to measure the lateral force (F_H), which can be considered as a tool to study the bit stability. By changing the location of the cutters on a bit, the horizontal forces and the lateral force are tended to be reduced (or even increased due to some special purposes). In next chapter, 5 different sets of cutters arrangements are evaluated based on this method to study the impact of the cutters layout on the bit performance.

6.3 Proposed Model to Experiments

Various sets of cutters arrangements are used to cut several rock samples based on the described method in previous chapter and forces, torque, removed volume, and MSE are measured. The forces in x , y , and z directions on a bit profile are composed of the main forces (F_n , F_t , and F_r) on every cutter. The forces on the cutters on a bit and their directions are shown in Figure 6-6 for both sets. It is worth noting that forces, cutting area, and depth of cut are constant (at least) in every quarter of revolution.

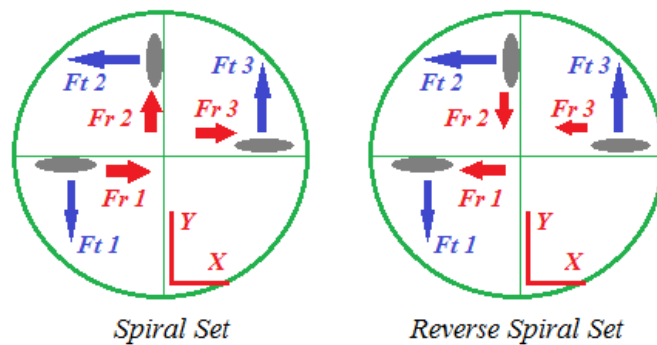


Figure 6-6: all forces and directions on the cutters on a bit of triple cutters

Thus, the forces in three directions are developed by the proposed model following the sets of equations below. The equations would be slightly different for spiral set and reverse spiral set because of the direction of CM movement for those sets.

For Spiral Set:

$$Fx = \sum_{i=1}^{n=3} Fx_i = Fr_1 - Ft_2 + Fr_3 \quad (6-10)$$

$$Fy = \sum_{i=1}^{n=3} Fy_i = -Ft_1 + Fr_2 + Ft_3 \quad (6-11)$$

$$Fz = \sum_{i=1}^{n=3} Fz_i = Fn_1 + Fn_2 + Fn_3 \quad (6-12)$$

For Reverse Spiral Set:

$$Fx = \sum_{i=1}^{n=3} Fx_i = -Fr_1 - Ft_2 - Fr_3 \quad (6-13)$$

$$Fy = \sum_{i=1}^{n=3} Fy_i = -Ft_1 - Fr_2 + Ft_3 \quad (6-14)$$

$$Fz = \sum_{i=1}^{n=3} Fz_i = Fn_1 + Fn_2 + Fn_3 \quad (6-15)$$

By plotting the forces obtained through the experiments and the forces developed by the model, the validity of the model can be evaluated. The calibrated rock properties applied in the model (ζ, ε, μ) and the cutting area (A) for both sets must be the same. For instance, for sample *marble 1*, the rock dependent parameters are presented in Table 6-2. Figure 6-7 compares the forces measured from experiment and developed per model for the spiral set and Figure 6-8 presents those forces for the reverse spiral set. The RPM is 120, the feeding rate is 1 *mm/rev*, the depth of cut is 0.5 *mm/rev*, the drilling fluid is water, the cutters radiuses are 60, 65.5,

and 71 mm (set 1&2). Forces on a bit containing triple cutters, in x -axis (graph a), in y -axis (graph b), in z -axis (graph c), and *lateral* on a plane (graph d) are plotted in the figures 6-6, and 6-7. Every colored dot in the plots represents the force in a quarter of revolution. In addition, for *limestone 1* rock sample, the rock dependent parameters for both sets are presented in the same table. The distance of the cutters from the bit center is the same as the previous test, but drilling conditions have been changed as provided in the table below. Figure 6-9 and Figure 6-10 present the forces measured and modeled to cut *limestone 1* sample.

Table 6-2: rock parameters obtained to model forces to cut the samples

Sample	ε (psi)	μ	ζ	RPM	ROP (mm/s)	DOC (mm/rev)
Marble 1	6000	0.17	1.6	120	1	0.5
Limestone 1	4200	0.15	1	75	1.25	1

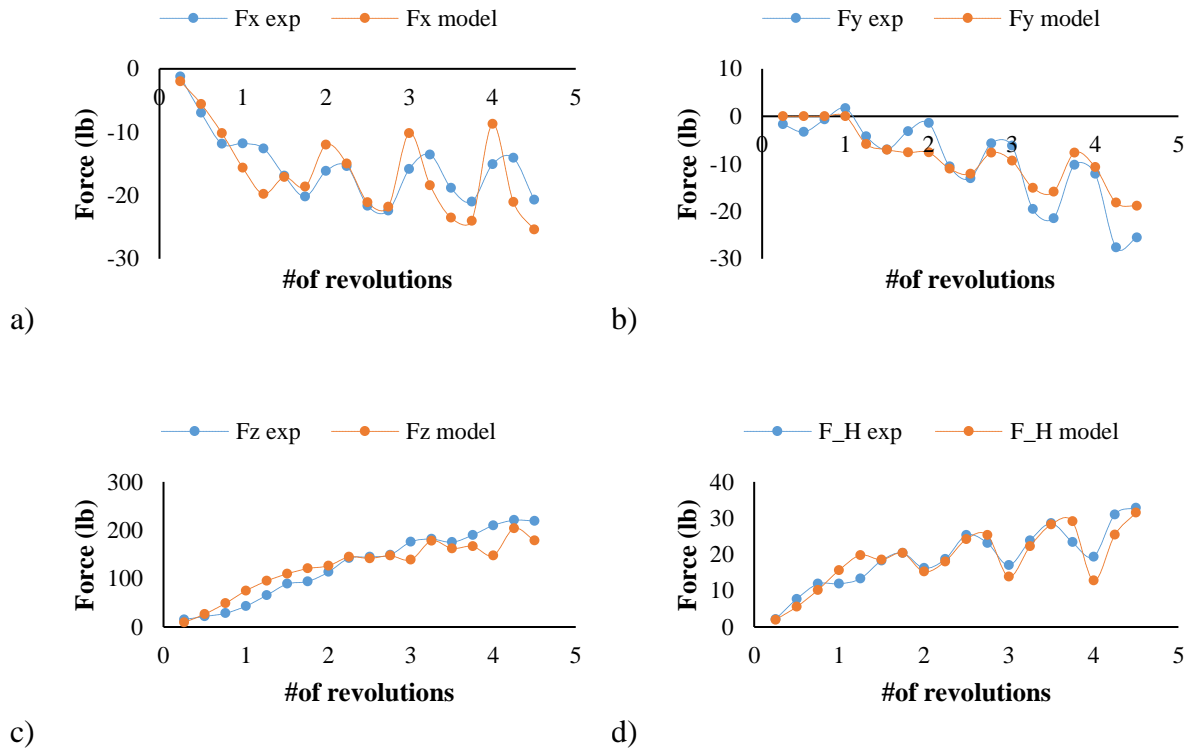


Figure 6-7: comparing forces from experiment and model, spiral set on marble 1

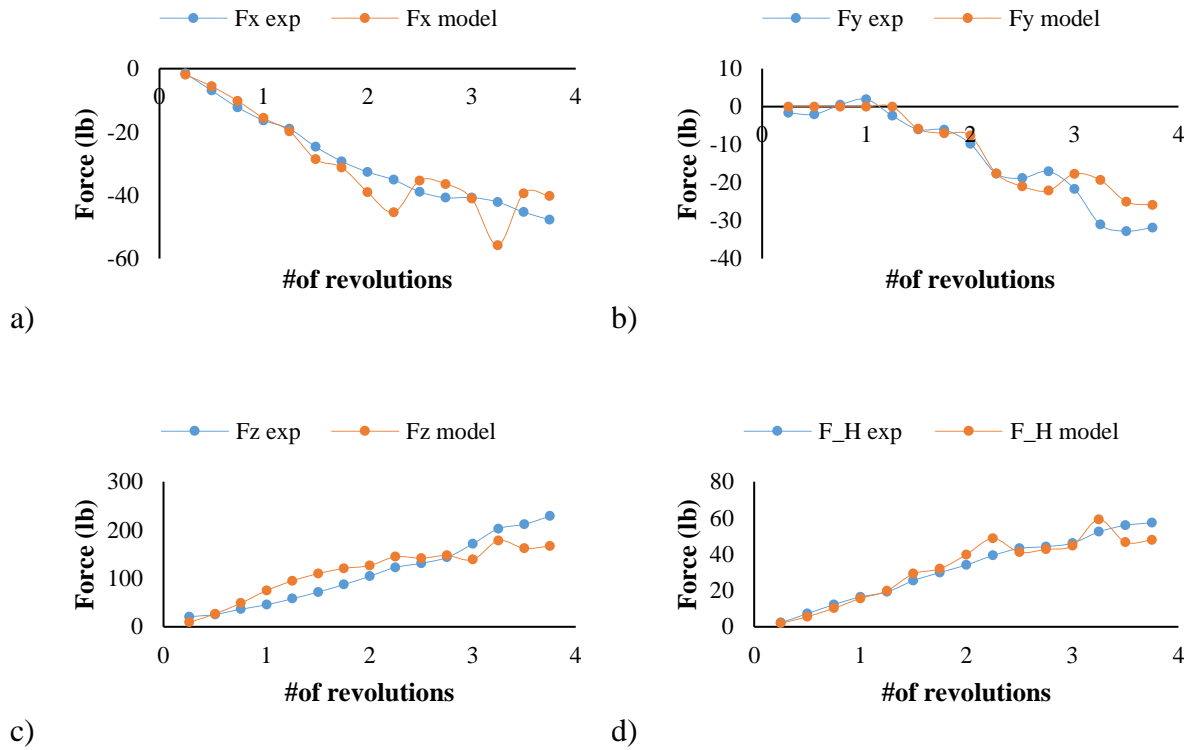


Figure 6-8: comparing forces from experiment and model, reverse spiral set on marble 1

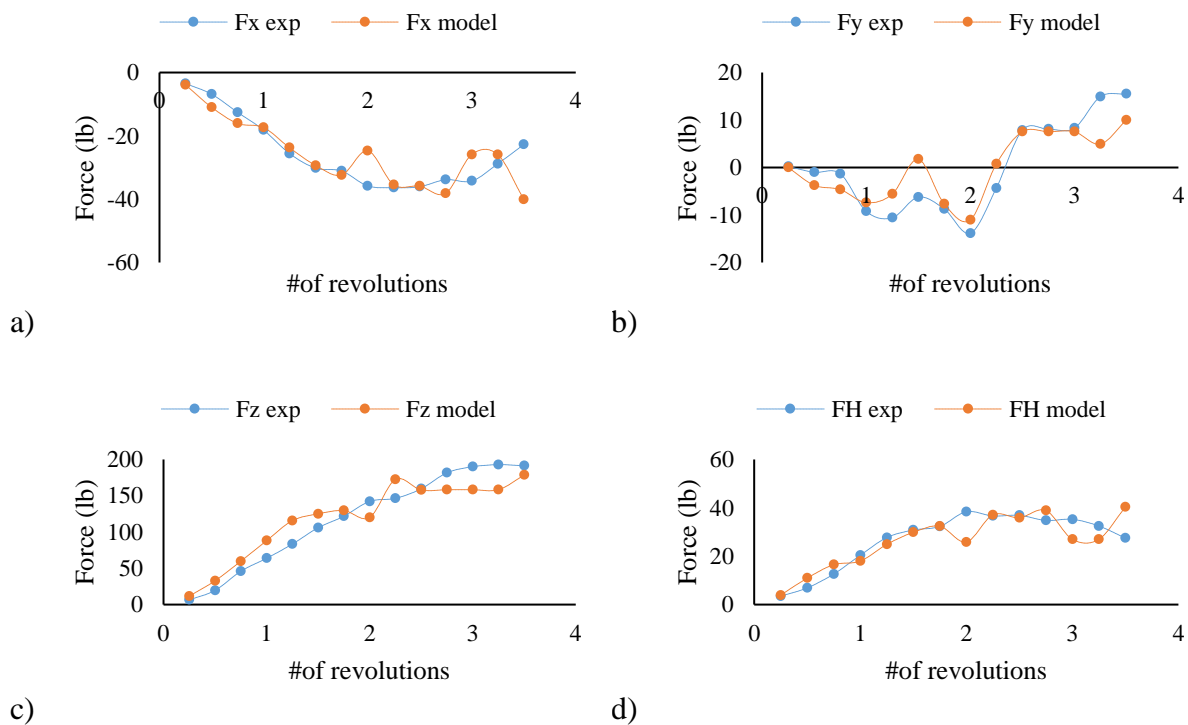


Figure 6-9: comparing forces from experiment and model, spiral set on limestone 1

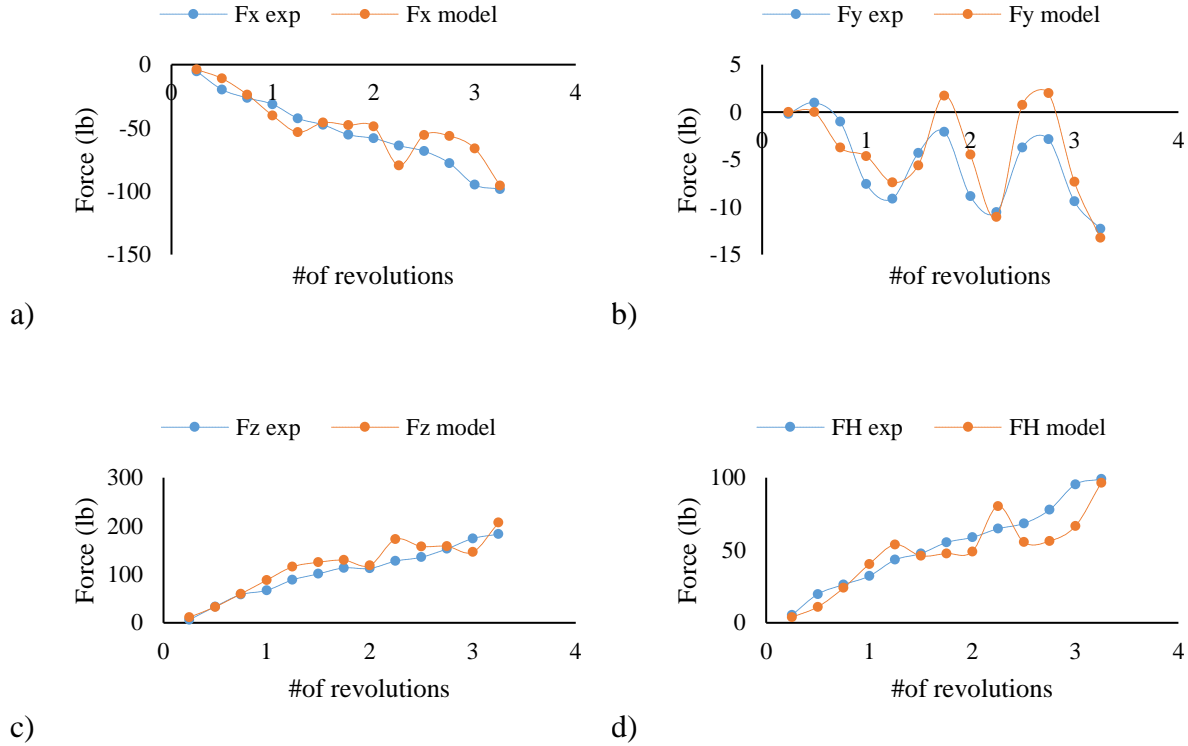


Figure 6-10: comparing forces from experiment and model, reverse spiral set on limestone 1

These figures show the agreement between the forces obtained for every quarter of revolution through the experiments and the forces developed by the model. Table 6-3 presents the average of the forces for two sets of cutters arrangements (*set 1* & *4*) based on the drilling parameters in the previous table. It is seen that the reverse spiral set (*set 4*) for both rocks generates higher forces on the plane of the bit when all other drilling conditions are constant. For all other tests, details of forces obtained from the experiments and the model are presented in the tables in Appendix C. Figure 6-11 depicts how accurate the model matches with experimental forces. The forces are averaged from the first touch between the rock and the cutter to the last touch, when the rotation is stopped.

Table 6-3: average results for the experimental and model forces on two discussed samples

No.	Sample	SET	F_X (lb)	F_Y (lb)	F_Z (lb)	F_H (lb)
1	Marble 1	Set 1 (Exp.)	-15.3	-9.5	126.7	17.4
		Set 1 (Model)	-16.1	-7.6	123.5	17.9
2	Marble 1	Set 4 (Exp.)	-28.9	-13.1	110.8	32.3
		Set 4 (Model)	-29.7	-11.3	112.8	31.9
3	Limestone 1	Set 1 (Exp.)	-25.1	1	117.9	26.5
		Set 1 (Model)	-25.8	-1.2	119.3	27.4
4	Limestone 1	Set 4 (Exp.)	-53	-5.5	104.1	53.4
		Set 4 (Model)	-48.3	-4.1	117.1	48.6

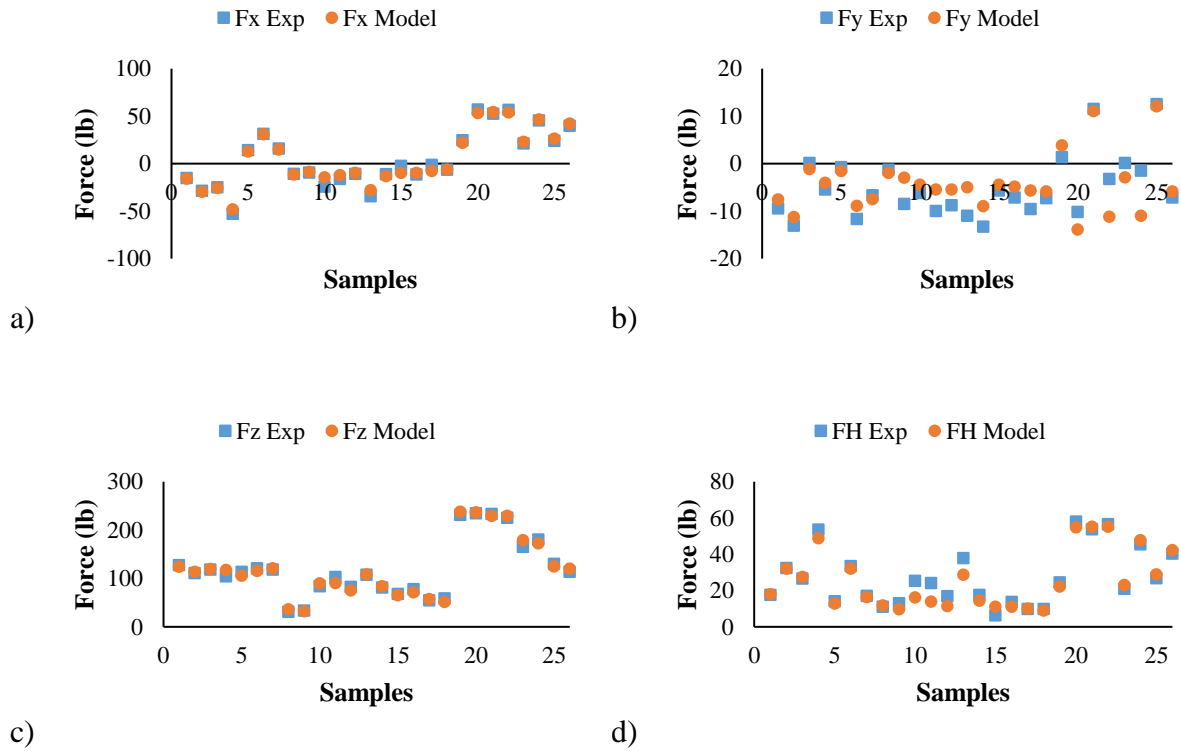


Figure 6-11: comparing the results obtained from the experiments and the model for 26 samples

Comparing the average forces, (average of the entire process) obtained from the experiments and the applied model in Table 6-4 provides the accuracy of the model. The deviation of the model from the experiments on lateral force on the plane is less than 2 *lb* and in vertical

force is 1 *lb*. It seems that the model provides a robust tool to predict the forces on the bit plane (F_H) and normal to the bit profile (F_Z).

Table 6-4: deviation of the model from the experiments

Sample	F_X	F_Y	F_Z	F_H
Average of Experiments (lb.)	4.51	-5.70	119.15	27.07
Average of Model (lb.)	4.78	-4.30	119.04	25.4
Error or Deviation (%)	6 %	24.5 %	0.1 %	6.2 %

6.3.1 Reasons for Deviation of the Results

The main sources of the error in results obtained from the model include:

- It is assumed that the rock is completely flat, the cutters are the same and they have no exposure or difference in height from the bit plane. Therefore, they all meet the rock at the same time. If for any reason, the tested rock surface is not precisely flat or all the cutters could not touch and cut the rock at the same time, then, this affects the calculation of the cutting area, which is precisely done, based on that initial assumption.
- The load cell capacity is 5000 *lb* in *z*-axis and 2500 *lb* in *x*, and *y*-axis. The range of the measured forces in whole the process is usually less than 20% of the maximum capacity. This also may reduce the accuracy of the force sampling.
- The sensor is placed in a stainless steel box with 1" thickness, and the wiring has been connected the sensor through the rotating shaft to the data acquisition system 20 *ft* away from the source. As the portion of the wiring is not covered by the highly sensitive materials, having small range of the noise is predictable during the sampling.

- In a part of the experiments, the low rate of penetration ($doc=0.5 \text{ mm/rev}$) mainly engaged the chamfer into the cutting action; while, for the sake of simplicity, in the analysis of the results and calculation of the engagement area, the chamfer impact is neglected.

It should be also reported that about 15% of all the experiments conducted in this work (~80 tests), have been removed from the analysis part due to very large error that they had, because of the possible practical mistakes or the abovementioned sources of error.

6.3.2 Parameters Applied to Force Model

It is being said that three parameters (ζ, ε, μ) are needed to build the force model on the cutters. To find the parameters and calibrate them into the model, there are two remarks to start with.

1. Friction coefficient (μ) can be estimated through the $w-t$ diagram (will be discussed later in section 6.5).
2. Specific intrinsic energy (ε) and the value of ζ are dependent (equation 6-16).

Because the total normal force on the bit (WOB) is the summation of all axial forces on every cutter, while ζ and ε are constant for a given formation. Rock strength can be estimated from single cutter tests or the sonic test results.

$$F_z = \sum_{i=1}^{n=k} F_{n_i} = \sum_{i=1}^{n=k} (\zeta \varepsilon A)_i = (\zeta \varepsilon) \sum_{i=1}^{n=k} (A)_i \quad (6-16)$$

Using the abovementioned method, the required parameters to obtain the forces on the cutters from the model are calibrated and presented in Table 6-5.

Table 6-5: rock parameters obtained to model forces on all other samples

Sample	ϵ (psi)	μ	ζ	DOC
Marble 2	6000	0.20	1.6	1
Sandstone 3	5000	0.12	1.55	1
Limestone 2	4000	0.20	1.5	1
Sandstone 4	3800	0.15	1.1	1
Shale (Oil)	3000	0.09	1	0.5
Sandstone 1 (Oil)	4000	0.13	1.5	0.5
Sandstone 1 (Water)	4000	0.11	1.5	0.5
Sandstone 1 (Air)	4000	0.18	1.3	0.5
Marble 1	4200	0.17	1.9	0.5

6.4 Impact of Cutters Arrangements on Bit Performance

The impact of different cutter layouts (spiral and reverse spiral sets of cutters with different distances between the cutters) on a few parameters (MSE, torque, and the removed rock volume) can be studied.

6.4.1 Effect on Torque and MSE

Every cutter has its own cutting area engaged with the formation during the rock cutting process. The cutting area passes a circular path, removes rock volume, and leaves a groove. Multiplication of the cross-section of a groove and the length of the cutting path for every cutter provides the amount of rock volume that is supposed to be removed by a cutter. The impact of each cutter share in removing rock volume can be studied to find the optimum cutters arrangement. A question is raised here to see if there is any relation between the bit performance or drilling results and the way of cutters engagement in the process. In other words, having the cutters evenly engaged is more efficient or uneven engagement. The percentage of every cutter engagement in rock volume removing process is showed by $\%V_i$ and the parameter of Δ , (*total volume share*), $\Delta = \%V_1 * \%V_2 * \%V_3$, is used to evaluate the bit impact. The higher value of Δ implies more

evenly cutters engagement. For instance, if all cutters have the equal share in cutting the rock ($1/3$), then $\Delta = \% 1/27$. To obtain $\%Vi$ for every cutter, the cutting area of the cutter in every $1/4$ of revolution is measured, then, it is multiplied by the $1/4$ of perimeter of the cutting path.

The relationship between the scaled torques (will be introduced in next section) and Δ for different tests using triple cutters in spiral and reverse spiral sets have been presented in figures below. Although, it seems by decreasing the total volume share, the scaled torque for every test increases; there are some exceptions, as well. For instance, the trend is not followed in cutting the shale with a spiral set of cutters. It should be noted that all of these tests have been conducted under atmospheric pressure, with $DOC = 0.5 \text{ mm/rev}$, and $RPM = 120$ in presence of oil /water.

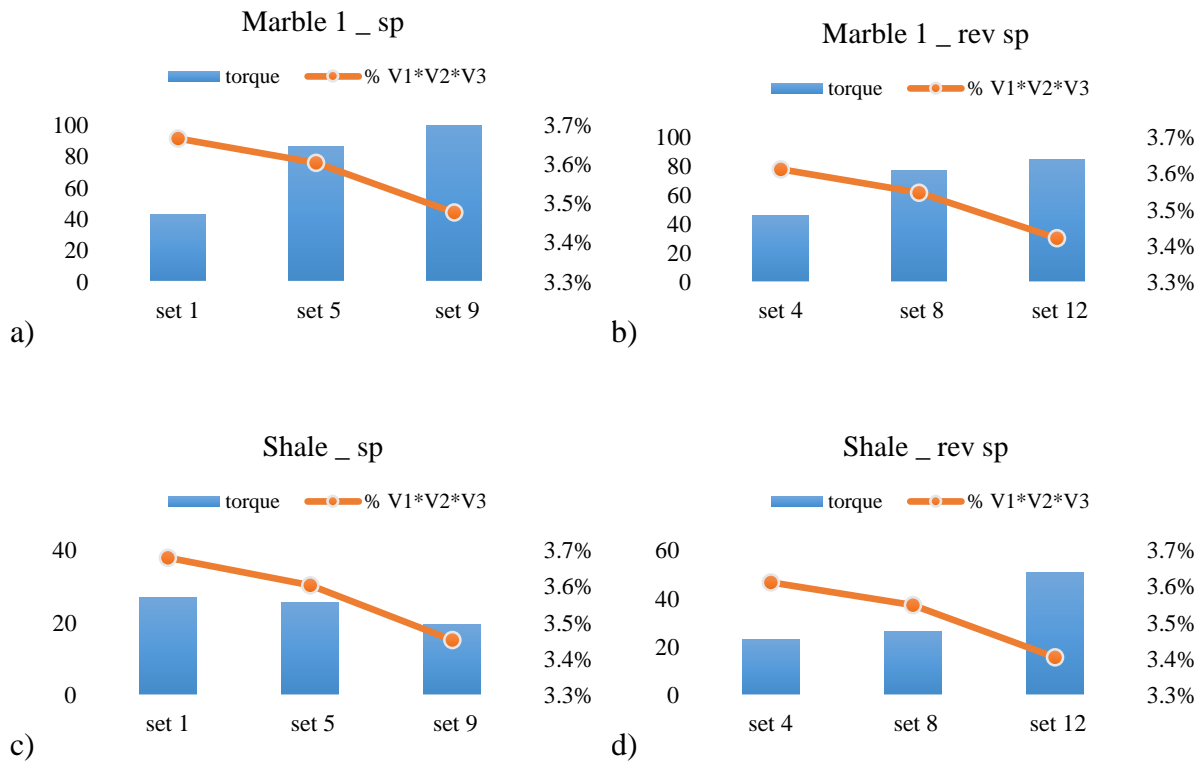


Figure 6-12: relation between total volume share and torque for different samples

Nevertheless, by comparing the total volume share (Δ) and MSE, no specific trend can be defined. It appears that among the cutters sets used in this study, the impact of the bit from the total volume share perspective does not provide a reliable trend on the MSE.

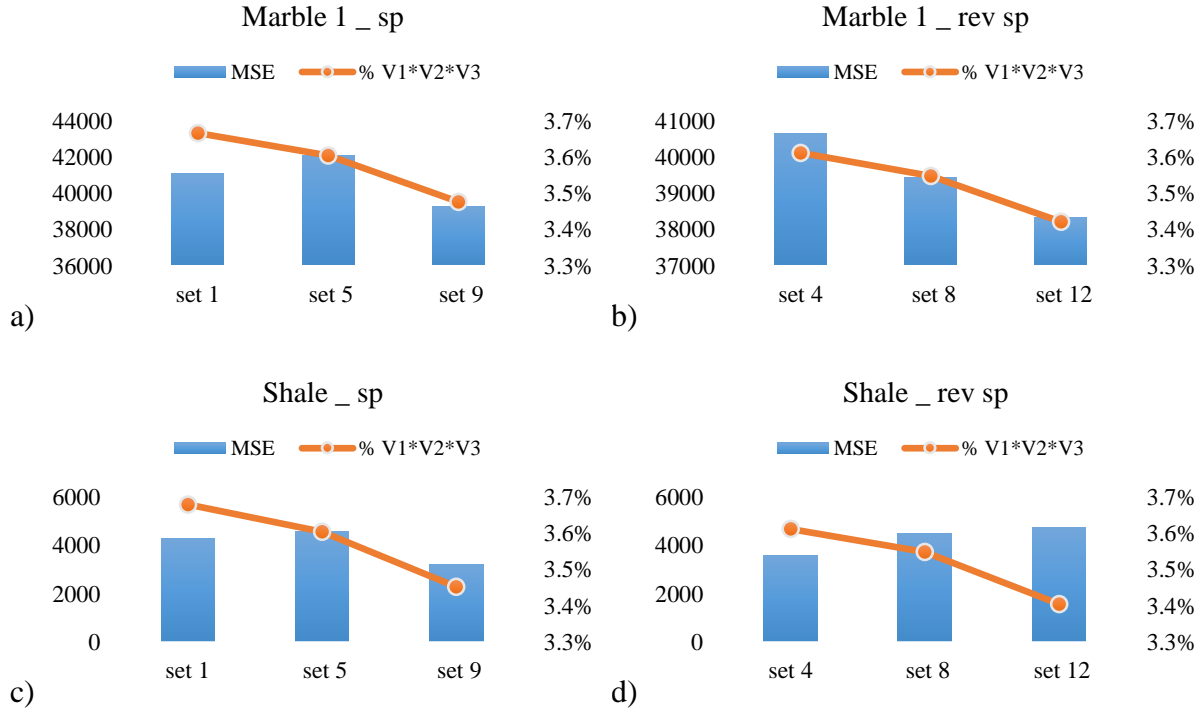


Figure 6-13: relation between total volume share and MSE for different samples

Another method to evaluate the effect of cutters arrangements on MSE is to plot and study the trend of both graphs (MSE and Δ) at entire process (Figure 6-14). It is recognized that they strongly depend on each other. For a set of cutters that the total volume share smoothly changes, same trend is seen for MSE. However, for a set of cutters where Δ fluctuates harder (such as *set 9*) the changes in MSE is heavier, as well. In other words, for a bit with closer cutters (less space between the cutters in 2D plane projection) the percentage of rock volume cut by every cutter is extremely changed and ended up to the extreme frequency of MSE. Because, if they are set so close to each other, in some portions of revolutions, the engagement area of some cutters may be drastically dropped and causes the big changes in the total volume share of cutters. It can be

mentioned that arranging the cutters with larger space in between, may cause a smoother (less changes in) experienced MSE. It is realized that as expected, increasing the Δ , causes decreasing in MSE. Hence, it is recommended in designing the cutters locations, to consider the amount of volume that one cutter is supposed to cut comparing to others.

Figure 6-14 demonstrates the effect of various distances between the cutters on a bit used to cut the sandstone samples. All other drilling parameters are constant.

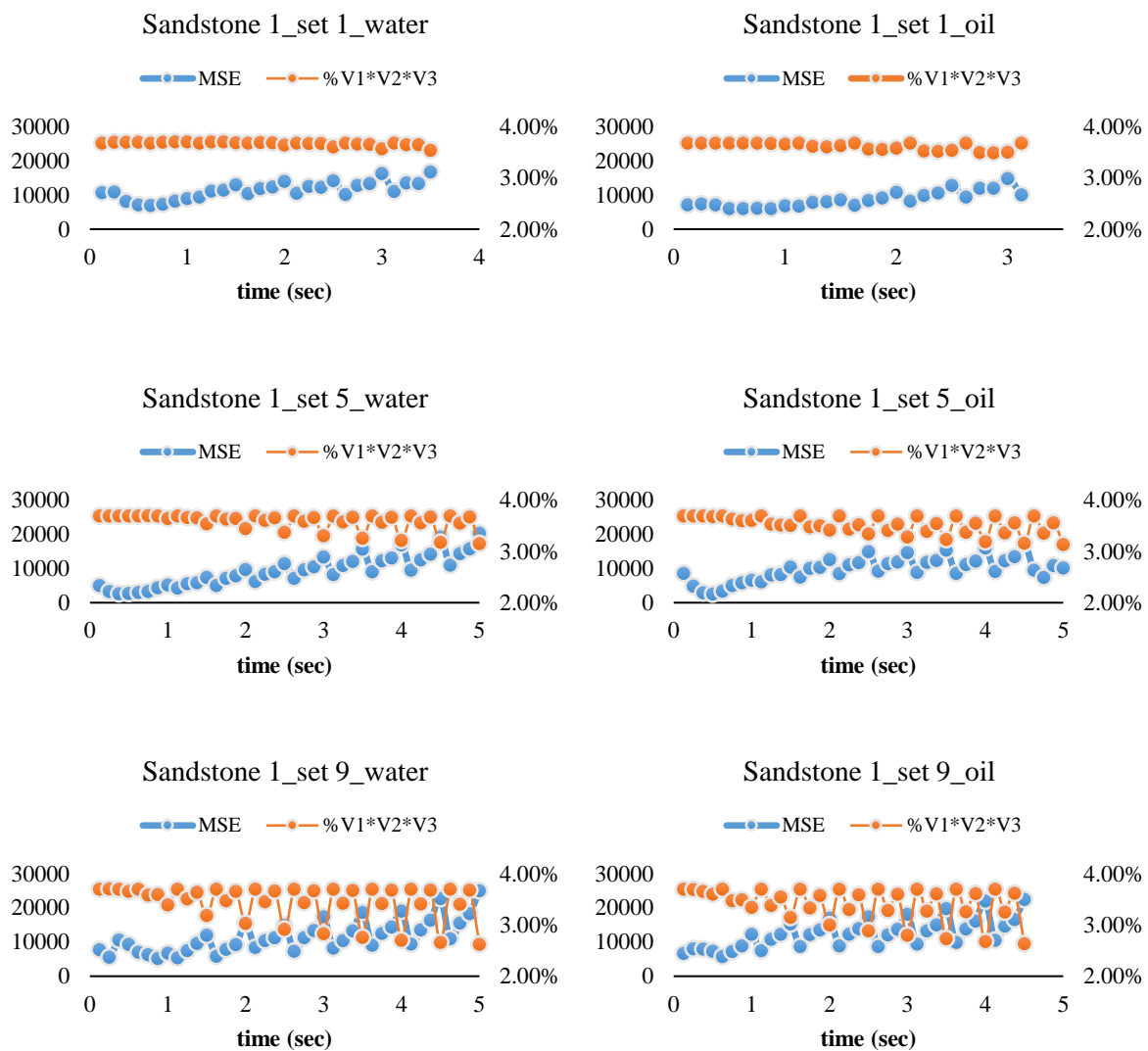


Figure 6-14: impact of total volume share on MSE based on time

6.4.2 Effect on Work Done by Bit

A comparison among the triple cutter tests on different rock samples has been done to study the effect of cutters arrangements (*spiral or reverse spiral sets*) on the work done by the cutters based on the measured MSE and lateral force per removed rock volume. In other words, to analyze which rock sample provides higher removed volume of the rock with lower lateral force or consumed energy. They can be considered as the more stable (lower lateral force) bit with higher drilling rate and more efficient (lower MSE) with higher rate of drilling.

It is depicted in Figure 6-15 that among all tests, the ratio of the lateral force to the removed rock volume for all rocks are lower with spiral sets of cutters than the reverse spiral sets. The top 4 performances based on the lateral force (Figure 6-15) are seen for *limestone 1 sp*, *sandstone 4 sp*, *limestone 2 sp*, and *marble 2 sp*, respectively. While, in MSE point of view (Figure 6-16), more efficient tests have been done on *limestone 1 sp*, *limestone 1 rev sp*, *limestone 2 rev sp*, and *limestone 2 sp*, respectively (Figure 6-16).

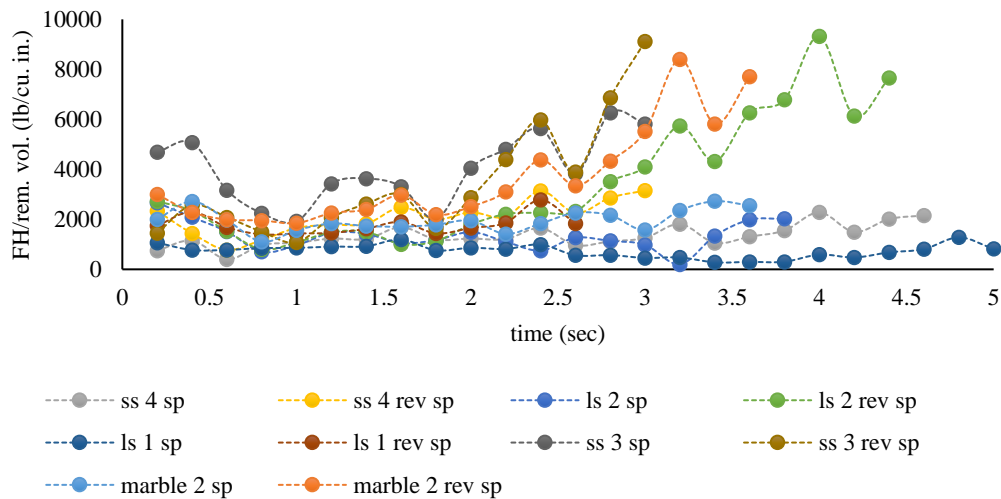


Figure 6-15: comparing lateral force per rock volume for different triple cutter tests

It can be concluded that considering both the stability (lateral force) and the removed rock volume is ended up to choose the spiral sets of cutters arrangements. While, to achieve the most efficient cutting process (lower MSE and higher removed volume), no globally comment can be added and it depends on the type of rock formation to drill. Looking lonely at MSE indicates the reverse spiral sets as the efficient sets of cutters.

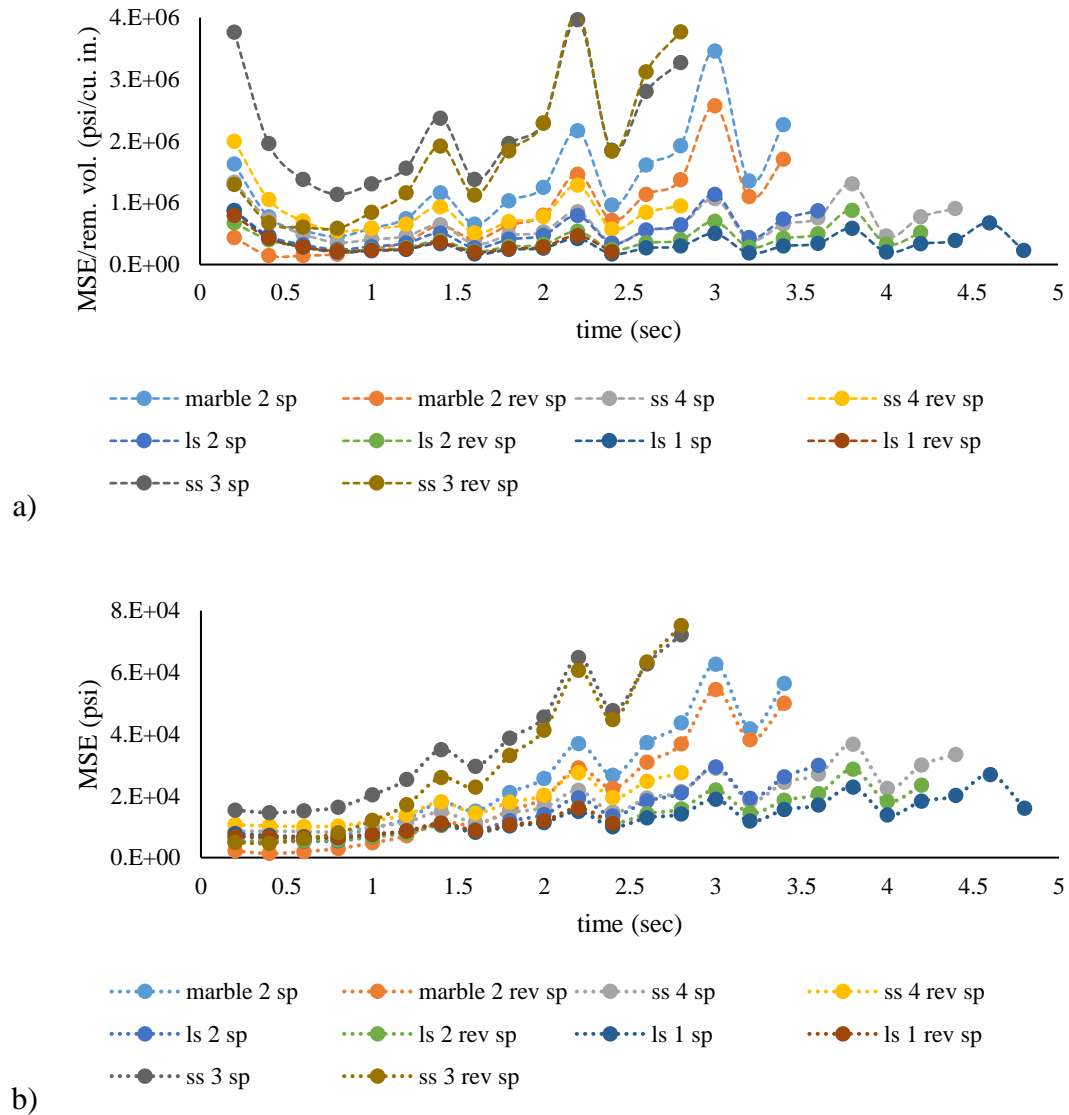


Figure 6-16: a) comparing MSE per rock volume for different triple cutter tests b) comparing MSE.

6.4.3 Effect on Rate of Removing Rock Volume

A short comparison is done only to consider the relation between the cutters arrangement (spiral or reverse spiral sets) and rate of removing volume by the cutters (in^3/sec). The relationship is depicted based on the MSE and volume rate. In all figures, the left axis is the rate of removed volume (in^3/sec), and the right axis is MSE (psi).

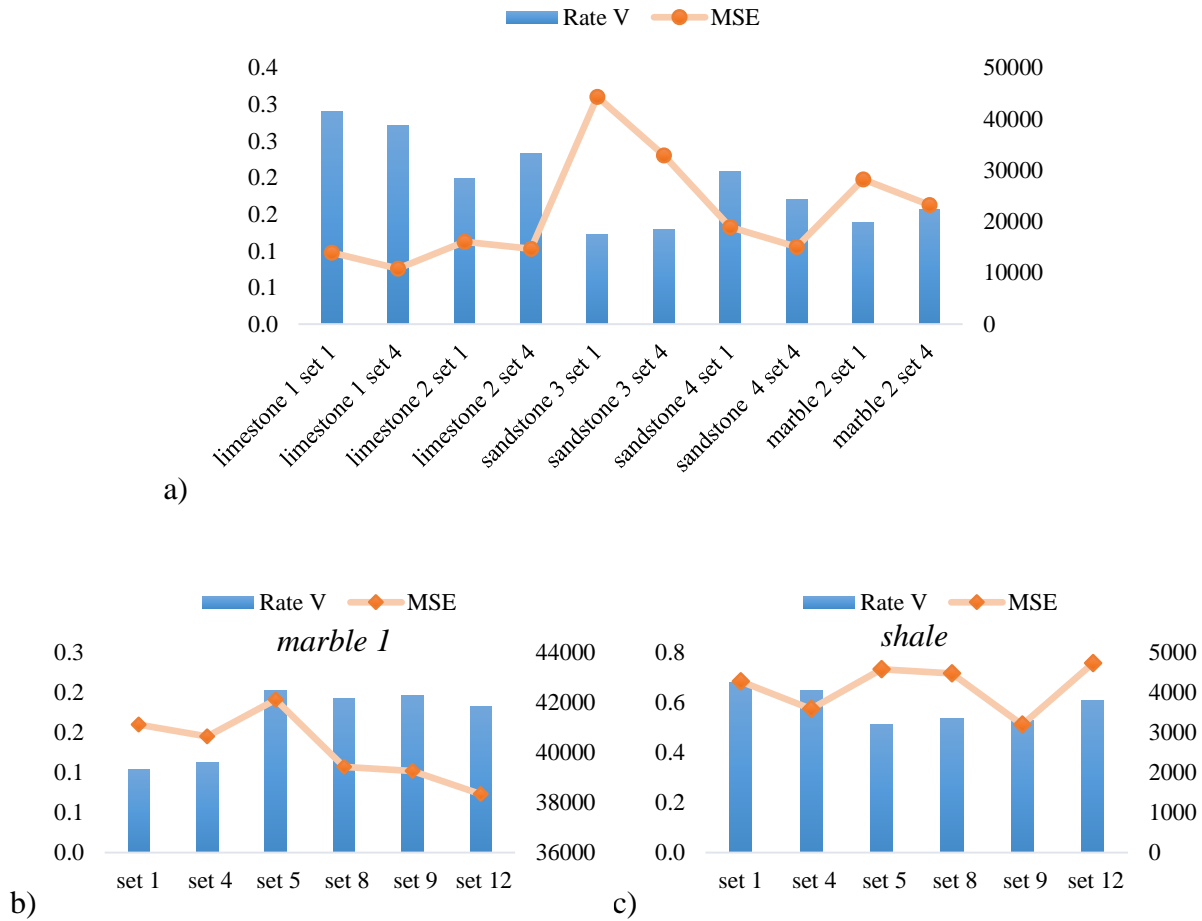


Figure 6-17: comparing MSE with the rate removing volume for (a) various samples DOC=1, RPM=75 (b) marble 1 DOC=0.5, RPM=120 (c) shale DOC=0.5 mm/rev, RPM=120

Almost in all tests, if all the drilling parameters are kept constant and only the direction of arrangement is changed, MSE is lower for reverse spiral sets (*set 4, 8, 12*) than the spiral sets (*set 1, 5, 9*). The trend for rate of volume removed is opposite, where it is higher for reverse spiral sets

and then decreases for spiral sets. This trend is repeated dominantly for all the tests, regardless of the distance between the cutters.

6.5 Bit Design

It was mentioned in chapter 2, that in 2008, Detournay *et al.* [50] developed their earlier model [39] into a more complete model for drag bits by further investigations on previous version. It was postulated that the cutting force could be decomposed into cutting component and frictional contact component. It was established by [50] that the drilling response of PDC bits obeys a linear constraint between torque, weight on bit, and depth of cut. They proposed a complete PDC bit response, based on the recognition of different drilling regimes. The drilling response model implies that forces on the bit, torque and weight on bit, only depend on the rate of penetration and angular velocity, which builds the depth of cut. Scaled weight (w) and scaled torque (t) are defined as following equations. Depth of cut per revolution (d) is proportional to the velocity ratio of ROP to angular velocity (ω). It should be noted that in this study, due to the some experimental restrictions regarding the depth of cut, another parameter should be defined and considered as called the equivalent cut thickness (ECT). This subject is explained in chapter 7.

$$w = \frac{WOB}{r_b(1 - \rho)} \quad (6-17)$$

$$t = \frac{2TOB}{r_b^2(1 - \rho^2)} \quad (6-18)$$

$$d = 2\pi/\omega * ROP \quad (6-19)$$

where r_b is bit radius and ρ is the ratio of inner to outer bit radius. In this work, it implies the ratio of the closest edge of the first cutter when touches the rock to furthest edge. [50] defined *alpha* (α) as the angle between the normal to cutting edge and the bit axis, which for a flat bit profile is zero *e.g.* the one is used in this study.

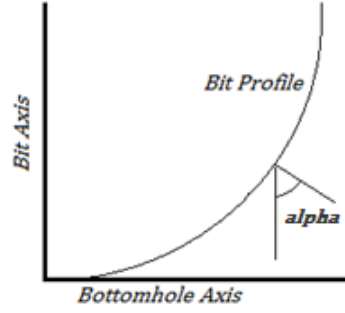


Figure 6-18: : Schematic of Bit Profile (after [50])

It is said that the general relationship between the scaled torque and scaled weight is introduced the drilling response of a drag bit. This is an assumed linear constraint between t and w based on the depth of cut, d , and can be defined as:

$$t = (\mu\gamma)w + (1 - \mu\gamma\zeta)\varepsilon d \quad (6-20)$$

where ε , d , and ζ are defined earlier. μ is the interface friction coefficient between rock and cutter and γ is the bit constant. It should be noted that ε depends on rock strength and borehole pressure and weakly on back rake angle of the cutter in a typical range of 10° to 20° .

6.5.1 Equivalent Cut Thickness (ECT) for Triple Cutter Bit

Similar to the single cutter tests (section 5.1) to better representing the depth of cut before reaching the stable condition (*e.g.* in transitional drilling), equivalent cut thickness (ECT) is introduced as the ratio of the total engagement area to the total width of cut. Different ECT's for several sets are plotted in Figure 6-19. It should be noted that total cutting area, total width of cut and accordingly, ECT are equal for both sets of spiral and reverse spiral sets as long as other parameters are constant. In Figure 6-19, blue dots show ECT when the nominal depth of cut is 1 mm/rev ($RPM = 75$ and $ROP = 1.25 \text{ mm/sec}$). Orange dots show ECT when the nominal $DOC = 0.5 \text{ mm/rev}$ ($RPM = 120$ and $ROP = \text{mm/sec}$) and the distance between the center of

adjacent cutters in a 2D plane is 5.5 *mm*. Same drilling conditions are followed for grey triangles; only the distance between the centers of cutters is reduced to 4 *mm/sec*. This distance is decreased to 2.5 *mm/sec* for yellow squares (the details of different sets are described in Table 4-1). The higher ECT is acquired when the cutters are farther (*set 1&2*) and depth of cut is higher (*blue dots*). The ECT will be used in next part, instead of *d* in obtaining the drilling response of a drag bit.

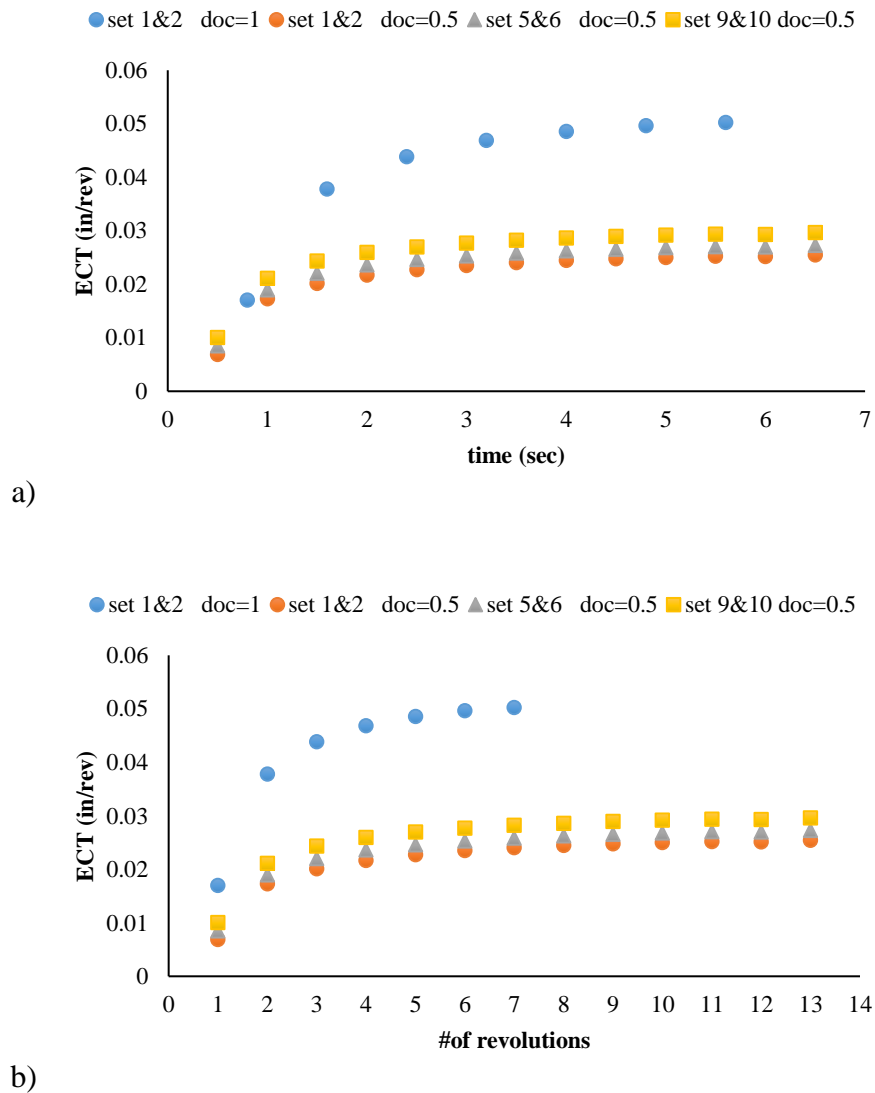


Figure 6-19: ECT for different sets based on (a) time and (b) number of revolutions

6.5.2 Drilling Response of Bit (t-w Diagram)

If the scaled torque of a test is plotted based on the scaled weight, then following the equation 6-20, the general response of the bit is achieved. The slope of the fitted line gives $(\mu\gamma)$ and the intercept provides $(1 - \mu\gamma\zeta)\varepsilon d$. For instance, this diagram is plotted for *sandstone 4* with *set 1* on *Bit 1* (Figure 6-20a). As the slope only depends on the friction and bit constant, then using a unique bit to cut one type of rock but under different drilling parameters, should give the same results. It is verified for single cutter tests but different depth of cuts in Figure 6-20b.

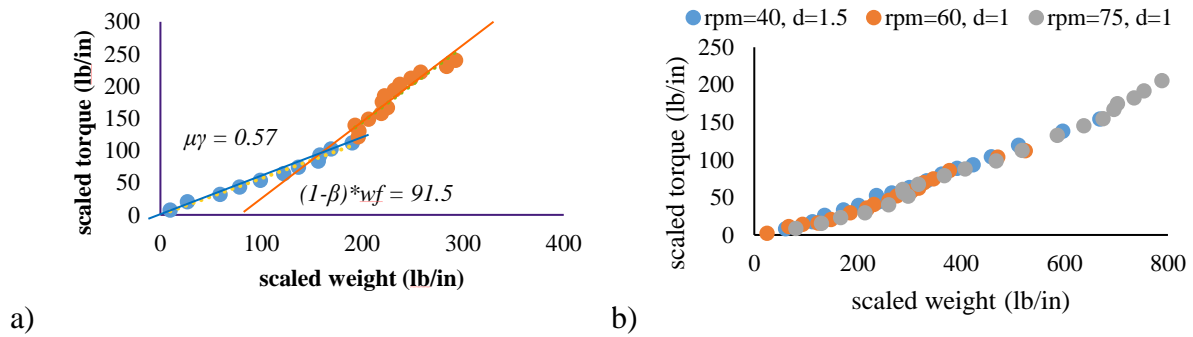


Figure 6-20: (a) conceptual response of triple cutter bit in t-w space (b) drilling response of one bit is independent from the drilling conditions.

A series of experiments by using triple PDC cutters in several arrangements have been presented to study the drilling response of different bits. In every test (every row in the table below), all the parameters are constant and only the location of the cutters is changed. Table 6-6 represents the slope of the linear drilling response of the bit $(\mu\gamma)$. It is seen the value of the slopes reduces when the distance between the adjacent cutters decreases (*Bit 1* is *set 1*, *Bit 2* is *set 5* and *Bit 3* is *set 9* in Table 4-1). Decreasing slopes for a given rock but different bits implies the reduction of the bit constants, since the friction coefficient is not changed for the same sample.

Therefore, the slope of the fitted line represents the changes in bit constants. Only, in cutting *Marble 1 sp* while the cutters are placed spirally, the trend is opposite and the slopes are increased.

Table 6-6: changes in slope of drilling response of the bit due to changes in the cutters arrangements on a given rock

Sample		Saturated	Bit 1	Bit 2	Bit 3
Sandstone 1	<i>sp</i>	water	0.75	0.72	0.68
Sandstone 1	<i>sp</i>	oil	0.77	0.75	0.74
Shale	<i>sp</i>	oil	0.77	0.67	0.52
Marble 1	<i>rev sp</i>	water	0.49	0.37	0.25
Marble 1	<i>sp</i>	water	0.31	0.36	0.49

The contents of the table are illustrated in Figure 6-21.

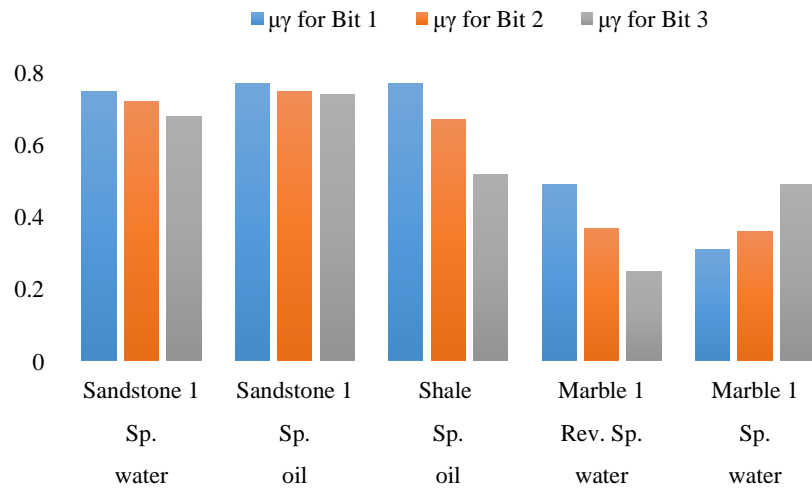


Figure 6-21: comparing the slope changes for different bits on a given rock sample

To the author, the only reason behind the observing different behavior on cutting the marble samples is due to the type of rock formation and the rock strength. Among the rocks that have been tested in this part of work to study the bit constant, *marble 1* is strongest rock that shows the highest MSE, torque and normal force along with lowest rate of removed rock volume (lowest cutting efficiency). Linear drilling response is based on the weight on bit and torque on bit and the ratio

of ring of cutters (ρ) and it can be used to get the bit constant. It seems that due to the nature of the rock, when the cutters are placed closer to each other (projected in a 2D plane), they cut more efficient (less MSE is required as measured in Table 5-6) and therefore, the bit constants increases.

6.5.3 Bit Constant

Bit constant can mathematically calculated based on the bit design parameters. It is said in [39] that the bit constant γ , encapsulates the influence of the orientation and distribution of the contact forces acting on the bit, which are strongly influenced by the bit design. In other words, a drill bit may be represented simply by a value as the constant γ . This constant can be controlled by the shape of the cutting edge and the cutters distribution on the bit; meaning that the cutter density or diamond density on a bit is formulated to design a bit for a given formation. Diamond density is a significant factor in bit design that represents the radial distribution of the cutters on a bit. It shows the number of cutters needed on a bit, their locations, and the distance between them. Number of cutters (n) that exist radially in different blades at any point (from bit center toward the gauge) is needed to calculate the bit constant following the method of [39]. Two quantities (κ_1, κ_2) are defined to consider the effect of the bit profile and the distribution of the cutters.

$$\Delta(\rho) = 1 + n\rho \quad (6-21)$$

$$\kappa_1 = \int_0^1 \Delta(\rho) d\rho \quad (6-22)$$

$$\kappa_2 = 2 \int_0^1 \frac{\rho \Delta(\rho)}{\cos \alpha(\rho)} d\rho \quad (6-23)$$

$$\gamma = \kappa_2 / \kappa_1 \quad (6-24)$$

where Δ is the radial contact length density, and ρ is the dimensionless radial coordinate based on r and α .

To simplify the calculation of bit constant proposed method by [39], it is found that for the circular PDC cutters, those equations for parameters κ_1 and κ_2 , can be converted to new equations.

$$\kappa_1 = N \times D_{cutter} \div R_{bit} \quad (6-25)$$

$$\kappa_2 = \sum_{i=1}^{i=k} n_i \times ((\frac{l_i}{R_{bit}})^2 - (\frac{l_{i-1}}{R_{bit}})^2) \quad (6-26)$$

where, N is total number of PDC cutters. D_{cutter} is the diameter of PDC cutter, and R_{bit} is the radius of the bit. In the second equation, n_i is the number of cutters in every portion of the cutting interval (n_i is an integer) which are engaged with the formation, l is the distance of every interval to the center, k is number of the intervals. The details of calculating the bit constant is explained in chapter 7.

In this work, a flat bit containing three circular and flat PDC cutters placed in different sets of radiuses is used to create three different drill bits (distance between the cutters varies). The way of cutters arranging (spiral or reverse spiral set) does not affect γ . The quantities of κ_1 , and κ_2 for different sets of cutters and the bit constants γ are presented in Table 6-7. The bit constants are reduced when the cutters on a bit placed closer to each other on a 2D plane. Figure 6-22 depicts schematically the number of cutters in all blades engaged in the cutting process at every portion of the interval. It counts the number of cutters involved in the engagement when they are projected on a 2D plane.

Table 6-7: bit constants based on the bit design parameters for different bits

	κ_1	κ_2	γ
Bit 1	0.446	0.667	1.497
Bit 2	0.446	0.652	1.463
Bit 3	0.446	0.637	1.429

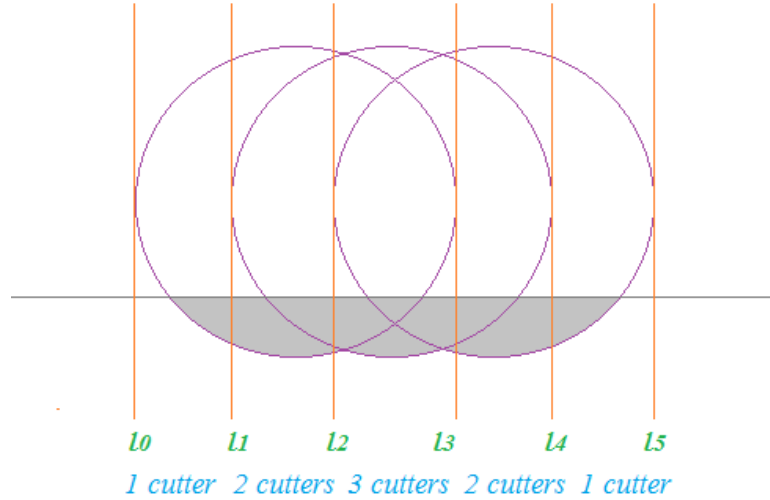


Figure 6-22: quantity of cutters involved in rock cutting process in every portion of an interval

The last step is to compare the calculated bit constant by the mathematical definition and the obtained bit constant based on the proposed model. In fact, having the slope of the drilling response of the bits and the friction coefficient applied in the model to predict the forces on the cutters can generate new bit constants, which is expected to be the same as the one obtained from the bit design (*Table 6-7*). It is verified that for all tests but *marble 1 sp*, it decreases as the cutters distances reduces. However, the range of value of these constants does not match with the ones obtained in *Table 6-7*.

Table 6-8: obtained bit constants follow the trend but not in the expected range

Sample		Saturated	Bit 1	Bit 2	Bit 3
Sandstone 1	<i>sp</i>	water	6.82	6.55	6.18
Sandstone 1	<i>sp</i>	oil	5.92	5.77	5.69
Shale	<i>sp</i>	oil	8.56	7.44	5.78
Marble 1	<i>rev sp</i>	water	2.88	2.18	1.47
Marble 1	<i>sp</i>	water	1.82	2.12	2.88

This can be due to the friction coefficient used in the proposed force model. The point is that friction coefficient was not measured in experimental tests and only was calibrated to assign in the force model. For instance, if the assigned friction coefficient to *sandstone 4 oil* changes to 0.51, then the obtained bit constants and calculated ones would be equal. Generally, it can be concluded that the proposed trend by [39] on the bit constants has been verified but the value of the constants strongly depend on the friction coefficient of the rock sample. This issue needs deeper study and experiments to be clarified.

7 APPLICATIONS

In drilling a deep well, proper bit selection and cutter forces prediction might be challenging, for the fact that most formations are not pure and homogenous. Heterogeneity that is typically found in drilling a downhole interval causes the changes in the stresses. The constant applied weight on bit while the formation strengths changes may constantly change the formation engagement with the bit. The abrupt transition from one type of rock to another type can be recognized at the surface as the fluctuations in rotary torque and ROP, which leverage the depth of cut to be changed. These ongoing changes in depth of cut could reduce ROP, stability, steerability, and durability of the bit or the cutters. Usually, the cost of the drilling process is defined in terms of these disfavor factors such as shocks and vibrations to downhole tools, slow penetration rate and damaged bits. It is desired to control these sudden changes on DOC to save the PDC cutters from breaking or damaging. It is said that due to some limitations in the MPC facility, the conducted experiments are all done before reaching the steady state condition, which is similar to the drilling condition in transitional interval between hard and soft formations. Therefore, the result of this method can be used to better understanding the bit-rock interaction in the transitional drilling. The proposed model can be employed to optimize the force distribution over the bit and reduce the bit instability. Bit stability may be enhanced by laying out the cutters, aiming to minimize the lateral forces on a bit. It is called a force-balanced PDC bit [4, 33, 53]. In this chapter, new cutters layouts are designed to study the bit performance by applying the proposed force model and comparing them with the numerical results from the simulation process.

7.1 Different Cutters Arrangements on a Bit

As noted previously, the bit-rock interaction model plays a key role in PDC bit design optimization. This optimization process requires the model to predict any changes in efficiency of

the bit if any design variable is changed. The global design variables *e.g.* cutters layout or number of cutters or blades, can widely affect the drilling efficiency [53]. A drill bit is made of tens of PDC cutters laying out on different blades. A ring of cutters on a drill bit contains few PDC cutters placed on different blades. In this work, two cutters arrangements have been experimentally studied on cutting different rock samples. However, there are many ways of laying out the cutters on a bit profile. In this chapter, different cutters arrangements are selected to study the bit performance. The proposed force model is applied to predict the forces on every cutter and then, evaluate the total horizontal forces on the bit. The engagement area and expected removed rock volume for every cutter are calculated by using a computer-aided design program. The equivalent cut thickness and the bit constants are computed for all bits. The location of the center of mass (CM) for each cutter and the direction of its movement after every revolution are considered to assign the radial force to a cutter with a proper direction. Five different bits (or five rings of cutters) are simulated via finite element method in a commercial package with exactly the same method and parameters as explained and used in chapter 3, for the triple cutter sets.

It is assumed that all bits are made of 5 PDC cutters with 13 *mm* diameter and 20° back rake angle. The cutters are placed on 5 blades (blades are symmetric to the *y axis*) with the constant 72° angular difference in between. In every set, the shortest distance between a cutter and the center of the bit is 60 *mm* and the longest distance can be maximum 80 *mm*. The cutters on *bit 1* are laid out spirally, where the cutters on *bit 2* are placed reverse spirally. Track set and Double Track set of cutters are assigned to *bit 3*, and *bit 4*. Track set means two cutters are located on the same radial locations. Double Track set can be pointed to a condition when two pairs of cutters are placed on the same radial locations. Cutters on *bit 5* are arranged differently (called in this chapter as Chen's model), following a model proposed by Chen *et al.* in [53]. The specification

of the bits (*i.e.* rings of cutters) are presented in Table 7-1. Figure 7-1 illustrates how the cutters and blades are named.

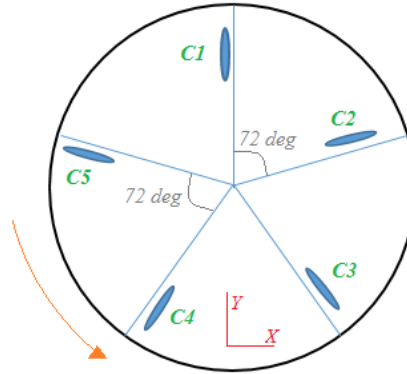


Figure 7-1: illustration of how the cutters are placed on a bit

Table 7-1: cutters setup on different bits

Cutters Arrangements	Name	R_1 mm	R_2 mm	R_3 mm	R_4 mm	R_5 mm
Spiral	Bit 1	60	65	70	75	80
Reverse Spiral	Bit 2	80	75	70	65	60
Track Set	Bit 3	75	80	70	75	60
Double Track Set	Bit 4	70	60	80	60	70
Chen's Model	Bit 5	70	80	65	75	60

The cutting area and the location of center of mass for every cutter are obtained through the CAD program. The movement direction of the CM (d_{CM}) for every cutter is obtained as Table 7-2: direction of the side force for every cutter. If the direction of the side (radial) force is toward the shoulder of the bit, then $d_{CM} = +1$ (in green), and if it points the side force to the center of the bit, then $d_{CM} = -1$ (in blue).

Table 7-2: direction of the side force for every cutter

	C_1	C_2	C_3	C_4	C_5
Bit 1	-1	+1	+1	+1	+1
Bit 2	+1	-1	-1	-1	-1
Bit 3	-1	+1	-1	+1	-1
Bit 4	+1	-1	+1	-1	+1
Bit 5	-1	+1	-1	+1	-1

The table shows that for a ring of cutters on a bit, when the distance of the adjacent cutters on a 2D plane continuously increases (spiral set) or decreases (reverse spiral), the radial (side) force for all cutters except C_1 , is toward the shoulder or toward the center, respectively. However, for other sets, when the cutters distances do not follow a straight trend, the direction of the side force is constantly changing. This is an important factor to consider in forming the lateral force on the plane of the bit. It is worth noting that technically, for the bit designers the significant cutters to study are the middle cutters in the rings (*cutter 2*, *cutter 3*, and *cutter 4*) and the edge cutters in the rings (*cutter 1* and *cutter 5*) are not much interested based on the current conditions in this study. Because, in our designed plane, there is no cutter after the edge cutters and the engagement portion of the bit is suddenly finished; while in a real bit, when the cutters are projected on a 2D plane, there is always another cutter in a row until gradually vanishing the cutting area and reaching the gauge pad.

The width of cut, the cutting area and the equivalent cut thickness for bits are plotted below. It is seen that the width of cut is equal for all bits. As expected, total cutting area is less for *bit 3* and *bit 4*, where the cutters are covered by other cutters (Track set and Double track set). Therefore, the ECT would be lower for these two bits. These two features (area and ECT) are almost equal for other three bits (Figure 7-2).

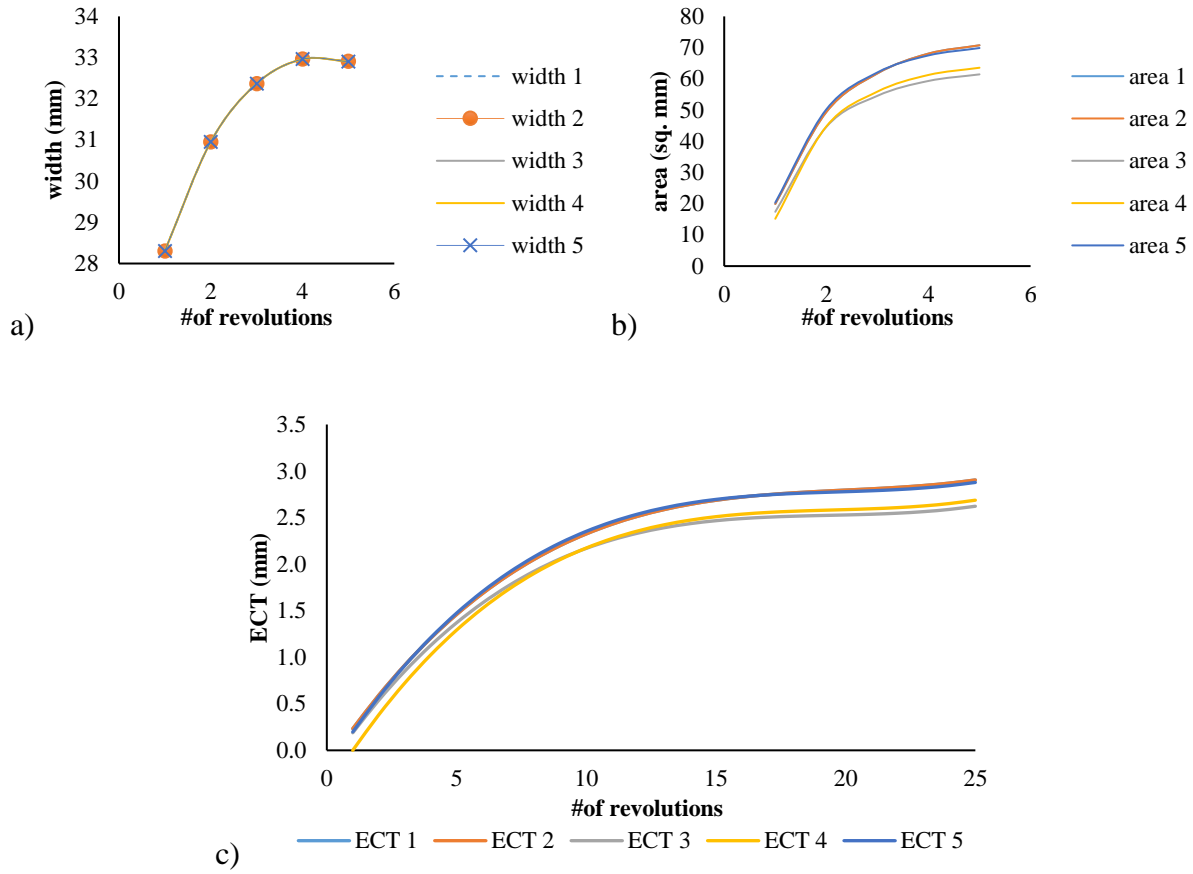


Figure 7-2: (a) total width of cut, (b) total cutting area, (c) ECT for all bits

The contribution of each cutter is calculated as well. Table 7-3 shows the cutters contribution in rock cutting process for every ring of cutters. It shows how much every cutter is engaged with the formation while the cutting progresses. A disproportionately high engagement by one cutter may accelerate the rate of dullness for that cutter, which needs more study to clarify.

Table 7-3: cutters contribution in rock cutting process by each cutter

	% C_1	% C_2	% C_3	% C_4	% C_5
Bit 1	24.9	18.5	18.5	18.5	19.7
Bit 2	23.8	17.9	17.9	17.9	18.8
Bit 3	15.2	23.3	16.2	15.2	27.7
Bit 4	9.8	17.9	28.4	20.5	21.8
Bit 5	17.6	20.8	17.6	18.4	21.8

7.1.1 Bit Constant

Bit constant (the concept was presented by [39]) is calculated for all the bits. It is said that for the circular PDC cutters in this study, the complicated equations to obtain the parameters of κ_1 and κ_2 , can be simply found by using the following equations.

$$\kappa_1 = N \times D_{cutter} \div R_{bit} \quad (7-1)$$

$$\kappa_2 = \sum_{i=1}^{i=k} n_i \times \left(\left(\frac{l_i}{R_{bit}} \right)^2 - \left(\frac{l_{i-1}}{R_{bit}} \right)^2 \right) \quad (7-2)$$

$$\gamma = \kappa_2 / \kappa_1 \quad (7-3)$$

where, N is total number of PDC cutters. D_{cutter} is the diameter of PDC cutter, and R_{bit} is the radius of the bit. In the second equation, n_i is the number of cutters in every portion of the cutting interval (n_i is an integer) which are engaged with the formation, l is the distance of every interval to the center, k is number of the intervals. Figure 7-3 schematically shows the number of cutters engaged in every portion of the cutting interval. The parameters l and n are seen for *Bit 1* where the cutters are laid out spirally; it would be the same for *Bit 2*, and *Bit 5*.

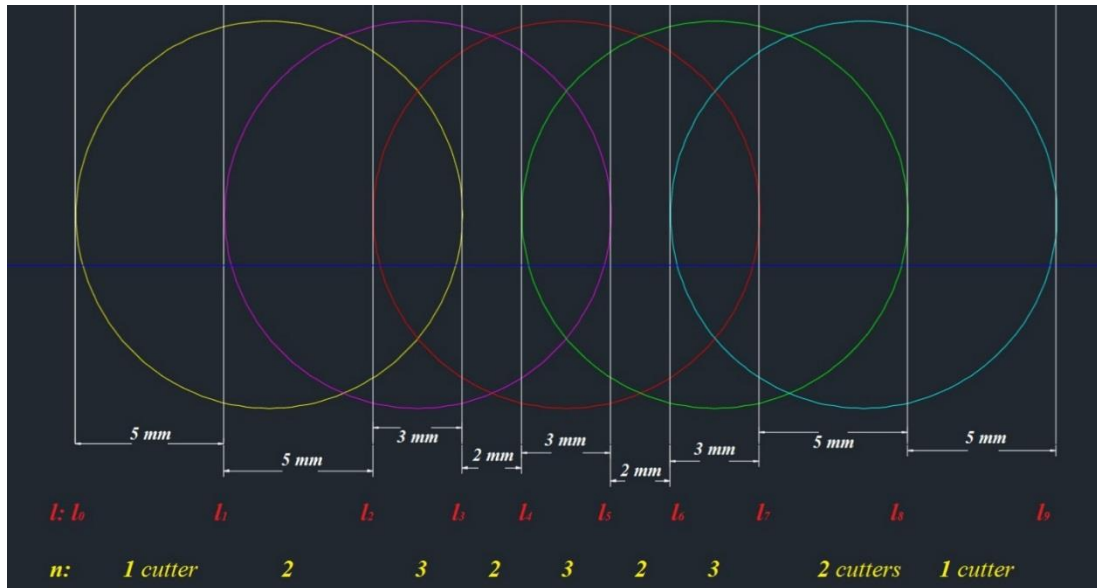


Figure 7-3: schematic of the cutters laid out for Bit 1, 2, and 5

The bit constants obtained mathematically are showed in Table 7-4. The values show that the location of the cutters affect the bit constant, where ultimately can affect the drilling response of a drag bit based on the w-t diagram presented by [50]. The location of the PDC cutters indicates the diamond density on a bit. It seems if diamonds are placed denser and closer to the center of the bit, the bit constant is lower; while, for a bit that the cutters are spread out wider and more toward the shoulder, this constant increases. This trend was found for triple cutter sets of cutters, as well.

Table 7-4: bit constants for different designed bits

	Bit 1	Bit 2	Bit 3	Bit 4	Bit 5
Bit Constant	1.40	1.40	1.44	1.36	1.40

7.2 Simulation of Cutting Process via FEM

Similar to section 3-4, the rock cutting process is simulated via finite element method/explicit but by assigning 5 cutters on a bit. All the parameters applied to the model are the same as the previous section. Only, the depth of cut is increased to 1.5 mm/rev . The rock properties assigned to the sample are selected in target of simulating shale cutting. The interaction property or the friction coefficient is set to 0.6. The density is 2700 kg/m^3 and the stress triaxiality is set to 0.25. The yield stress is 2900 psi , the friction angle is 60° and the dilation angle is set to 5° . The rock sample a square surface of 200 mm and 100 mm height. Height is divided into two partitions of 15 and 85. In 3D mesh model, a fine mesh with average element size of 0.5 mm is formed on top of the sample, while a coarse mesh with average element size of 3.5 mm is distributed throughout the rest of the rock piece, which makes totally 100800 elements assigned to the rock. Element type C3D8R is set to the elements in top partition of rock. The bottom of the rock sample is set to ENCASTRE while the boundary conditions for the sides are set to zero displacement. The bit is moving toward the rock with speed of 3 mm/sec and rotational

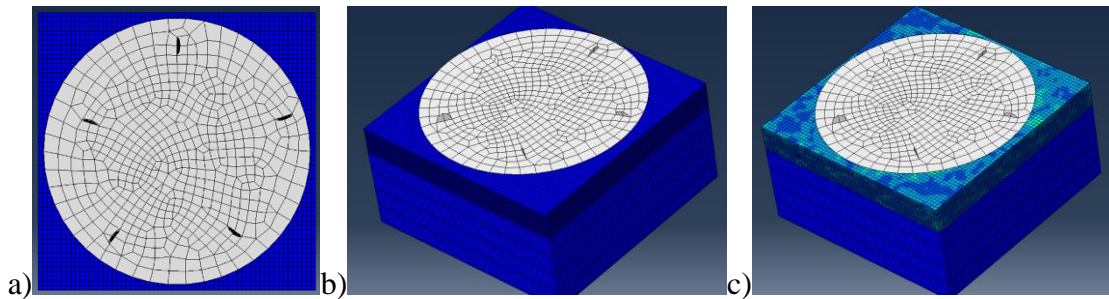
speed of 12.56 rad/sec , therefore, DOC be 1.5 mm/rev . The number of removed elements, the forces and torques on cutters in x , y and z direction are measured to calculate MSE and lateral force on the bit plane.

The numerical results show that changing the cutters arrangement on a bit can improve the MSE up to 22%; where *Bit 4 (Double Track)* has the lowest MSE while *Bit 1 (Spiral)* has the highest MSE. The lateral force can be interpreted as a tool to measure the bit stability [53]. Balanced or minimum lateral force could provide more stable bits. Double track set of cutters presents lower lateral force on the plane but the lowest removed rock volume, as well. *Bit 1, Bit 2*, cut the most volume of rock with higher MSE. Similar to report of [53], the single set cutters (e.g. *Bit 2, Bit 5*) drills more efficient. Single set means no cutters at the same radial or axial position after projecting into a 2D plane. Table 7-5 presents the numerical results. (M_z is torque around z).

Table 7-5: numerical results for all bits

	$F_X \text{ (lb)}$	$F_Y \text{ (lb)}$	$F_Z \text{ (lb)}$	$M_Z \text{ (in-lb)}$	$F_H \text{ (lb)}$	MSE (psi)	Removed Volume (cu. in.)
Bit 1	18	2.1	202.2	308.1	18.1	4204	0.920
Bit 2	18.5	0.7	189.6	296.1	18.5	4040	0.920
Bit 3	0.2	14.1	152.5	254.5	14.1	3480	0.918
Bit 4	1.5	1.1	182.6	237.4	1.8	3280	0.910
Bit 5	6.8	20.7	199.7	292.1	21.8	4004	0.916

In the figures below, different steps of rock cutting simulation are presented.



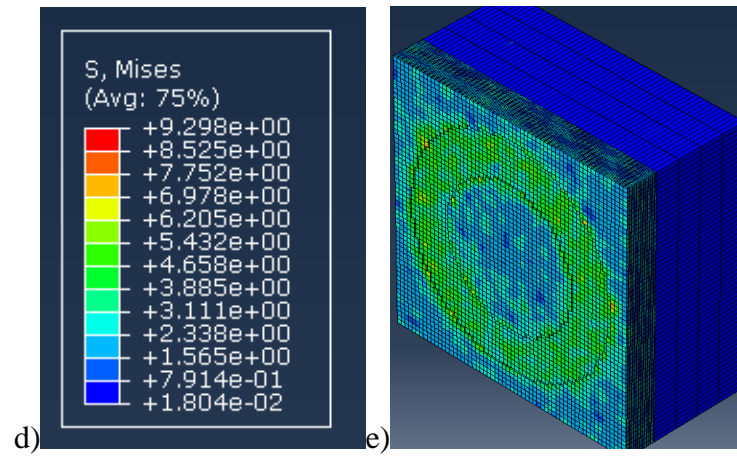


Figure 7-4: (a) bit plane containing the cutters right above the rock sample (b) before cutting starts (c) at the end of process (d) distortion energy density table (e) final shape of rock surface after the cut

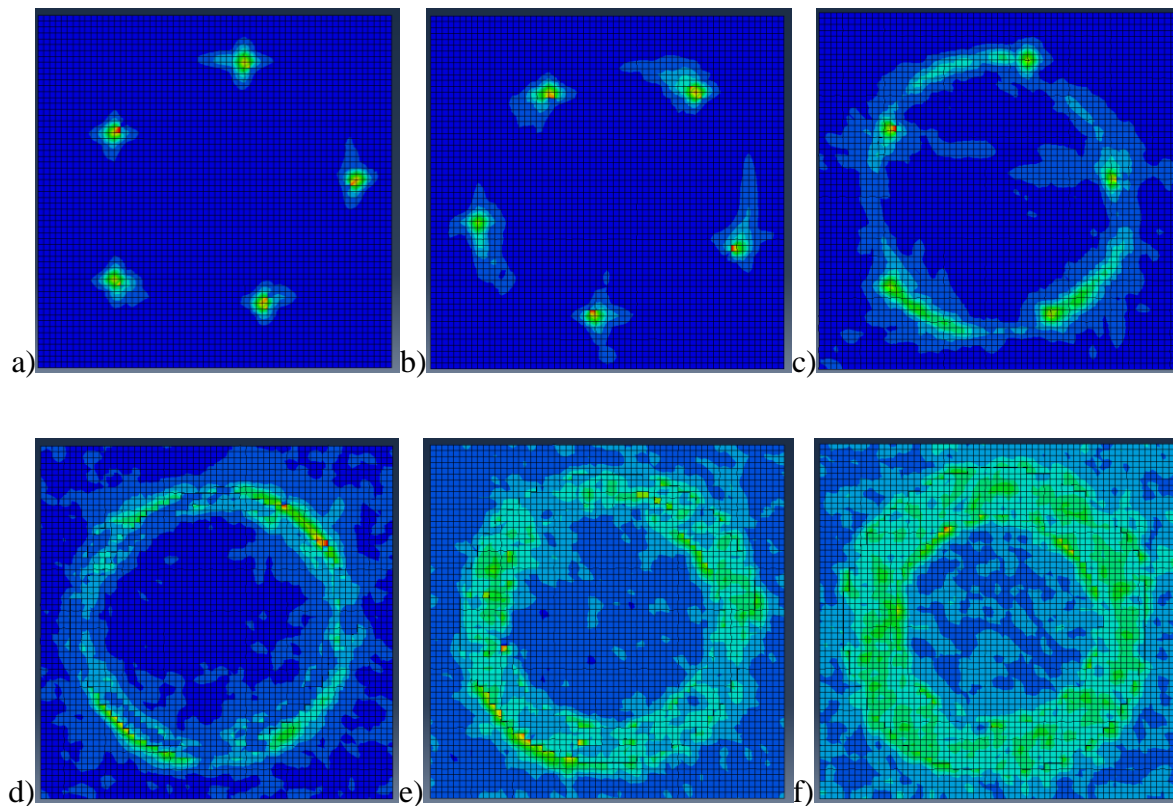


Figure 7-5: the screenshots of simulating the cutting process by using a bit of five cutters

7.3 Applied Forces Model to Cutters on Various Bits

By applying the force model to every cutter and then breaking the forces on a bit plane into x , and y directions, total forces on bit plane can be obtained. Table 7-6 shows the magnitude and direction of the forces on the cutters on *Bit 1* that are broken into x and y directions. For all other bits and cutters, cutters distribution over the bit is the same as Figure 7-6, only the direction of radial force should be considered. The contents of Table 7-2 play a key role in assigning the proper direction into the radial forces. It should be noted that the same method prescribed in the previous chapter is used to apply the model and obtain normal force, tangential force and radial force on every cutter on a bit.

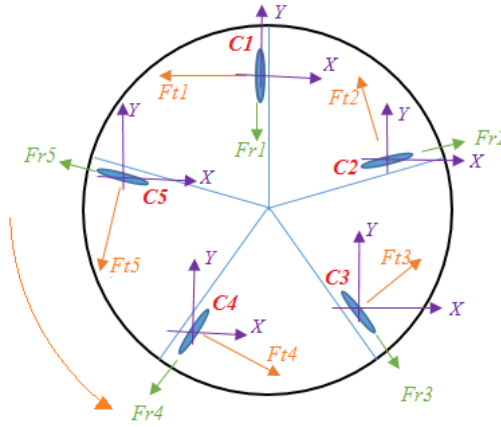


Figure 7-6: force components on every cutter decomposed in x and y directions

Table 7-6: breaking two forces into x and y components for cutters on Bit 1

	C_1	C_2	C_3	C_4	C_5
X	$-Ft1$	$Fr2 * \cos18$ $-Ft2 * \sin18$	$Fr3 * \sin36$ $+Ft3 * \cos36$	$-Fr4 * \sin36$ $+Ft4 * \cos36$	$-Fr5 * \cos18$ $-Ft5 * \sin18$
Y	$-Fr1$	$Fr2 * \sin18$ $+Ft2 * \cos18$	$-Fr3 * \cos36$ $+Ft3 * \sin36$	$-Fr4 * \cos36$ $-Ft4 * \sin36$	$Fr5 * \sin18$ $-Ft5 * \cos18$
Z	$Fn1$	$Fn2$	$Fn3$	$Fn4$	$Fn5$

$$F_x = \sum_{i=1}^{i=5} F_{Ci} \quad \text{in } x \text{ direction} \quad (7-3)$$

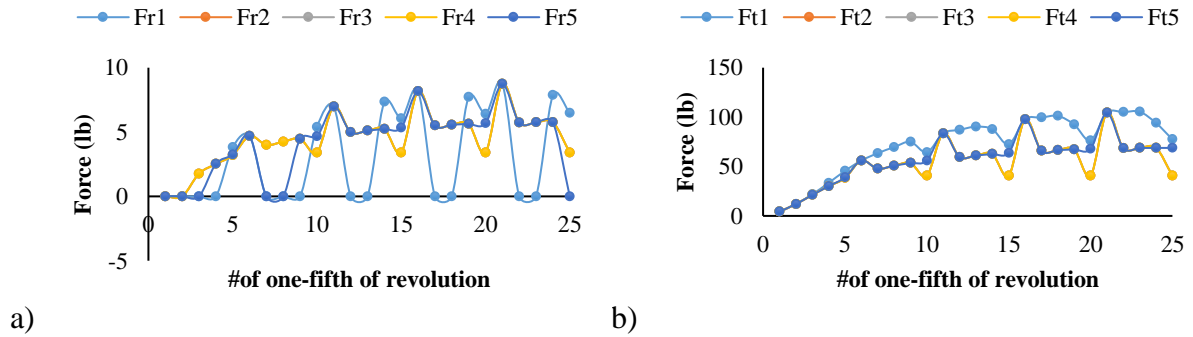
$$F_y = \sum_{i=1}^{i=5} F_{Ci} \quad \text{in } y \text{ direction} \quad (7-4)$$

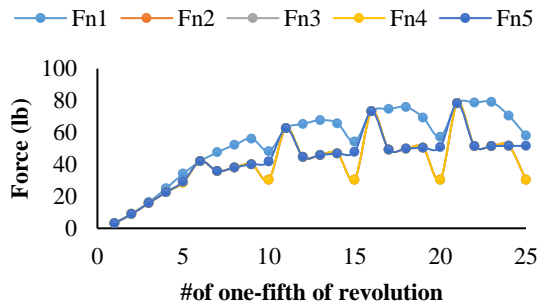
$$F_z = \sum_{i=1}^{i=5} F_{Ci} \quad \text{in } z \text{ direction} \quad (7-5)$$

where C_i varies from *cutter 1* to *cutter 5*. Summation of the forces in first row of the table provides F_x , and summation of the forces in second row, gives F_y . Torque around z -axis and forces estimated on every cutter on different bits are plotted in figures below.

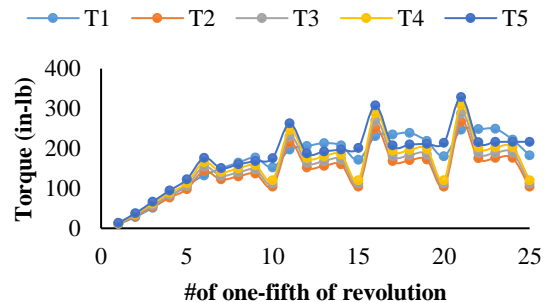
7.3.1 Cyclic loading (Fatigue) Effect on Cutters

Fatigue is the progressive and localized damage to molecular structure of a material and occurs when the material is subjected to cyclic loading [79]. PDC cutters experience cyclic loading and impact loading during the drilling that may cause the crack growth or the fracture on the specimen [80]. Overall, the repeated loading and unloading on polycrystalline diamond compact (PDC) reduce the resistance and durability of the cutter. Therefore, in bit design, the cyclic loading on the cutters should be considered. The model of force-distribution on the cutters demonstrates the cutters that are subjected to repeated impact or loading. Then, they can be treated by either changing the cutter layout or substituting with high-resistance materials. Figures below can be used to study this phenomenon on the cutters.



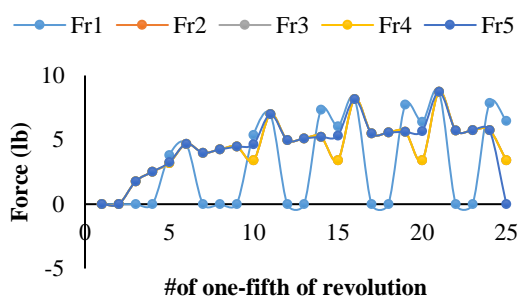


c)

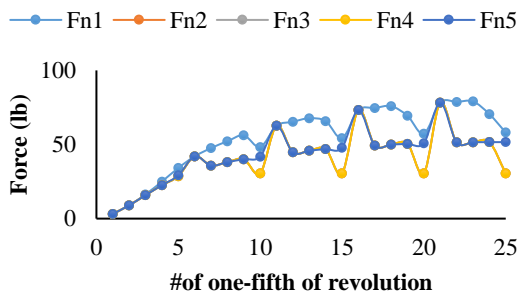
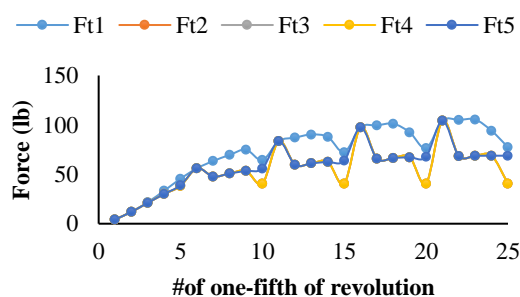


d)

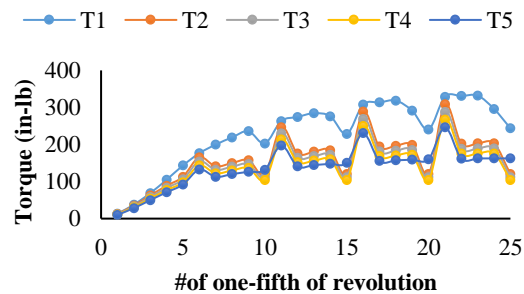
Figure 7-7: forces and torque on the cutters laid out on Bit 1, Spiral Seta)



b)

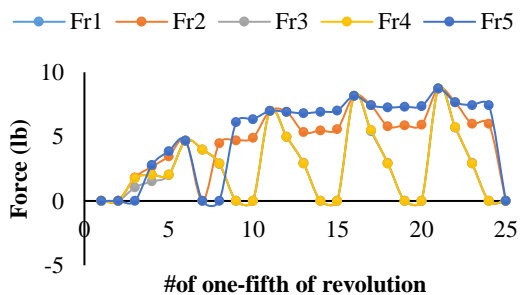


c)

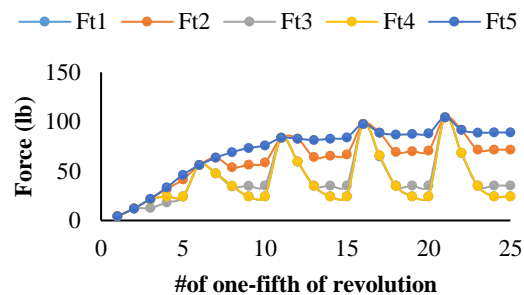


d)

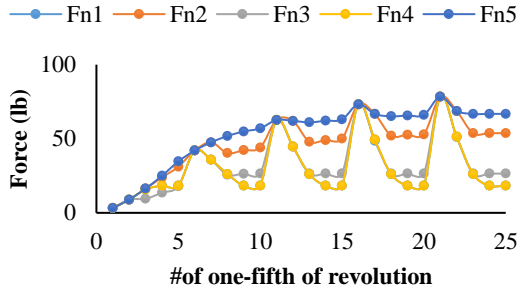
Figure 7-8: forces and torque on the cutters laid out on Bit 2, Reverse Spiral Set



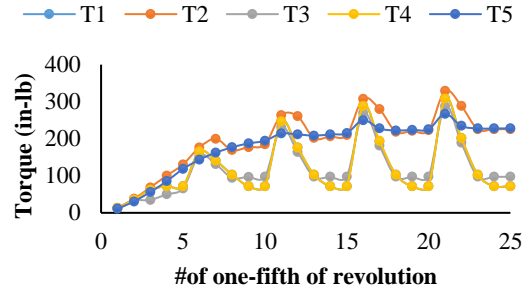
a)



b)

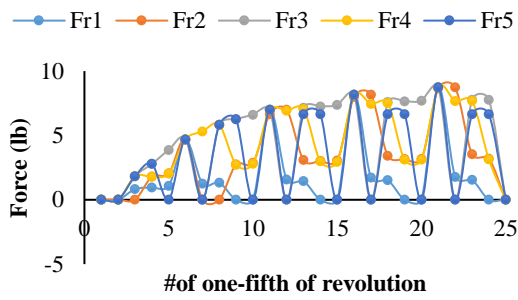


c)

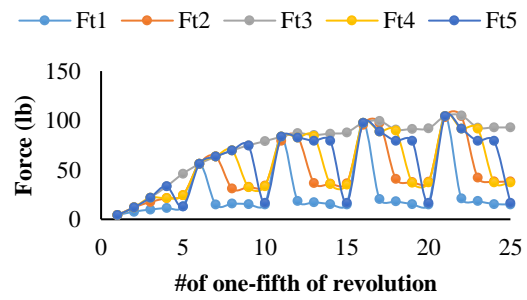


d)

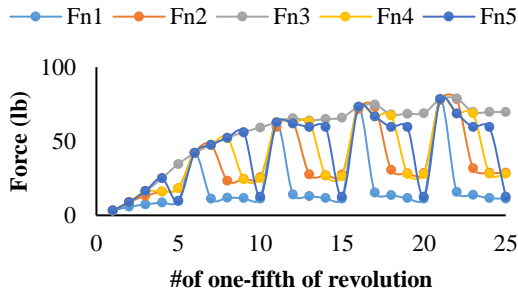
Figure 7-9: forces and torque on the cutters laid out on Bit 3, Track Set



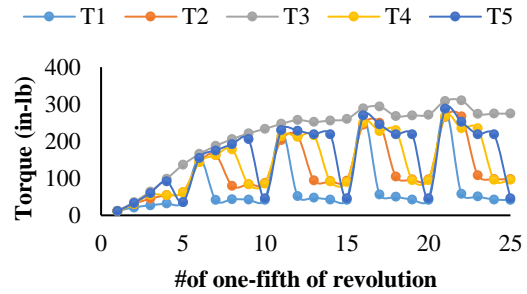
a)



b)

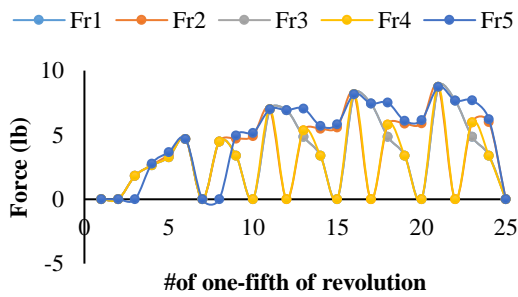


c)

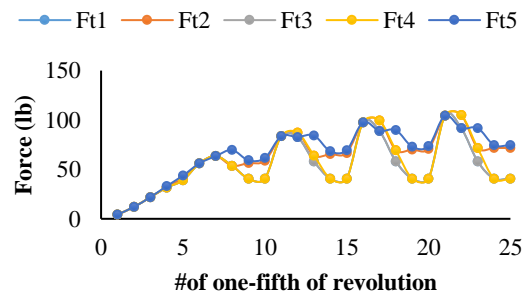


d)

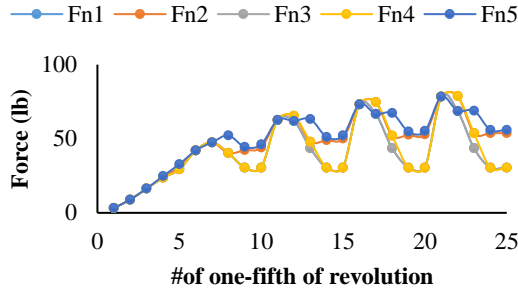
Figure 7-10: forces and torque on the cutters laid out on Bit 4, Double Track Set



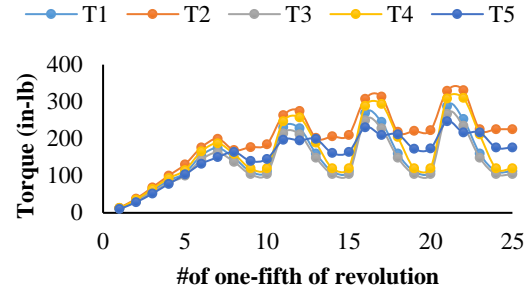
a)



b)



c)

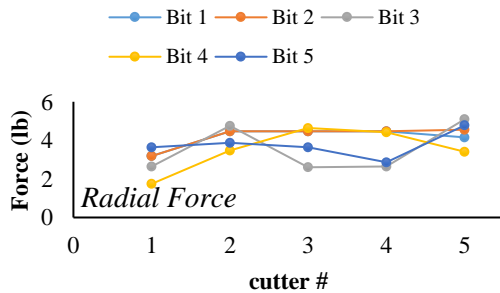


d)

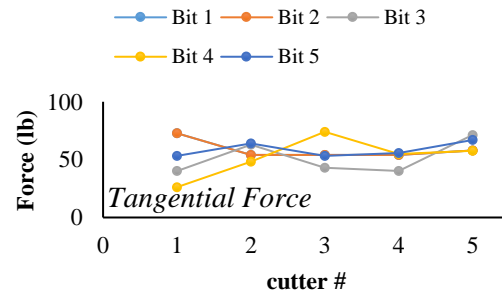
Figure 7-11: forces and torque on the cutters laid out on Bit 5 Chen's Model

The detail of the forces that the cutters are experienced during the pre-steady state condition (during the transitional drilling from one formation to the other) show that in *Bit 1* (spiral) and *Bit 2* (reverse spiral), almost all cutters are evenly distributed. In *Bit 3* (single track) and *Bit 5* (Chen's), the high frequency of loading and unloading is observed on *cutter 3* and *cutter 4*, and on *Bit 4* (double track) *cutter 2* and *cutter 4* are prone to be damaged. These cutters need more attention in bit design or in material selection.

In Figure 7-12, the contribution and the engagement of every cutter on different bits and the amount of the forces that the cutter experiences might be used as a tool to predict how fast one cutter can be worn or damaged. For instance, on *Bit 3* (colored grey), *cutter 2* and *cutter 5* withstand higher forces in all three directions. On the other hand, *cutter 3* in *Bit 3* (yellow) is the potential cutter in that ring to be worn or fractured.



a)



b)

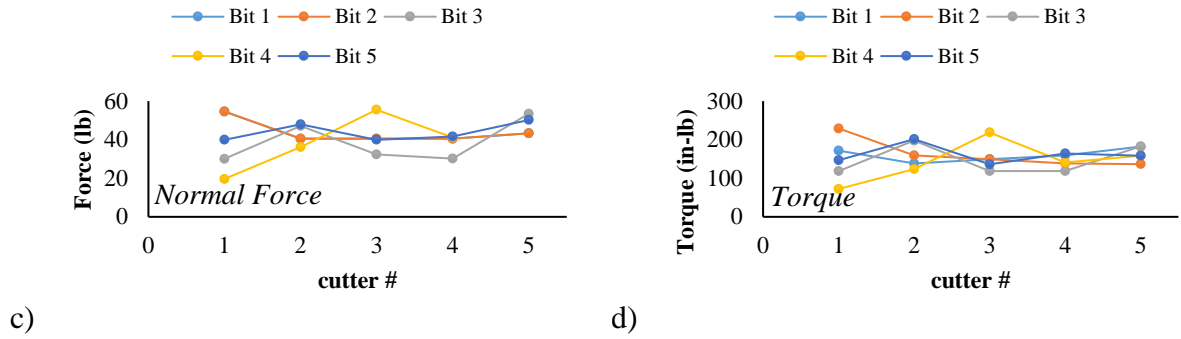


Figure 7-12: comparing different forces on every cutter on a bit

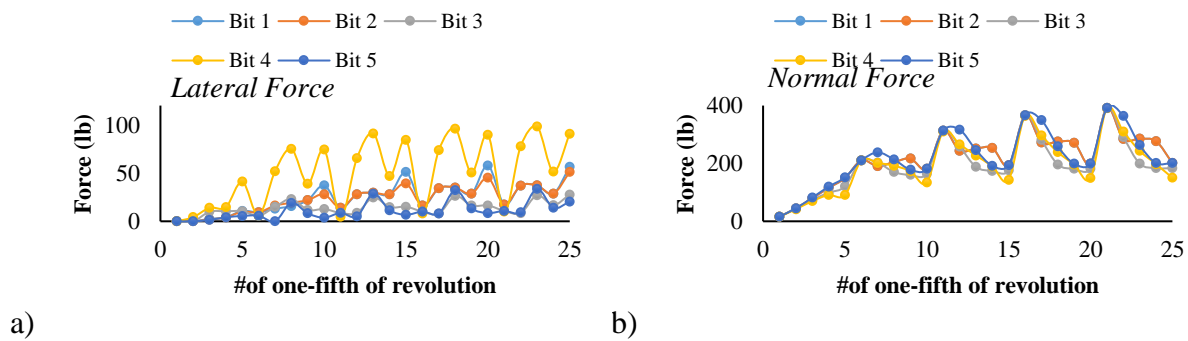


Figure 7-13: (a) lateral force and (b) normal force for all bits based on the model

The general performance of the bits shows the high fluctuation of lateral force and high level of potential instability (maybe bit whirl) for *Bit 4*, where the most stability is possibly predicted for *Bit 3* and *Bit 5*.

7.3.2 Comparing with Numerical Results

The average results from the numerical simulation is compared to the average results from the force model. Except *Bit 4*, a good agreement is seen between the results. For *Bit 4*, it was expected based on the simulation results to obtain much lower lateral force, but the model could not meet the expectation.

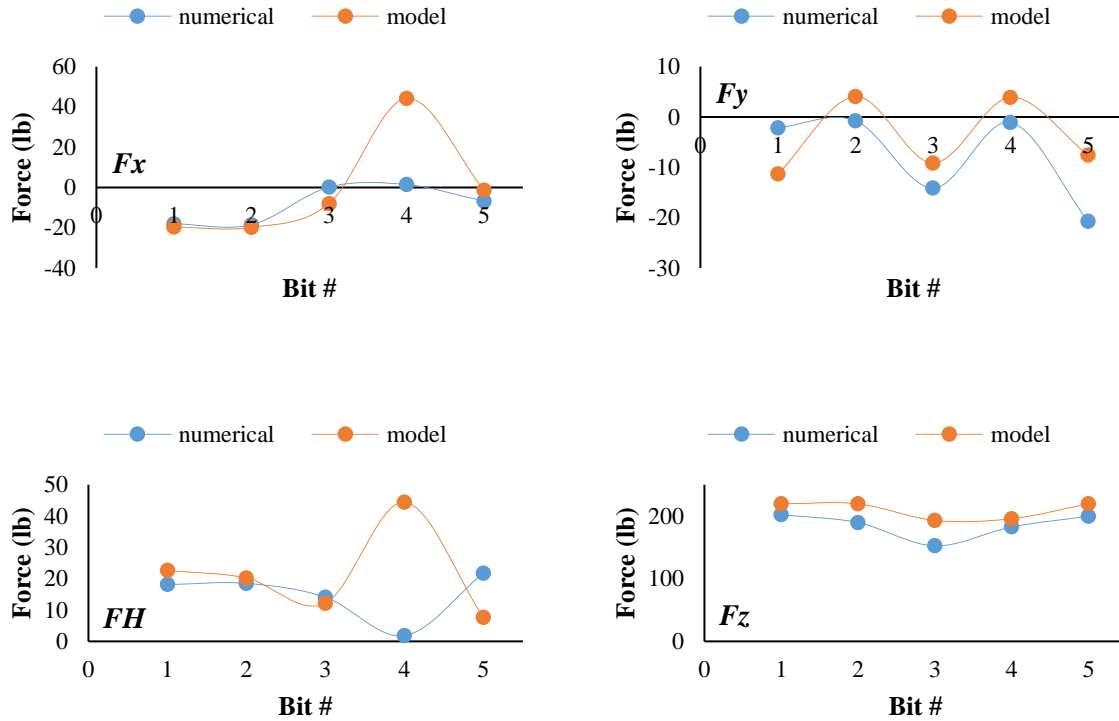
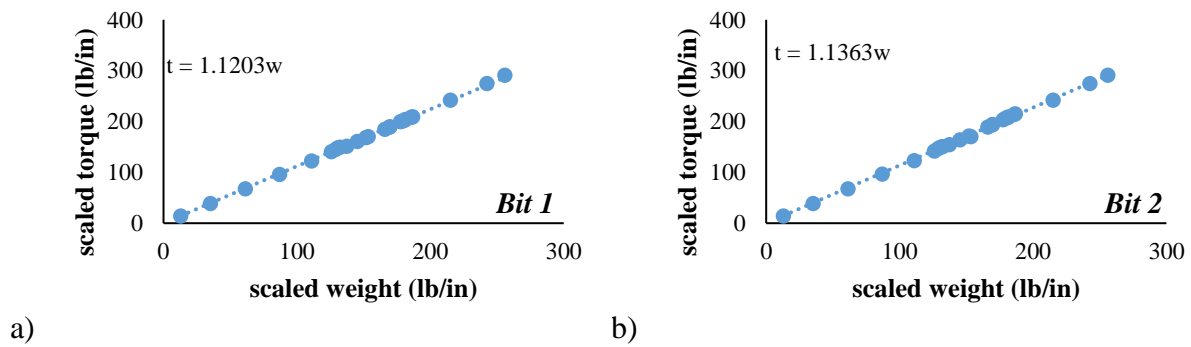


Figure 7-14: comparing the average of numerical results with results from the model

7.3.3 t-w Diagram

Scaled weight and scaled torque for every bit are calculated to plot the linear drilling response based on the bit parameters (ρ and R_{bit}) and computed WOB and TOB from the model. The slope of the line should indicate $\gamma \cdot \mu$. The bit constant, γ has been calculated in Table 7-4 and the obtained frictions based on the bit constants have been presented in Table 7-7.



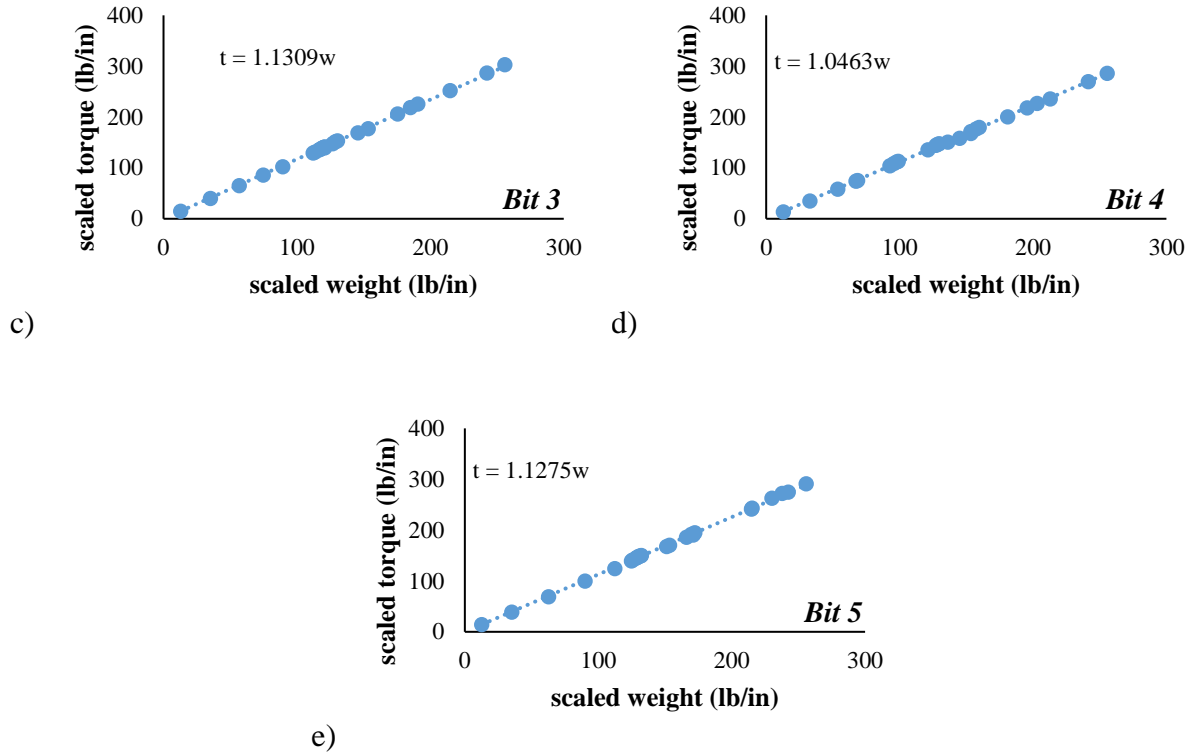


Figure 7-15: w-t diagram for all bits

Table 7-7: friction coefficients obtained based from t-w space

	Bit 1	Bit 2	Bit 3	Bit 4	Bit 5
Friction Coefficient	0.80	0.81	0.79	0.77	0.81

7.4 Summary

New rings of cutters containing five PDC cutters have been designed. Besides spiral and reverse spiral sets of cutters, three other bits are presented to study the effect of cutters arrangements on the bit performance and on the cutters. The variety of the bit parameters such as CM movement, ECT, bit constant, *etc.* are calculated. The rock cutting process is simulated to evaluate the bit performance. The proposed force model is applied to the bits with consideration of the direction of radial force for every cutter. The horizontal forces on the bit plane are measured. These forces on a bit plane may depict the bit tendency to driving off the center and the bit whirl.

Then, the model is employed to evaluate the cyclic loading on the cutters to consider damage or fracture on the diamond structure. It is demonstrated that in every sets of cutters layout, some cutters are subjected to higher stresses or cyclic loading and unloading. These cutters have to be protected either by changing the cutters arrangements on the bit or by strengthening them with high-quality material resistance. Last, the drilling response of the bit and the friction coefficient based on the bit constant is obtained. It is found that *Bit 1* and *Bit 2* (spiral and reverse spiral sets of cutters) operate very similar to each other; however, the MSE is slightly better when *Bit 2* is used. *Bit 3* and *Bit 5* (Track set and Chen's layout, respectively) give the lowest lateral force (instability), while *Bit 3* also provides the lowest MSE. Regardless of the performance for *Bit 4*, almost all cutters on that ring experience high cyclic loading, which indicates lowest bit life. Nevertheless, all the results have been obtained based on the cutting the shale sample, which is considered as a soft formation. To better understanding the bit performance of different cutters arrangements on the bit, harder formation is strongly recommended to consider.

8 CONCLUSIONS AND FUTURE WORK RECOMMENDATIONS

8.1 Summary

This dissertation reports on improvements made during the author's work by using multiple PDC cutters in conducting experiments, modeling, numerical simulation and data analysis. The first phase of the author's work at the beginning of the program was to fix, repair and modify a non-operational single point cutter (SPC) equipment to the current multipoint cutters (MPC) facility. In next phase, a database of single cutter and multiple PDC cutters experiments on different rock samples under atmospheric was generated during the study. The experiments were conducted under atmospheric (drilling fluid) pressure on the variety of partially saturated and unsaturated rock samples, including shale, limestone, sandstone and marble samples. New bit profile was designed to hold (up to) four PDC cutters on perpendicular blades, which allows the cutters to have various distances from the bit center. The forces in three directions were measured through a tri-axial load cell. Torque and MSE were calculated based on the electrical power consumed to rotate the bit. The engagement area of the cutters that involves with the formation and the geometry of the cut in every portion of a revolution were precisely calculated via a computer-aided design (CAD) program. The response of the multiple PDC cutters on a bit were evaluated based on the MSE and the lateral force on the bit plane. Lateral force on the bit can be heeded as the bit stability.

Rock characterization was done to obtain the rock strength. For one type of rock (Catoosa shale), the uniaxial compression strength test was conducted to gain the Mohr-Coulomb and Drucker-Prager criterion. The sonic test were conducted on all the samples to gain the rock strength based on the proposed empirical relations in the literature. The result of UCS test was used to find

the best correlation between the travel time measurement and the rock strength for all the tests. The scratch test was studied in this work to obtain the rock strengths but results were not satisfying.

Rock cutting simulation with using triple PDC cutters was done via finite element method (FEM). Rock properties of the sample were obtained based on the related tests *e.g.* UCS test. Four different cutters layouts containing three PDC cutters on a bit were proposed. The numerical results verified that different cutters layouts on the bit, provides different performances on the bit. The cutting area of the cutters cannot be assumed as the only factor affecting the bit performance. Because, for different cutters arrangements but with the same engagement area, different bit responses (MSE and the lateral force) have been obtained. In addition, numerical analysis indicated that among the designed arrangements, the reverse spiral sets of cutters gives the lowest MSE.

Several sets of experiments with triple PDC cutters were executed on different rock samples. The samples had 8" diameter, 1" thickness. In most cases, a drilling fluid was either water or mineral oil. The samples were left in the fluid at least for 2 days before the experiments to presume they were partially saturated. In a few tests, the dry samples were cut with no drilling fluid. Due to the restrictions on the MPC facility, the cutting process was stopped before reaching the steady state drilling condition. This fact can be driven to the fact that the cutting process in this study presents the transitional drilling situation between hard and soft formations.

In framework of this study, it is found that the cutters arrangements on the bit affect the bit performance. The experimental results indicated that although the engagement area of the cutters in the spiral and reverse spiral sets of cutters is similar, the bit responses are different; where, the reverse spiral set of cutters on the bit shows the lower MSE but higher lateral force on the plane. This fact verifies the effect of radial force of the cutters on the bit response. The radial force strongly depend on the changes on the center of mass (CM) of the cutters. The direction of

movement of the CM can be used to assign the side force to the cutters. Due to the changing in the cutting area in every portion of revolution.

A mechanistic model was presented to predict the main forces (normal, tangential and radial force) on the cutting face of the cutters. The parameters of the proposed model can be decomposed into the rock properties, the engagement area of the cutters, and the friction coefficient between the rock and the cutter. A good agreement between the results developed by the model and the experimental results were obtained, which validates the method of measuring the radial force on the cutters. The bit constant can be used as a tool to represent the bit design and particularly to highlight the impact of the diamond density. It is calculated for different bits used in this study. The linear drilling response based on the bit parameters is obtained that indicates the friction coefficient. If depth of cuts varies, the drilling response of the bit can be used to study the different regimes in drilling.

The proposed model then was employed to study and compare different cutters arrangements on 5 common cutters layouts on the bits. The results were compared to the numerical results, as well. Based on the modeling analysis, it can be concluded that applying the double track sets of cutters in a ring may ended up with the lowest MSE. Reverse spiral sets of cutters also presents low MSE and low lateral force on the bit.

Besides the evaluation of the general response of different bits, the proposed modeling can be used as a beneficial tool to predict the cutters conditions on the rings during the cutting process. Using this method demonstrates the possible fatigue on the cutters that may cause damage and fracture on the cutters. In this case, it is suggested to either enhance the cutters arrangement on the bit to reduce the cyclic loading or to compose the diamonds of those cutters with high quality materials to improve the resistance against bouncing.

The results of this study can be used to optimize the current cutters layouts models on the bits. They can be applied to the PDC cutters on a bit to predict the cutters conditions during the drilling process. The enhancement and optimization on the cutters arrangement may increase the bit performance and durability and reduce the drilling cost.

8.2 Future Work

This work provides data and model to predict the forces on the cutters and investigate on the cutters arrangement of the cutters on a bit. Based on the results of the experiments the following recommendation may improve the subject of this study.

- Switch from the current capability of the equipment in having the constant feeding rate (vertical distant) to the constant weight on bit (normal force in this study). This feature would allow us to study the drilling response of the bit more realistic and similar to the field practices.
- New bit design is needed to allow the cutters to involve with formation long enough to reach the maximum engagement area on the bit and experience the steady state condition for better investigation in rock cutting process.
- Cutters arrangements on the bits can be placed symmetric to better understanding the effect of different cutters arrangements on the bit stability and the imbalance force on the bits. It is recommended to have three PDC cutters with 120° angular difference or four PDC cutters with 90° . Possibly, the best way is to use six PDC cutters placed on different blades with 60° angular difference. That would greatly simulate the bit performance.
- Several rock samples in large range of strengths from soft to hard with known properties are required to validate the force modeling. It is predicted that some considerations may be risen in the study on the hard formations.

- New sets of cutters arrangements with different distances to the bit center can be used to better study the impact of the diamond density on the bits. Large flexibility of placing the cutters on the bit is needed to study the density of the cutters on bit design. This factor can be used to optimize the bit selection based on the given formation.
- In a geometrical study such as the presented work, it is significantly important to have the cutters all in the same height. Preparing the rock samples precisely even and flat, can be dramatically improved the quality of the force analysis. It is recommended that the sample preparation should be done automatically via an appropriate machine. That would reduce the level of error analysis and increase the validity of results.
- It is suggested to use strong adhesive or glue to attach the PDC cutters to the cutter holders rather than brazing or welding method that may damage the polished cutting face of the cutters.
- Conducting the experiments under the elevated pressures can provide a new perspective on the subject of this study. Considering the effect of the wellbore pressure is recommended to improve the force modeling on the cutters.

REFERENCES

- [1] D. Scott, "A bit of history: Overcoming early setbacks, PDC bits now drill 90%-plus of worldwide footage," *Drilling contractor anthology series—DC drill bits*. Houston, TX: IADC, pp. 1-7, 2015.
- [2] C. A. Deen, C. Kitagawa, B. Schneider, and G. King, "Aligned Materials and Design Development of High ROP Drill Bits," in *IADC/SPE Asia Pacific Drilling Technology Conference*, 2014: Society of Petroleum Engineers.
- [3] B. G. Lewis A, S. Miska, and M. Ziaja, "Experimental study of layouts of PDC cutters in core bit drilling," *AGH Drilling, Oil, Gas*, vol. 33, no. 2, 2016.
- [4] D. A. Glowka, "Use of single-cutter data in the analysis of PDC bit designs: Part 1-development of a PDC cutting force model," *Journal of Petroleum Technology*, vol. 41, no. 08, pp. 797-849, 1989.
- [5] L. Sinor, J. Powers, and T. Warren, "The effect of PDC cutter density, back rake, size, and speed on performance," in *IADC/SPE drilling conference*, 1998: Society of Petroleum Engineers.
- [6] J. R. Smith, "Diagnosis of Poor PDC Bit Performance in Deep Shales," 1998.
- [7] D. A. Glowka, "Development of a method for predicting the performance and wear of PDC (polycrystalline diamond compact) drill bits," Sandia National Labs., Albuquerque, NM (USA)1987.
- [8] T. Warren and W. Armagost, "Laboratory drilling performance of PDC bits," *SPE drilling engineering*, vol. 3, no. 02, pp. 125-135, 1988.
- [9] P. Hariharan and J. Azar, "PDC bit hydraulics design, profile are key to reducing balling," *Oil and Gas Journal*, vol. 94, no. 50, pp. 58-63, 1996.
- [10] S. Chen, G. Grosz, S. Anderle, R. Arfele, and K. Xun, "The role of 3D rock chips and cutting area shapes in PDC bit-design optimization," in *Abu Dhabi International Petroleum Exhibition and Conference*, 2014: Society of Petroleum Engineers.
- [11] T. Richard, "Determination of rock strength from cutting tests," University of Minnesota, 1999.
- [12] M. C. Jaime, "Numerical modeling of rock cutting and its associated fragmentation process using the finite element method," University of Pittsburgh, 2011.

- [13] L. Jing, "A review of techniques, advances and outstanding issues in numerical modelling for rock mechanics and rock engineering," *International Journal of Rock Mechanics and Mining Sciences*, vol. 40, no. 3, pp. 283-353, 2003.
- [14] B. Ortiz, C. Casallas, and H. Parra, "Improved bit stability reduces downhole harmonics (vibrations)," in *SPE/IADC Asia Pacific Drilling Technology*, 1996: Society of Petroleum Engineers.
- [15] M. Ziaja, "Rock/Bit imbalance force prediction," *Journal of Canadian Petroleum Technology*, vol. 38, no. 05, 1999.
- [16] G. Mensa-Wilmot, R. L. Garrett, and R. S. Stokes, "PAO lubricant inhibits bit balling, speeds drilling," *Oil and Gas Journal*, vol. 95, no. 16, 1997.
- [17] L. Ledgerwood III, "PFC modeling of rock cutting under high pressure conditions," in *1st Canada-US Rock Mechanics Symposium*, 2007: American Rock Mechanics Association.
- [18] R. Teale, "The concept of specific energy in rock drilling," in *International journal of rock mechanics and mining sciences & geomechanics abstracts*, 1965, vol. 2, no. 1, pp. 57-73: Elsevier.
- [19] D. Zijsling, "Single cutter testing-a key for PDC bit development," in *Offshore Europe*, 1987: Society of Petroleum Engineers.
- [20] E. Kuru and A. Wojtanowicz, "An experimental study of sliding friction between PDC drill cutters and rocks," in *International Journal of Rock Mechanics and Mining Sciences and Geomechanics Abstracts*, 1995, vol. 6, no. 32, p. 278A.
- [21] T. Richard, C. Coudyzer, and S. Desmette, "Influence of groove geometry and cutter inclination in rock cutting," in *44th US Rock Mechanics Symposium and 5th US-Canada Rock Mechanics Symposium*, 2010: American Rock Mechanics Association.
- [22] N. Rafatian, S. Z. Miska, L. W. Ledgerwood, M. Yu, R. Ahmed, and N. E. Takach, "Experimental study of MSE of a single PDC cutter interacting with rock under simulated pressurized conditions," *SPE Drilling & Completion*, vol. 25, no. 01, pp. 10-18, 2010.
- [23] V. Rajabov, S. Z. Miska, L. Mortimer, M. Yu, and M. E. Ozbayoglu, "The effects of back rake and side rake angles on mechanical specific energy of single PDC cutters with selected rocks at varying depth of cuts and confining pressures," in *IADC/SPE Drilling Conference and Exhibition*, 2012: Society of Petroleum Engineers.
- [24] B. Akbari, *PDC cutter-rock interaction-experiments and modeling*. The University of Tulsa, 2014.

- [25] B. Akbari, S. Miska, Y. Mengjiao, and E. Ozbayoglu, "Effect of Rock Pore Pressure on Mechanical Specific Energy of Rock Cutting Using Single PDC Cutter," in *47th US Rock Mechanics/Geomechanics Symposium*, 2013: American Rock Mechanics Association.
- [26] C. J. Kerr, "PDC drill bit design and field application evolution," *Journal of petroleum technology*, vol. 40, no. 03, pp. 327-332, 1988.
- [27] R. Feenstra, "Status of Polycrystalline-Diamond-Compact Bits: Part I Development (includes associated papers 19032 and 19900)," *Journal of petroleum technology*, vol. 40, no. 06, pp. 675-684, 1988.
- [28] R. Knowlton and R. Kester, "Curved Cutters Extend Range of Formations Drilled With PDC Bits," in *SPE/IADC Drilling Conference*, 1989: Society of Petroleum Engineers.
- [29] R. Knowlton, "PDC bits using positive rake cutters," in *SPE/IADC Drilling Conference*, 1990: Society of Petroleum Engineers.
- [30] F. Appl, C. C. Wilson, and I. Lakshman, "Measurement of forces, temperatures and wear of PDC cutters in rock cutting," *Wear*, vol. 169, no. 1, pp. 9-24, 1993.
- [31] E. Andersen and J. Azar, "PDC bit performance under simulated borehole conditions," *SPE drilling & completion*, vol. 8, no. 03, pp. 184-188, 1993.
- [32] D. Zijssling and R. Illerhaus, "Eggbeater PDC drillbit design eliminates balling in water-based drilling fluids," *SPE drilling & completion*, vol. 8, no. 04, pp. 246-252, 1993.
- [33] G. Weaver and R. Clayton, "A new PDC cutting structure improves bit stabilization and extends application into harder rock types," in *SPE/IADC drilling conference*, 1993: Society of Petroleum Engineers.
- [34] A. Ersoy, "Automatic drilling control based on minimum drilling specific energy using PDC and WC bits," *Mining Technology*, vol. 112, no. 2, pp. 86-96, 2003.
- [35] G. Hareland, R. Nygaard, W. Yan, and J. L. Wise, "Cutting efficiency of a single PDC cutter on hard rock," *Journal of Canadian Petroleum Technology*, vol. 48, no. 06, pp. 60-65, 2009.
- [36] M. E. Merchant, "Mechanics of the metal cutting process. I. Orthogonal cutting and a type 2 chip," *Journal of applied physics*, vol. 16, no. 5, pp. 267-275, 1945.
- [37] E. E. Bray and E. D. Evans, "Hydrocarbons in non-reservoir-rock source beds," *AAPG Bulletin*, vol. 49, no. 3, pp. 248-257, 1965.

- [38] Y. Nishimatsu, "The mechanics of rock cutting," in *International Journal of Rock Mechanics and Mining Sciences & Geomechanics Abstracts*, 1972, vol. 9, no. 2, pp. 261-270: Elsevier.
- [39] E. Detournay and P. Defourny, "A phenomenological model for the drilling action of drag bits," in *International journal of rock mechanics and mining sciences & geomechanics abstracts*, 1992, vol. 29, no. 1, pp. 13-23: Elsevier.
- [40] J. Cheatham and W. Daniels, "A Study of Factors Influencing the Drillability of Shales: Single-Cutter Experiments With STRATAPAX (T) Drill Blanks," *Journal of Energy Resources Technology*, vol. 101, no. 3, pp. 189-195, 1979.
- [41] M. Lebrun, *Etude théorique et expérimentale de l'abattage mécanique: application à la conception de machines d'abattage et de creusement*. École Nationale Supérieure des Mines de Paris, 1978.
- [42] J. I. Adachi, "Frictional contact in rock cutting with blunt tools," University of Minnesota, 1996.
- [43] J. Brych, N. Nsenga, and X. Shan, "Destructibility Of Rocks With Rotation Drilling Bits," in *6th ISRM Congress*, 1987: International Society for Rock Mechanics.
- [44] C. Fairhurst and W. Lacabanne, "Hard rock drilling techniques," *Mine Quarry Eng*, vol. 23, pp. 157-161, 1957.
- [45] F. Dagrain, "Influence of the cutter geometry in rock cutting: an experimental approach," *University of Minnesota, Minneapolis*, 2001.
- [46] L. Gerbaud, S. Menand, and H. Sellami, "PDC bits: all comes from the cutter rock interaction," in *IADC/SPE Drilling Conference*, 2006, p. 1.
- [47] R. Rahmani, J. Smith, and A. D. Taleghani, "Analytical modeling of PDC single cutter-rock interaction under confining pressure," in *46th US Rock Mechanics/Geomechanics Symposium*, 2012: American Rock Mechanics Association.
- [48] M. Ziaja, "Mathematical Model of the Polycrystalline Diamond Bit Drilling Process and Its Practical Application," in *SPE Annual Technical Conference and Exhibition*, 1985: Society of Petroleum Engineers.
- [49] T. Warren and A. Sinor, "Drag bit performance modeling," in *SPE Annual Technical Conference and Exhibition*, 1986: Society of Petroleum Engineers.

- [50] E. Detournay, T. Richard, and M. Shepherd, "Drilling response of drag bits: Theory and experiment," *International Journal of Rock Mechanics and Mining Sciences*, vol. 45, no. 8, pp. 1347-1360, 2008.
- [51] C. A. Deen, J. Maw, C. Knull, and J. M. Clegg, "Departure From the Norm in Polycrystalline Diamond Bit Design Allows Significant Performance Gains in Highly Erosive and Abrasive Formations," in *SPE Annual Technical Conference and Exhibition*, 2012: Society of Petroleum Engineers.
- [52] W. Thomson, *Theory of vibration with applications*. CrC Press, 2018.
- [53] S. Chen, R. Arfele, S. Anderle, and J. Romero, "A new theory on cutter layout for improving PDC bit performance in hard and transit formation drilling," in *IPTC 2013: International Petroleum Technology Conference*, 2013.
- [54] C. Galarraga, J. C. Fierro, I. Al Riyami, I. Al Azizi, and Y. Al Salehi, "An Unconventional Fixed Cutter Cutting Structure Layout to Drill Through Hard, Abrasive Conglomerates in Deep Wells—A Case Study," in *Abu Dhabi International Petroleum Exhibition & Conference*, 2016: Society of Petroleum Engineers.
- [55] S. Chen, G. Grosz, S. Anderle, R. Arfele, and K. Xun, "The Role of Rock-Chip Removals and Cutting-Area Shapes in Polycrystalline-Diamond-Compact-Bit Design Optimization," *SPE Drilling & Completion*, vol. 30, no. 04, pp. 334-347, 2016.
- [56] J. Lund, C. Cooley, J. Gonzalez, and T. Sexton, "Laboratory drill rig for PDC bearing and cutter development, Diamond Tool," ed: J, 2009.
- [57] C. Chang, M. D. Zoback, and A. Khaksar, "Empirical relations between rock strength and physical properties in sedimentary rocks," *Journal of Petroleum Science and Engineering*, vol. 51, no. 3-4, pp. 223-237, 2006.
- [58] G. Block and H. Jin, "Role of failure mode on rock cutting dynamics," in *SPE Annual Technical Conference and Exhibition*, 2009: Society of Petroleum Engineers.
- [59] J. C. Jaeger, N. G. Cook, and R. Zimmerman, *Fundamentals of rock mechanics*. John Wiley & Sons, 2009.
- [60] O. Mohr, *Abhandlungen aus dem gebiete der technischen mechanik*. 1906.
- [61] D. Drucker, W. Prager, and H. Greenberg, "Extended limit design theorems for continuous media," *Quarterly of applied mathematics*, vol. 9, no. 4, pp. 381-389, 1952.

- [62] M. D. Nazzal, "Laboratory characterization and numerical modeling of geogrid reinforced bases in flexible pavements," 2007.
- [63] O. Katz and Z. e. Reches, "Microfracturing, damage, and failure of brittle granites," *Journal of Geophysical Research: Solid Earth*, vol. 109, no. B1, 2004.
- [64] N. Sivakugan, B. Das, J. Lovisa, and C. Patra, "Determination of c and ϕ of rocks from indirect tensile strength and uniaxial compression tests," *International Journal of Geotechnical Engineering*, vol. 8, no. 1, pp. 59-65, 2014.
- [65] E. Detournay, A. Drescher, and D. A. Hultman, "Portable rock strength evaluation device," ed: Google Patents, 1997.
- [66] S. Y. Xie and J. F. Shao, "An Experimental Study and Constitutive Modeling of Saturated Porous Rocks," *Rock Mechanics and Rock Engineering*, vol. 48, no. 1, pp. 223-234, 2014.
- [67] K. Zhang, H. Zhou, and J. Shao, "An Experimental Investigation and an Elastoplastic Constitutive Model for a Porous Rock," *Rock Mechanics and Rock Engineering*, vol. 46, pp. 1499-1511, 2013.
- [68] C. Sachpazis, "Correlating Schmidt hardness with compressive strength and Young's modulus of carbonate rocks," *Bulletin of the International Association of Engineering Geology-Bulletin de l'Association Internationale de Géologie de l'Ingénieur*, vol. 42, no. 1, pp. 75-83, 1990.
- [69] M. C. Jaime, Y. Zhou, J.-S. Lin, and I. K. Gamwo, "Finite element modeling of rock cutting and its fragmentation process," *International Journal of Rock Mechanics and Mining Sciences*, vol. 80, pp. 137-146, 2015.
- [70] H. Liu, "Numerical modelling of the rock fragmentation process by mechanical tools," Luleå tekniska universitet, 2004.
- [71] I. Reyes Martinez, S. Fontoura, N. Inoue, C. Carrapatoso, A. Lourenco, and D. Curry, "Simulation of Single Cutter Experiments in Evaporites Through Finite Element Method," in *SPE/IADC Drilling Conference*, 2013: Society of Petroleum Engineers.
- [72] J. A. Mendoza Rizo, "Modeling Rock cutting using DEM with crushable particles," University of Pittsburgh, 2010.
- [73] J. Rojek, E. Onate, C. Labra, and H. Kargl, "Discrete element simulation of rock cutting," *International Journal of Rock Mechanics and Mining Sciences*, vol. 48, no. 6, pp. 996-1010, 2011.

- [74] M. Aubertin and R. Simon, "A damage initiation criterion for low porosity rocks," *International Journal of Rock Mechanics and Mining Sciences*, vol. 34, no. 3-4, pp. 17. e1-17. e15, 1997.
- [75] B. Wu and C. Tan, "Effect of water-cut on sandstone strength and implications in sand production prediction," in *DC Rocks 2001, The 38th US Symposium on Rock Mechanics (USRMS)*, 2001: American Rock Mechanics Association.
- [76] A. Hawkins and B. McConnell, "Sensitivity of sandstone strength and deformability to changes in moisture content," *Quarterly Journal of Engineering Geology and Hydrogeology*, vol. 25, no. 2, pp. 115-130, 1992.
- [77] P. Colback and B. Wiid, "The influence of moisture content on the compressive strength of rocks," *Geophysics*, 1965.
- [78] A. Fogden, M. Kumar, N. R. Morrow, and J. S. Buckley, "Mobilization of fine particles during flooding of sandstones and possible relations to enhanced oil recovery," *Energy & Fuels*, vol. 25, no. 4, pp. 1605-1616, 2011.
- [79] N. E. Dowling, *Mechanical behavior of materials: engineering methods for deformation, fracture, and fatigue*. Pearson, 2012.
- [80] K. Zacny, "Fracture and fatigue of polycrystalline-diamond compacts," *SPE Drilling & Completion*, vol. 27, no. 01, pp. 145-157, 2012.
- [81] O. Lopez *et al.*, "Quick Core Assessment from CT Imaging: from Petrophysical Properties to Log Evaluation," in *International Symposium of the Society of Core Analysts, Snomass, CO, paper SCA2016-031*, 2016, p. 12.

APPENDIX A: μ – CT SCANNING OF A SAMPLE AFTER CUT

It is assumed that the rock surface is virgin and intact at $t = 0$. By ignoring the small possible fractures/changes at the surface that have been occurred while coring and preparing the rock before test, it is assumed that the rock surface is intact. Once the cutter meets (touches), the rock surface some inevitable small fractures or changes in the patterns of the rock particles are maybe produced. These fractures, microscopically speaking, would make some changes on the boundary conditions of the rock and on the rock specifications. It means that only during the first revolution the cutters might meet the known presumed rock surface.

Likewise, in modelling and simulating the rock cutting process, the possible changes in the rock properties at the surface are not considered. Usually, it is supposed that in every revolution, the rock behavior remains the same as the first revolution. Therefore, this inaccurate assumption may affect the results. Applying an additional precise method of surface analyzing such as X-ray Computed Tomography would be strongly helpful. Computerized Tomography scanning (CT) is now widely used in the oil and gas industry, both for imaging of multiphase core flooding experiments and for the rock characterization. Core properties such as bulk density, mean atomic number and photoelectric factor can be derived directly from CT scans performed at two different energy levels. A CT scanner consists of an X-ray source and detectors. The X-rays penetrate the sample from different angles; either by rotating the source or the sample, and the detectors records the transmitted X-ray intensity [81].

In rock drilling perspective, only those fractures and cracks are important that their size is in range of micro or larger. First thing is to observe and analyze the so-called virgin rock surface. The samples have been scanned by the micro CT scanner (capable to see the fractures in magnitude of micrometer) and medical CT scanner (where no fractures smaller than 0.5 mm is visible). The

CT scanning by the medical device was done by cooperation of Dr. K. Matthews, Department of Physics & Astronomy at LSU. The micro CT scanning was carried out by the assist from Dr. M. Osborn, Department of Comparative Biomedical Sciences in School of Veterinary Medicine at LSU. The only difference in these two types of scanner is that better resolution comes with the restrictions on the size of the sample. By computed tomography scanning that is a common method in medical imaging, any changes in densities is scanned. In fact, when a material is homogenized and integrated, nothing is seen but once any fracture, crack or hole is produced, it will be scanned because of changing of densities between the material and the hole/fracture contents. For instance, in the samples used on this study, as the materials of rock has a greater density than any other fracture which contents water, oil or air, those fractures can be recognized due to the density. Therefore, it is planned to study and measure the dimensions of possible fractures in both width and height. Figure below shows the intact rock surfaces before cutting by PDC cutters.

It is seen that the medical CT scanner does not provide a high quality image on the fractures that is desired. Therefore, using micro CT scanner is the next step that accepts the samples no larger than 1 *inch* in any dimension. The saw that is used to shorten the 8" diameter rock into the acceptable specimens for the scanner, might produce new fractures or make changes at the edges that should not be confused with the former fractures due to main PDC rock cutting.

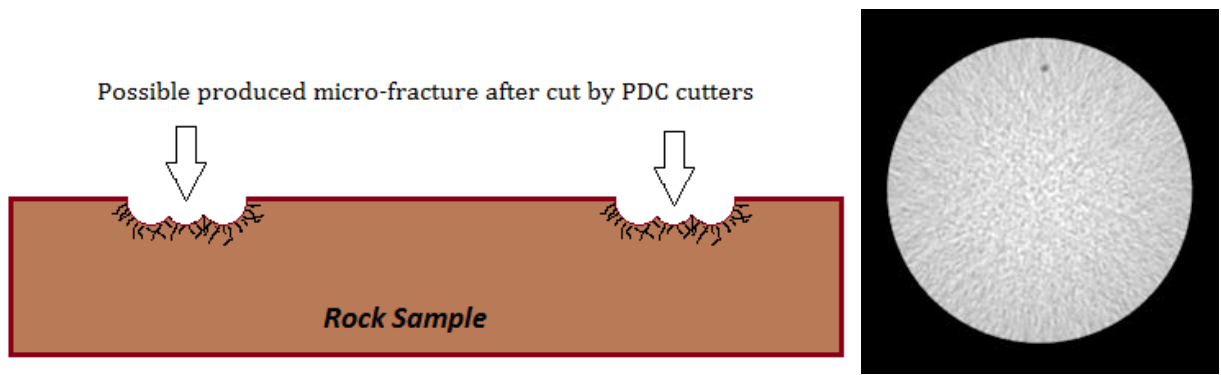


Figure A-1: Berea sandstone intact surface scanned by CT scanner

Small pieces of Berea sandstone that are cut by PDC cutters have been scanned. The scanner could provide 40 KV level of energy to see anything bigger than 80 micrometer. First sample (1) is assumed as an intact rock and other two samples (2 and 3) are cut by the cutters. The specific program (ImageJ) is used to analysis the images.

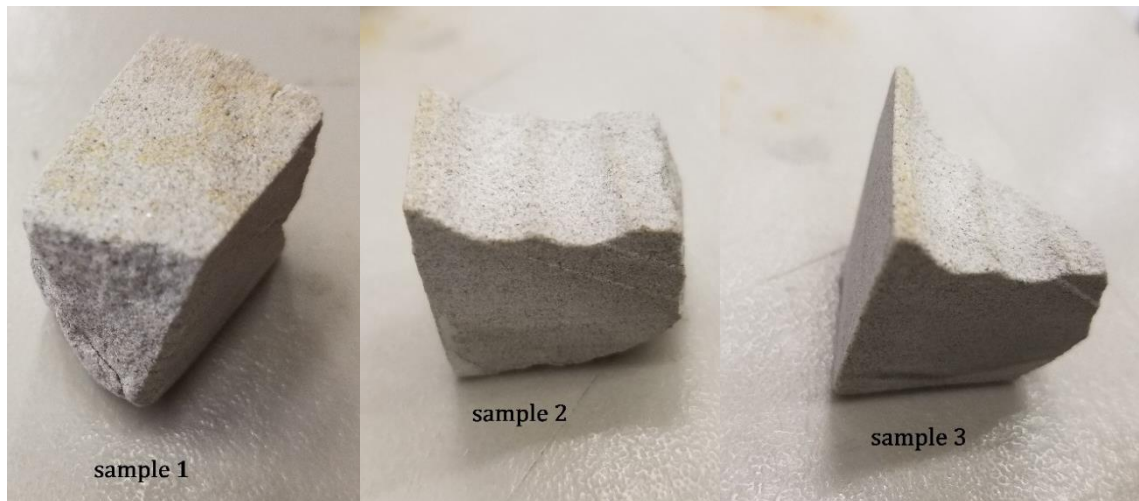


Figure A-2: sample 1 is intact rock and samples 2 & 3 are cut by cutters

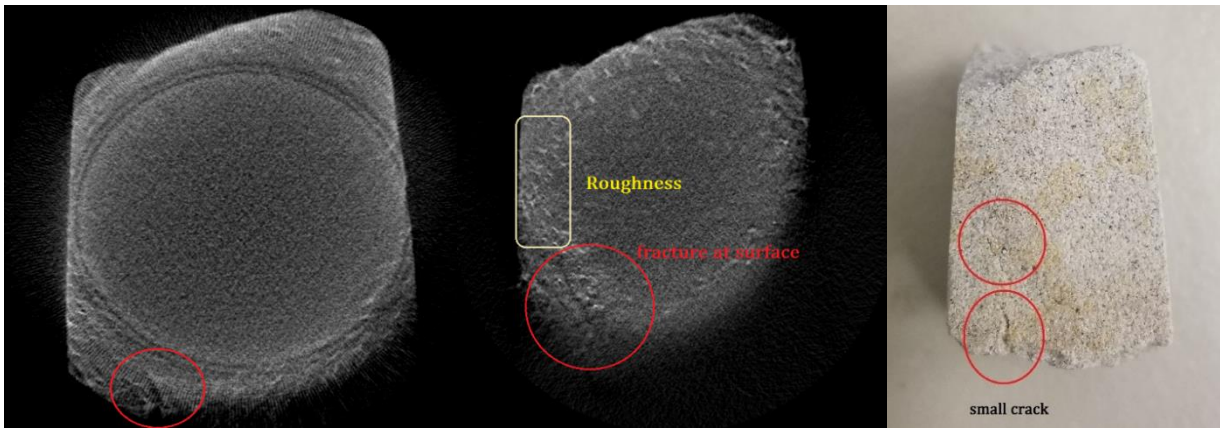
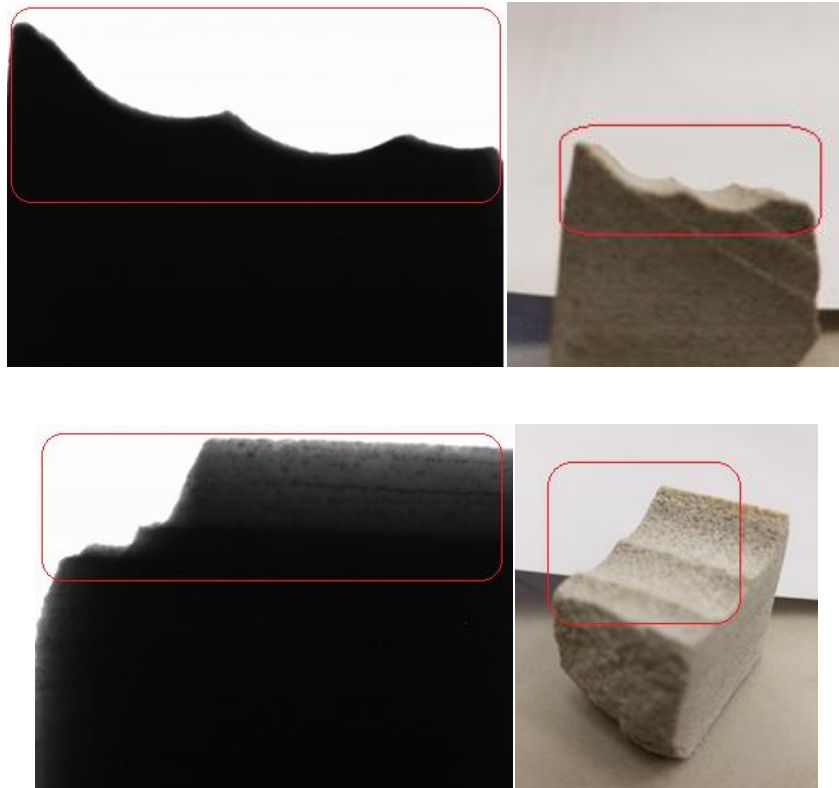


Figure A-3: scanned images for sample 1



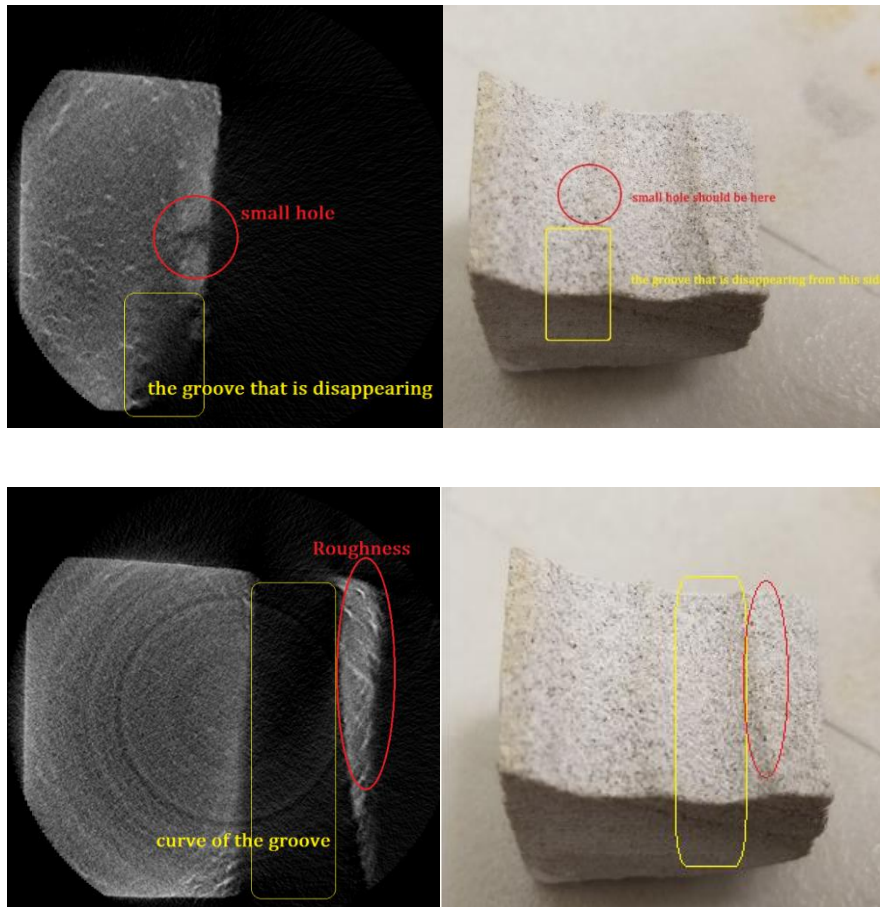


Figure A-4: scanned images for sample 2



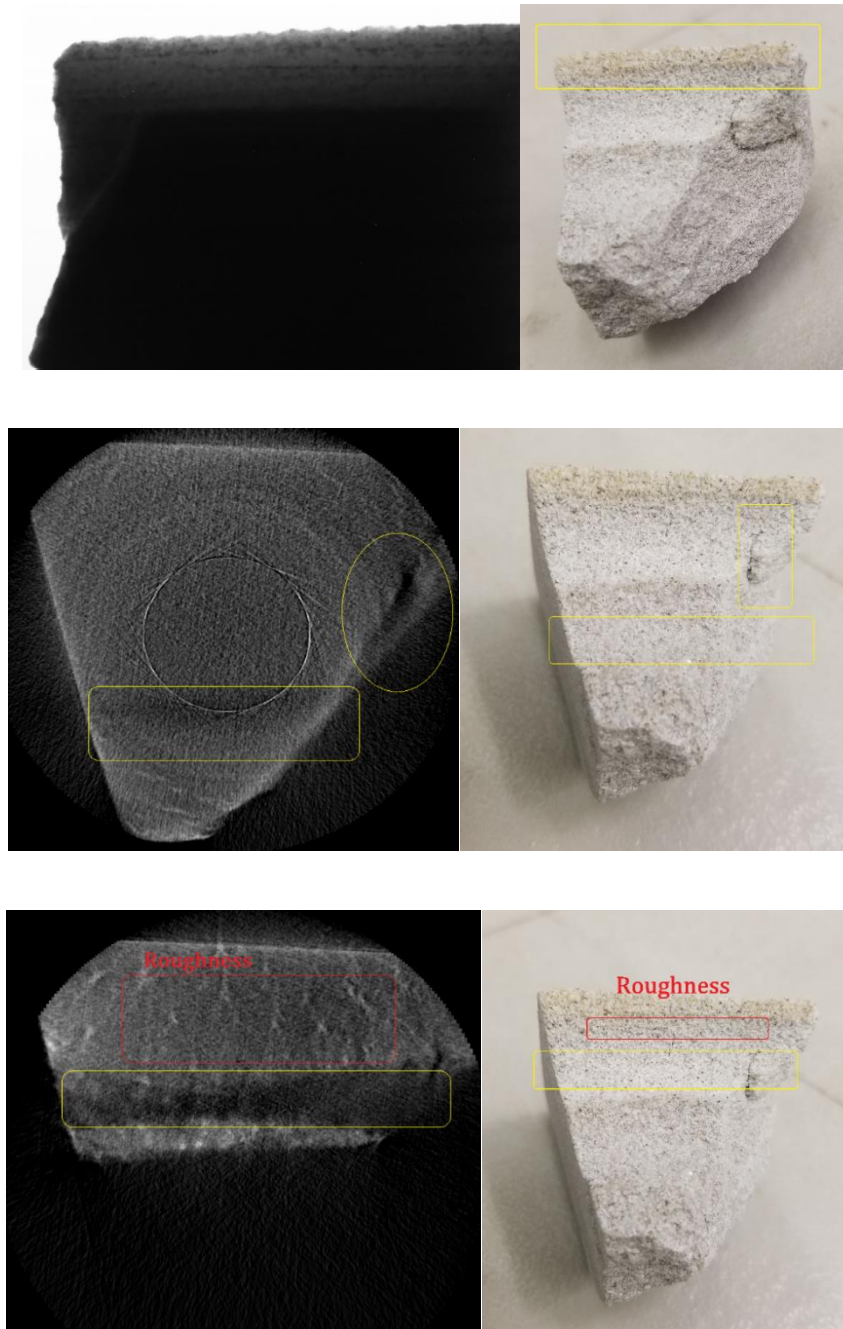
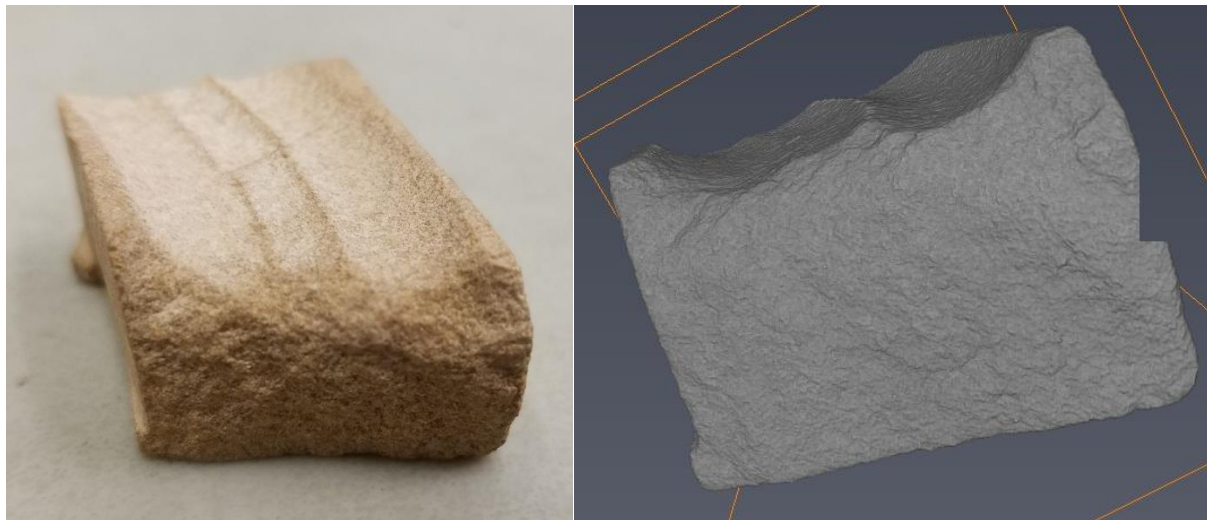


Figure A-5: scanned images for sample 3

The first attempt to visualize and analyze the rock surface after cutting was not satisfying due to low quality of the scanning and almost weak software to process the images. Then, a powerful micro CT scanner is employed (in Vet School at LSU) to scan the specimens of Torrey Buff sandstone. This device is capable to scan larger samples (up to 75 mm in length) with a higher

level of energy. Therefore, the better images with higher resolutions are expectable. Furthermore, for better analysis, a professional licensed software (*Avizo*) is employed.

In X-Ray CT images, the intensity values are linked to mass density. In a CT scan of a rock sample, different intensity ranges may represent surrounding air or pores (void spaces), water, clay or mineral. The ranges of intensities can be defined so that better visualization and computation modules can be taken. The fact in 3D volume rendering is of showing different densities and X-Ray absorptions by changing the intensities ranges. Therefore, the pattern visible on the rock surfaces represent different densities and X-Ray absorptions. When the cutters start to touch and cut the rock with implying axial and tangential forces, a compressed layer under the cutters can be produced. The changes on the patterns show the compression, which might be interpreted as the slightly changes in the rock properties. In fact, it can cause new layer or surface for new revolution of the cutters in next rotation that differs from what it used to be. This hypothesis needs more study to assure.



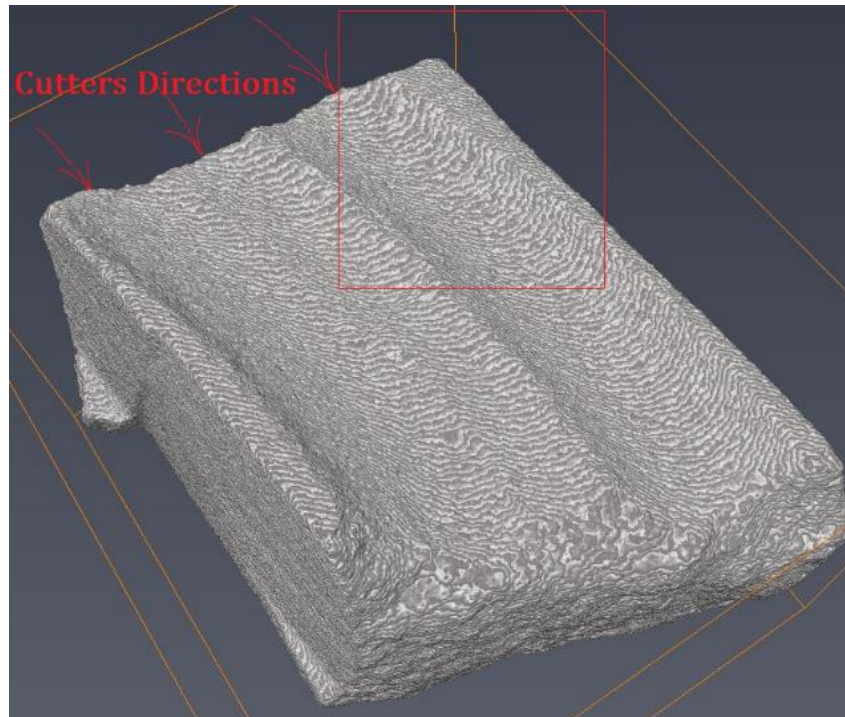
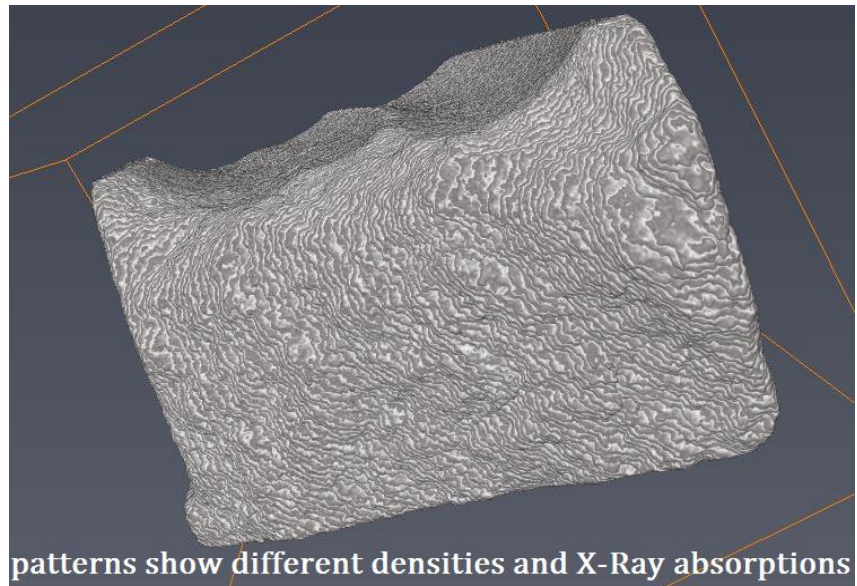


Figure A-6: image processing after micro CT scanning

Figures depict the changes in densities and consequently in X-Ray absorptions due to compression by cutting forces. It shows that less void spaces will be remained after cutting the rock. This phenomenon is seen on all sides of the sample, because of using saw to braking a 8"

dimeter rock disk to a small specimen for fitting into the micro CT scanner tube. The figure show the dragging and compressing of the layers under the PDC cutters in the same directions with the cutters. Next figures demonstrate the beneath the sample that have not been cut with the PDC cutters. The parallel patterns remain the same and they are produced due to the using a 14" rock saw blade to slice the initial core.

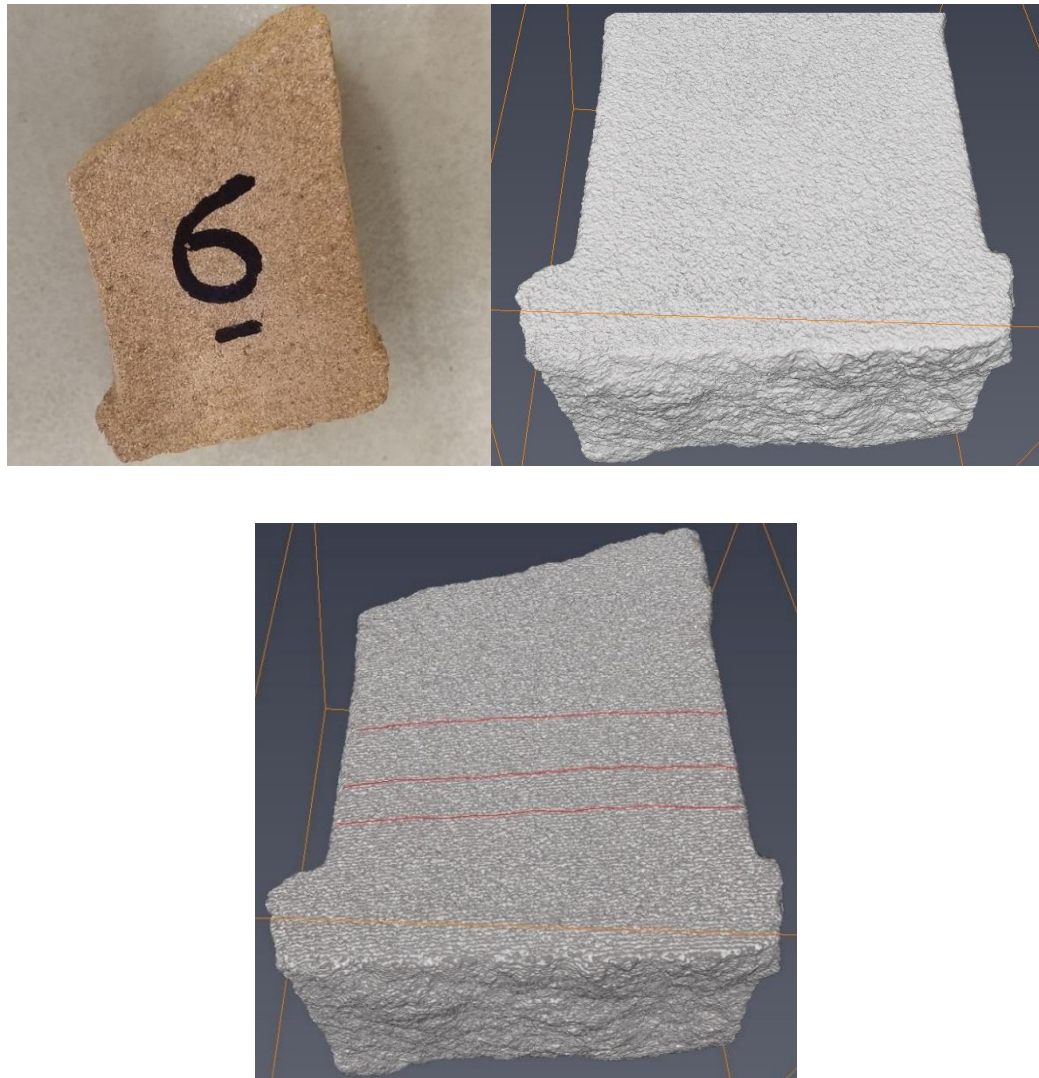


Figure A-7: image-processing, bottom of the sample

To better representing the changes in densities, two horizontal slides of the inside of the object are taken. One from almost 2 millimeter above the bottom surface where is predicted that

is not compressed due to the cutting. In addition, the other slide comes from almost 0.2 millimeter under the grooves. The precise comparison in densities shows that the (molecular) pattern of layers with the same density have been manipulated. Those layers are lying East-West on the lower slide while the North-South grooves have changed them, even in small ranges.

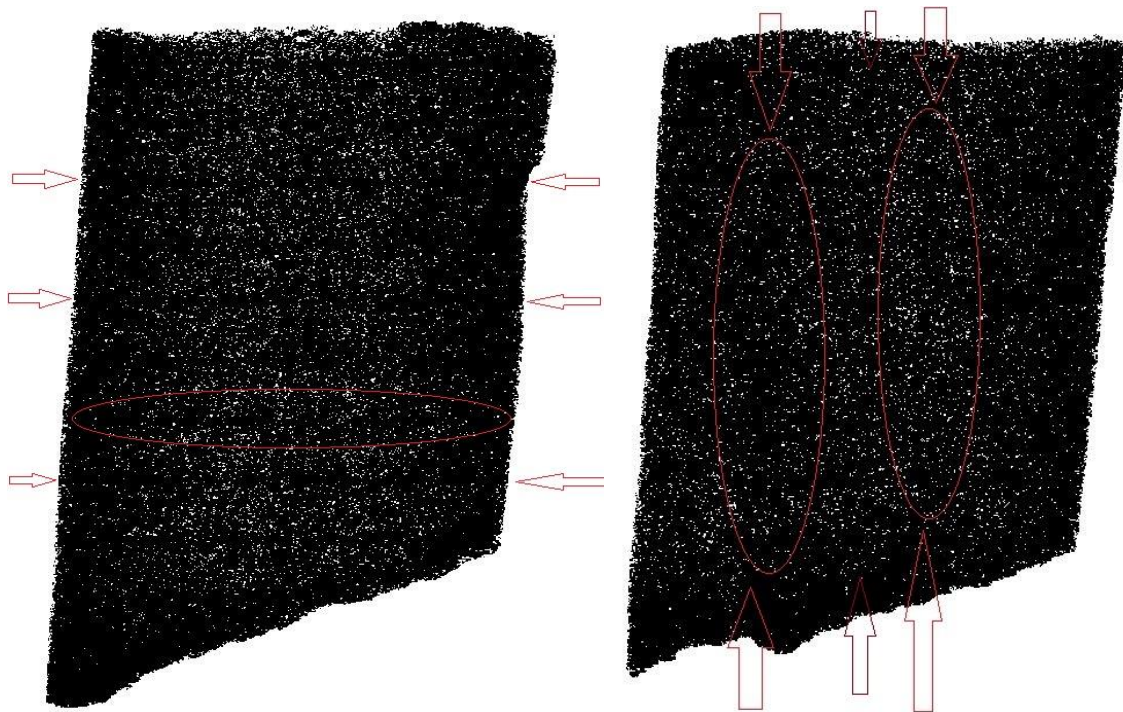
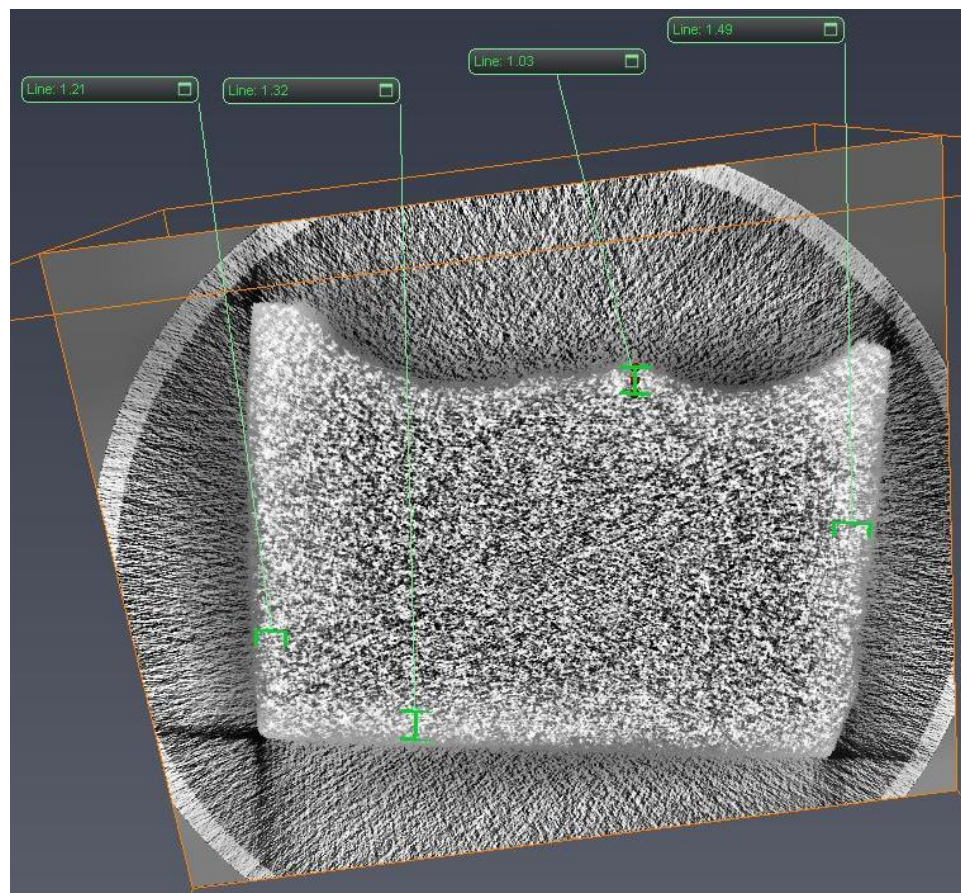


Figure A-8: horizontal internal slide from about 2 millimeter above the bottom surface of the rock. (a) The East-West black lines among the white dots show the pattern of density map. (b) 3 North-South black lines among the white dots can be interpolated of impact of the cutters on the molecular density of layers

The same hypothesis can be implied to another sample (Berea Sandstone) which was scanned by another device in lower level of energy. The analysis of the slides shows the possible compression on the layers near to the sides. This affect can be seen for one-millimeter length inside the rock. Last figure shows the internal slides in different distances from the front view.



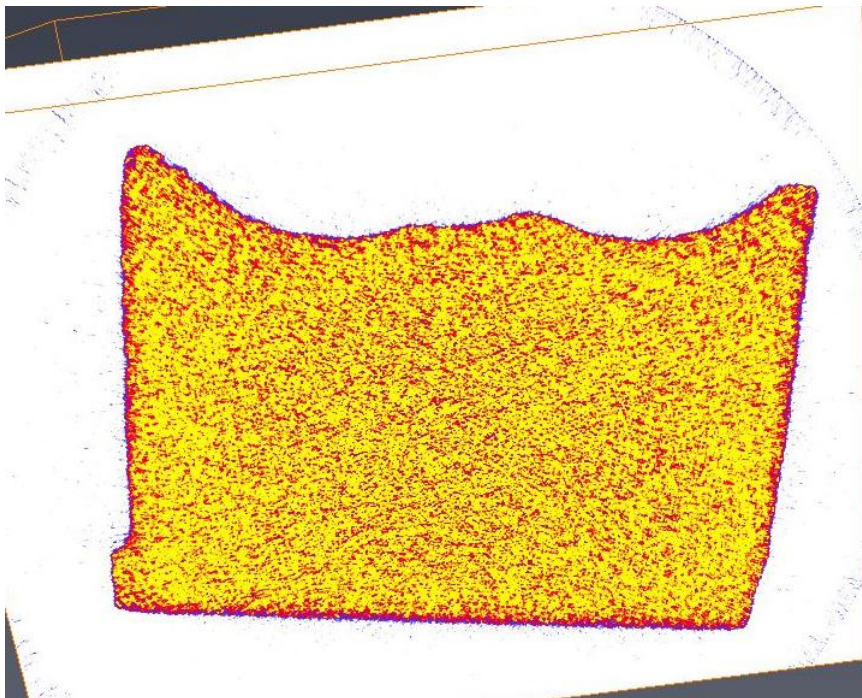
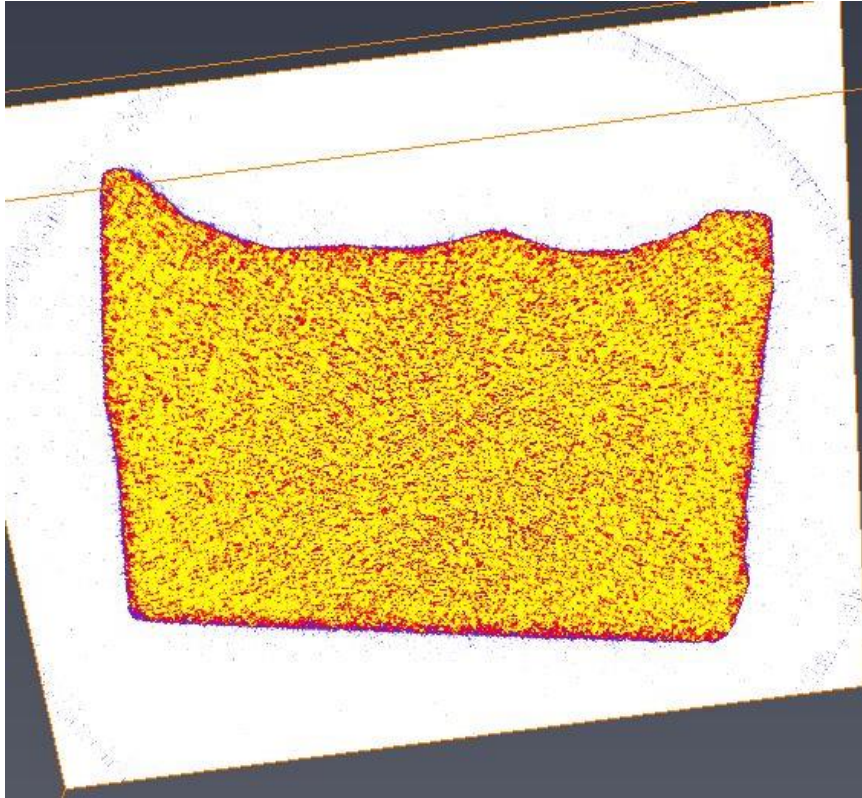


Figure A-9: The heavy density of red dots surround the object in different internal ortho-slides shows that from front view side to the end, these phenomena of changing densities due to the cutting forces can be seen.

APPENDIX B: SAMPLE PREPARATION

The sample preparation from the raw core is the time-consuming and hard but valuable process to improve the quality of the experiments. The procedure of the sample preparing has been presented in figures below.



Figure B-1: Core Driller and Rock Saw



Figure B-2: Rock Samples (Catoosa Shale, Torrey Buff, collection of sandstone, limestone and marble sample)

The samples must have 8" diameter and 1" thickness. The biggest sample was Catoosa shale that always have to be protected from the ambient conditions. First, it sliced to lighter and smaller pieces and then cored and cut to the desired size. The entire process of coring and cutting the shale was done by using oil as the cutting fluid. The other rock samples were cut to the required size, as well.



Figure B-3: coring and protecting Catoosa shale



Figure B-4: Final shape of the samples, prepared to be tested by the PDC cutters

APPENDIX C: COMPARING RESULTS: EXPERIMENTS & MODEL

Average forces from experiments with the forces developed based on the proposed model.

Table C-1: Comparing all the experimental and model forces for triple cutter tests. If the drilling/saturation fluid is not specified, then it is water.

No.	Sample	SET	F _x (lb)	F _y (lb)	F _z (lb)	F _H (lb)
1	Marble 1	Set 1	-15.3	-9.5	126.7	17.4
1	Marble 1	Set 1	-16.1	-7.6	123.5	17.9
2	Marble 1	Set 2	-28.9	-13.1	110.8	32.3
2	Marble 1	Set 2	-29.7	-11.3	112.8	31.9
3	Limestone 1	Set 1	-25.1	0.1	117.9	26.5
3	Limestone 1	Set 1	-25.8	-1.2	119.3	27.4
4	Limestone 1	Set 2	-53	-5.5	104.1	53.4
4	Limestone 1	Set 2	-48.3	-4.1	117.1	48.6
5	Marble 1	Set 5	13.9	-0.8	113.3	13.9
5	Marble 1	Set 5	12.6	-1.57	105	12.7
6	Marble 1	Set 6	31.1	-11.7	120.3	33.3
6	Marble 1	Set 6	30.8	-8.9	115	32
7	Marble 1	Set 10	15.6	-6.7	117.7	17
7	Marble 1	Set 10	14.5	-7.5	120.2	16.2
8	Shale 1 Oil	Set 1	-10.9	-1.3	30.2	11
8	Shale 1 Oil	Set 1	-11.5	-2	36	11.6
9	Shale 1 Oil	Set 5	-9.7	-8.5	33.4	12.9
9	Shale 1 Oil	Set 5	-9	-3	31.5	9.5
10	Sandstone 1 Oil	Set 1	-24.4	-6.2	83.1	25.2
10	Sandstone 1 Oil	Set 1	-14.6	-4.5	89.2	16
11	Sandstone 1 Oil	Set 5	-16.5	-17	102.3	24
11	Sandstone 1 Oil	Set 5	-12.4	-5.5	89.7	13.7
12	Sandstone 1 Oil	Set 9	-10.9	-12.8	82.3	16.8
12	Sandstone 1 Oil	Set 9	-9.9	-5.5	74.8	11.3
13	Sandstone 1 Water	Set 1	-34.7	-15.2	107.1	37.8
13	Sandstone 1 Water	Set 1	-28	-5	107.6	28.5
14	Sandstone 1 Water	Set 5	-11.3	-13.3	80.4	17.4
14	Sandstone 1 Water	Set 5	-13.3	-5	83.06	14.3
15	Sandstone 1 Water	Set 9	-2.5	-5.7	67.8	6.1
15	Sandstone 1 Water	Set 9	-10	-4.5	65	11
16	Sandstone 1 Water	Set 1	-11.6	-7.2	77.3	13.6
16	Sandstone 1 Air	Set 1	-9.8	-4.9	70.5	10.9
17	Sandstone 1 Air	Set 5	-1.6	-9.6	54	9.7
17	Sandstone 1 Air	Set 5	-7.9	-5.7	56.9	9.8

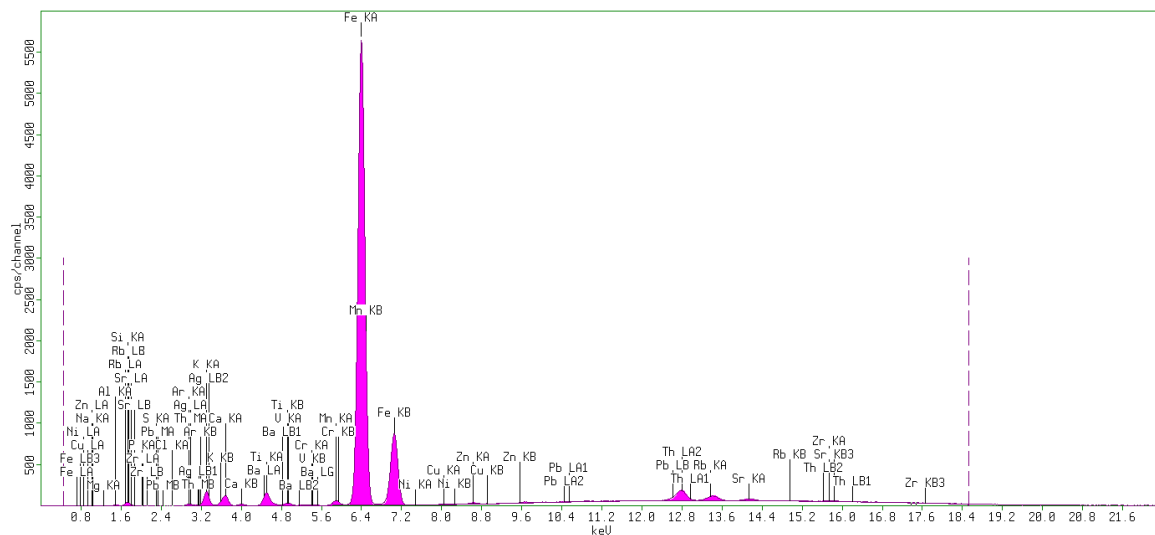
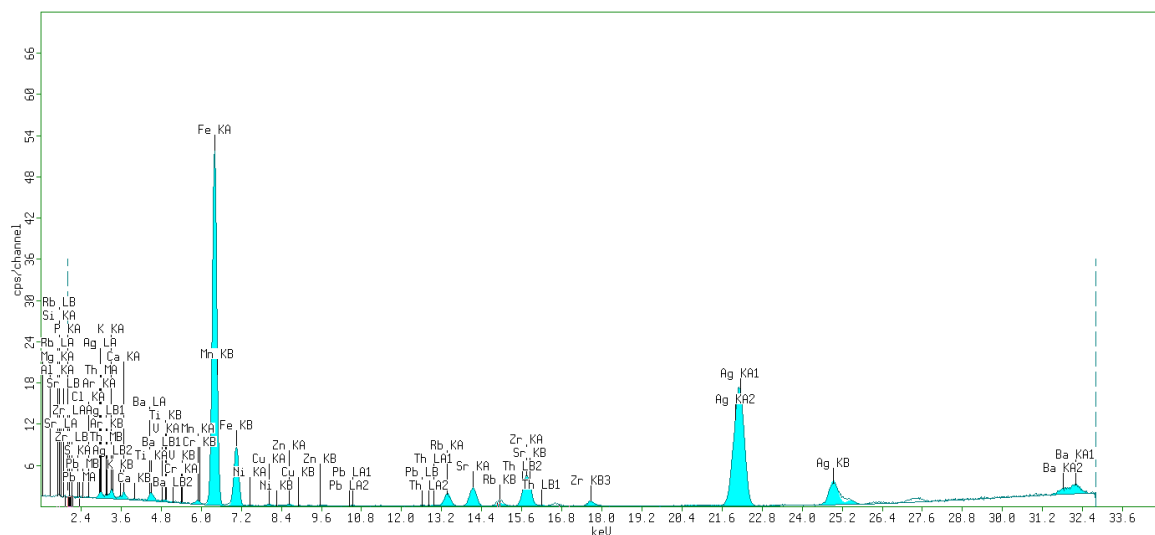
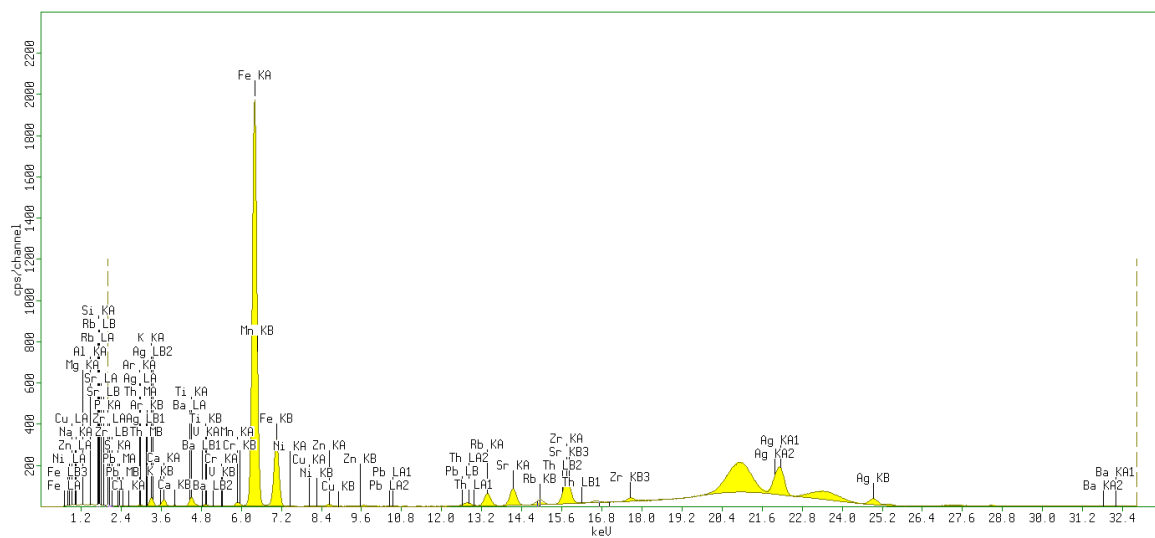
No.	Sample	SET	Fx (lb)	Fy (lb)	Fz (lb)	FH (lb)
18	Sandstone 1 Air	Set 9	-6.4	-7.3	58	9.7
18	Sandstone 1 Air	Set 9	-6.6	-5.9	51	8.8
19	Marble 2	Set 1	24.3	1.3	231	24.4
19	Marble 2	Set 1	21.6	3.8	237.7	22
20	Marble 2	Set 2	56.8	-10.2	234.2	57.8
20	Marble 2	Set 2	53	-13.9	235.9	54.7
21	Sandstone 3	Set 1	52.5	11.5	233	53.7
21	Sandstone 3	Set 1	54	11	229	55
22	Sandstone 3	Set 2	56.3	-3.3	225.2	56.5
22	Sandstone 3	Set 2	53.9	-11.2	229	55.1
23	Limestone 2	Set 1	20.9	0.1	165	20.9
23	Limestone 2	Set 1	22.7	-2.9	178.8	22.9
24	Limestone 2	Set 2	45.4	-1.5	180	45.4
24	Limestone 2	Set 2	46.3	-11	172	47.7
25	Sandstone 4 Air	Set 1	23.6	12.5	129.4	26.7
25	Sandstone 4 Air	Set 1	26	12	124.5	28.7
26	Sandstone 4 Air	Set 2	39.6	-7.2	113.3	40.3
26	Sandstone 4 Air	Set 2	41.8	-5.9	120	42.2

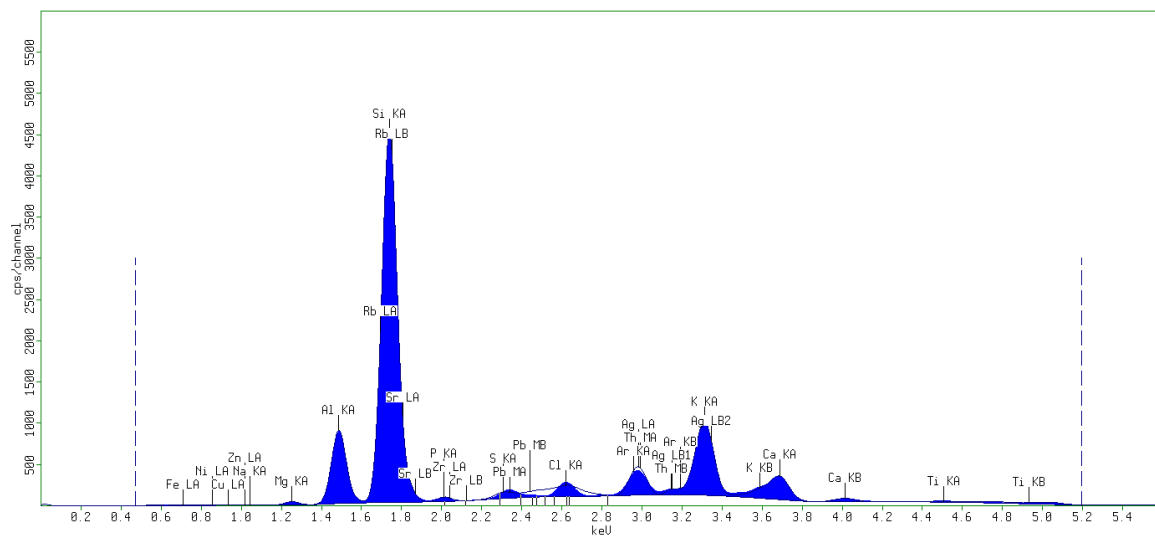
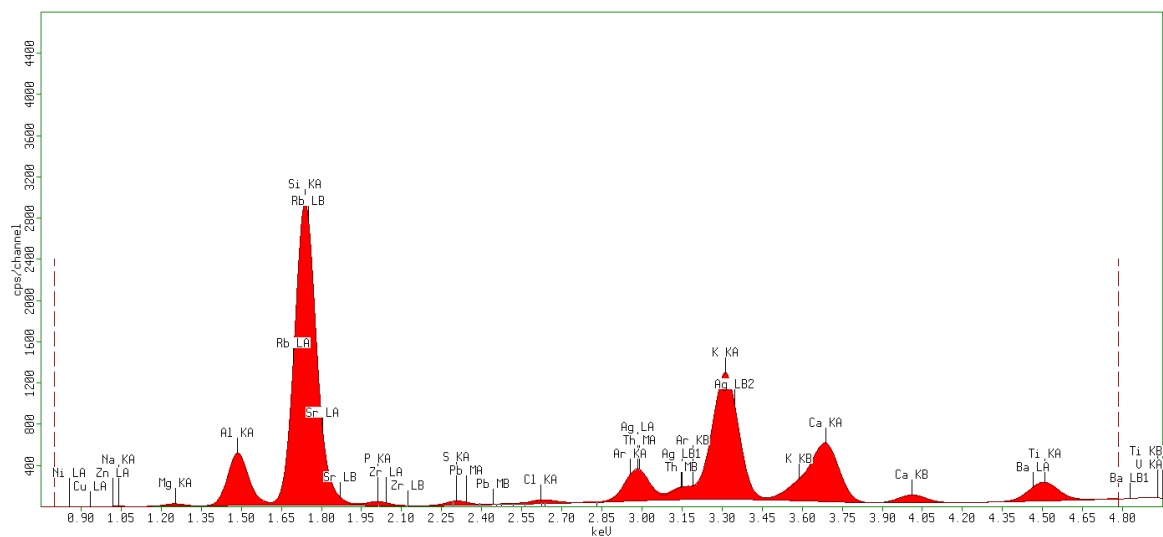
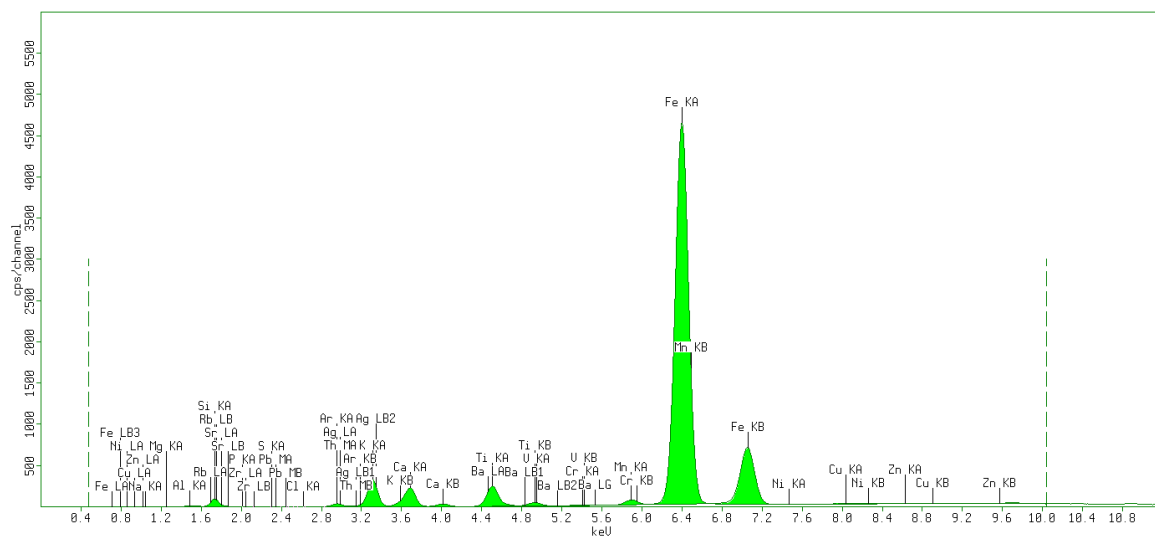
APPENDIX D: SHALE SPECIFICATIONS (*X-RAY & XRF*)

The mineral composition of the Catoosa shale have been presented as the table below.

Table D-1: Mineral composition of Catoosa Shale via XRF

Compound	Conc.	Unit
Na	0.466	%
Mg	1.331	%
Al	8.937	%
Si	26.884	%
P	0.251	%
S	0.147	%
Cl	734.2	ppm
K	4.075	%
Ca	1.733	%
Ti	0.88	%
V	189.3	ppm
Cr	161.5	ppm
Mn	0.125	%
Fe	8.862	%
Ni	106.9	ppm
Cu	68.1	ppm
Zn	165.9	ppm
Rb	290.7	ppm
Sr	345.3	ppm
Zr	445.1	ppm
Ba	368.5	ppm
Pb	61.6	ppm
Th	18.3	ppm





APPENDIX E: GROOVES AND CUTTING REMAIN AFTER CUT

The cutting path, grooves after the cutters, and the cuttings remain on the cutter faces have been presented in figures below.



Figure E-1: Torrey Buff Set 2 (71, 60, 65.5 mm) in oil and water



Figure E-2: Catoosa shale set 1 and set 3



Figure E-3: limestone and sandstone cutting with water set 1



Figure E-4: steady state drilling provides large path of cut

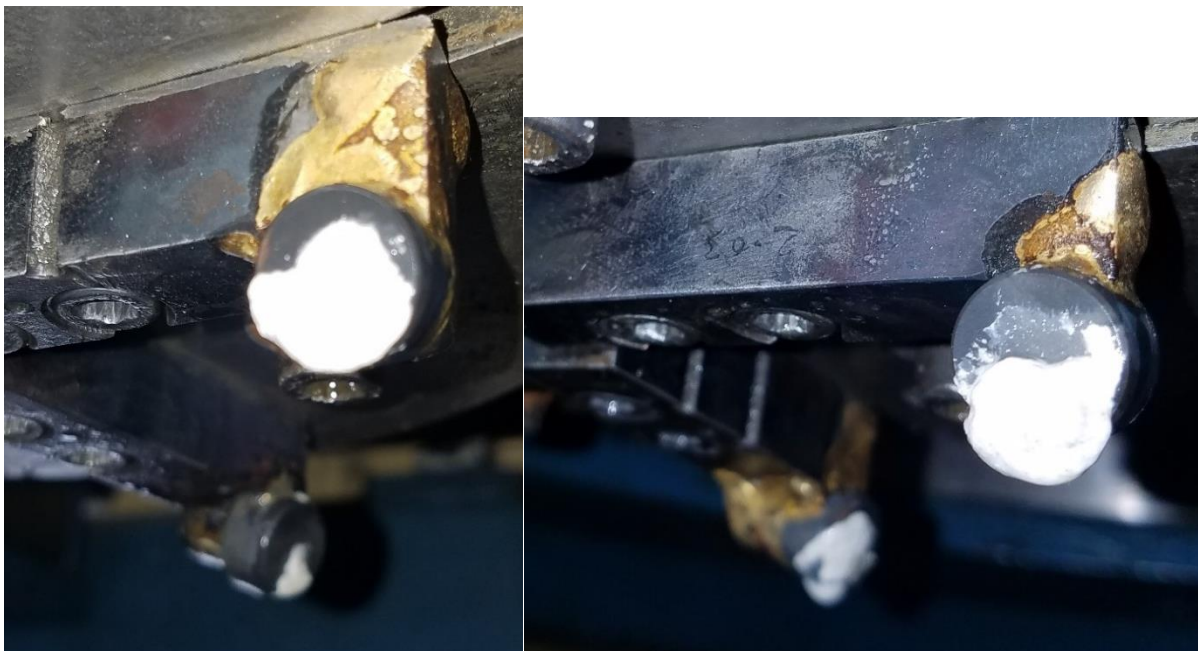


Figure E-1: marble cutting on the cutters



Figure E-6: sandstone cuttings on the cutters



Figure E-7: shale cuttings under atmospheric pressure

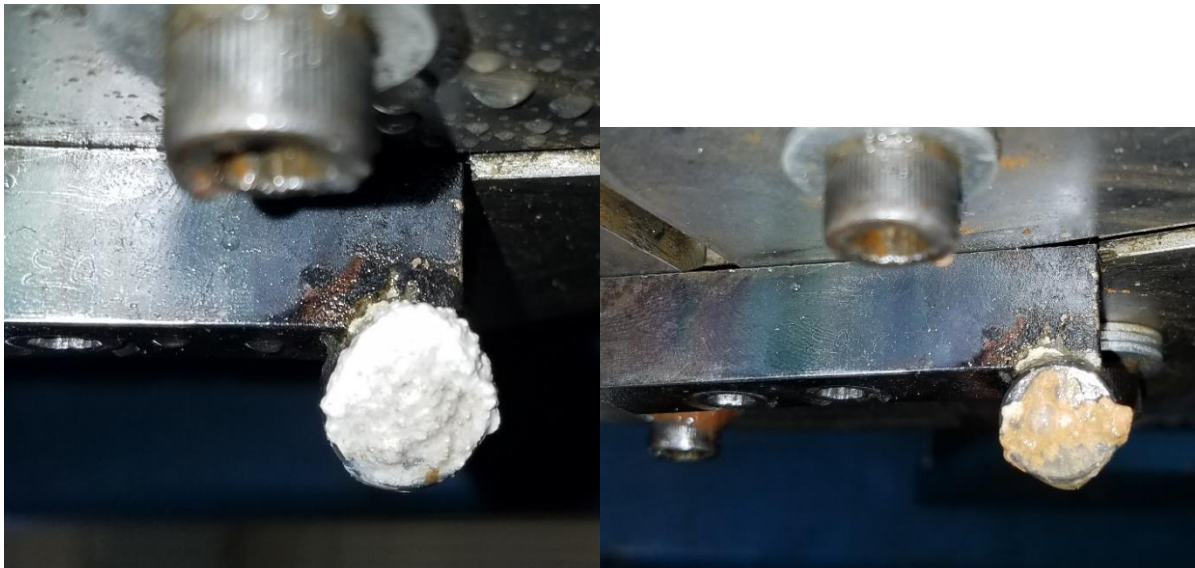


Figure E-8: cuttings remain after the single cutter tests with same conditions. (a) marble (b) sandstone

APPENDIX F: EMPRICAL RELATIONS TO OBTAIN UCS

Table 1

Empirical relationships between unconfined compressive strength (UCS) and other physical properties in sandstone

Eq. no.	UCS (MPa)	Region where developed	General comments	Reference
(1)	$0.035V_p - 31.5$	Thuringia, Germany	–	Freyburg (1972)
(2)	$1200\exp(-0.036\Delta t)$	Bowen Basin, Australia	Fine grained, both consolidated and unconsolidated sandstones with all porosity range	McNally (1987)
(3)	$1.4138 \times 10^7 \Delta t^{-3}$	Gulf Coast	Weak and unconsolidated sandstones	Fjaer et al. (1992)
(4)	$3.3 \times 10^{-20} \rho^2 V_p^4 [(1+\nu)/(1-\nu)]^2 (1-2\nu) [1+0.78V_{clay}]$	Gulf Coast	Applicable to sandstones with UCS > 30 MPa	
(5)	$1.745 \times 10^{-9} \rho V_p^2 - 21$	Cook Inlet, Alaska	Coarse grained sandstones and conglomerates	Moos et al. (1999)
(6)	$42.1\exp(1.9 \times 10^{-11} \rho V_p^2)$	Australia	Consolidated sandstones with $0.05 < \phi < 0.12$ and UCS > 80 MPa	Bradford et al. (1998) Vernik et al. (1993)
(7)	$3.87\exp(1.14 \times 10^{-10} \rho V_p^2)$	Gulf of Mexico	–	
(8)	$46.2\exp(0.027E)$	–	–	
(9)	$2.28 + 4.1089E$	Worldwide	–	
(10)	$254 (1 - 2.7\phi)^2$	Sedimentary basins worldwide	Very clean, well-consolidated sandstones with $\phi < 0.3$	
(11)	$277\exp(-10\phi)$	–	Sandstones with $2 < \text{UCS} < 360 \text{ MPa}$ and $0.002 < \phi < 0.33$	

Table 2

Empirical relationships between unconfined compressive strength (UCS) and other physical properties in shale

Eq. no.	UCS (MPa)	Region where developed	General comments	Reference
(12)	$0.77 (304.8 / \Delta t)^{2.93}$	North Sea	Mostly high porosity Tertiary shales	Horsrud (2001)
(13)	$0.43 (304.8 / \Delta t)^{3.2}$	Gulf of Mexico	Pliocene and younger	
(14)	$1.35 (304.8 / \Delta t)^{2.6}$	Globally	–	Lal (1999)
(15)	$0.5 (304.8 / \Delta t)^3$	Gulf of Mexico	–	
(16)	$10 (304.8 / \Delta t - 1)$	North Sea	Mostly high porosity Tertiary shales	Horsrud (2001)
(17)	$7.97E^{0.91}$	North Sea	Mostly high porosity Tertiary shales	
(18)	$7.22E^{0.712}$	–	Strong and compacted shales	Lashkaripour and Dusseault (1993)
(19)	$1.001\phi^{-1.143}$	–	Low porosity ($\phi < 0.1$) high strength (~ 79 MPa) shales	
(20)	$2.922\phi^{-0.96}$	North Sea	Mostly high porosity Tertiary shales	Horsrud (2001)
(21)	$0.286\phi^{-1.762}$	–	High porosity ($\phi > 0.27$) shales	

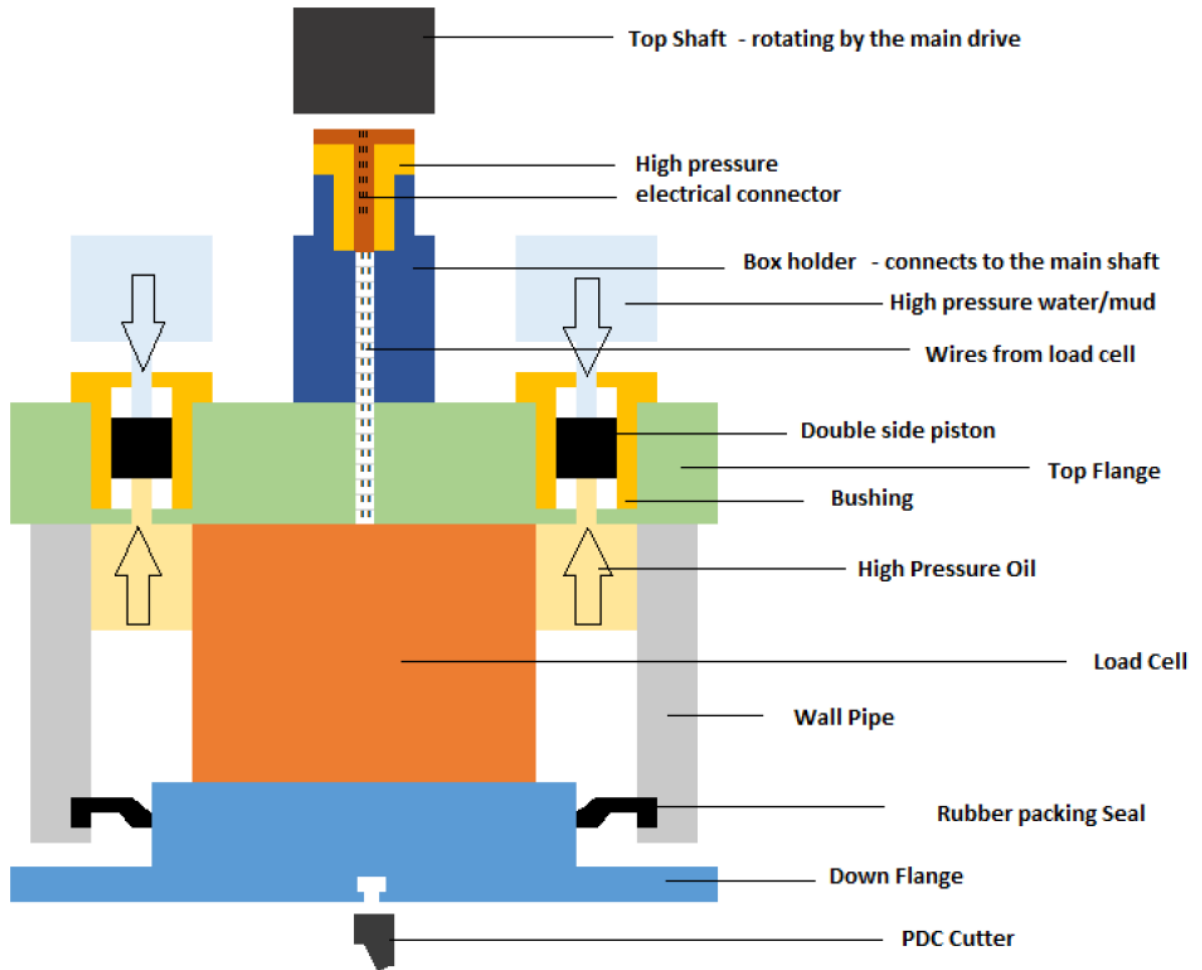
Table 3

Empirical relationships between unconfined compressive strength (UCS) and other physical properties in limestone and dolomite

Eq. no.	UCS (MPa)	Region where developed	General comments	Reference
(22)	$(7682 / \Delta t)^{1.82} / 145$	–	–	Militzer and Stoll (1973)
(23)	$10^{(2.44+109.14/\Delta t)} / 145$	–	–	Golubev and Rabinovich (1976)
(24)	$13.8E^{0.51}$	–	Limestone with $10 < \text{UCS} < 300 \text{ MPa}$	Rzhevsky and Novick (1971)
(25)	$25.1E^{0.34}$	–	Dolomite with $60 < \text{UCS} < 100 \text{ MPa}$	
(26)	$276 (1 - 3\phi)^2$	Korobcheyev deposit, Russia	–	
(27)	$143.8 \exp(-6.95\phi)$	Middle East	Representing low to moderate porosity ($0.05 < \phi < 0.2$) and high UCS ($30 < \text{UCS} < 150 \text{ MPa}$)	
(28)	$135.9 \exp(-4.8\phi)$	–	Representing low to moderate porosity ($0 < \phi < 0.2$) and high UCS ($10 < \text{UCS} < 300 \text{ MPa}$)	

APPENDIX G: SENSOR PROTECTIVE BOX

A protective box is designed and built to save the sensor from the harsh environment inside the vessel, especially in pressurized test.



VITA

Kian Sheikhezadeh was born in 1986 in Tehran, Iran. In 2004, he entered the Chemical Engineering program of the Amirkabir University of Technology, Tehran, Iran and got his bachelor in 2008. He then, worked for 5 years as a manager in a branch of a company manufacturing the insulation products. Meanwhile, due to his serious interest to the management programs, Kian applied to Payam Noor University in Tehran to pursue his degree in master of business administration (MBA) and graduated in 2011. A year after, Kian married to his love, Marmar. In spring 2015, he joined the Craft & Hawkins Department of Petroleum Engineering at Louisiana State University (LSU). In May 2019, Kian successfully defended his dissertation entitled “An Experimental Study on the Impacts of Using Multiple PDC Cutters on Rock Cutting Process”. Upon the graduation, he started his career as a development engineer and joined to National Oilwell Varco (NOV) in summer 2019.